Universidad Complutense de Madrid

Facultad de Farmacia

Departamento de Química Inorgánica y Bioinorgánica

Síntesis de Fosfatos de Calcio en Presencia de Surfactantes Iónicos, Fosfolípidos y Nanopartículas de Sílice Mesoporosa para Controlar la Mesoestructura de la Biocerámica

Synthesis of Calcium Phosphates in the Presence of Ionic Surfactants, Phospholipids and Mesoporous Silica Nanoparticles to Control the Bioceramic Mesostructure

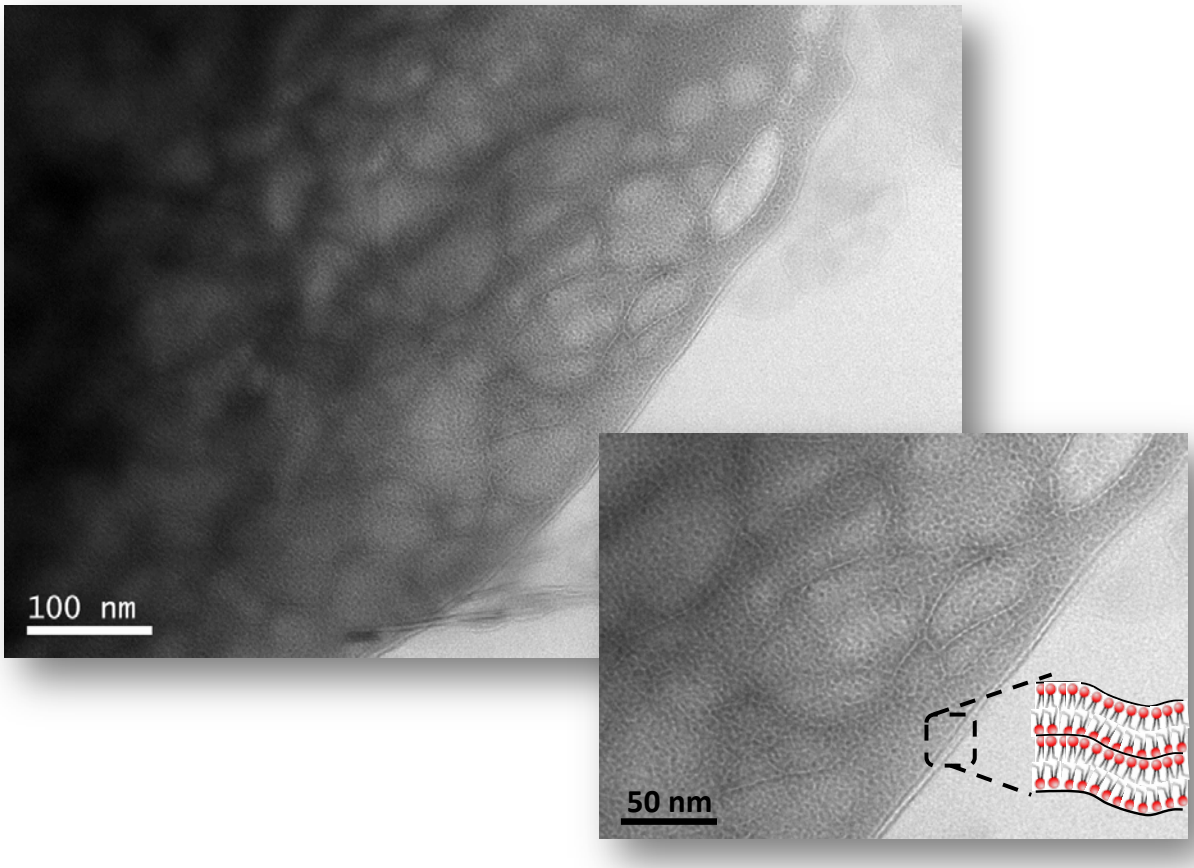

Okan Mersinlioğlu

TESIS DOCTORAL

Madrid, Septiembre 2015

Universidad Complutense de Madrid
Facultad de Farmacia
Departamento de Química Inorgánica y Bioinorgánica

TESIS DOCTORAL

Síntesis de Fosfatos de Calcio en Presencia de Surfactantes Iónicos, Fosfolípidos y Nanopartículas de Sílice Mesoporosa para Controlar la Mesoestructura de la Biocerámica

Memoria presentada por
Okan Mersinlioğlu
para optar al grado de Doctor por la Universidad Complutense de Madrid

Directores
Dr. Antonio J. Salinas Sánchez y Dra. Blanca González Ortiz

Madrid, Septiembre 2015

Universidad Complutense de Madrid

Facultad de Farmacia

Departamento de Química Inorgánica y Bioinorgánica

DOCTORAL THESIS

Synthesis of Calcium Phosphates in the Presence of Ionic Surfactants, Phospholipids and Mesoporous Silica Nanoparticles to Control the Bioceramic Mesostructure

A dissertation presented by

Okan Mersinlioğlu

to apply for the degree of Doctor by Universidad Complutense de Madrid

Supervisors

Dr. Antonio J. Salinas Sánchez and Dra. Blanca González Ortiz

Madrid, September 2015

Universidad Complutense de Madrid

Dr. Antonio J. Salinas Sánchez y **Dra. Blanca González Ortiz**, Profesores Titulares del Departamento de Química Inorgánica y Bioinorgánica de la Facultad de Farmacia de la Universidad Complutense de Madrid, en calidad de directores de esta Tesis Doctoral,

CERTIFICAN:

Que la presente memoria titulada ***"Synthesis of Calcium Phosphates in the Presence of Ionic Surfactants, Phospholipids and Mesoporous Silica Nanoparticles to Control the Bioceramics Mesostructure"*** ha sido realizado por **Okan Mersinlioğlu** bajo nuestra dirección, en el Departamento de Química Inorgánica y Bioinorgánica de la Facultad de Farmacia de la Universidad Complutense de Madrid, y que reúne las condiciones necesarias para ser presentada como requisito para optar al grado de Doctor por la Universidad Complutense de Madrid.

Madrid, 22 de Septiembre de 2015

Dr. Antonio J. Salinas Sánchez **Dra. Blanca González Ortiz**

Universidad Complutense de Madrid

Dr. Antonio J. Salinas Sánchez and **Dr. Blanca González Ortiz**, Associate Professors of the Department of Inorganic and Bioinorganic Chemistry of Faculty of Pharmacy at Universidad Complutense de Madrid, Spain, as supervisors of this Doctoral Thesis,

CERTIFICATE:

That the present PhD dissertation entitled ***"Synthesis of Calcium Phosphates in the Presence of Ionic Surfactants, Phospholipids and Mesoporous Silica Nanoparticles to Control the Bioceramics Mesostructure"*** has been developed by **Okan Mersinlioğlu** under our supervision, at the Department of Inorganic and Bioinorganic Chemistry of Faculty of Pharmacy at Universidad Complutense de Madrid, and that it fulfils all the requirements to apply for the degree of Doctor by Universidad Complutense de Madrid.

Madrid, September 22nd 2015

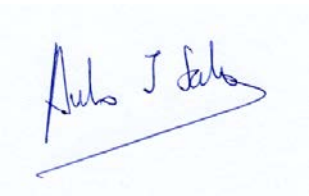

Dr. Antonio J. Salinas Sánchez

Dr. Blanca González Ortiz

To ***Hanife,*** the most beautiful woman in my life&heart.

Hayatımda ki & Kalbimde ki en güzel kadına, ***Hanifeme***.

To my family,

Aileme,

This thesis would not have been possible without the support and advice of many of my colleagues and friends, and I want to thank them. A scientific work is never the result of individual efforts but always the result of teamwork.

I thank my supervisors **Dr. Antonio J. Salinas Sánchez** and **Dr. Blanca González Ortiz** for all their support and patience during all of my study years. Thank you for believing in me.

I thank **Prof. Dr. María Vallet-Regí**, head of the Research Group in Intelligent Biomaterials (GIBI), for the opportunity of doing this project and for all her support and ideas. Her work has been an inspiration for me. Also, I thank **Dr. Juan Carlos Doadrio**, head of the Department, for let me conclude this thesis in the department.

I thank **Prof. Dr. Matthias Epple** for accepting me in his group in my three months stay at Institute of Inorganic Chemistry of the University of Duisburg–Essen, Germany. I also thank all my new friends at Institute of Inorganic Chemistry.

I also thank all my friends and colleagues at Department of Inorganic and Bioinorganic Chemistry of the Universidad Complutense de Madrid. You are great and make my life richer and funnier than ever. **Montse**, your help is also unforgettable! Thanks for all those funny conversations. You are always a hard worker. **Dani, María Teresa, África, Antonio Luis** and **Isabel,** thank you for your time and help, and for sharing your energy. Ha *acido* un placer conoceros y gracias por ser tan amables. **Jesus, Juan Peña** and **Vicky** thank you for your time and for making me laugh every time. **Alejandro Baeza**, call me back if you ever go to Turkey again, if I'm not available, my expensive guide book will help you in Istanbul better than me. It's unique and you know it. **Miguel** eres muy español tío, you are awesome and a very friendly person. And your son, Rodriguito, es más guapo que tú. Dear **Merche**, may be you don't remember it but your help was unforgettable when we met at the commercial centre of Mar Negro region, Thank you! **Ana Fontecha**, I've never known anyone as optimistic and positive as you! Your help is unforgettable. Thank you very much! **Sandra**, enhorabuena por tu boda, wishing you the best in your new life. **Edu Ruiz**, thank you for your time and sharing your ideas! Thank you **Jose, Pilar** and **Ana Martín** for your support and help all time. **Marina**, there are no words to explain what a person you are. Thank you for being in my life and my life wouldn't be the same without you. You are lucky because you have a great family in Murcia! You and your family are unforgettable! **Mónica, Rafael, Nati, Paris, Rocío, Sandra Moltalvo** and **Gonzalo** I couldn't possibly have funnier friends than all of you. I was very happy with you guys, thank you all. **Edu G** and **Ángel**, thank you for hosting me in your house and making a ninja of me. It was very funny to be a part of your family, Thank you! **Chico**, you know that nunca me caes bien tío. Pero tuve muchos momentos increíbles contigo. Eres grande, muy grande colega, un abrazote muy fuerte. **Dr. Fernando Conde**, evet evet, eres muy grande, educado, abierto y muy internacional. I had a great time with you here, and in Turkey when we drank "Çay" and "Ayran".

Acknowledgements in Turkish for my family and Turkish friends:

Sekiz yıl önce İspanya'ya ilk adımlarımı attığımda, yeni doğmuş bebek gibiydim herşeyden habersiz, dilsiz, tecrübesiz, ailesiz ve eğitimsiz. Uçağa binerken nasılsa geri dönerim düşüncesiyle dokuz yıl geçirdiğim İspanya'da, hayatımın ikinci dönemini adlandırdığım bu bambaşka bölümde, bu emekleyen çocuğu büyüttüm ve eğittim… Zorlukları öğrendi, zoru başarmayı, imkansızı basitleştirdi, çok çalışmanın zeki olmaktan daha akıllıca bir hamle olduğunu keşfetti, her insanın fikrini dinlemeyi öğrendi, zoluklara göğüs görmeyi, sorumluluklarını…Geliştikçe yeni yerler keşfetti, keşfettikçe yeni insanlar tanıdı, tanıdıkça yeni hayatlar öğrendi, öğrendikçe insanlara güvenmeyide. Nasıl yaşarsa öyle insanlarla karşılasacağını öğrendi… Hayatta herseyin zor olduğunu ama pes etmemek kaydıyla her şeyın imkansız olmadığını, Ve herkesin değil, kendi yaptıklarının daha doğru olduğunu keşfetti…

Hiçbir başarı tesadüf değildir ve her başarı mutlaka görünmeyen bir ekibin eseridir…

Yürüdüğüm bu yolda bana destek olan, güvenen ve asla unutamayacağım insanları saymaya kalksam sayfalar yetmez… Saygı değer Hocam Yrd.Doç.Dr. M. Galip İçduygu, laboratuvarda bi şeker karıştırmanın kimyasal bir deney olduğunu bilmeden çıktığım bu yolda, destek olduğunuz, ve hayatımın en değerli anlarında İspanya macerasında bana cesaret verdiğiniz, önderlik ettiğiniz ve en önemlisi güvendiğiniz için sonsuz teşekkür ederim…

En başta Aileme teşekkürler, Annem babama, Onur abim, Emine Yengeme ve şirin kızları Şevval-Ecrine, İsa kardeşim ve Ailesine, bana her daim destek oldunuz, Ailemden uzaklaştıkça geri dönülmez bir yola çıktığımı anladım… Kardeşim Abdullah, abisinin en değerlisi, abisini tanıyamasada onu hiç yalnız bırakmadı... Manevi ailem; Ahmet Yılmaz abim, Hatun yenge ve kızları…

Mersinlioğlu ailesi; çınar ağacımız Hayati, Baştacımız Yadigar, abimiz Hakan, mühendisimiz Gökhan, kardeşlerim Yahya, Meryem, Esra, kalecimiz Osman ve aileleri... Bana kendi ailem gibi destek çıktığınız, inandığınız ve güvendiğiniz için teşekkürler… Siz olmasaydınız bu öyküm yarıda kalırdı, eminim…

Sak Ailesi; Havva yengem, Mehmet abim, Kick bokscumuz Rıdvan ve Eşi Hanife, Furkan ve Sena, kardeşim Engin ve ailesine, Hollanda'dan Hasan abim ve ailesine, Ayhan amcama ve beni hayata hazırlayarak hep güvenen Miyase yengeme, Mevlüt ve Zehra'ya ; Ne kadar teşekkür etsem azdır. Beni sürekli kardeşiniz olarak gördüğünüz ve sürekli güleryüzlü davrandığınız için çok teşekkür ederim… Ömrümde tanıdığım tek ve en değerli Halama (unutulmaz böreklerine), Eniştem Ferhat abime (ve 20 lirasına), pırlanta gibi çocukları Fatih'e, Miyase ve şeyma'ya… Her daim güler yüzünüzü eksik etmediniz…

Yılmaz Ailesine; Bayram dayım, Nurgül yengem, Bünyamin-Ensar ve Fezyullah kardeşlerim… Diğer büyük ailem… Her zaman destekçim oldunuz, kapınızı açık tuttunuz, ekmeğinizi paylaştınız… Ne kadar teşekkür etsem azdır. Bu zorlu yolda hep yanımda oldunuz ve güvendiniz… Teşekkür demek az kalır ama manevi anlamı büyüktür anlayana… Sebahittin hocam, Genç Nuran yengemiz ve değerli kızları… Gülüşünüze neşenize benide ortak ettiniz, teşekkürler…

DJ Gökhan Tüysüz, gülüşünü esirgemedin, kardeşten öteydin, Nutellalı ekmeğini bölüştün ve en önemlisi İspanya'da evime misafirim oldun. Her zaman kardeşten öte sıcak samimi içten doğallığın ve desteklerin için teşekkür ederim..

Ailem ne kadarda büyükmüş… Bir çınar gibi sağlam, güçlü ve büyük…!

Tübitak'ın saygı değer Yüksek mühendis ve Doktor araştırmacıları Yasemin, Ayşegül, Meral ve Ayşen… Her daim misafirliğinizden çok mutlu oldum, sizi tanımak çok güzeldi. Yasemin, çekinerek kapınızdan girdiğim gün ailenin inanılmaz saygın misafirperverliği ve bana içten samimi davranışları beni mahçup etti, asla unutmıycam! Mühendis Hanım Eda Elmas arkadaşım… Elmas gibi bir kalbe sahip dost ve arkadaşım. İçten samimi davranışların ve ögrencilik sıralarından beri devam eden dostluğumuz hiç solmasın... Senin gibi daha nice iyi dostlarıma, Betül Güneş Mercan, Sinem Mercan Kalaycı, dostum Ahmet Gökhan Taşpınar, taze anne Gündem, Ünlü fizikçim Adem Öztürk, Milli sporcumuz Aynur Samat, Murat bostan ve dahası…

Daha isimlerini sayamayacağım ve anlıkta olsa hayatıma giren herkes; Malaga'dan Meltem, İstanbul'dan Kemal Dalyan, Madrit'ten Ankara'ya uzanan Ramazan çınar, Zaragoza'dan Ankara'ya uzanan kısa hikâyede Burçin ve Gökhan Güzel ailesi, Portekiz'deki esrarengiz rehberime, İtalya Venedik'te ki beni misafir eden arkadaşlara ve saçları limonlu İtalyan otobüs şoförüne, Slovenya'da ki esrarengiz tren istasyonuna, eski erasmus arkadaşlarıma ve Slovenya'da kaybettiğim fotoğraf makineme, Fransa'da ki Eyfel kulesine, Estonya'da ki arkadaşıma, Brüksel'de ki dostlara, Hollanda'nın esrar-engiz kokusuna, Almanya'daki arkadaşlara, Essen'de ki soğuk alman polislerine ve laboratuvardaki çalışma arkadaşlarıma, İsveç Stockholm ve İsviçre Zürih'de ki tanımadığım içten sıcak insanlara ve unutulmaz doğasına, küçücük şirin ülke olan Andorra Prensliği'nin dağlarına, Bilbao'daki gezgin dostum Deniz Derin ve annesine, Huelva'da hiç tanımadığım ve beni evinde misafir eden dostlarıma, Barcelona-San sebastian-Sevilya ve Salamanca sokaklarına, Mayorca adasındaki yoldaşım dostum Sinan'a, Avusturya Viyana'nın türklerine, uykusuz gecelerime, herkese selam olsun… Hayatıma bir anlıkta olsa neşe kattınız…

Ve İspanya… Endülis Huelva'da sıradan bir erasmusla başlayıp, Madrid Başkentte çınar gibi büyüyen bir profille, Araştırmacı-mühendis-doktor ve tercümanlık iş tercübelerini elde ettiğim dokuz yıl boyunca her yerini gezdiğim, tabiri caizse, ikinci evim, vatanım yurdum dediğim ve acısıyla tatlısıyla gençliğimin en güzel ve unutulmaz yıllarını yaşadığım bu sıcacık ülkem… Bana kattıkların, verdiğin hayat deneyimi, iş tecrübesi ve eşsiz eğitim için ne kadar teşekkür etsem azdır…

Ve…hayatımın geriye kalanını emanet ettiğim en değerlime, Eşime, ve bana güvenip destek olan Atmaca ailesinin reisi Günaydın babam, patronu Emine annem ve pırlanta gibi kardeşlerim Ümit-Derya-Uğur-Yağmur'a sevgilerimle…

Hayatımda bana engel olanlara, kötü davrananlara veya beni görmezden gelenlere… Sizede teşekkürler, bilmeden beni doğru yola yönlendirdiğiniz için…

Hayatımda, bir dönemi kapatıp, yeni döneme Doktor olarak girdiğim bugünüme sayenizde ulaşabildim… Hiçbir başarı tesadüf değildir, aksine bedeli ödenmiştir…

Sevgiler

Okan

Okan Mersinlioğlu is grateful to the Ministry of Science and Innovation of Spain (MICINN) for the financial support through a predoctoral fellowship, FPI BES-2009-027503.

I thank the following for funding this work: the Ministry of Science and Innovation of Spain (MICINN) through project MAT2008–00736, the Ministry of Economy and Competitiveness of Spain (MINECO) through project MAT2012–35556 and Community of Madrid (CAM) through Consortium BITI, ref S2009/MAT–1472. This work was also supported by the Networking Research Center on Bioengineering, Biomaterials and Nanomedicine (CIBER-BBN), Spain.

I also thank Dr. Mª Luisa Ruiz González (Department of Inorganic Chemistry, UCM) for the acquisition of TEM images of samples prepared by precipitation of CaP during the synthesis of mesoporous silica nanospheres (MSNSs), Dr. Fernando Conde (X–ray Diffraction CAI, UCM), Isabel Salido Herranz (Library of Faculty of Pharmacy, UCM), Dr. Francisco Javier García García (National Center of Electron Microscopy, UCM) and Dr. Adrián Gómez Herrero (National Center of Electron Microscopy, UCM) for their kind technical support.

- POSTER – *Precipitation of Calcium phosphates in the presence of Ionic Surfactants*
  Blanca González, Antonio J. Salinas, **Okan Mersinlioğlu**, María Vallet-Regí
  23rd European Conference on Biomaterials, 11–15 September, 2010, Tampere, Finland.

- RAPID-FIRE PRESENTATION AND POSTER – *Nanostructured Calcium Phosphates from Phospholipids Templates*
  Okan Mersinlioğlu, Antonio J. Salinas, Blanca González, María Vallet-Regí
  24th European Conference on Biomaterials, 4–8 September, 2011, Dublin, Ireland.

- ORAL PRESENTATION – *Apatite coatings on MCM–41 nanospheres*
  Okan Mersinlioğlu, Blanca González, Antonio J. Salinas, María Vallet-Regí
  EUROMAT2013– European Congress and Exhibit on Advanced Materials and Processes, 8–13 September 2013, Sevilla, Spain.

Manuscripts in preparation:

- Lamellar discontinuous mesostructured hydroxyapatite in the presence of sodium dodecyl benzene sulfonate (Chapter II)
- Mesostructured calcium phosphates in the presence of phospholipids (Chapter III)
- Mesoporous silica nanospheres coated by apatite nanoparticles (Chapter IV)

Abbreviation	Full Name
° / °C	Degree, Degree celsius (centigrade)
ζ	Zeta Potential
U	Electrophoretic mobility
H	Viscosity of water
e	Dielectric constant of water
λ	Wavelength
θ	Theta
[ ]	Concentration
α–TCP	α–tricalciumphosphate
β–TCP	β–tricalciumphosphate
β–CPP	β–Calcium pyrophosphate
a_o	Unit cell parameter
Å	Angstrom
ACP	Amorphous calcium phosphate
ATR	Attenuated total reflectance
BET	Brunauer–Emmett–Teller
BJH	Barrett–Joyner–Halenda
C_o	Spontaneous curvature
CaP	Calcium phosphate
CDHA	Calcium–deficient hydroxyapatite
CMC	Critical micelle concentration
CTAB	Cetyltrimethylammonium bromide
d	Days
d_{hkl}	Interplanar distance
DCPA	Dicalcium phosphate anhydrous, mineral monetite
DCPD	Dicalcium phosphate dihydrate, DCPD, mineral brushite
DEPETES	Diethylphosphatethyltriethoxy silane
DLS	Dynamic light scattering
DNA	Deoxyribonucleic acid
Dp	Pore diameter
ED	Electron diffraction
EDS	Energy dispersive X–ray spectroscopy
EPG / EPG®BB	Empigen®BB detergent
EtOH	Ethanol
FA	Fluorapatite
FHA	Fluorescent hydroxyapatite
FTIR	Fourier transform infrared spectroscopy
H	Hour
HA	Hydroxyapatite
HLB	Hydrophilic lipophilic balance
HMM	Hybrid mesoporous material
HRTEM	High resolution transmission electron microscopy
ICDD	International centre for diffraction data
IUPAC	International union of pure and applied chemistry
LDHASi	Lanthanide-doped HA/silica composite
MAP	Monoalkyl phosphate

List of abbreviations

MBGs	Mesoporous bioactive glasses
MCM	Mobil composition of matter: class of mesoporous silica materials
MCM–41	Mobil composition of matter No. 41
MCM–48	Mobil composition of matter No. 48
MCM–50	Mobil composition of matter No. 50
MCPA	Monocalcium phosphate anhydrous
MCPM	Monocalcium phosphate monohydrate
MSNSs	Mesoporous silica nanospheres
NPs	Nanoparticles
OCP	Octacalcium phosphate
P/P_o	Relative pressure
PC	Phosphatidylcholine
PC33	Asolectin from soybean, about 33 % of PC
PC60	L-α-Lecithin from egg yolk, about 60 % of PC
PC94	Lipoid-S100 from soybean, about 94 % of PC
PEI	Poly(ethyleneimine)
PLs	Phospholipids
S_{BET}	BET surface area
SBA–15	Santa Barbara amorphous type material–15
SBF	Simulated body fluid
SDS	Sodium dodecyl sulfate
SDBS	Sodium dodecyl benzene sulfonate
SEM	Scanning electron microscopy
SA–XRD	Small angle X–ray diffraction
t	Time
T	Temperature
TEM	Transmission electron microscopy
TEOS	Tetraethyl orthosilicate
TEP	Triethyl phosphate
TG/DTA	Thermogravimetric / differential thermal analysis
TIP	Triethyl phosphite
THSMP	Trihydroxysilylpropyl methylphosphonate
TTCP	Tetracalcium phosphate
UV	Ultra violet
WA–XRD	Wide angle X–ray diffraction

Sample Code	Full name
NHCaP	Nanostructured hybrid calcium phosphates
NHHA	Nanostructured hybrid hydroxyapatite
MHCaP	Multistructured hybrid calcium phosphate
HMM	Hybrid mesostructured material
LCaP	Lamellar structured calcium phosphate
CaPX / PCaX	Nano–structured calcium phosphate
PC33	Hybrid material synthesized in the presence of Asolectin from soybean
PC60	Hybrid material synthesized in the presence of L-α-Lecithin from egg yolk
PC94–1 & PC94–2	Hybrid materials synthesized in the presence of lipoid-S100 from soybean
MSNSs	Mesoporous silica nanospheres
MSNS-HA-X	Mesoporous silica nanospheres coated with HA
NSFD	MSNSs functionalized with DEPETES
NSFT	MSNSs functionalized with THSMP
NSFD-HA	MSNSs functionalized with DEPETES and then coated with HA
NSFT-HA	MSNSs functionalized with THSMP and then coated with HA
LDHASix	Lanthanide-doped HA/silica composite

SUMMARY

Synthesis of Calcium Phosphates in the Presence of Ionic Surfactants, Phospholipids and Mesoporous Silica Nanoparticles to Control the Bioceramic Mesostructure

Introduction

Currently, there is a great interest in the development of new biomaterials because of their foreseeable enormous contribution for the demands of an aging society that needs alternatives in the treatment of hard tissues diseases or cancer. First biomaterials developed were as bioinert as possible. Then, in the years 70´s and 80´s of the past Century, bioactive and biodegradable biomaterials, including calcium phosphates and bioactive glasses, started to be investigated. At present, the interest is focused towards the synthesis of biomaterials with controlled mesostructure and functionalized surface to improve and tailor at demand their behaviour into the body. Moreover, for bone tissue engineering applications, biomaterials are processed as 3D scaffolds able to be decorated with biochemical signals and cells. Nevertheless, for cancer therapy some recent strategies are based on mesoporous nanoparticles able to transport drugs or genes when injected in the blood stream, without being recognised and withdrawn by macrophages.

Calcium phosphates (CaPs) exhibit chemical and structural similarities to the mineral component of hard tissues (biological apatite). Thus, they are biocompatible and bioactive and were widely investigated as bioceramics for over 40 years, mainly for applications in Orthopedics or Dentistry. In that time the research effort was focused in aspects such as the phase obtained, the microstructure, the particle size or the calcium deficiency. Very recently, it was proposed that a control of the mesostructure during the synthesis of CaPs would improve its current performance as well as allow adjusting their properties for the requirements of new clinical applications.

On the other hand, in 2001 ordered mesoporous silicas were proposed as matrices in drug delivery systems. More recently, these mesoporous systems synthesized as nanoparticles have gained much attention for applications in nanomedicine, such as cell targeted drug/gene delivery nanosystems or nanosystems incorporating moieties for diagnosis. Mesoporous silica nanospheres (MSNSs), with a diameter ranging 50-300 nm and mesopores of approximately 2-3 nm, use to be ordered in the 2D hexagonal arrangement of MCM-41 material. Moreover, they possess high pore volume and surface area rich in silanol groups (Si–OH) that can be functionalized with a great variety of organic moieties.

The high number of mesoporous silica families makes one wonders if it would be possible to synthesise an analogous family of mesoporous materials based in CaPs. Hereafter, the first approaches can be to use analogous strategies to those used in the syntheses of mesoporous silicas. Thus is, to employ organic amphiphilic molecules which could act as a template of the CaPs mesostructure via supramolecular assemblies. Up to now, the efforts made in this line had little success because the chemistry of essentially ionic compounds, such as CaPs, is far from the chemistry of essentially network covalent compounds, such as silica. Consequently, the interactions between the surfactants and calcium and phosphate ions in solution are quite different than with silicate species. However, the synthesis of new CaP-based mesostructured materials could allow new clinical applications or improve current performance. Moreover, the new knowledge acquired in this effort could also bring new bioceramics and organic-inorganic hybrids based in CaP.

Objectives

The first main objective of this thesis has been to investigate the synthesis of CaPs in the presence of different types of ionic surfactants, pure and mixtures, and in the presence of different concentrations of phosphatidylcholine, trying to obtain mesostructured CaPs (Chapters II and II). The second essential objective has been to investigate the synthesis of CaPs in the presence of mesoporous silica nanospheres to obtain *core@shell* systems of the type mesoporous silica@hydroxyapatite (Chapters IV and V). This multiple approach was attempted to show if it is possible to obtain CaPs with controlled mesostructure.

Chapter I contains the Introduction of this thesis. Therefore, it describes the background and current status of the subject matters.

Chapter II addresses the synthesis and characterization of CaPs in the presence of various ionic surfactants, pure and mixture of them, aimed to behave as structure directing agents. The investigated surfactants were: sodium dodecyl sulphate (SDS), sodium dodecyl benzene sulphonate (SDBS), cetyltrimethyl ammonium bromide (CTAB) and mono-n-dodecyl phosphate (MAP). Moreover, EMPIGEN®BB detergent (EPG), a zwitterionic surfactant, was tested as mesostructure template for the first time as an alternative approach. Surfactants in water can be organized in different mesostructures such as micellar, lamellar, hexagonal or cubic. Synthesis conditions and surfactants have been optimized looking for interactions with the precipitated CaP, *i.e.*, to obtain materials with mesostructural characteristics different to materials prepared in the absence of surfactant.

In ***Chapter III*** we aimed at synthesizing HA based hybrids with a sponge-like mesostructure via precipitation of CaP in the presence of three phospholipid (PL) sources with substantially different contents of phosphatidylcholine (PC): asolectin 33%, lecithin 60% and lipoid 94% of PC. The different structures of the nanohybrids as a function of the synthesis conditions, pH of solution (basic or neutral) and Ca/P molar ratio (1.0 or 1.67) and concentration of PC, were investigated. In this case, given the biocompatibility of PLs, it arises the synthesis of CaP-PLs hybrids, *i.e.*, PLs were not removed from the final material. The new CaP-PLs hybrid materials were characterized and the mechanisms of formation for the nanostructured materials were proposed.

Given the difficulty found in the previous chapters to obtain CaP systems as ordered mesoporous materials, in ***Chapter IV*** various strategies were investigated to obtain CaP coatings, namely HA, on mesoporous silica nanospheres (MSNSs) with MCM-41 structure. In this case our approach implies the use of a well-defined mesoporous material as the basis of the final nanosystem. The purpose of this study was to design multifunctional *core@shell* nanoparticles that can be applied in bone regeneration, as well as specific intracellular carriers of drugs, proteins or agents for image, which could be used for applications such as the treatment of cancer. The nanospheres coated by CaP would exhibit well interconnected pore structures and excellent *in vitro* bioactivity that made them useful for several biomedical applications. For instance, an HA coating could act as a nanogate allowing the controlled release of the biomolecules enclosed in the silica mesopores under specific conditions, for instance a pH decrease. The attempted approaches to obtain MSNSs coated by CaPs were: *(i)* co-synthesis of CaP and MSNSs, *(ii)* soaking and *(iii)* wetting MSNSs in a sol precursor of CaP,

and *(iv)* functionalization of MSNSs with organic moieties containing phosphate-like groups to facilitate the CaP coating after wetting them into a sol precursor of CaP. Except in the first approach, in which both processes are simultaneous, the synthesis of materials is performed in two steps: *(1)* the synthesis of MSNSs ranging 150-250 nm of diameter and around 2 nm of pore diameter and *(2)* the step to coat MSNSs with CaP.

An improvement of these systems is dealt with in ***Chapter V***, where the subject investigated is the coating of MSNSs with HA doped with europium as fluorescent element via the precipitation of fluorescent CaP on previously synthetized MSNSs, which would give greater visibility and traceability of the nanosystem during the biological application, such as cell trafficking or tumour localization.

Chapter VI summarizes the principal conclusions derived from this thesis. Finally, the general conditions and detailed experimental work, as well as structural characterization and analysis techniques employed, are included in ***Chapter VII*** of this report.

Results and Conclusions

Chapter II. Precipitation of Mesostructured Calcium Phosphates in the Presence of Ionic Surfactants

- Ionic surfactants, namely anionic, containing S or P atoms in their polar head, such as SDS, SDBS and MAP, can be used to obtain mesostructured organic-inorganic hybrids based in CaPs.

- The interaction of amphiphilic molecules of surfactant with calcium and phosphate ions, during the CaP precipitation from aqueous solutions, yield hybrid materials exhibiting lamellar or discontinuous lamellar mesostructures, but no mesoporous order.

- In the synthesis conditions, *i.e.*, Ca/P molar ratio 1 and 1.67, surfactant concentration from 15 to 90 mM and 240 mM and pH not buffered, the CaP most common phases present in the lamellar hybrids were brushite, hydroxyapatite or monetite.

- SDS is a suitable surfactant to obtain highly mesostructured lamellar CaP hybrids.

- Relatively high SDBS concentrations and Ca/P molar ratio of 1 yield discontinuous lamellar or curved lamellar mesostructures, forming meshes, of poorly crystallized HA. The formation of HA at this low Ca/P molar ratio is attributed to the pH increase (7 to 9) of medium due to the protonation of the sulphate polar heads of SDBS.

- The mixture of an anionic surfactant, such as SDS, SDBS or MAP, with the cationic cetyltrimethyl ammonium bromide (CTAB) produces hybrids with mesostructure analogous to that obtained with the pure anionic surfactants, suggesting a non-effective interaction of CTAB with calcium and phosphate ions.

- TEM analysis of materials obtained using a surfactant mixture shows two types of particles: *(i)* rod-like particles exhibiting lamellar mesostructure and (ii) sheet-like particles unstable under the electron beam. The bubbles formed when these sheet-like particles were investigated, attributed to the organic matter combustion and to the removal of crystallization water

molecules in brushite, avoid the identification of the possible mesostructure in the sheet-like particles.

- The use of energetic synthesis procedures, such as ageing in an autoclave or refluxing after the CaP precipitation, leads to monetite, a CaP phase derived from brushite after remove the two water molecules of crystallization.

- The use of EPG, a zwitterionic surfactant containing one carboxybetaine group, as mesostructure template for CaP fails and no interactions with calcium and phosphate ions are detected. For the future, the investigation of another zwitterionic surfactant containing a sulfobetaine groups is suggested.

Chapter III. Precipitation of Mesostructured Calcium Phosphates in the Presence of Phospholipids

- The precipitation of CaPs in phospholipids (PLs) suspensions containing different concentrations of phosphatidylcholine (PC) yields to the synthesis of CaP-PLs hybrid materials.

- The inorganic components of the hybrids are poorly crystallized HA, when pH is basic and Ca/P molar ratio 1.67, and brushite at pH neutral and Ca/P = 1.

- The organic matter content is similar in both hybrid types, around 20% in brushite-containing hybrids and around 17% in HA-containing ones. CaP-PLs hybrid materials subjected to a thermal process to remove the organic matter evolve to non-porous HA. Since no mesoporous materials were obtained after calcination, this Chapter has been focused in the characterization of the CaP-PLs hybrid materials.

- TEM analysis of hybrids revealed four types of nanostructures: *(i) lamellar bilayer* with 4.2 nm in thickness of layer (apatite, asolectin), *(ii) bilayer vesicles* around 35 nm in diameter of vesicles and 4.7 nm in thickness of bilayer (brushite, lecithin), *(iii) micelles* of about 4.3 nm in diameter (brushite, lipoid) and *(iv) bilayer sponge–like* or *worm–like tubular* mesostructures with 4.3 nm in thickness of disordered bilayer sponge–like structure (apatite, lipoid).

- Since both components of CaP-PLs hybrid materials are biocompatible they can be investigated as drug delivery platforms via the encapsulation of a drug within the phospholipid structure of the hybrid.

Chapter IV. Hydroxyapatite Coatings on Mesoporous Silica Nanospheres

In this chapter, MCM–41 mesoporous silica nanospheres (MSNSs) were tried to be coated with HA nanoparticles or with a HA layer, to expand the clinical applications of both materials. According to this goal, the conclusions derived from each synthetic route attempted are:

- *Co-synthesis of CaP and MSNSs.* The CaP precipitation simultaneous to the sol-gel synthesis of MSNSs yield a mixture of independent particles of poorly crystallized HA rods and polydisperse MSNSs (S_{BET} 594 m^2/g).

- *Soaking of MSNSs into a sol precursor of CaP.* First, pure SiO_2 MSNSs (S_{BET} = 1230 m^2/g) were synthesized. After soaking them in the sol precursor of CaP for 3 hours, the nanospheres (S_{BET} = 250 m^2/g) convert in ellipsoids with the elements Si, Ca, P and O in their composition. The ellipsoids exhibit a radial mesopore channels arrangement close to the particles surface. Moreover, the obtained material exhibits a moderate *in vitro* bioactive response in simulated body fluid.

- *Wetting of MSNSs by a sol precursor of CaP.* In this approach, pure SiO_2 MSNSs (S_{BET} = 1230 m^2/g) were synthesized first, then soaked for 30 minutes in the sol precursor of CaP and subsequently subjected to a washing process mimicking a dip-coating procedure with the sol. TEM images after wetting confirm the successful formation of HA NPs covering the MSNSs surface. In this case, the S_{BET} of the coated material suffer a drastic decrease of ≈90 % compared to the initial MSNSs. Unlike the previous method, in this approach MSNSs are not altered in shape neither in composition.

- *Functionalization of MSNSs with phosphate-like groups and subsequent wetting with a sol precursor of CaP.* MSNSs were functionalized with diethylphosphatoethyl triethoxysilane (DEPETES) or 3-trihydroxysilylpropylmethylphosphonate (THSMP) to facilitate the subsequent interaction of their phosphate-like groups with calcium ions and then phosphate ions in the sol.

    - DEPETES-functionalized MSNSs exhibiting MCM-41 hexagonal arrangement and high S_{BET} (878 to 1190 m^2/g) were synthesized by co-condensation or post-synthesis. After functionalization, P-containing MSNSs were wetted with a sol precursor of CaP. A homogeneous distribution of a HA layer around the MSNSs and some HA NPs are observed by TEM. S_{BET} of 335 m^2/g indicates a partial coating of the MSNSs surface.

    - MSNSs were functionalized with THSMP by a co-condensation method. The obtained material exhibits a high S_{BET} of 1316 m^2/g. THSMP-functionalized MSNSs were wetted with a sol precursor of CaP. TEM analysis showed that a *core@shell* structure MSNS@HA was obtained. Coated MSNSs are non-porous showing a decrease in S_{BET} of around 97% regarding the initial MSNSs.

Chapter V. Coating of Mesoporous Silica Nanospheres with Fluorescent Hydroxyapatite Nanoparticles

- The precipitation of Eu^{3+} doped HA (fluorescent HA, FHA) in the presence of MCM-41 type MSNSs yields to the synthesis of FHA/MSNSs composites.

- Some FHA/MSNSs composites exhibit the red luminescence of lanthanides under UV light. The luminous intensity is dependent on the amount of Eu^{3+} ion in the composite.

- A *core@shell* structure (MSNS@HA) is observed by TEM for one of the samples investigated. However, this sample does not show a fluorescent emission due to its low Eu^{3+} content.

RESUMEN

Síntesis de Fosfatos de Calcio en Presencia de Surfactantes Iónicos, Fosfolípidos y Nanopartículas de Sílice Mesoporosa para Controlar la Mesoestructura de la Biocerámica

Introducción

Actualmente, hay un gran interés en el desarrollo de nuevos biomateriales debido a su enorme contribución a las demandas de una sociedad cada vez más envejecida que necesita alternativas para el tratamiento del cáncer o las enfermedades de los tejidos duros. Los primeros biomateriales se desarrollaron para que fuesen lo más bioinertes posible. A partir de los años 70´s y 80´s del siglo XX, comenzaron a investigarse biomateriales bioactivos o biodegradables, incluyendo algunos fosfatos de calcio y los vidrios bioactivos. En la actualidad, el interés se enfoca hacia la síntesis de biomateriales con mesoestructura controlada y funcionalizados para mejorar y adaptar su comportamiento en el cuerpo. Por otra parte, para aplicaciones de ingeniería de tejido óseo, los biomateriales se procesan como andamios 3D capaces de ser funcionalizados con señales bioquímicas y células. Asimismo, algunas estrategias recientes para la terapia del cáncer se basan en nanopartículas mesoporosas que son capaces de transportar drogas o material genético cuando se inyectan en el torrente sanguíneo, sin ser retiradas de la circulación por los macrófagos.

Los fosfatos de calcio (CaPs) exhiben muchas semejanzas químicas y estructurales con el componente mineral de los tejidos duros (la apatita biológica). Por ello, son biocompatibles y bioactivos y han sido ampliamente investigados como biocerámicas durante más de 40 años, principalmente para aplicaciones en Ortopedia u Odontología. A lo largo de ese tiempo el esfuerzo investigador se ha centrado en aspectos como la fase de fosfato de calcio, su microestructura, el tamaño de partícula o la deficiencia en calcio. Más recientemente, se ha propuesto que un control de la mesoestructura durante la síntesis de los CaPs permitiría mejorar sus prestaciones actuales así como ajustar sus propiedades a las necesidades de nuevas aplicaciones clínicas.

Por otra parte, en 2001 se propuso la utilización los materiales de sílice mesoporosa ordenada como matrices en sistemas de liberación controlada de fármacos. Estos sistemas mesoporosos sintetizados en forma de nanopartículas están recibiendo recientemente mucha atención para aplicaciones en nanomedicina, tales como nanosistemas dirigidos a células para el suministro de fármacos o material genético y también en nanosistemas que incorporen componentes de diagnóstico. Las nanoesferas de sílice mesoporosa (MSNSs), con un diámetro entre 50-300 nm y mesoporos de unos 2-3 nm, ordenados en una simetría hexagonal 2D típica del material MCM-41. Además, poseen elevado volumen de poros y una alta superficie específica que es rica en grupos silanol (Si-OH) que pueden ser funcionalizados con una gran variedad de moléculas orgánicas.

El elevado número de familias de sílice mesoporosa existentes lleva a preguntarse si sería posible sintetizar una familia análoga de materiales mesoporosos basados en CaPs. En este sentido, los primeros intentos podrían basarse en estrategias análogas a las utilizadas en la síntesis de sílices mesoporosas, es decir, emplear moléculas orgánicas anfifílicas para que actúen como plantilla de la mesoestructura de los CaPs mediante ensamblaje supramolecular. Hasta ahora, los esfuerzos realizados en esta línea han tenido poco éxito debido fundamentalmente a que la química de compuestos esencialmente iónicos, tales como los CaPs, difiere mucho de la química de compuestos esencialmente covalentes en red, como la sílice. En consecuencia, las interacciones entre los surfactantes y los iones calcio y fosfato en disolución son bastante diferentes que con las especies silicato. Sin embargo, la síntesis de nuevos materiales mesoestructurados basados en CaPs podría

permitir nuevas aplicaciones clínicas o mejorar las actuales. Por otra parte, los nuevos conocimientos adquiridos en este esfuerzo también podrían llevar a la obtención de nuevas biocerámicas e híbridos orgánico-inorgánicos basados en CaPs.

Objetivos

El primer objetivo de esta tesis ha sido investigar la síntesis de CaPs en presencia de diferentes tipos de surfactantes iónicos, puros y mezclas, así como de diferentes concentraciones de fosfatidilcolina, intentando obtener CaPs mesoestructurados (Capítulos II y II). El segundo objetivo fundamental ha sido investigar la síntesis de CaPs en presencia de nanoesferas de sílice mesoporosa para obtener sistemas núcleo@corteza del tipo MSNSs@HA (Capítulos IV y V). Con este enfoque múltiple se ha intentado demostrar si es posible conseguir CaPs con mesoestructura controlada.

El ***Capítulo I*** contiene la introducción de esta tesis. Por lo tanto, describe los antecedentes y el estado actual de las materias de estudio.

El ***Capítulo II*** aborda la síntesis y caracterización de los CaPs en presencia de varios surfactantes iónicos, puros y una mezcla de ellos, destinados a comportarse como agentes directores de estructura. Los surfactantes investigados han sido: dodecil sulfato de sodio (SDS), dodecil benceno sulfonato de sodio (SDBS), bromuro de cetiltrimetil amonio (CTAB) y mono-*n*-dodecil fosfato (MAP). Por otra parte, un surfactante zwitteriónico, EMPIGEN ® BB (EPG), ha sido probado por primera vez, en un enfoque alternativo, como plantilla de la mesoestructura. Los surfactantes en agua se organizan en diferentes mesostructuras formando micelas, lamelas, o fases de simetría hexagonal o cúbica. Se han optimizado el tipo de surfactante y las condiciones de síntesis buscando interacciones con el CaP que se obtiene por precipitación, es decir, para obtener materiales con características mesostructurales diferentes a los sintetizados en ausencia de surfactante.

En el ***Capítulo III*** se han intentado sintetizar híbridos basados en HA con una mesoestructura tipo esponja mediante la precipitación de CaPs en presencia de tres fuentes de fosfolípidos (PL) con distinto contenido en fosfatidilcolina (PC): *Asolectin* 33%, *Lecitina* 60% y *Lipoid* 94%. Se han investigado las diferentes estructuras obtenidas para los nanohíbridos en función de: las condiciones de síntesis, el pH de la disolución (básico o neutro), la relación molar Ca/P (1.0 o 1.67) y la concentración de PC. En este caso, dada la biocompatibilidad de los PLs, se presenta la síntesis de híbridos CaP-PLs, es decir, sin eliminar los fosfolípidos del material. Se han caracterizado los nuevos híbridos CaP-PLs y se han propuesto los mecanismos de formación de las nanoestructuras formadas.

Dada la dificultad encontrada en los capítulos anteriores para obtener materiales de CaPs como sistemas mesoporosos ordenados, en el ***Capítulo IV*** se investigan diversas estrategias para obtener recubrimientos de CaP, principalmente HA, en nanoesferas de sílice mesoporosa (MSNSs) con estructura tipo MCM-41. En este caso nuestro enfoque implica el uso de un material mesoporoso bien definido que actúe como base de los nanosistemas finales. El propósito de este estudio ha sido diseñar nanopartículas núcleo@corteza multifuncionales que puedan ser aplicadas en la regeneración ósea, así como nanosistemas portadores de drogas, proteínas o agentes de imagen a nivel intracelular que podrían ser utilizados para aplicaciones como el tratamiento del cáncer. Las nanoesferas recubiertas por CaPs exhibirían estructuras de poros bien interconectados y excelente bioactividad *in vitro* que les haría útiles para diversas aplicaciones biomédicas. Por ejemplo, una capa de HA podría actuar como una nanocompuerta que permitiese la liberación controlada de

biomoléculas alojadas los mesoporos de la sílice bajo condiciones específicas, por ejemplo la disminución del pH. Los procedimientos que se han intentado para obtener MSNSs recubiertas por CaP han sido: *(i)* co-síntesis de CaP y MSNSs, inmersión *(ii)* e *(iii)* impregnación de las MSNSs en un sol precursor de CaP y *(iv)* funcionalización de MSNSs con moléculas orgánicas que contienen grupos fosfato para facilitar el recubrimiento durante la impregnación con un sol precursor de CaP. Excepto en la primera ruta, en la que ambos procesos son simultáneos, la síntesis de los materiales se realiza en dos pasos: *(1)* síntesis de las MSNSs de 150-250 nm de diámetro y unos 2 nm de diámetro de poro y *(2)* recubrimiento de las MSNSs con una fase de CaP.

En el ***Capítulo V*** se aborda una mejora de estos sistemas, donde el tema investigado es el recubrimiento de las MSNSs con HA dopada con un elemento fluorescente como el europio, mediante la precipitación de CaP fluorescente sobre MSNSs sintetizadas previamente. Se busca dar una mayor visibilidad y trazabilidad de los nanosistemas durante la aplicación de biológica, permitiendo la localización del recorrido de las nanopartículas por el interior de la célula o la acumulación de las mismas en el tumor.

El ***Capítulo VI*** resume las principales conclusiones derivadas de esta tesis. Por último, las condiciones generales y el trabajo experimental detallado, así como las técnicas de caracterización y análisis estructurales empleados, se incluyen en el ***Capítulo VII*** de esta memoria.

Resultados y Conclusiones

Capítulo II. Precipitación de fosfatos de calcio mesoestructurados en presencia de surfactantes iónicos

- Los surfactantes iónicos, principalmente aniónicos, que contienen átomos de S o P en su cabeza polar, como el SDS, SDBS y MAP, pueden utilizarse para obtener híbridos orgánico-inorgánicos mesoestructurados basados en CaPs.

- La interacción de las moléculas anfifílicas de surfactante con los iones calcio y fosfato, durante la precipitación de CaPs de soluciones acuosas, produce materiales híbridos que exhiben mesostructura lamelar o lamelar discontinua, pero sin orden mesoporoso.

- En las condiciones de síntesis, es decir, relación molar Ca/P 1 o 1,67, concentración de surfactante de 15 a 90 mM o 240 mM y sin tamponar el pH, las fases de CaP más comunes que presentan los híbridos lamelares formados son brushita, hidroxiapatita o monetita.

- El SDS es un surfactante adecuado para obtener CaPs híbridos con mesoestructura lamelar.

- Concentraciones relativamente altas de SDBS y una relación molar Ca/P de 1 dan lugar a mesostructuras discontinua lamelar o curvada lamelar, formando redes de HA poco cristalina. La formación de HA a pesar de la baja relación molar Ca/P se atribuye al aumento de pH (de 7 a 9) del medio debido a la protonación del grupo sulfato de la cabeza del SDBS en la síntesis.

- La mezcla de un surfactante aniónico, como SDS, SDBS o MAP, con el catiónico cetiltrimetil bromuro de amonio (CTAB) produce híbridos con mesoestructura análoga a la obtenida con los surfactantes aniónicos puros, lo que sugiere una interacción no efectiva del CTAB con los iones calcio y fosfato.

- El análisis mediante TEM de los materiales obtenidos con mezcla de surfactantes muestra dos tipos de partículas: *(i)* tipo-barra con mesoestructura lamelar y *(ii)* tipo-hoja que son inestables bajo el haz de electrones. Las burbujas que se forman cuando se enfocan estas partículas, atribuidas a la combustión de la materia orgánica y la eliminación del agua de cristalización de la brushita, evitan la identificación de su posible mesoestructura.

- La utilización de procedimientos de síntesis más enérgicos, como el envejecimiento en autoclave o el reflujo después de la precipitación del CaP, lleva a la formación de monetita, una fase de CaP derivada de brushita tras eliminar las dos moléculas de agua de cristalización.

- La utilización de EPG, surfactante zwitteriónico que contiene un grupo de carboxibetaína, como plantilla de la mesoestructura del CaP no tiene éxito ya que no se detecta su interacción con los iones calcio y fosfato. Para investigaciones futuras, se sugiere la utilización de otro surfactante zwitteriónico que contenga grupos sulfobetaína.

Capítulo III. Precipitación de fosfatos de calcio mesoestructurados en presencia de fosfolípidos

- La precipitación de CaPs en suspensiones de fosfolípidos (PLs) con diferentes concentraciones de fosfatidilcolina (PC) conduce a la síntesis de materiales híbridos CaP-PLs.

- Los componentes inorgánicos de los híbridos son HA poco cristalina, cuando el pH es básico y la relación molar Ca/P = 1.67 y brushita a pH neutro y Ca/P = 1.

- El contenido de materia orgánica en ambos tipos de híbridos es semejante: alrededor del 20% en los que contienen brushita y alrededor del 17% en los que contienen HA. Los híbridos CaP-PLs sometidos a un proceso térmico para eliminar la materia orgánica evolucionan a HA no porosa. Puesto que ninguno de los materiales obtenidos después de la calcinación presenta mesoporosidad, este capítulo se ha centrado en la caracterización de los híbridos CaP-PLs.

- El análisis mediante TEM de los híbridos reveló cuatro tipos de nanoestructuras: *(i)* bicapa lamelar de 4.2 nm de espesor de capa (apatita, Asolectin), *(ii)* vesículas bicapa alrededor de 35 nm de diámetro y 4.7 nm de espesor de pared bicapa (brushita, Lecitina), *(iii)* micelas de unos 4.3 nm de diámetro (brushita, Lipoid) y *(iv)* mesostructuras tipo esponja o gusano con bicapas tubulares de 4.3 nm de grosor de bicapa de la estructura desordenada (apatita, Lipoid).

- Puesto que ambos componentes de los híbridos CaP-PLs son biocompatibles, estos materiales son susceptibles de utilizar como plataformas de liberación de fármacos mediante la encapsulación del fármaco en la estructura de los fosfolípidos que forman el híbrido.

Capítulo IV. Recubrimientos de hidroxiapatita en nanoesferas de sílice mesoporosa

En este capítulo, se intentó recubrir nanoesferas de sílice mesoporosa tipo MCM-41 (MSNSs) con NPs de HA o con una capa de HA, para ampliar las aplicaciones clínicas de ambos materiales. Según este objetivo, las conclusiones derivadas de cada ruta sintética empleada son:

- *Co-síntesis de CaP y MSNSs.* La precipitación de CaP simultánea a la síntesis sol-gel de MSNSs produce una mezcla de partículas independientes de HA poco cristalina y en forma de barras y MSNSs con una amplia dispersión de tamaños y una S_{BET} de 594 m^2/g.

- *Immersion de MSNSs en un sol precursor de CaP.* En primer lugar se sintetizaron MSNSs de SiO_2 pura (S_{BET} = 1230 m^2/g). Después de sumergirlas en el sol precursor de CaP durante 3 horas, las nanoesferas se transforman en elipsoides con Si, Ca, P y O en su composición y una S_{BET} de 250 m^2/g. Las partículas elipsoidales exhiben una disposición radial de canales mesoporosos cerca de su superficie. Además, el material obtenido exhibe una moderada respuesta bioactiva *in vitro* en fluido corporal simulado (SBF).

- *Impregnación de MSNSs por un sol precursor de CaP.* En esta aproximación, las MSNSs de SiO_2 pura (S_{BET} = 1230 m^2/g), se sumergieron 30 minutos en el sol precursor de CaP y posteriormente se sometieron a un proceso de lavado repetidas veces con el sol, imitando un procedimiento de recubrimiento por inmersión. Las imágenes de TEM tras la impregnación confirman la formación de NPs de HA que recubren la superficie de las MSNSs. En este caso, la S_{BET} del material recubierto sufre una drástica disminución del ≈90% comparado con las MSNSs iniciales. A diferencia del método anterior, con este método de síntesis las MSNSs no se alteran, ni en su forma ni en su composición.

- *Funcionalización de MSNSs con grupos fosfato y posterior impregnación con un sol precursor de CaP.* Las MSNSs se funcionalizaron con dietilfosfatoetil trietoxisilano (DEPETES) o con 3-trihidroxisililpropilmetilfosfonato (THSMP) para facilitar la posterior interacción de sus grupos tipo fosfato con los iones calcio y fosfato del sol.

    - Las MSNSs funcionalizadas con DEPETES mediante co-condensación o post-síntesis mostraron una mesoporosidad ordenada tipo MCM-41 y altas S_{BET} (878 y 1190 m^2/g, respectivamente). Tras la impregnación con un sol precursor de CaP, el análisis por TEM muestra una distribución homogénea de una capa HA alrededor de las MSNSs junto con NPs de HA. La elevada S_{BET} de 335 m^2/g indica que la superficie de las MSNSs sólo se ha recubierto parcialmente.

    - Se funcionalizaron MSNSs con THSMP por co-condensación. El material obtenido que presenta una alta S_{BET} de 1316 m^2/g fue impregnado con un sol precursor de CaP. El análisis TEM muestra una estructura MSNS@HA tipo núcleo@corteza. Las MSNSs recubiertas son no porosas mostrando una disminución en S_{BET} de alrededor del 97% con respecto a las MSNSs iniciales.

Capítulo V. Recubrimiento de Nanoesferas de sílice mesoporosa con nanopartículas de hidroxiapatita fluorescente

- La precipitación de HA dopada con Eu^{3+} (HA fluorescente, FHA) en presencia de MSNSs tipo MCM-41 conduce a la síntesis de materiales compuestos FHA/MSNSs.

- Algunos materiales compuestos FHA/MSNSs exhiben luminiscencia roja propia de los elementos de lantánidos irradiados con luz UV. La intensidad luminosa depende de la cantidad de iones Eu^{3+} en el material.

- En una de las muestras investigadas se observa por TEM una estructura núcleo@corteza (MSNS@HA). Sin embargo, esta muestra no presenta emisión fluorescente debido a su bajo contenido en Eu^{3+}.

I. INTRODUCTION

I.1 Biomaterials for hard tissues regeneration

Biomaterials are materials that play their role in contact with biological systems. Therefore, they must be biocompatible because their implantation creates interfaces between the biological and the physical worlds. That way, they must interact with biological systems and should be biologically active within the human body. Figure I.1 displays some examples of biomaterials improving the quality of life of people. The current ageing of the population due to the increase of the life span and the subsequent increase in degenerative problems, arthritis, osteoporosis and others, as well as the incidence of road traffic accidents, justify the large demand of biomaterials to sustain and improve the quality of life of thousands of people. For this reason they have experienced a great development in the last decades due to the multidisciplinary effort of investigators from different areas, including: Science and Engineering of Materials, Chemistry, Physics, Medicine, Biology or Pharmacy [1-3].

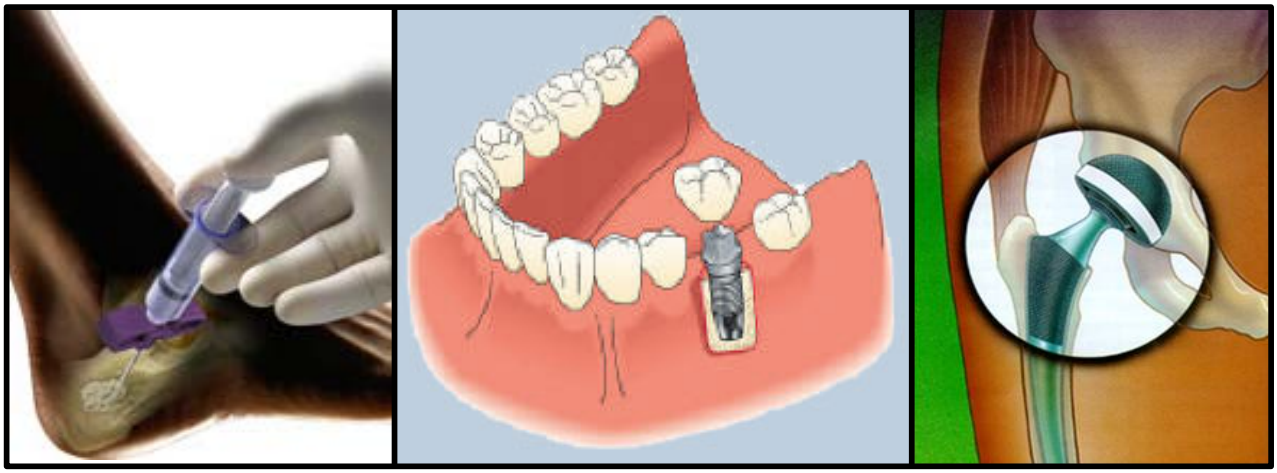

Figure I.1 Biomaterials in the human body (Source: *www.bilgiustam.com/biyomalzeme-vucutta-kullanilan-yapay-malzemeler-2/)*.

Different definitions of "biomaterial" can be found in the literature. Several ones are included below. In 1982 *Hench* and *Erthridge* stated in their book [4]: *A biomaterial is used to make the devices to replace a part or a function of the body in a safe, reliable, economic, and physiologically acceptable manner.*

Perhaps the most popular definition of biomaterials is the one endorsed in 1987 by a consensus of experts [5]. *A biomaterial is a nonviable material used in a medical device, intended to interact with biological systems.*

In 2004 *Ratner et al* in the second edition of their noteworthy book "Biomaterials Science" removed from the previous definition the words "medical" and "nonviable", to address the new tissue engineering and hybrid artificial organ applications, where living cells are used [6]. Therefore the actual simpler definition of a biomaterial is: *Material used in a device, intended to interact with biological systems*.

The science of biomaterials has shown continuous and rapid growth in the last 50 years, and biomaterials are now in direct interaction with the fields of medicine, chemistry and materials

science [7]. In medical applications, biomaterials are rarely used as they are, but integrated into medical devices or implants. Compulsory characteristics of biomaterials are to be non–toxic, non–carcinogenic, non–allergenic, and non–inflammatory. In addition they must be biocompatible, applicable and biofunctional throughout their lifetime [3, 7]. The new generation of biomaterials can be produced from metallic, polymeric, ceramic, or composite components. In the last 20 years, humans have realized that ceramics and their composites can be used to replace various parts of the body, particularly for bone regeneration applications [8]. In this sense, it is very common to classify the bioceramics in terms of their reactivity within the human body as bioinert, usually considered as first generation bioceramics, or as biorebsorbable and bioactive, *i.e.* able to bond directly with the living tissues, as second generation bioceramics. However in the last years a different type of biomaterials is being studied. These biomaterials include a second generation bioceramic that behaves just as a scaffold and exhibits a hierarchical porosity able to host cells and/or osteoinductor agents. Such materials are considered nowadays as third generation biomaterials [9].

Thus, the ceramics that are used in the body are classified as bioceramics and they are used as biomaterials in the medical science. Furthermore, they are considered as inorganic materials in chemistry science. Their relative inertness to the body fluids, high compressive strength, and esthetically pleasant appearance led to the use of bioceramics in dentistry as dental filling and also in medicine. These materials can be used in granulated form, with predefined shapes or in porous form, for coating and artificial bone filling applications. Porous calcium phosphate (CaP) bioceramics have more potential applications in bone tissue engineering because of its large surface area and pore volume [10, 11]. Bioceramics are biocompatible with living cells and with the body, and they are suitable for bone regeneration and tissue engineering. Besides, porous bioceramics have received much attention because their porosity allows vascularization and cell growth in body by chemical self–interaction. For this reason calcium phosphate bioceramics have been under constant study in the last forty years as potential candidates for hard tissues replacement. Nowadays, the advent of Nanotechnology to the Biomaterials world has evidenced the importance of designing the new implants not only at the macrometric scale but also at the mesoscopic scale and even at the molecular level. In fact, the control of the biomaterials mesostructure is revealing as a requisite for an effective control of their *in vivo* behavior, including their bone regeneration capability [12, 13]. Depending on this, it is possible to synthesize porous materials in varying pore sizes: microporous, containing pores with diameters less than 2 nm; mesoporous, containing pores between 2 and 50 nm, and macroporous containing pores larger than 50 nm.

This memory is devoted towards the design and characterization of mesostructured calcium phosphates to be used for the design of implants aimed at repairing hard tissues, and their employ as biomaterials. For this purpose, in this thesis calcium phosphate and silica based bioceramics were developed as third generation bioceramics by novel methods. In the future, these novel methods and synthesized hybrid materials may play an important role in the development of new bioceramics based on calcium phosphate and mesoporous silica materials [14].

I.2 Calcium phosphate bioceramics

In the last 50 years, there is increased interest in the use of calcium phosphates as bioceramic material. CaP bioceramics are widely being investigated and applied in diverse areas of bone regeneration and hard tissue engineering. Their chemical and structural similarities to biological apatite make them perfect candidates in bone filling applications [14, 15]. Bone structure is naturally formed by 60 – 75 % of inorganic components (mainly calcium phosphates), 25 % of organic components (principally collagen) and 5 – 8 % water [16, 17]. Hence, calcium phosphates are often used for bone substitution because: *(i)* their chemical similarity to the mineral component of hard tissues (bone and teeth) [18, 19]; *(ii)* they are bioactive, biocompatible and biologically form a strong bond with the surrounding bone tissue [20, 21]; and *(iii)* they integrate into living tissue and induce the remodeling of natural bone [22-25].

The most habitual CaPs used as biomaterials are listed in Table I.1 [26]. From this list, HA is selected to be used for application as bioceramics in the field of bone and hard tissue regeneration, because its similarity with the main crystalline component of the mineral phase of bone, and also because it can be adequately synthesized at the laboratory by chemical methods [27-30]. CaPs can be obtained in different crystalline forms by changing experimental synthesis conditions (such as temperature, pressure and pH) and the Ca/P molar ratio. Thus, by changing synthesis conditions, other crystalline calcium phosphates besides HA can be synthesized such as tetracalcium phosphate (TTCP), brushite (or dicalcium phosphate dehydrate, DCPD), monetite (dicalcium phosphate anhydrous, DCPA), α–TCP or β–TCP [31-33].

Table I.1 Calcium phosphates used as biomaterials [26].

Ca/P molar ratio	Compound	Acronym	Formula
0.5	Monocalcium phosphate monohydrate	MCPM	$Ca(H_2PO_4)_2{\cdot}H_2O$
0.5	Monocalcium phosphate anhydrous	MCPA	$Ca(H_2PO_4)_2$
1.0	Dicalcium phosphate dihydrate, brushite	DCPD	$CaHPO_4{\cdot}2H_2O$
1.0	Dicalcium phosphate anhydrous, monetite	DCPA	$CaHPO_4$
1.33	Octacalcium phosphate	OCP	$Ca_8(HPO_4)_2(PO_4)_4{\cdot}5H_2O$
1.5	α–Tricalcium phosphate	α–TCP	α–$Ca_3(PO_4)_2$
1.5	β–Tricalcium phosphate	β–TCP	β– $Ca_3(PO_4)_2$
1.2-2.2	Amorphous calcium phosphate	ACP	$Ca_xH_y(PO_4)_z{\cdot}nH_2O$
1.5-1.67	Calcium–deficient hydroxyapatite	CDHA	$Ca_{10-x}(HPO_4)_x(PO_4)_{6-x}(OH)_{2-x}(0<x<1)$
1.67	Hydroxyapatite	HA	$Ca_{10}(PO_4)_6(OH)_2$
1.67	Fluorapatite	FA	$Ca_{10}(PO_4)_6F_2$
2.0	Tetracalcium phosphate, hilgenstockite	TTCP	$Ca_4(PO_4)_2O$

I.2.a Synthesis of calcium phosphates by precipitation

The wet chemistry precipitation method is mostly used to obtain crystalline CaPs, especially HA. The $Ca(OH)_2$–H_3PO_4–H_2O system allows only a limited number of calcium phosphates to be obtained by

precipitation in crystalline solid form with well-defined stoichiometry, physical and thermodynamic properties. In fact, attention in the biomedical field is generally focused on monocalcium phosphate monohydrate (MCPM), dicalcium phosphate dihydrate (DCPD), octacalcium phosphate (OCP), precipitated HA, calcium-deficient hydroxyapatite (CDHA) and amorphous calcium phosphate (ACP) because their respective solubility products are well established. It should be noted that dicalcium phosphate (DCP) is rarely obtained by precipitation from an aqueous solution at room temperature. It is usually obtained by heating DCPD at temperatures between 120 and 170 °C. Likewise, the hydration processes of DCP are usually effective at temperatures higher than 50 °C. Therefore, when analysing singular points between any calcium phosphate and DCP at ambient or body temperature care should be taken in drawing any conclusions. Although less well documented than the abovementioned phosphates, there are other calcium phosphates obtained by precipitation playing an important role in the solution behaviour of the $Ca(OH)_2$–H_3PO_4–H_2O system. In the case of precipitation, where the temperature does not exceed 100°C, nanocrystals are obtained. They have shapes of blades, needles, rods, or equiaxed particles [34]. Their crystallinity and Ca/P molar ratio depend strongly upon the preparation conditions and are in many cases lower than that of well–crystallized stoichiometric HA. Also, during synthesis it is necessary to take into account these parameters: pressure, pH value, temperature of synthesis and Ca/P molar ratio, because they play an important role in obtaining different crystalline calcium phosphates [35-37]. Precipitation of calcium phosphate takes place according to the following chemical reactions:

$$CaCl_{2\,(aq)} + Na_2HPO_{4\,(aq)} + 2H_2O \rightarrow CaHPO_4{\cdot}2H_2O_{(s)} + 2NaCl \quad (1)$$

$$CaHPO_4{\cdot}2H_2O \text{ (brushite)} \xrightarrow{\geq 300\ ^\circ C\ /\ 2H_2O\uparrow} CaHPO_4 \text{ (monetite)} \quad (2)$$

As seen in the reaction 1, calcium and phosphate sources are dissolved and Ca^{2+} and HPO_4^{2-} ions are precipitated in the aqueous solution to obtain brushite. In the reaction 2, the transition to monetite occurs at temperatures above 300°C due to evaporation of the crystalline water of brushite [38].

As explained above, HA crystals can be prepared by the following wet chemical reaction of precipitation [39]:

$$10\ Ca(OH)_2 + 6\ H_3PO_4 \xrightarrow{\text{basic media of aqueous solution}} Ca_{10}(PO_4)_6(OH)_2 + 18\ H_2O \quad (3)$$

This formulation shows that Ca/P molar ratio of 1.67 and OH^- ions are sufficient to form crystalline HA. One of the features of precipitation is that the particle deposition of the calcium phosphate can momentarily be observed as it rapidly occurs forming needle–like crystals [40-42]. The precipitation method of CaP was used during this thesis and calcium chloride dihydrate and sodium phosphate dibasic dihydrate were used as sources of calcium and phosphate, respectively.

I.2.b Hydroxyapatite

In Biomaterial Science, synthetic hydroxyapatite (HA) crystals are widely studied and used for their important biological applications, including coatings for implant devices, bone substitutes and scaffolds as well as vehicles for drug, protein and gene delivery [43-45]. There are many reported methods for preparation of HA powders. The most commonly used techniques are precipitation,

solid–state reaction, co–precipitation, hydrothermal synthesis and sol–gel chemistry [46-50]. Hydroxyapatite is chemically formulated as $Ca_{10}(PO_4)_6(OH)_2$, and as stated above, it is similar to the main mineral component in body.

HA can be produced by chemical reaction, with Ca/P molar ratio of 1.67, in basic media of aqueous solutions [51]. The Ca/P molar ratio and pH of the aqueous solution are important to obtain HA, because the compounds with a Ca/P ratio lower than 1 are less suitable for implantation [6, 52].

For quantitative reactions in solution, the inorganic reactants must be $Ca(OH)_2$ and H_3PO_4 or their salts, with ions that are to be incorporated in the apatite lattice. Thus, calcium chloride dehydrate and calcium nitrate tetrahydrate are the most commonly used calcium source precursors in the synthesis of calcium phosphate [53, 54]. Likewise, the most used phosphorous precursors are triethyl phosphite (TIP) with formula $P(OCH_2CH_3)_3$ or triethyl phosphate (TEP) with formula $O=P(OCH_2CH_3)_3$ in sol–gel synthesis, and diammonium hydrogen phosphate or sodium phosphate dibasic dihydrate in precipitation synthesis.

The interaction of HA with solid inorganic surfaces is the key to several important and novel applications [55]. The surface functionalization of HA nanocrystals with bioactive molecules makes them able to transfer information and to act selectively on the biological environment. In particular, the functionalization with drugs could represent a local treatment for bone diseases by direct application of HA modified [24, 55, 56]. In the field of biomaterials, HA–surface adhesion is the first event in the integration of an implanted device or material with biological tissues. In nanotechnology, HA–surface interactions are pivotal for the assembly of interfacial biocompatible constructs, such as functional components at the biological/chemical function [57]. The detailed mechanistic understanding of the HA–surface interaction and the ability to tailor HA surface interaction in mesostructured materials would be of value to bio–/nano–assembly technologies. The study of HA–solid surface interaction may also increase our general knowledge of hybrid materials synthesis and coating [55].

In the biomaterial field, calcium phosphates are widely used as bone grafts. Here, a knowledge of the underlying principles of solid inorganic interaction with calcium phosphates, specially HA, is required not only in evaluating their potential application but also in their ability to act as bioactive implants. By synthesis of functionalized HA, it is possible to enhance bioactivity (HA nanocrystals/biomolecules) and biocompatibility [55].

I.2.c Lanthanide–doped hydroxyapatite

In recent years several strategies have been developed to produce luminescent HA nanoparticles (NPs) doped with different lanthanides [58-61], that could be used as luminescent labels or luminescent drug carriers [58, 62]. The emitted wavelength (colour) can be modified by selecting a specific dopant or a combination of dopants. In general, the luminescence intensity of a material is dependent on the concentration of the doping ions, the crystal structure and the degree of crystallinity of the host material [63, 64].

In this memory, we tried to coat the mesoporous silica nanospheres (MSNSs) with lanthanide–doped HA nanoparticles (NPs) and these are promising biomaterials with fluorescent properties that after optimization could be highly appropriate for biomedical applications [61, 65, 66]. Such applications include: luminescent labels, luminescent drug carriers, biological probes, biological labelling and fluorescent probes that follow an excitation in the visible domain [67-69].

I.3 Mesoporous Silica Nanoparticles

In recent years, mesoporous silica nanoparticles (NPs), which exhibit unique pore size, high surface area and pore volume, are being widely employed as carriers for controlled drug delivery. Compared with amorphous colloidal and porous silica, mesoporous silica exhibit higher drug loading abilities and provide a controlled drug release if modified by functionalization [70]. Since the discovery of ordered mesoporous silica materials in 1990s, synthesis and applications of mesoporous solids have received intensive attention due to their mesostructures, large pore size, and high surface area. Particle diameter, surface area and pore size of mesoporous silica NPs are below 500 nm, above 900 m^2/g and between 2–10 nm, respectively. In the past decade, mesoporous silica materials have found many applications in separation, catalysis, sensors and devices [71, 72]. Due to their stable mesoporous structure and well–defined surface properties, silica mesoporous materials seem ideal for encapsulation of pharmaceutical drugs, proteins and other biologically active molecules. In recent years, employment of silica mesoporous materials for hosting and further delivering of a variety of molecules of pharmaceutical interest has been reviewed [73, 74]. It has been shown that both small and large molecular drugs can be entrapped within the silica mesoporous by impregnation process and liberated via a diffusion–controlled mechanism. Since the report by *M. Vallet–Regí et al.* in 2001 using MCM–41 (Mobil Composition of Matter No 41) as a new drug delivery system [75], numerous investigations have been carried out in this area, developing different types of silica mesoporous materials with varying porous structure and functionality for sustained drug release and stimuli–responsive release [70]. Mesoporous silica nanoparticles are commonly used and their use as bioceramics is increasing in medicine and pharmaceutical devices applications [76, 77].

Silica mesoporous materials are being investigated for drug delivery, stimulate cell growth and other biomedical applications such as loading of anticancer drugs [78]. Besides, mesoporous materials in granulated form, or with predefined shapes, in either porous or dense pieces, can be a very useful tool for an orthopaedic surgeon or pharmaceutical working in bone reconstruction [79]. Porous bioceramics act as scaffolds for cells and inducting molecules, are able to drive tissue self–regeneration and help in cell growth [26, 46]. The pore diameter of mesoporous materials is between 2 – 50 nm according to IUPAC pore classification. The formation mechanism of the mesostructure relies on the use of templating molecules, such as long chain quaternary amphiphilic surfactants self–assembled as a liquid crystal onto which silica precursor molecules are hydrolyzed and condensed.

The 2D–hexagonal mesostructured MCM–41 is the best known and most widely studied material of the mesoporous silica family. Other members of this family are MCM–48 and MCM–50 [48]. These

three materials have hexagonal, cubic and lamellar mesostructures for MCM–41, MCM–48 and MCM–50, respectively [49, 50, 80, 81].

Structure directing agents, or surfactants, play an important role in nanostructured materials due to their self–assembly features in water. Cetyl TrimethylAmmonium Bromide (CTAB) is the most used structure directing agent to synthesize MCM–41 type mesostructure, with pore diameters around 2-3 nm.

There are several methods to synthesize mesoporous silica particles. For the preparation of nanoparticles the usual method is as follows: *(i)* synthesis of amorphous silica by sol–gel chemistry (hydrolysis and condensation), *(ii)* obtaining the mesostructure by performing the synthesis in the presence of structure directing agents and *(iii)* preparation of nanospheres by Stöber method [77, 82]. Then, the general synthesis method of silica mesoporous nanoparticles can be explained as follow: CTAB is dissolved in aqueous solution to obtain hexagonal mesostructure, the pH is set to a basic value with NaOH or ammonia and then the silica precursor is added. Micellar nanorods are formed by self-assembly of CTAB during the hydrolysis and condensation of silica precursor [47]. Finally, the silica nanoparticles with hexagonal packed mesoporosity, MCM–41, are obtained after removing surfactant, see Figure I.2.

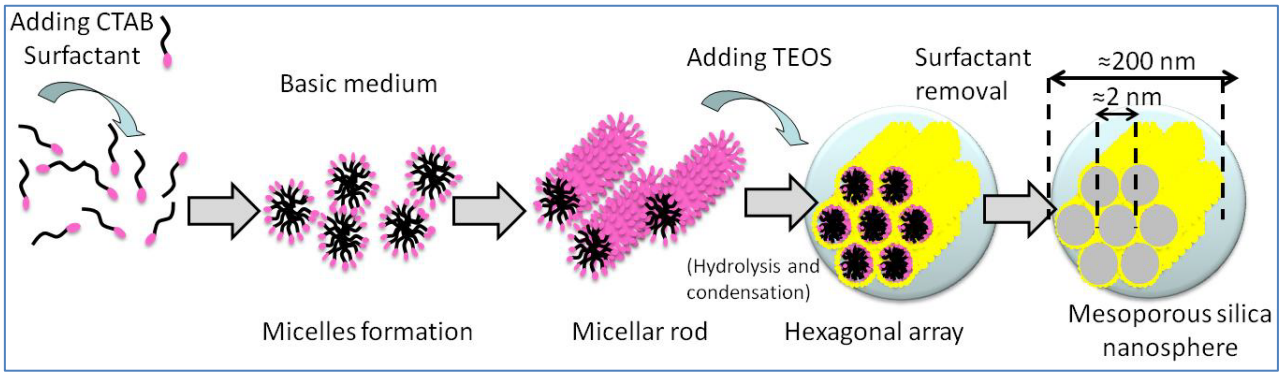

Figure I.2 Synthesis of hexagonally ordered mesoporous silica nanospheres (MCM–41 type).

The experimental conditions employed in the so–called "Stöber process" for preparing SiO_2 powders are hydrolysis of TEOS with H_2O/Si molar ratio values ranging from 20 to over 50 and concentrations of ammonia ranging from ≈ 1 to 7 M, which result in monodisperse and spherical particles [83]. In the modified Stöber method the silica spherical mesoporous nanoparticles are achieved at high temperature using CTAB as structure directing agent. The diameter of these spherical mesoporous particles is between 100 and 300 nm [84]. In this memory, MSNSs have been synthesized by modified Stöber method and have also been functionalized with phosphate–like groups by co-condensation and post-synthesis and then coated with HA [85-87].

I.3.a Functionalization of mesoporous silica phases

The combination of the properties of organic and inorganic building blocks within a single material is particularly attractive from the viewpoint of materials scientists because of the possibility to combine

the enormous functional variation of organic chemistry with the advantages of a thermally stable and robust inorganic substrate. The symbiosis of organic and inorganic components can lead to materials whose properties differ considerably from those of their individual, isolated components.

Adjustment of the polarity of the pore surfaces of an inorganic matrix by the addition of organic building blocks extends considerably the range of materials that can be used, for example, in drug delivery. Equally interesting is modification with organic functionalities such as C–C multiple bonds, alcohols, thiols, sulfonic and carboxylic acids, and amines, *etc.*, which allow, for example, localized organic or biochemical reactions to be carried out on a stable, solid inorganic matrix [88].

In Chapter IV, two pathways are used for the functionalization of mesoporous silica materials: 1) the simultaneous condensation of corresponding silica and organosilica precursors (co–condensation method), and 2) the subsequent modification of the pore surface of a purely inorganic silica material (post–synthesis method).

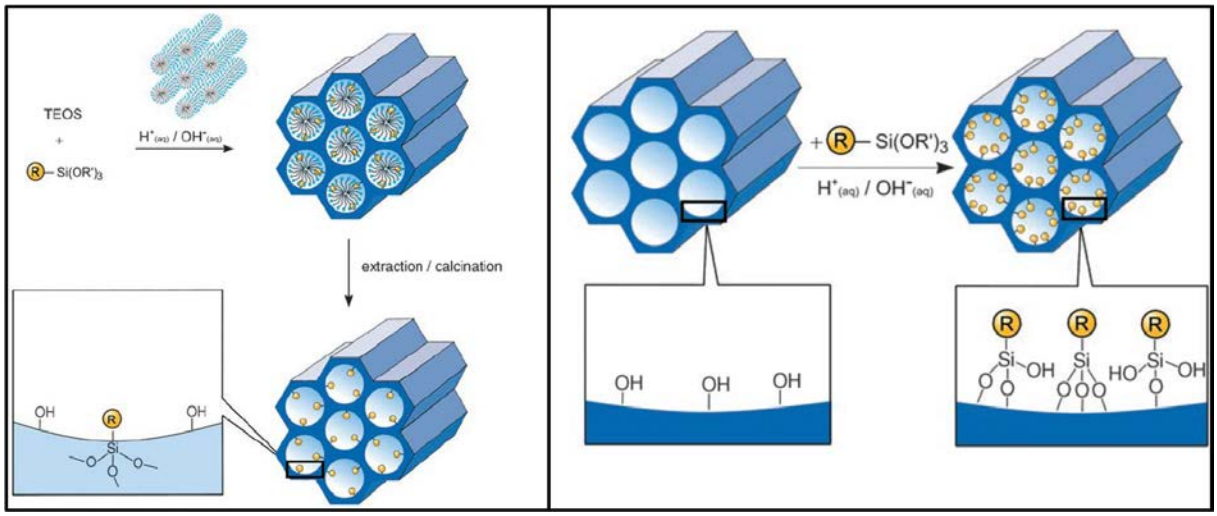

Figure I.3 *Left:* Co-condensation method (direct synthesis) for the organic modification of mesoporous pure silica phases. R=organic functional group. *Right:* Grafting (post–synthetic functionalization) for organic modification of mesoporous pure silica phases with terminal organosilanes of the type $(R'O)_3SiR$. R=organic functional group (right), taken from *Angew. Chem. Int. Ed.* **2006**, *45*, 3216 [88].

Co–condensation method: The process to synthesize organically functionalized mesoporous silica phases is the co–condensation method. It is possible to prepare meso–structured silica phases by the co–condensation of tetra–alkoxysilanes $[(RO)_4Si]$ with terminal trialkoxyorganosilanes of the type $(R'O)_3SiR$ in the presence of structure directing agents leading to materials with organic residues anchored covalently to the pore walls (see Figure I.3, left). By using structure directing agents known from synthesis of pure mesoporous silica phases (*e.g.,* MCM or Santa Barbara Amorphous type material (SBA) silica phases), organically modified silicas can be prepared in such a way that the organic functionalities project into the pores.

Since the organic functionalities are direct components of the silica template, pore blocking is not a problem in the co–condensation method. Furthermore, the organic units are generally more homogenously distributed than in materials synthesized with the post–synthesis. However, the co–condensation method also has a number of disadvantages: generally, the degree of mesoscopic order of the products decreases with increasing concentration of $(R'O)_3SiR$ in the reaction mixture, which ultimately leads to totally disordered products, consequently, the content of organic functionalities in the modified silica phases does not normally exceed 40 mol%. Furthermore, the proportion of terminal organic groups that are incorporated into the pore–wall network is generally lower than would correspond to the starting concentration of the reaction mixture. These observations can be explained by the fact that an increasing proportion of $(R'O)_3SiR$ in the reaction mixture favours homocondensation reactions at the cost of cross–linking co–condensation reactions with the silica precursors. The tendency towards homocondensation reactions, which is caused by the different hydrolysis and condensation rates of the structurally different precursors, is a constant problem in co–condensation because the homogeneous distribution of different organic functionalities in the framework cannot be guaranteed. Moreover, an increase in loading of the incorporated organic groups can lead to a reduction in the pore diameter, pore volume, and specific surface areas. A further, purely methodological disadvantage that is associated with the co–condensation method is that care must be taken not to destroy the organic functionality during removal of the surfactant, which is why commonly only extractive methods can be used, and calcination is not suitable in most cases.

Post–synthesis method: It refers to the subsequent modification of the inner surfaces of mesostructured silica phases with organic groups. This process is carried out primarily by reaction of organosilanes of the type $(R'O)_3SiR$, or less frequently chlorosilanes $ClSiR_3$ or silazanes $HN(SiR_3)_2$, with the free silanol groups of the pore surfaces (see, Figure I.3, right). In principle, functionalization with a variety of organic groups can be realized in this way by variation of the organic residue R. This method of modification has the advantage that, under the synthetic conditions used, the mesostructure of the starting silica phase is usually retained, whereas the lining of the walls is accompanied by a reduction in the porosity of the hybrid material (albeit depending upon the size of the organic residue and the degree of occupation). If the organosilanes react preferentially at the pore openings during the initial stages of the synthetic process, the diffusion of further molecules into the center of the pores can be impaired, which can in turn lead to a nonhomogeneous distribution of the organic groups within the pores and a lower degree of occupation. In extreme cases (*e.g.,* with very bulky grafting species), this can lead to complete closure of the pores (pore blocking).

I.4 Surfactants for mesophases formation

Surfactants are compounds that decrease the surface tension (or interfacial tension) between a liquid and a solid [89]. They are usually organic compounds that are amphiphilic, meaning they contain hydrophobic groups (their tails) and hydrophilic groups (their heads), see Figure I.4.

A surfactant contains both a water insoluble component and a water soluble component. Surfactants diffuse in water and adsorb at interfaces between air and water or at the interface between oil and water, in the case where water is mixed with oil [90]. The water–insoluble hydrophobic group may extend out of the bulk water phase, into the air, while the water–soluble head group remains in the water phase. This alignment of surfactants at the surface modifies the surface properties of water at the water/air boundary [91].

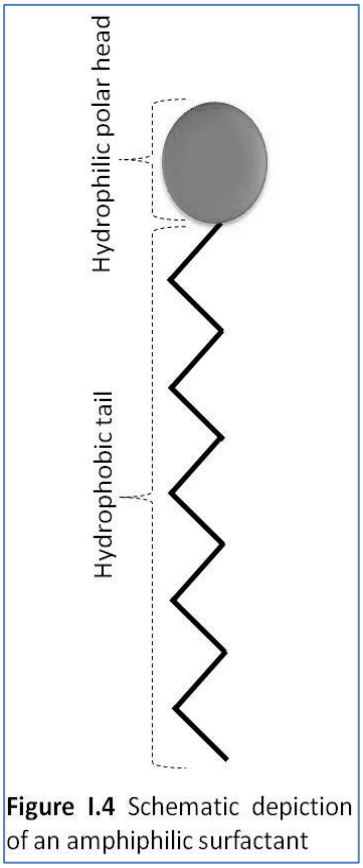

Figure I.4 Schematic depiction of an amphiphilic surfactant

Surfactant molecules have either one tail or two; those with two tails are said to be *double–chain.* Most commonly, surfactants are classified according to polar head such as lower alkyl group, branching alkyl chains, aromatic ring such as benzene or naphthalene [92]. A non–ionic surfactant has no charge groups in its head. The head of an ionic surfactant carries a net charge. If the charge is negative, the surfactant is more specifically called anionic; if the charge is positive, it is called cationic [93]. If a surfactant contains a head with two oppositely charged groups, it is termed zwitterionic. Commonly encountered surfactants of each type include: non–ionic, anionic, cationic and zwitterionic surfactant.

Most known and used surfactants to obtain mesophases are classified in 3 main types as ionic, non ionic and zwitterionic in Table I.2.

Surfactants are classified according to their use or application: soap, detergent, emulsion former, bactericide, corrosion inhibit or dispersant, tensioactive, etc [94].

In aqueous phase, surfactants form aggregates, such as micelles, where the hydrophobic tails form the core of the aggregate and the hydrophilic heads are in contact with the surrounding liquid. Other types of aggregates such as spherical or cylindrical micelles or bilayers can be formed. The shape of the aggregates depends on the chemical structure of the surfactants, depending on the balance of the sizes of the hydrophobic tail and hydrophilic head [95]. This is known as the HLB, hydrophilic–lipophilic balance [96].

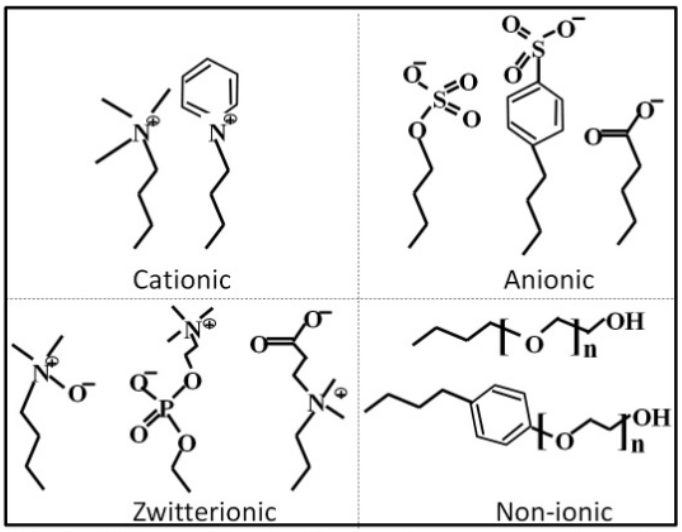

Figure I.5 Examples of polar head groups was showed with formula.

Table I.2. Some surfactants that play an important role in the formation of mesostructures.

Types		Examples
Ionic	*Anionic*	Sodium lauryl sulphate, alkylbe nzene sulphonates, paraffin sulphonate, alkyl ether sulphates, phosphate esters.
	Cationic	Quaternary ammonium compounds, hexadecyl trimethyl ammonium bromide, cetylpyridinium chloride**,** trimethylhexadecyl ammonium chloride, Bronidox.
Non ionic		Polyoxyethylene, Sorbitan monooleate (Polysorbate 80 = Tween 80), Cetyl alcohol, Oleyl alcohol, Monolaurin.
Zwitterionic		Cocamidopropyl betaine, Sodium lauroamphoacetate, Empigen®BB.

I.4.a Hydrophilic–lipophilic balance

Surfactants consist of a molecule that combines both hydrophilic and lipophilic groups (or polar and non–polar groups) and it is the balance of the size and strength of these two opposing groups that we call hydrophilic–lipophilic balance (HLB) [97]. The hydrophilic–lipophilic balance of a surfactant is a measure of the degree to which it is hydrophilic or lipophilic, determined by calculating values for the different regions of the molecule [98].

There is an arbitrary scale from 0 to 20 depicting the HLB balance of a surfactant. Products with low HLB are more soluble in oil. High HLB represents good water solubility. HLB values can determine surfactant suitability as follows [99]:

–Anti–foaming agent	(HLB = 0 – 3)
–Emulsifying agent w/o	(HLB = 4 – 6)
–Wetting/spreading agent	(HLB = 7 – 9)
–Emulsifying agent o/w	(HLB = 8 – 18)
–Detergent	(HLB = 13 – 15)
–Solubilizing agent	(HLB = 10 – 18)

I.4.b Critical micelle concentration

After saturation of the liquid surface with surfactant molecules, any excess will be distributed in the bulk of the solution. At low temperature the solution looks like any other, solute distributed randomly throughout the water [100]. However, when the concentration gets enough, the molecules begin to arrange themselves in hollow spheres, rods and disks called *micelles.* Critical Micelle Concentration (CMC), organic chain length and polar head of surfactant, temperature and pressure of synthesis play important roles in mesostructure formation, see Figure I.6. Some factors affecting critical micelle concentration in case of polar solvents (*e.g.* water) are:

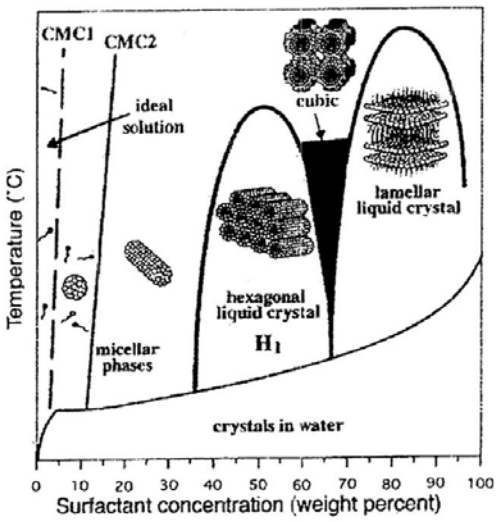

Figure I.6 Mesostructures depending on CMC value and temperature.

- Increased length of hydrocarbon chain: minor interaction with water facilitates the transfer from an aqueous phase to micelles and produces a decrease in CMC.
- Increased polarity of the polar portion: greater interaction with water retards the transfer from an aqueous phase to micelles and produces an increase in CMC.

I.4.c Nanostructure formation

Many nanostructures can be synthesized by using different surfactants as structure templates. The self–assembly characteristic of surfactants can yield various nanostructures such as micelle, inverse micelle, lamellar bilayer, bilayer vesicle, hexagonal or inverse hexagonal [101, 102]. In addition many research groups have described other possible mesostructures like rod–like or worm–like [46, 103].

Figure I.7 schematically depicts the six more relevant mesostructures discussed in this memory, these are: lamellar, micelles, worm–like, vesicle, rod and hexagonal. The structure type depends on the CMC value. It is possible to obtain mesostructured silica materials with the shown nanostructures by using surfactants, detergents or phospholipids.

To date, the main focus in the study of calcium phosphates as bioceramics has been bioactivity (HA) and resorption (α–TCP, β–TCP…). Nevertheless, a designed mesostructure would be useful to achieve new functions, such as the confinement and controlled release of biologically active molecules and the possibility of functionalization [104].

Due to the self–assembly feature of surfactants and phospholipids in water, various nanostructures can be synthesized in presence of inorganic materials such as silica and calcium phosphate [38, 105, 106].

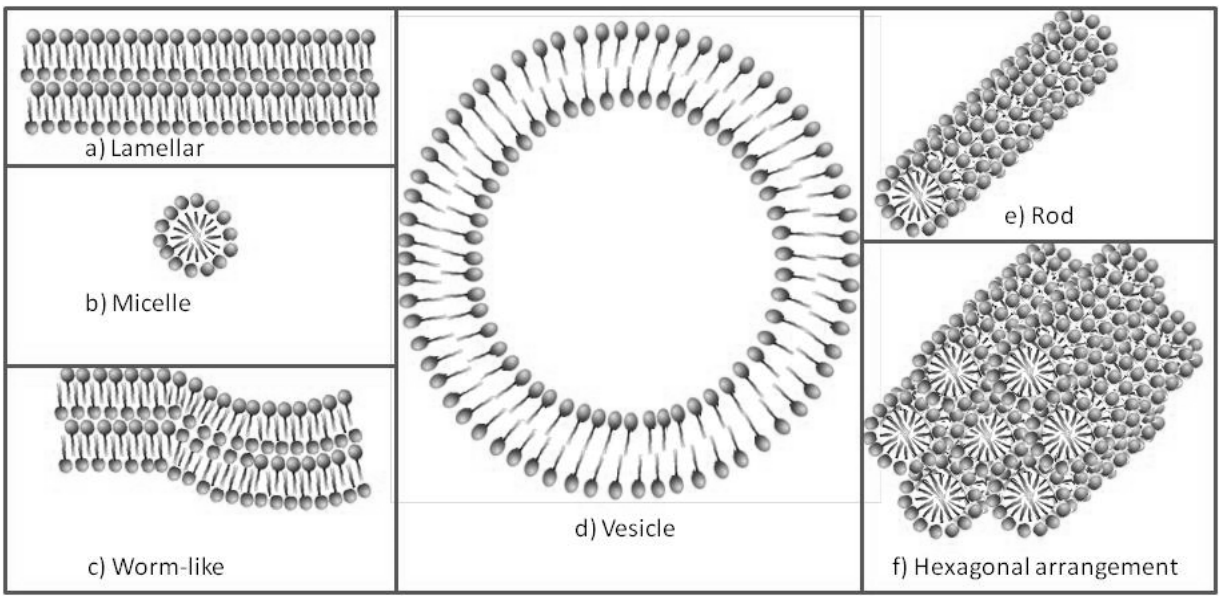

Figure I.7 Six possible nanostructure formations of surfactants in aqueous solution.

I.5 Synthesis of mesostructured hybrid materials

Nowadays, organic–inorganic hybrid materials are synthesized in porous form for bone regeneration, tissue engineering and drug delivery. The mechanical requirements of prostheses, however, severely restrict the use of low–strength porous ceramics to non–load bearing applications. Studies reviewed by *Hench* and *Ethridge* [4], *Swain et al*. [107], and *Chen et al*. [108] have shown that when load bearing is not a primary requirement, porous ceramics can provide a functional implant. Mesostructured porous scaffolds can display several advantages such as: *(i)* Improving control over sustained delivery of therapeutic agents, signaling biomolecules and pluripotent stem cells, *(ii)* Introducing porosity and/or improving the mechanical properties of bulk scaffolds by acting as porogen or reinforcement phase, *(iii)* supplying compartmentalized nano–reactors for specific biochemical process, functioning as cell delivery vehicle, *(iv)* possibility of preparing injectable and/or moldable formulations to be applied by using minimally invasive surgery [109].

Mesostructured hybrid materials can be synthesized by different chemical methods such as sol–gel, precipitation or evaporation induced self-assembly (EISA). The goal is to obtain an inorganic mesophase by directing agents using these chemical methods. In this memory, sol–gel and precipitation methods were selected to synthesize crystalline CaP with mesostructure and the modified Stöber method to synthesize mesoporous silica nanospheres.

I.6 Sol–gel processing of bioceramics

The sol–gel process is a chemical synthesis where an oxide network is formed by polymerization reactions of chemical precursors dissolved in a liquid medium. It was initially used for the preparation of inorganic materials such as glasses and ceramics at relatively low temperatures. The most common precursors for forming colloidal suspensions are metal alkoxides, which consist of a metal or metalloid element (Si, Al, Zr, Sn…) bonded to various alkoxide groups. Hydrolysis and condensation and direct condensation of metal alkoxides form large metal oxide molecules [110, 111].

The sol–gel chemical process may be described as: "Formation of an oxide network through polycondensation reactions of a molecular precursor in a liquid solution". A *sol* is a stable dispersion of colloidal particles or polymers in a solvent. The particles may be amorphous or crystalline. An aerosol is formed by particles in a gas phase, while a sol is particles in a liquid. A *gel* consists of a

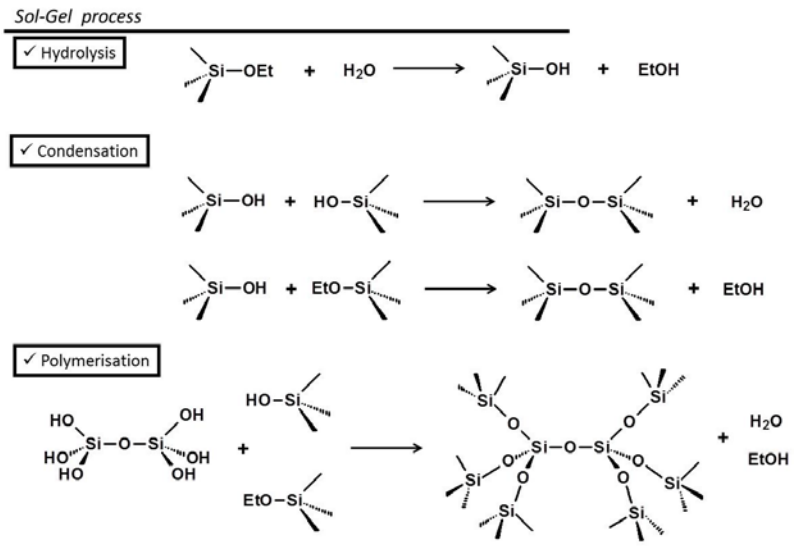

Figure I.8 Sol–gel process to obtain SiO_2 takes place in three steps: hydrolysis, condensation and polymerisation.

three dimensional continuous network, which encloses a liquid phase; in a colloidal gel, the network is built from an agglomeration of colloidal particles. In a polymer gel the particles have a polymeric sub−structure made by aggregates of sub−colloidal particles. Generally speaking, the *sol* particles interact by van der Waals forces or hydrogen bonds. A *gel* may also be formed from linking polymer chains. In most *gel* systems used for materials synthesis, the interactions are of a covalent nature and the gel process is irreversible. The gelation process may be reversible if other interactions are involved. The sol−gel process to obtain SiO_2 is schematically shown in Figure I.8.

In summary, the sol–gel process involves the generation of colloidal suspensions (*sols*) of solid particles in a liquid. One of the main features of the sol–gel process regarding CaPs is that the hydroxyapatite layer can be obtained as a homogenous matrix. During the process, these colloids are converted to viscous *gels* (gelation) and then to solid materials (ageing). In this memory, this process was used to synthesize HA for coating silica mesoporous nanospheres.

I.7 Nanoparticles

Nanoparticles (NPs) are generally acknowledged as particles with dimensions below 100 nm. However, the term nanoparticles is also used when dealing with particles with diameters between 100−300 nm. From a purely physical perspective, nanoparticles are small enough to interface with objects that control some of the most basic cellular function (e.g. ~2 nm diameter DNA). In comparison, cells are much larger (average diameter ~10 μm). Moreover, their small size allows them to interface with existing microelectronic components, such as field effect transistors, enabling the development of diagnostic biosensors. Some of the uses of NPs in biology and medicine include: drug delivery, gene delivery systems in gene therapy, genetic and tissue engineering etc. In addition, NPs are also interesting biomaterials because of their unique, size−dependent physical properties. For example, semiconductor quantum dots and gold NPs produce optical responses that are not evident in bulk materials. Iron oxide particles display a different type of magnetism when presented as NPs than when presented as microparticles or in bulk. These properties originate from different principles, but are all derived from the size of the material, which lies between bulk and atomic scales. Because of these interesting properties, NPs have found application as contrast agents in biomedical imaging, signaling molecules that enhance diagnostic ability, carriers for drug delivery, and as therapeutic agents [112].

As above mentioned, CaP has excellent biocompatibility due to its chemical similarity to human hard tissue (bone and teeth). Moreover, in nanoparticulate dispersed form, it can be used as a carrier in biological systems, e.g. to transfer nucleic acids or drugs. CaP NPs have gained increasing interest in medicine thanks to their high biocompatibility and good biodegradability. Therefore, they complement typical nanoparticulate systems which are used in medicine, e.g. polymers, metallic nanoparticles (like gold), iron oxide NPs (like magnetite) and quantum dots (like CdS). The preparation of CaP NPs can be conveniently carried out from aqueous solutions, provided that a suitable functionalization agent is used, e.g. a polymer or a charged adsorbing molecule. In the reference [113], a number of applications where calcium phosphate nanoparticles were successfully applied in biological systems is highlighted.

I.8 Objectives and distribution of the Memory

The fact that bone calcium phosphates are carbonated nanoapatites, deficient in calcium and with large number of structural defects that are placed in the cavities that leave the collagen fibres, has made many authors consider to obtain mesostructure, mainly nanohydroxyapatite, by strategies similar to those used for obtaining mesoporous silica materials using amphiphilic molecules which act as a template. The effort has result in little success since the chemistry of essentially ionic compounds, such as calcium phosphates, is far from the chemistry of essentially covalent compounds as silica, and the relationship that is established between the surfactants used as structure directing agents and the ions calcium and phosphate is much different than with the silica. However, in the world of biomaterials science new materials are becoming more necessary tailored for specific clinical applications.

The first main objective of this thesis has been to investigate the synthesis of CaPs in the presence of different types of ionic surfactants, pure and mixtures, and in the presence of different concentrations of phosphatidylcholine, trying to obtain mesostructured CaPs (Chapters II and II). The second essential objective has been to investigate the synthesis of CaPs in the presence of mesoporous silica nanospheres to obtain *core@shell* systems of the type mesoporous silica@hydroxyapatite (Chapters IV and V). This multiple approach was attempted to show if it is possible to obtain CaPs with controlled mesostructure. To attain these aims different synthetic strategies have been used and are described in the memory together with the characterization of the obtained bioceramics.

This initial introduction ***Chapter I*** has presented the background and current status of the subject matter.

Chapter II addresses the synthesis and characterization of CaPs in the presence of various ionic surfactants, pure and mixture of them, aimed to behave as structure directing agents. The investigated surfactants were: sodium dodecyl sulphate (SDS), sodium dodecyl benzene sulphonate (SDBS), cetyltrimethyl ammonium bromide (CTAB) and mono-n-dodecyl phosphate (MAP). Moreover, EMPIGEN®BB detergent (EPG), a zwitterionic surfactant, was tested as mesostructure template for the first time as an alternative approach. Surfactants in water can be organized in different mesostructures such as micellar, lamellar, hexagonal or cubic. Synthesis conditions and surfactants have been optimized looking for interactions with the precipitated CaP, *i.e.*, to obtain materials with mesostructural characteristics different to materials prepared in the absence of surfactant.

In ***Chapter III*** we aimed at synthesizing HA based hybrids with a sponge-like mesostructure via precipitation of CaP in the presence of three phospholipid (PL) sources with substantially different contents of phosphatidylcholine (PC): asolectin 33%, lecithin 60% and lipoid 94% of PC. The different structures of the nanohybrids as a function of the synthesis conditions, pH of solution (basic or neutral) and Ca/P molar ratio (1.0 or 1.67) and concentration of PC, were investigated. In this case, given the biocompatibility of PLs, it arises the synthesis of CaP-PLs hybrids, *i.e.*, PLs were not removed from the final material. The new CaP-PLs hybrid materials were characterized and the mechanisms of formation for the nanostructured materials were proposed.

Given the difficulty found in the previous chapters to obtain CaP systems as ordered mesoporous materials, in ***Chapter IV*** various strategies were investigated to obtain CaP coatings, namely HA, on mesoporous silica nanospheres (MSNSs) with MCM-41 structure. In this case our approach implies the use of a well-defined mesoporous material as the basis of the final nanosystem. The purpose of this study was to design multifunctional *core@shell* nanoparticles that can be applied in bone regeneration, as well as specific intracellular carriers of drugs, proteins or agents for image, which could be used for applications such as the treatment of cancer. The nanospheres coated by CaP would exhibit well interconnected pore structures and excellent *in vitro* bioactivity that made them useful for several biomedical applications. For instance, an HA coating could act as a nanogate allowing the controlled release of the biomolecules enclosed in the silica mesopores under specific conditions, for instance a pH decrease. The attempted approaches to obtain MSNSs coated by CaPs were: *(i)* co-synthesis of CaP and MSNSs, *(ii)* soaking and *(iii)* wetting MSNSs in a sol precursor of CaP, and *(iv)* functionalization of MSNSs with organic moieties containing phosphate-like groups to facilitate the CaP coating after wetting them into a sol precursor of CaP. Except in the first approach, in which both processes are simultaneous, the synthesis of materials is performed in two steps: *(1)* the synthesis of MSNSs ranging 150-250 nm of diameter and around 2 nm of pore diameter and *(2)* the step to coat MSNSs with CaP.

An improvement of these systems is dealt with in ***Chapter V***, where the subject investigated is the coating of MSNSs with HA doped with europium as fluorescent element via the precipitation of fluorescent CaP on previously synthetized MSNSs, which would give greater visibility and traceability of the nanosystem during the biological application, such as cell trafficking or tumour localization.

Chapter VI summarizes the principal conclusions derived from this thesis. Finally, the general conditions and detailed experimental work, as well as structural characterization and analysis techniques employed, are included in ***Chapter VII*** of this report.

I.9 References:

1. J. A. Planell, *Bone Repair Biomaterials. ISBBN 978-1-84569-385-5*. **2009**: Woodhead Publishing Ltd. 478 pp.

2. S. Deb. *Calcium phosphate cements*. **2013**: Imperial College Press.

3. T. J. Keane, S. F. Badylak. *Semin. Pediat. Surg.* **2014**, *23*, 112-8. Biomaterials for tissue engineering applications.

4. LL. Hench, E.C. Ethridge, *Biophysics and Bioengineering Series, Vol. 4: Biomaterials: An Interfacial Approach*. **1982**: Academic Press. 385 pp.

5. D.F. Williams. *Elsevier* **1987**, 72. Definitions in Biomaterials.

6. B. D. Ratner, A. S. Hoffman, F. J. Schoen, J. E. Lemons. *Elsevier Academic Press* **2004**, 162. Biomaterials science: an Introduction to materials in medicine, 2nd Edition.

7. S. Sánchez-Salcedo, D. Arcos, M. Vallet-Regí. *Key Eng. Mat.* **2008**, *377*, 19-42. Upgrading calcium phosphate scaffolds for tissue engineering applications.

8. F. He, F. Yang, J. Zhu, Y. Peng, X. Tian, X. Chen. *J. Am. Ceram. Soc.* **2015**, *98*, 223-228. Fabrication of a novel calcium carbonate composite ceramic as bone substitute.

9. A. J. Salinas, M. Vallet-Regí. *Z. Anorg. Allg. Chem.* **2007**, *633*, 1762-1773. Evolution of ceramics with medical applications.

10. Y. Xiao, Q. Yin, L. Wang, C. Bao. *Ceram. Int.* **2015**, *41*, 995-1003. Macro-porous calcium phosphate scaffold with collagen and growth factors for periodontal bone regeneration in dogs.

11. F. Stergioudi, A. Choleridis, E. Paulidou, E. Smyrnaios, N. Michailidis. *Ceram. Int.* **2015**, *41*, 3822-3832. Novel production and characterization of porous calcium phosphate suitable for bone tissue engineering applications.

12. M. Iafisco, S. Sprio, M. Sandri, S. Panseri, G. Filardo, E. Kon, M. Marcacci, A. Tampieri. *Woodhead Publ. Ser. Biomater.* **2014**, *76*, 249-280. Composite biomedical foams for engineering bone tissue.

13. A. H. Choi, J. P. Matinlinna, G. Heness, B. Ben-Nissan. *Nanocomposites for biomedical and dental applications*. **2014**: Handbook of Functional Nanomaterials.

14. B. D. Ratner, A. S. Hoffman, F. J. Schoen, J. E. Lemons. *Elsevier Academic Press* **2013**, p. 25. Biomaterials science: An evolving, multidisciplinary endeavor 3rd edition.

15. M. Iafisco, B. Palazzo, T. Ito, M. Otsuka, M. Senna, J. M. Delgado-Lopez, J. Gomez-Morales, A. Tampieri, M. Prat, L. Rimondini. *J. Mater. Sci.: Mater. Med.* **2012**, *23*, 2659-2669. Preparation of core-shell poly(l-lactic) acid-nanocrystalline apatite hollow microspheres for bone repairing applications.

16. N. Pramanik, T. Imae. *Langmuir* **2012**, *28*, 14018-14027. Fabrication and characterization of dendrimer-functionalized mesoporous hydroxyapatite.

17. M. Vallet-Regí, J. M. Gonzalez-Calbet. *Prog. Solid State Chem.* **2004**, *32*, 1-31. Calcium phosphates as substitution of bone tissues.

18. I. Izquierdo-Barba, M. Colilla, M. Manzano, M. Vallet-Regí. *Micropor. Mesopor. Mat.* **2010**, *132*, 442. In vitro stability of SBA-15 under physiological conditions.

19. M. Iafisco, G. B. Ramirez-Rodriguez, Y. Sakhno, A. Tampieri, G. Martra, J. Gomez-Morales, J. M. Delgado-Lopez. *Cryst. Eng. Comm.* **2015**, *17*, 507-511. The growth mechanism of apatite nanocrystals assisted by citrate: relevance to bone biomineralization.

20. A. J. Salinas, M. Vallet-Regí. *RSC Adv.* **2013**, *3*, 11116-11131. Bioactive ceramics: from bone grafts to tissue engineering.

21. I. Izquierdo-Barba, A. J. Salinas, M. Vallet-Regi. *Int. J. Appl. Glass Sci.* **2013**, *4*, 149-161. Bioactive glasses: from macro to nano.

22. V. Q. Le, A. Cochis, L. Rimondini, G. Pourroy, V. Stanic, H. Palkowski, A. Carrado. *RSC Adv.* **2013**, *3*, 11255-11262. Biomimetic calcium-phosphates produced by an auto-catalytic route on stainless steel 316L and bio-inert polyolefin.

23. S. Prieto, A. Shkilnyy, C. Rumplasch, A. Ribeiro, F. J. Arias, J. C. Rodriguez-Cabello, A. Taubert. *Biomacromolecules* **2011**, *12*, 1480-1486. Biomimetic calcium phosphate mineralization with multifunctional elastin-like recombinamers.

24. N. Roveri, M. Iafisco. *Nanotechnol. Sci. Appl.* **2010**, *3*, 107-125. Evolving application of biomimetic nanostructured hydroxyapatite.

25. X. Li, Y. Chen, M. Wang, Y. Ma, W. Xia, H. Gu. *Biomaterials* **2013**, *34*, 1391-1401. A mesoporous silica nanoparticle - PEI - Fusogenic peptide system for siRNA delivery in cancer therapy.

26. S. V. Dorozhkin. *J. Mater. Sci.* **2007**, *42*, 1061-1095. Calcium orthophosphates.

27. L. Podaropoulos, A. A. Veis, S. Papadimitriou, C. Alexandridis, D. Kalyvas. *J Oral Implantol* **2009**, *35*, 28-36. Bone regeneration using beta-tricalcium phosphate in a calcium sulfate matrix.

28. R. Palanivelu, A. M. Saral, A. R. Kumar. *Spectrochim. Acta, Part A* **2014**, *131*, 37-41. Nanocrystalline hydroxyapatite prepared under various pH conditions.

29. K. Lin, C. Wu, J. Chang. *Acta Biomater.* **2014**, *10*, 4071-4102. Advances in synthesis of calcium phosphate crystals with controlled size and shape.

30. P. Pokale, S. Shende, A. Gade, M. Rai. *Environ. Chem. Lett.* **2014**, *12*, 393-399. Biofabrication of calcium phosphate nanoparticles using the plant Mimusops elengi.

31. T. Konishi, M. Honda, T. Yoshioka, S. Hayakawa, M. Aizawa. *J. Biomimetics, Biomater. Biomed. Eng.* **2014**, *20*, 113-118, 7 pp. Preparation of α-tricalcium phosphate powders surface-modified with inositol phosphate for cement fabrication.

32. M. A. Miller, M. R. Kendall, M. K. Jain, P. R. Larson, A. S. Madden, A. C. Tas. *Ceram. Eng. Sci. Proc.* **2014**, *34*, 77-91. Maturation of brushite ($CaHPO_4{\cdot}2H_2O$) and in situ crystallization of brushite micro-granules.

33. K. A. Gross, E. Rozite. *J. Biomimetics, Biomater. Biomed. Eng.* **2014**, *20*, 93-98, 7 pp. Synthesis of tetracalcium phosphate at reduced temperatures.

34. S. C. Cox, P. Jamshidi, L. M. Grover, K. K. Mallick. *J. Mater. Sci.: Mater. Med.* **2014**, *25*, 37-46. Low temperature aqueous precipitation of needle-like nanophase hydroxyapatite.

35. M. Aizawa, H. Ueno, K. Itatani, I. Okada. *J. Eur. Ceram. Soc.* **2006**, *26*, 501-507. Syntheses of calcium-deficient apatite fibres by a homogeneous precipitation method and their characterizations.

36. H. Zhang, Y. Wang, Y. Yan, S. Li. *Ceram. Int.* **2003**, *29*, 413-418. Precipitation of biocompatible hydroxyapatite whiskers from moderately acid solution.

37. M. Vallet-Regí, L. M. Rodriguez-Lorenzo, A. J. Salinas. *Solid State Ionics* **1997**, *101-103*, 1279-1285. Synthesis and characterization of calcium deficient apatite.

38. N. Kawa, Y. Oumi, T. Kimura, T. Ikeda, T. Sano. *J. Mater. Sci.* **2008**, *43*, 4198-4207. Synthesis of lamellar mesostructured calcium phosphates using n-alkylamines as structure-directing agents in alcohol/water mixed solvent systems.

39. E. Bouyer, F. Gitzhofer, M. I. Boulos. *J. Mater. Sci.: Mater. Med.* **2000**, *11*, 523-531. Morphological study of hydroxyapatite nanocrystal suspension.

40. Y. Zhang, J. Lu, J. Wang, S. Yang, Y. Chen. *J. Cryst. Growth* **2009**, *311*, 4740-4746. Synthesis of nanorod and needle-like hydroxyapatite crystal and role of pH adjustment.

41. W. P. S. L. Wijesinghe, M. M. M. G. P. G. Mantilaka, E. V. A. Premalal, H. M. T. U. Herath, S. Mahalingam, M. Edirisinghe, R. P. V. J. Rajapakse, R. M. G. Rajapakse. *Mater. Sci. Eng. C.* **2014**, *42*, 83-90. Facile synthesis of both needle-like and spherical hydroxyapatite nanoparticles: Effect of synthetic temperature and calcination on morphology, crystallite size and crystallinity.

42. Q. Sun, J-.T. Lou, F. Kang, J-. F. Chen, J-. X. Wang. *Powder Technol.* **2014**, *261*, 49-54. Facile preparation of hydroxyapatite nanotubes assisted by needle-like calcium carbonate.

43. M. Iafisco, F. M. Di, S. Bonora, M. Prat, N. Roveri. *Dalton Trans.* **2011**, *40*, 820-827. Adsorption and spectroscopic characterization of lactoferrin on hydroxyapatite nanocrystals.

44. S. V. Dorozhkin, M. Epple. *Angew. Chem., Int. Ed.* **2002**, *41*, 3130-3146. Biological and medical significance of calcium phosphates.

45. R. A. Perez, S. H. Shin, C. M. Han, H. W. Kim. *Tissue Eng. Regener. Med.* **2015**, Ahead of Print. Bone-bioactive injectables based on calcium phosphates for the delivery of drugs and cells in hard tissue engineering: A recent update.

46. F. Ye, H. Guo, H. Zhang. *Nanotechnology* **2008**, *19*, 245605. Biomimetic synthesis of oriented hydroxyapatite mediated by nonionic surfactants.

47. M. Houmard, Q. Fu, E. Saiz, A. P. Tomsia. *J. Mater. Sci. Mater. M.* **2012**, *23*, 921-930. Sol-gel method to fabricate CaP scaffolds by robocasting for tissue engineering

48. J. Chen, Y. Wang, X. Chen, L. Ren, C. Lai, W. He, Q. Zhang. *Mater. Lett.* **2011**, *65*, 1923-1926. A simple sol-gel technique for synthesis of nanostructured hydroxyapatite, tricalcium phosphate and biphasic powders.

49. B. H. Fellah, P. Layrolle. *Acta Biomater* **2009**, *5*, 735-742. Sol-gel synthesis and characterization of macroporous calcium phosphate bioceramics containing microporosity.

50. C. H. Duan, J. X. Wang, S. B. Zhou, B. Feng, X. Lu, S. X. Qiu, J. Weng. *Adv. Appl. Ceram.* **2010**, *109*, 111-116. Study on liquid phase sintering of calcium phosphate.

51. B. D. Ratner, A. S. Hoffman, F. J. Schoen, J. E. Lemons. *Elsevier Academic Press* **2013**, 162. Biomaterials science 3rd Edition: Natural and Synthetic hydroxyapatites.

52. A. Galarneau, G. Renard, M. Mureseanu, A. Tourrette, C. Biolley, M. Choi, R. Ryoo, F. R. Di, F. Fajula. *Micropor. Mesopor. Mater.* **2007**, *104*, 103-114. Synthesis of sponge mesoporous silicas from lecithin/dodecylamine mixed-micelles in ethanol/water media: A route towards efficient biocatalysts.

53. J. P. Maity, T.-J. Lin, H. P.-H. Cheng, C.-Y. Chen, A. S. Reddy, S. B. Atla, Y.-F. Chang, H.-R. Chen, C.-C. Chen. *Int. J. Mol. Sci.* **2011**, *12*, 3821-3830. Synthesis of brushite particles in reverse microemulsions of the biosurfactant surfactin.

54. A. J. Salinas, M. Vallet-Regí. *Key Eng. Mat.* **2009**, *391*, 141-158. The sol-gel production of bioceramics.

55. M. Iafisco, B. Palazzo, G. Falini, F. M. Di, S. Bonora, S. Nicolis, L. Casella, N. Roveri. *Langmuir* **2008**, *24*, 4924-4930. Adsorption and conformational change of myoglobin on biomimetic hydroxyapatite nanocrystals functionalized with alendronate.

56. M. Iafisco, J. M. Delgado-Lopez, E. M. Varoni, A. Tampieri, L. Rimondini, J. Gomez-Morales, M. Prat. *Small* **2013**, *9*, 3834-3844. Cell surface receptor targeted biomimetic apatite nanocrystals for cancer therapy.

57. M. Iafisco, M. Sandri, S. Panseri, J. M. Delgado-Lopez, J. Gomez-Morales, A. Tampieri. *Chem. Mater.* **2013**, *25*, 2610-2617. Magnetic Bioactive and Biodegradable Hollow Fe-Doped Hydroxyapatite Coated Poly(l-lactic) Acid Micro-nanospheres.

58. A. Doat, F. Pelle, A. Lebugle. *J. Solid State Chem.* **2005**, *178*, 2354-2362. Europium-doped calcium pyrophosphates: Allotropic forms and photoluminescent properties.

59. R. Ternane, M. T. Cohen-Adad, G. Panczer, C. Goutaudier, C. Dujardin, G. Boulon, N. Kbir-Ariguib, M. Trabelsi-Ayedi. *Solid State Sci.* **2002**, *4*, 53-59. Structural and luminescent properties of new Ce^{3+} doped calcium borophosphate with apatite structure.

60. M. Mehnaoui, R. Ternane, G. Panczer, M. Trabelsi-Ayadi, G. Boulon. *J. Phys. Condens. Matter.* **2008**, *20*, 275227/1-275227/6. Structural and luminescent properties of new Pb^{2+}-doped calcium chlorapatites $Ca_{(10-x)}Pb_x(PO_4)_6.Cl_2$ ($0 \leq x \leq 10$).

61. M. Neumeier, A. L. Hails, A. S. Davis, S. Mann, M. Epple. *J. Mater. Chem.* **2011**, *21*, 1250-1254. Synthesis of fluorescent core-shell hydroxyapatite nanoparticles.

62. S. P. Mondejar, A. Kovtun, M. Epple. *J. Mater. Chem.* **2007**, *17*, 4153-4159. Lanthanide-doped calcium phosphate nanoparticles with high internal crystallinity and with a shell of DNA as fluorescent probes in cell experiments.

63. R. K. Singh, T-. H. Kim, K. D. Patel, C. Mahapatra, K. Dashnyam, M. S. Kang, H-. W. Kim. *J. Am. Ceram. Soc.* **2014**, *97*, 3071-3076. Novel hybrid nanorod carriers of fluorescent hydroxyapatite shelled with mesoporous silica effective for drug delivery and cell Imaging.

64. H. Liu, F. Chen, P. Xi, B. Chen, L. Huang, J. Cheng, C. Shao, J. Wang, D. Bai, Z. Zeng. *J. Phys. Chem. C.* **2011**, *115*, 18538-18544. Biocompatible fluorescent hydroxyapatite: synthesis and live cell Imaging applications.

65. W. Wang, D. Shi, J. Lian, Y. Guo, G. Liu, L. Wang, R. C. Ewing. *Appl. Phys. Lett.* **2006**, *89*, 183106/1-183106/3. Luminescent hydroxylapatite nanoparticles by surface functionalization.

66. A. Doat, M. Fanjul, F. Pelle, E. Hollande, A. Lebugle. *Biomaterials* **2003**, *24*, 3365-3371. Europium-doped bioapatite: a new photostable biological probe, internalizable by human cells.

67. F. Chen, Y.- J. Zhu, K.- H. Zhang, J. Wu, K.-W. Wang, Q.-L. Tang, X.- M. Mo. *Nanoscale Res. Lett.* **2011**, *6*, 67-69. Europium-doped amorphous calcium phosphate porous nanospheres: preparation and application as luminescent drug carriers.

68. A. Lebugle, F. Pelle, C. Charvillat, I. Rousselot, J. Y. Chane-Ching. *Chem. Commun.* **2006**, *6*, 606-608. Colloidal and monocrystalline Ln^{3+} doped apatite calcium phosphate as biocompatible fluorescent probes.

69. A. Doat, F. Pelle, N. Gardant, A. Lebugle. *J. Solid State Chem.* **2004**, *177*, 1179-1187. Synthesis of luminescent bioapatite nanoparticles for utilization as a biological probe.

70. S. Wang. *Micropor. Mesopor. Mater.* **2008**, *117*, 1-9. Ordered mesoporous materials for drug delivery.

71. A. Taguchi, F. Schueth. *Micropor. Mesopor. Mater.* **2004**, *77*, 1-45. Ordered mesoporous materials in catalysis.

72. B. J. Scott, G. Wirnsberger, G. D. Stucky. *Chem. Mater.* **2001**, *13*, 3140-3150. Mesoporous and mesostructured materials for optical applications.

73. M. Hartmann. *Chem. Mater.* **2005**, *17*, 4577-4593. Ordered Mesoporous Materials for Bioadsorption and Biocatalysis.

74. H. H. P. Yiu, P. A. Wright. *J. Mater. Chem.* **2005**, *15*, 3690-3700. Enzymes supported on ordered mesoporous solids: a special case of an inorganic-organic hybrid.

75. M. Vallet-Regí, A. Ramila, R. P. del Real, J. Perez-Pariente. *Chem. Mater.* **2001**, *13*, 308-311. A new property of MCM-41: drug delivery system.

76. J . Jinhua, F. Yong, Z. Lirong, Y. Hong, C. Yanli, Z. Dazhou, Z. Ping. *J. Mater. Sci.* **2011**, *46*, 3828-3834. Synthesis and characterization of multi-lamellar mesostructured hydroxyapatites using a series of fatty acids.

77. M. Manzano, M. Vallet-Regí. *Prog. Solid State Ch.* **2012**, *40*, 17-30. Revisiting bioceramics: bone regenerative and local drug delivery systems.

78. M. Vallet-Regí, D. Arcos. *Curr. Nanosci.* **2006**, *2*, 179-189. Nanostructured hybrid materials for bone tissue regeneration.

79. M. Vallet-Regí. *Materialwiss. Werkst.* **2006**, *37*, 478-484. Bone repair and regeneration: possibilities.

80. S. Mann. *Oxford University Press* **2001**. Biomineralization: principles and concepts in bioinorganic materials chemistry.

81. F. Schueth. *Chem. Mater.* **2001**, *13*, 3184-3195. Non-siliceous mesostructured and mesoporous materials

82. M. Vallet-Regí, M. Vila. *Key Eng. Mat.* **2010**, 392. Advanced bioceramics in nanomedicine and tissue engineering.

83. C. Brinker, G. Scherer, *Sol-Gel Science: The Physics and Chemistry of Sol-Gel Processing*. 1990: Academic press, Inc. Chapter 3: "Hydrolysis and Condensation II: Silicates".

84. W. Stöber, A. Fink, E. Bohn. *J. Colloid Interf. Sci.* **1968**, *26*, 62. Controlled growth of monodisperse silica spheres in the micron size range.

85. C. J. Brinker, Y. Lu, A. Sellinger, H. Fan. *Adv. Mater.* **1999**, *11*, 579-585. Evaporation-induced self-assembly. Nanostructures made easy

86. A. López-Noriega, D. Arcos, I. Izquierdo-Barba, Y. Sakamoto, O. Terasaki, M. Vallet-Regí. *Chem. Mater.* **2006**, *18*, 3137-3144. Ordered mesoporous bioactive glasses for bone tissue regeneration.

87. C. Vaid, S. Murugavel, C. Das, S. Asokan. *Micropor. Mesopor. Mater.* **2014**, *186*, 46-56. Mesoporous bioactive glass and glass-ceramics: Influence of the local structure on in vitro bioactivity.

88. F. Hoffmann, M. Cornelius, J. Morell, M. Fröba. *Angew. Chem., Int. Ed.* **2006**, *45*, 3216-3251. Silica-based mesoporous organic-inorganic hybrid materials.

89. M. J. Rosen, J. T. Kunjappu. *John Wiley & Sons* **2012**, 600. Surfactants and interfacial phenomena (4th ed.).

90. M. J. Scott, M. N. Jones. *Biochimica et Biophysica Acta (BBA) - Biomembranes* **2000**, *1508*, 235-251. The biodegradation of surfactants in the environment.

91. K.-O. Choi, H. P. Aditya, S. Ko. *Food Chemistry* **2014**, *147*, 239-244. Effect of aqueous pH and electrolyte concentration on structure, stability and flow behavior of non-ionic surfactant based solid lipid nanoparticles.

92. K. Narumi. *Setchaku no Gijutsu* **2010**, *30*, 51-59. Outline of surface active agents: application for dispersion (selection of dispersants).

93. J. Eastoe, *Blackwell Publishing Ltd.*, in *Colloid Science*. **2009**, Surfactant Aggregation and Adsorption at Interfaces. p. 50-76.

94. D. C. Cullum. *Blackie*. **1994**: Surfactant types; classification, identification, separation.

95. J. Texter. *Carl Hanser Verlag*. **1999**: Characterization of surfactants.

96. R. J. Farn. *Blackwell Publishing* **2006**. Chemistry and technology of surfactants.

97. J. T. Davies. *Proc. Int. Congr. Surf. Act., 2nd* **1957**, *1*, 426-438. A quantitative kinetic theory of emulsion type. I. Physical chemistry of the emulsifying agent.

98. W. C. Griffin. *J. Soc. Cosmet. Chem.* **1954**, *5*, 249. Calculation of HLB values of non-Ionic surfactants.

99. W. C. Griffin. *J. Soc. Cosmet. Chem.* **1949**, *1*, 311. Classification of surface-active agents by 'HLB'.

100. N. J. Phillips, M. A. Kelland. *Spec. Publ. - R. Soc. Chem.* **1999**, *230*, 244-259. The application of surfactants in preventing gas hydrate formation.

101. J. H. Collier, P. B. Messersmith. *Annu. Rev. Mater. Res.* **2001**, *31*, 237-263. Phospholipid strategies in biomineralization and biomaterials research.

102. S. Zhang, Y. Wang, K. Wei, X. Liu, J. Chen, X. Wang. *Mater. Lett.* **2007**, *61*, 1341-1345. Template-assisted synthesis of lamellar mesostructured hydroxyapatites.

103. S. A. Bagshaw., E. Prouzet., T. J. Pinnavaia. *Science (Washington, D. C.)* **1995**, *269*, 1242-1244. Templating of mesoporous molecular sieves by nonionic polyethylene oxide surfactants.

104. J. B. Park, J. D. Bronzino. *CRC Press* **2003**. Biomaterials: principles and applications.

105. M. S. Schmidt, J. McDonald, E. T. Pineda, A. M. Verwilst, Y. Chen, R. Josephs, A. E. Ostafin. *Micropor. Mesopor. Mater.* **2006**, *94*, 330-338. Surfactant based assembly of mesoporous patterned calcium phosphate micron-sized rods.

106. Q. Huo, D. I. Margolese, U. Ciesla, D. G. Demuth, P. Feng, T. E. Gier, P. Sieger, A. Firouzi, B. F. Chmelka, al et. *Chem. Mater.* **1994**, *6*, 1176-1191. Organization of organic molecules with Inorganic molecular species into nanocomposite biphase arrays.

107. S. K. Swain, S. Bhattacharyya, D. Sarkar. *Mater. Res. Bull.* **2015**, *64*, 257-261. Fabrication of porous hydroxyapatite scaffold via polyethylene glycol-polyvinyl alcohol hydrogel state.

108. Z. C. Chen, X. L. Zhang, K. Zhou, H. Cai, C. Q. Liu. *Adv. Appl. Ceram.* **2015**, *114*, 183-187. Novel fabrication of hierarchically porous hydroxyapatite scaffolds with refined porosity and suitable strength.

109. M. Iafisco, B. Palazzo, G. Martra, N. Margiotta, S. Piccinonna, G. Natile, V. Gandin, C. Marzano, N. Roveri. *Nanoscale* **2012**, *4*, 206-217. Nanocrystalline carbonate-apatites: role of Ca/P ratio on the upload and release of anticancer platinum bisphosphonates.

110. D. Zhao, Y. Wan, W. Zhou. *Wiley-Vch.* **2013**, *517*. Ordered mesoporous materials.

111. F. T. C. Moreira, A. P. Moreira-Tavares, M. G. F. Sales. *Curr. Top. Med. Chem.* **2015**, *15*, 245-255. Sol-Gel-Based Biosensing Applied to Medicinal Science.

112. B. D. Ratner, A. S. Hoffman, F. J. Schoen, J. E. Lemons. *Elsevier Academic Press* **2013**, pg:368. Biomaterials science: An Introduction to Materials in Medicine, 3rd Edition: Classes of Materials Used in Medicine.

113. M. Epple, K. Ganesan, R. Heumann, J. Klesing, A. Kovtun, S. Neumann, V. Sokolova. *J. Mater. Chem.* **2010**, *20*, 18-23. Application of calcium phosphate nanoparticles in biomedicine.

II. PRECIPITATION OF MESOSTRUCTURED CALCIUM PHOSPHATES IN THE PRESENCE OF IONIC SURFACTANTS

II.1 Introduction

Synthetic hydroxyapatite (HA) exhibits excellent osteoconductive properties, therefore it is widely used in bone surgery and dentistry as material for bone cavity fillings and metallic implant coatings [1]. In addition to HA, other calcium phosphates (CaPs) are receiving a good deal of attention as matrixes in drug delivery systems, due to their physical and chemical properties, high surface interaction properties and biocompatibility.

Since researchers at Mobil Oil Company synthetized the silica mesoporous ordered material MCM–41 using a supramolecular templating technique, silica mesoporous molecular sieves have attracted considerable attention because of their potential application as absorbents, catalysts, ion exchangers and containers for guest molecules [2]. The cooperative self–assembling of inorganic silicates and surfactants produces a mesostructured phase, and the removal of organic component yield well-organized porous structures. This methodology can be extended to prepare a variety of non-siliceous mesostructured materials such as mesostructured CaPs. Hence, mesoporous HA could be useful as a drug delivery system in hard tissues. But the synthesis of mesostructured calcium phosphate or HA has been rarely reported [3-10].

In this chapter, several calcium phosphates (HA, brushite, monetite, etc…) have been synthesized in the presence of various ionic surfactants aimed to be used as structure directing agents or templates. The aim of the work was the preparation of mesostructured CaPs, specially HA, which could be used in drug delivery systems [11-13] and bone regeneration [14] applications.

The precipitation method was selected to synthesize the mesostructured calcium phosphate materials since it is the most used wet chemistry approach to obtain CaPs, particularly HA. A significant feature of the precipitation method is that calcium phosphate deposition occurs rapidly forming needle–like particles of HA. The following features of this method should also be pointed out: CaPs are synthesized at low temperature and the synthesis conditions can be easily varied if necessary. In this method parameters such as the Ca/P molar ratio, pH value, pressure or temperature of synthesis play important roles in order to obtain different phases of CaP such as HA, brushite, monetite, octacalcium phosphate, α-/β-tricalcium phosphate, etc [15]. In general, synthesis of brushite by precipitation takes place through the following chemical reaction:

$$CaCl_{2\,(aq)} + Na_2HPO_{4\,(aq)} + 2H_2O \rightarrow CaHPO_4{\cdot}2H_2O\downarrow + 2NaCl_{\,(aq)} \quad (1)$$

As expressed in reaction (1), Ca^{2+} and HPO_4^{2-} ions precipitate as brushite ($CaHPO_4{\cdot}2H_2O$) in aqueous solution depending on the synthesis conditions. The wet chemical precipitation method was proven to be one of the easiest ways to prepare HA if the Ca/P molar ratio and pH of media are 1.67 and basic, respectively. Liu *et al*. prepared crystalline HA based on the reaction of calcium nitrate with ammonium phosphate dibasic [6], through the reaction (2):

$$10\ Ca(NO_3)_2{\cdot}4H_2O + 6\ (NH_4)_2HPO_4 + 20\ NaOH \rightarrow Ca_{10}(PO_4)_6(OH)_2\downarrow + 20\ NaNO_3 + 12\ NH_3\uparrow + 58\ H_2O \quad (2)$$

The formation of CaPs over a range of pH has been investigated at 37 °C using a precipitation method. The precipitation of octacalcium phosphate (OCP) appears to be limited to a pH range of 6

to 7 with a Ca/P molar ratio 1.67. Brushite (DCPD) is usually synthesized at pH 5.5 and Ca/P molar ratio 1, and HA can be synthesized at higher pH (7.4-10) with Ca/P molar ratio 1.67 [16].

To obtain various mesostructures, different ionic surfactants were used in this work as structure directing agents during the CaPs precipitation, due to their self-assembly characteristics in water and their possible interactions with Ca^{2+} and HPO_4^{2-} ions [3, 17]. The ionic surfactants used were: sodium dodecyl sulphate (SDS), sodium dodecyl benzene sulphonate (SDBS), cetyltrimethyl ammonium bromide (CTAB), mono-alkyl phosphate (MAP, in particular mono-*n*-dodecyl phosphate) and the zwitterionic N,N-dimethyl-N-dodecylglycine betaine or EMPIGEN®BB detergent (EPG), Figure II.1.

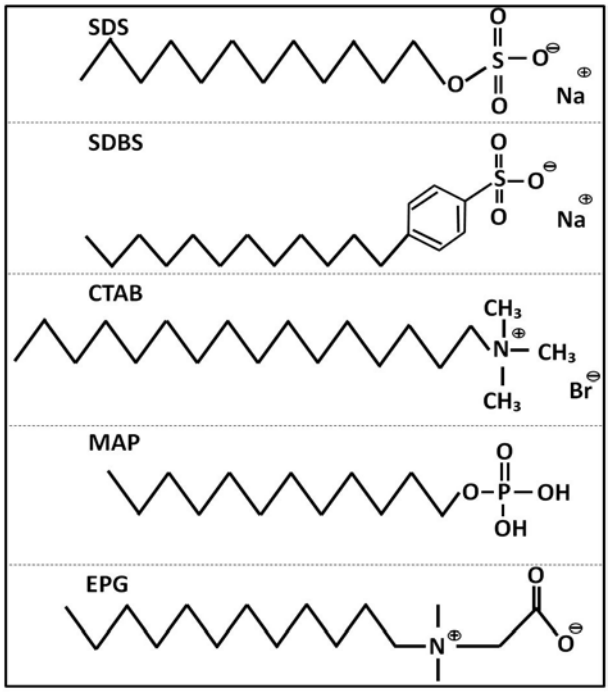

Figure II.1. Hydrophobic carbon tail (left) and hydrophilic head group (right) of surfactants used in this chapter.

Surfactants were dissolved in water to obtain mesophases [4, 18]. The interaction between the polar head of ionic surfactants and Ca^{2+} and HPO_4^{2-} ions could lead to obtain mesostructure during the precipitation of the CaPs. Dissolved surfactants in water can be organized in different shapes such as lamellar, hexagonal, micellar or cubic (see Figure I.6 in Chapter I). These shapes and layer size depend on concentration, temperature and the ionic surfactant used during synthesis.

The expected mesostructures in the presence of CaP are organized in several groups as follows:

- Lamellar mesostructure by using anionic SDS: sulphonate polar head interacts easily with Ca^{2+} ions [5].
- Lamellar mesostructure with extended layers by using SDBS: the bigger polar head group of this surfactant would favor the formation of wider layers that with SDS. Thus, we expected to obtain *(i)* extended layers of lamellar mesostructure or *(ii)* a worm-like mesostructure by covering the extra space during formation [6, 19].
- Extended mesostructure (enlarged lamellar, vesicles and worm-like structures) by using mixtures of surfactants: hybrid CaP materials were prepared in mixtures of surfactants such as SDS+CTAB [20], SDBS+CTAB, MAP+CTAB. In the presence of two surfactants, it is expected to synthesize larger mesostructures of calcium phosphate through the interaction between the surfactants and the calcium phosphates [8, 21, 22].
- A new mesophase by using EPG zwitterionic surfactant. Zwitterionic or amphoteric surfactants have both cationic and anionic charge in the same molecule. The cationic part is based on primary, secondary or tertiary amines or quaternary ammonium cation. The charge

separation causes a dipole moment in the head group. Therefore, the head group is polar and the molecule soluble in water forming micelles that can interact with ions.

Table II.1 Mesostructured CaP synthesis strategies, sample code and section of this Chapter where they are described.

Section	Strategy of Synthesis		Sample Code	Acronym mean
II.2	*Calcium phosphates in the presence of ionic surfactants*			
	II.2.a	CaPs in the presence of SDS	***NHCaP1-X*** ***NHCaP167-X*** ***NHCaP1A-2*** ***NHCaP1R-2***	Nanostructured Hybrid Calcium Phosphate: **NHCaP**
	II.2.b	CaPs in the presence of SDBS	***NHHA1-X***	Nanostructured Hybrid HydroxiApatite: **NHHA**
II.3	*Calcium phosphates in the presence of mixture of anionic and cationic surfactants*			
	II.3.a	CaPs in SDS + CTAB	***MHCaP-X***	Multi-structured Hybrid Calcium Phosphate: **NHCaP**
	II.3.b	CaPs in SDBS + CTAB	***HMM31*** ***HMM31***	Hybrid Mesostructured Material: **HMM**
	II.3.c	CaPs in MAP + CTAB	***LCaP***	Lamelar-structured Calcium Phosphate: **LCaP**
II.4	*Calcium phosphate in the presence of a zwitterionic surfactant*		***CaP1, CaP2, PCa1, PCa2***	Non-structured Calcium Phosphate: **NHCaP**

Lamellar layered mesostructures can be obtained by using SDS, SDBS and MAP surfactants, and there is reported evidence that lamellar brushite or HA structures can be synthesized in the presence of these surfactants [5, 6, 23]. On the other hand, micelle structures can be synthesized by using CTAB [7, 8, 20, 24]. Moreover, zwitterionic surfactant will be used for the first time as structure directing agent trying to obtain a mesostructured CaP.

II.2 Calcium phosphate in the presence of ionic surfactants

II.2.a Calcium phosphate in the presence of sodium dodecyl sulphate

Anionic sodium dodecyl sulphate (SDS), the most known surfactant to obtain lamellar mesostructured CaPs, was used as structure directing agent [6]. SDS dissolves well in water and the critical parameter for this surfactant is the optimal concentration value since it plays a crucial role in the synthesis of different ordered mesostructured CaP phases. Ca^{2+} and HPO_4^{2-} ions may easily interact with the ionic sulphate polar head. On the other hand, the pH of the solution and the Ca/P molar ratio are relevant parameters to obtain different CaP crystalline phases.

In this section, the concentration of SDS has been considered a variable parameter ranging from 15 to 90 mM in the final reaction volume. The pH of the medium was not modified neither buffered. 14 samples in total were synthesized in the following three batches:

(i) six samples prepared with [SDS] = from 15 to 90 mM and Ca/P molar ratio 1

(ii) six samples prepared with [SDS] = from 15 to 90 mM and Ca/P molar ratio 1.67

(iii) two samples prepared with [SDS] = 30 mM and Ca/P molar ratio 1, obtained by using reflux and autoclave processes.

Hybrid CaP materials were shortly named as NHCaP, which stands for nanostructured hybrid calcium phosphate: NHCaP1–X with Ca/P molar ratio 1, NHCaP167–X with Ca/P 1.67, and X indicates the number of sample (X = 1 to 6). NHCaP1A–2 for the samples synthesized with the experimental conditions for sample 2 (NHCaP1–2 prepared with [SDS] = 30 mM) by using Autoclave and NHCaP1R–2 for the sample synthesized under Reflux.

Thermogravimetric and Differential Thermal Analysis

Thermogravimetric and differential thermal analyses (TG/DTA) were used to quantify the organic matter present in the hybrid samples and to observe the possible phase changes from brushite to monetite. Weight loss curves are shown in Figure II.2. All samples showed analogous DTA curves, therefore only one DTA trace is shown. For all samples, TGA curves exhibited a slight weight loss between room temperature and 125 °C that is attributed to the loss of physisorbed water in the samples.

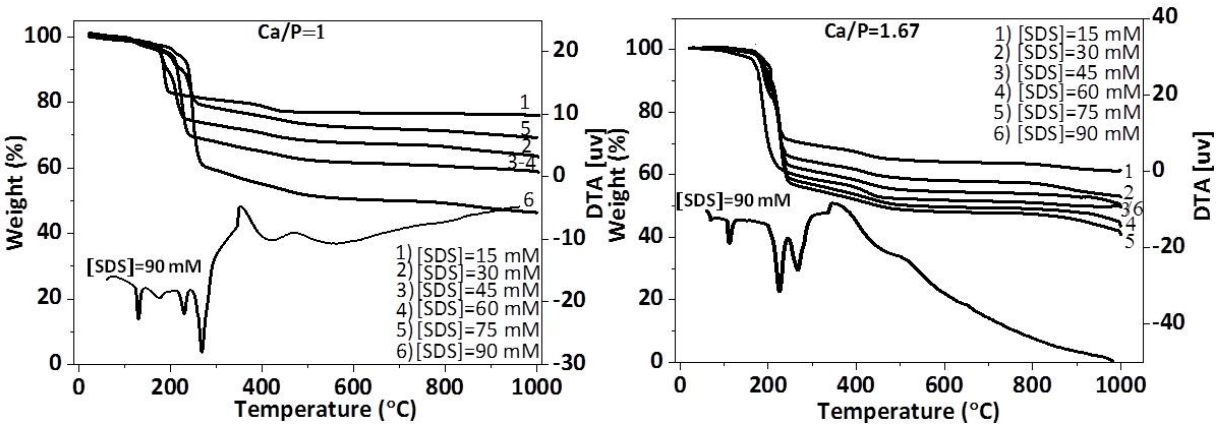

Figure II.2 TG/DTA curves for hybrid calcium phosphate samples precipitated in various concentrations of SDS, Ca/P = 1 (left) and Ca/P = 1.67 (right).

A sharp loss of weight was observed between 200 and 300 °C in the two series of hybrids, being more pronounced in the Ca/P = 1.67 series. This process in the TGA curve is observed together with two endothermic peaks in the DTA curve. Taking into account that a transition phase from brushite to monetite occurs at this temperature due to loss of the two water molecules in the crystal lattice of brushite (see reaction 3), these processes in the hybrid samples would be indicative of the presence of a brushite phase in both series of samples.

$$CaHPO_4 \cdot 2H_2O \text{ (brushite, DCPD)} \xrightarrow{\Delta\,°C} CaHPO_4 \text{ (monetite, DCPA)} + 2H_2O \qquad (3)$$

Regarding the surfactant combustion, exothermic peaks are registered in the DTA around 350 °C assigned to this process and amounted in the following weight losses for [SDS] = 15 to 90 mM: 6 up

to 11% for the Ca/P = 1 series and 7 up to 10% for the Ca/P = 1.67 series. Therefore, as expected, an increase in the amount of organic matter incorporated in the hybrid materials was observed in concordance with the increase of surfactant concentration during the synthesis.

Fourier Transform Infrared Spectroscopy

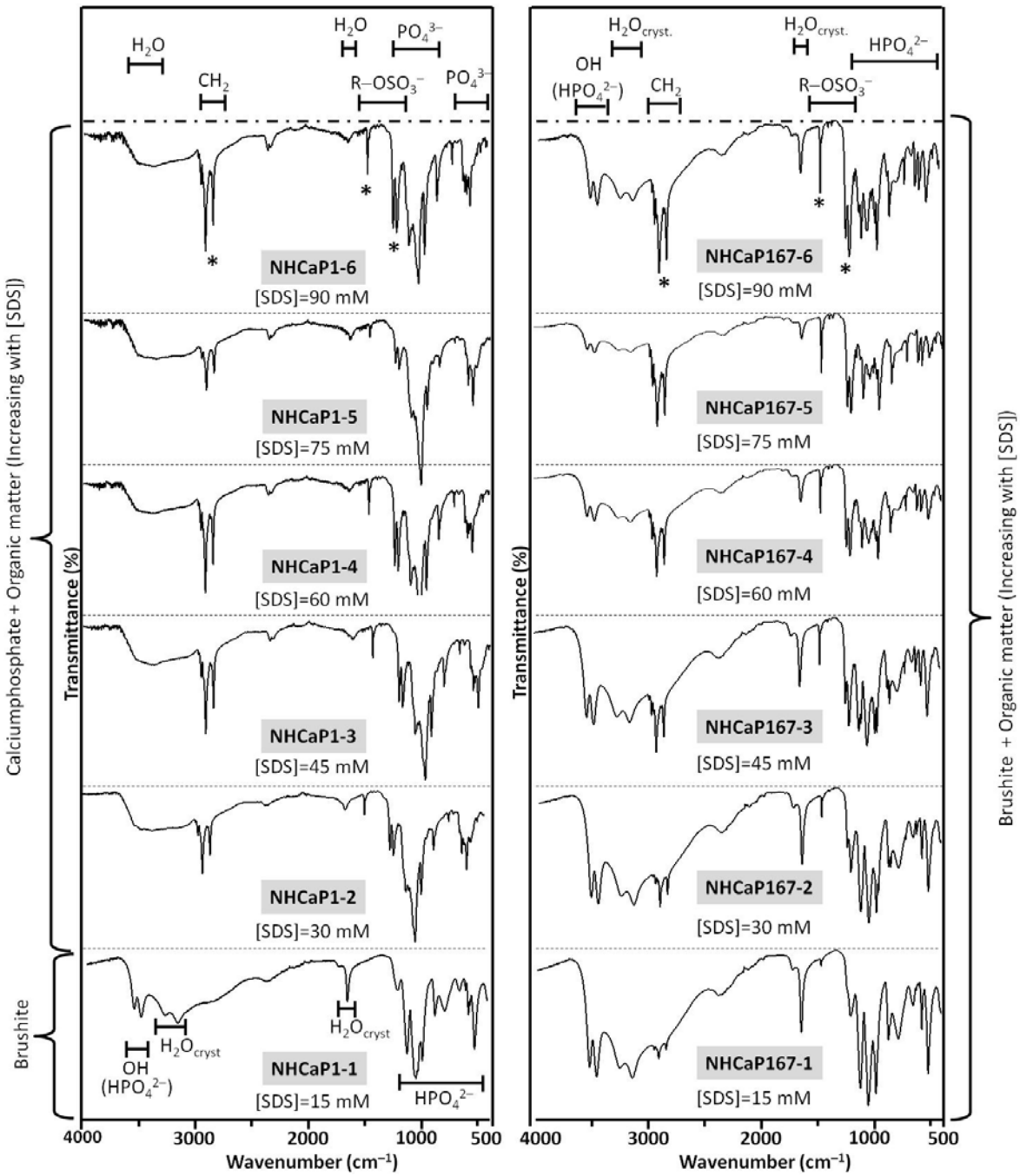

Figure II.3 FTIR spectra of NHCaP hybrid materials (Left: Ca/P = 1; right: Ca/P = 1.67). More characteristic bands from SDS are marked with a * in the spectra at the top.

FTIR spectra for hybrid materials obtained with **Ca/P molar ratio 1** and **[SDS] = from 15 to 90 mM** are shown in Figure II.3 (left) and present the following characteristics:

Sample prepared with **[SDS] = 15 mM** shows a typical brushite spectrum, with four bands due to crystalline water of brushite between 3700 and 2900 cm^{-1} and HPO_4^{2-} group around 1060 cm^{-1} [25]. The rest of the samples, prepared with **[SDS] = from 30 to 90 mM,** exhibit spectra attributable to HA, with three bands from CH_2 groups of surfactant around 2900 cm^{-1}. In general terms, the following facts can be ascertained from these spectra:

- The stretching vibration mode of C-H bonds of surfactant was observed with increasing intensity in materials synthesized with [SDS] = 30 to 90 mM: at 2956, 2918 and 2848 cm^{-1} for ν_{as}(CH) of the methyl group, ν_{as}(CH) and ν_s(CH) of the methylene groups.
- ν(S=O), ν_{as}(SO) and ν_s(SO) bands from the R-OSO_3^{2-} group appeared at 1450, 1250 and 1215 cm^{-1}, respectively, except in the spectrum of sample prepared with [SDS] = 15 mM. As well, the intensity of these three bands increases with the concentration of SDS.
- Physisorbed water in the spectra for HA: a broad band around 3500 for ν(OH) and at 1640 cm^{-1} for δ(HOH).
- Regarding the PO_4^{3-} structural unit: bands at 1117 and 1039 cm^{-1} for ν_{as}(PO) and at 982 cm^{-1} for ν_s(PO) from the PO_4^{3-} group, and at 600 and 575 cm^{-1} for δ(OPO) of PO_4^{3-} in crystalline environment.

FTIR spectra for hybrid materials obtained with **Ca/P** molar ratio **1.67** and **[SDS] = from 15 to 90 mM** are shown in Figure II.3 (right) and indicate that all hybrid materials exhibit characteristic brushite FTIR spectra [25].

- The absorption bands at 2950, 2916 and 2850 cm^{-1} are ascribed to the stretching vibration modes of C-H bonds of surfactant and present a higher intensity in [SDS] = 45 to 90 mM samples.
- At 1450, 1250 and 1215 cm^{-1} bands present in all spectra, assigned to ν(S=O), ν_{as}(SO) and ν_s(SO) from the R-OSO_3^{2-} group.
- The water molecules in the crystal lattice of the brushite give rise to the two typical bands at 3256 and 3149 cm^{-1} for ν_{as}(OH) and ν_s(OH). There is also the band due to δ(HOH) at 1640 cm^{-1} of the crystalline H_2O in brushite.
- *HPO_4^{2-} structural unit:* at 3530 and 3470 cm^{-1} bands for ν_{as}(OH) and ν_s(OH) of HPO_4^{2-}; at 1202 cm^{-1}, 1117 cm^{-1} and 1039 cm^{-1} bands for ν_{as}(PO) and ν_s(PO); at 784 cm^{-1} the band for δ(O-P-OH) and at 520 and 575 cm^{-1} bands for δ(OPO).

On the other hand, FTIR spectra of materials obtained with Ca/P = 1 and [SDS] = 30 mM **by using autoclave and reflux processes** (Figure II.4) exhibit a profile for calcium phosphate without water, neither crystalline water nor physisorbed water [25]. FTIR spectrum of NHCaP1–2 sample, obtained by precipitation, is included for reference purposes.

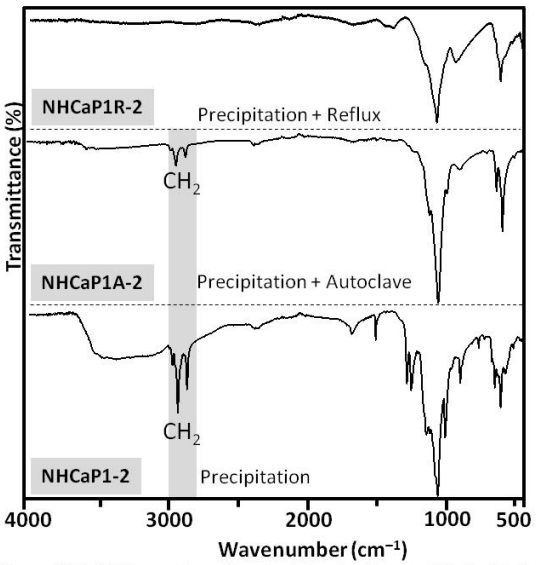

Figure II.4 FTIR spectra of materials obtained with Ca/P=1 and [SDS]=30 mM by using autoclave and reflux processes. FTIR spectrum of NHCaP1-2 sample is included for reference purposes.

Bands corresponding to the stretching vibration modes of the C-H bonds from methylene groups from surfactant are present in the material obtained by autoclave, while these bands are absent in the material obtained by reflux, indicating absence of organic matter in this material. In both materials, phosphate group bands are detected at 1085 and 1024 cm^{-1} for ν_{as}(PO) and 960 cm^{-1} for ν_s(PO). Regarding the δ(OPO) mode, it is identified as two bands at 600 and 575 cm^{-1} for PO_4^{3-} in crystalline environment in the material obtained by autoclave. However, only a band is observed at 575 cm^{-1} in the material obtained by reflux, which suggest a lower crystallinity of the HA here formed. Therefore, the accurate identification of the CaP phase will be done by XRD analysis.

Small and wide angle X–ray Diffraction

Lamellar mesostructure can be observed by small angle X–ray diffraction (SA–XRD) in the range 0.6 – 10° in 2θ (Cu Kα radiation), giving rise to three diffraction peaks identified as (100), (200) and (300) of a lamellar phase, respectively. For time saving purposes, a quick confirmation measurement of the first two peaks attributable to a lamellar mesostructure was performed in all materials. Hence, the SA–XRD measurement was performed only from 0.6 to 6.5° or to 8° in 2θ. However, the second and third peaks of the lamellar layer were also observed by wide angle X–ray diffraction (WA–XRD) measurements performed in the range 5 to 50° in 2θ. On the other hand, for comparison and reference purposes, the sample of hybrid material obtained from **Ca/P molar ratio 1.67** and **[SDS] = 90 mM** (NHCaP167-6) was measured by SA–XRD up to 10° in 2θ to obtain the three peaks of the lamellar structure in the same diffractogram, see Figure II.5 and Table II.2.

In the wide angle pattern, seven more intense reflections (020), (021), (040), (041), ($\bar{2}$21), (220) and (022) of brushite (B) are labelled, (see Figure II.5, right). This crystalline brushite with lamellar mesostructure is used as reference to compare with all the obtained materials.

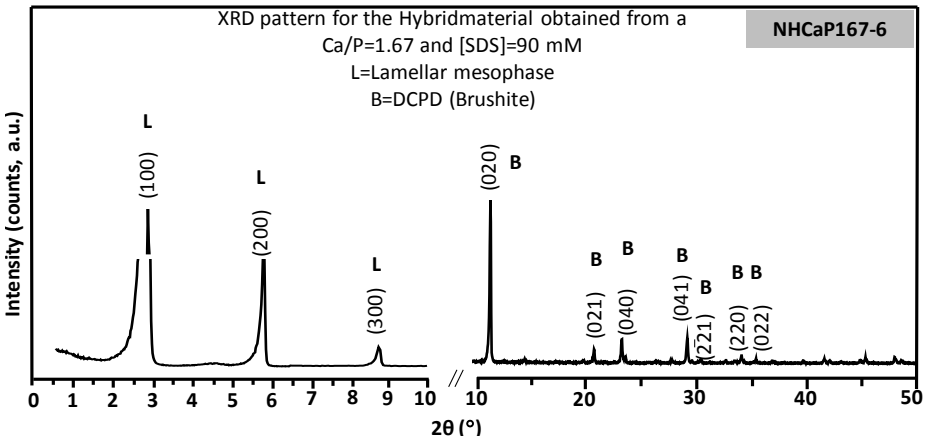

Figure II.5 SA-XRD (left) and WA-XRD (right) patterns of a highly ordered lamellar structure with brushite phase exhibited by NHCaP167-6 sample.

Table II.2 Small-angle X-ray diffraction data of the mesostructured NHCaP167-6 sample.

2θ (°)	*n*	*d (nm)*	*nd (nm)*	*(hkl)*
2.9	1	3.046	3.046	100
5.8	2	1.520	3.040	200
8.8	3	1.015	3.015	300

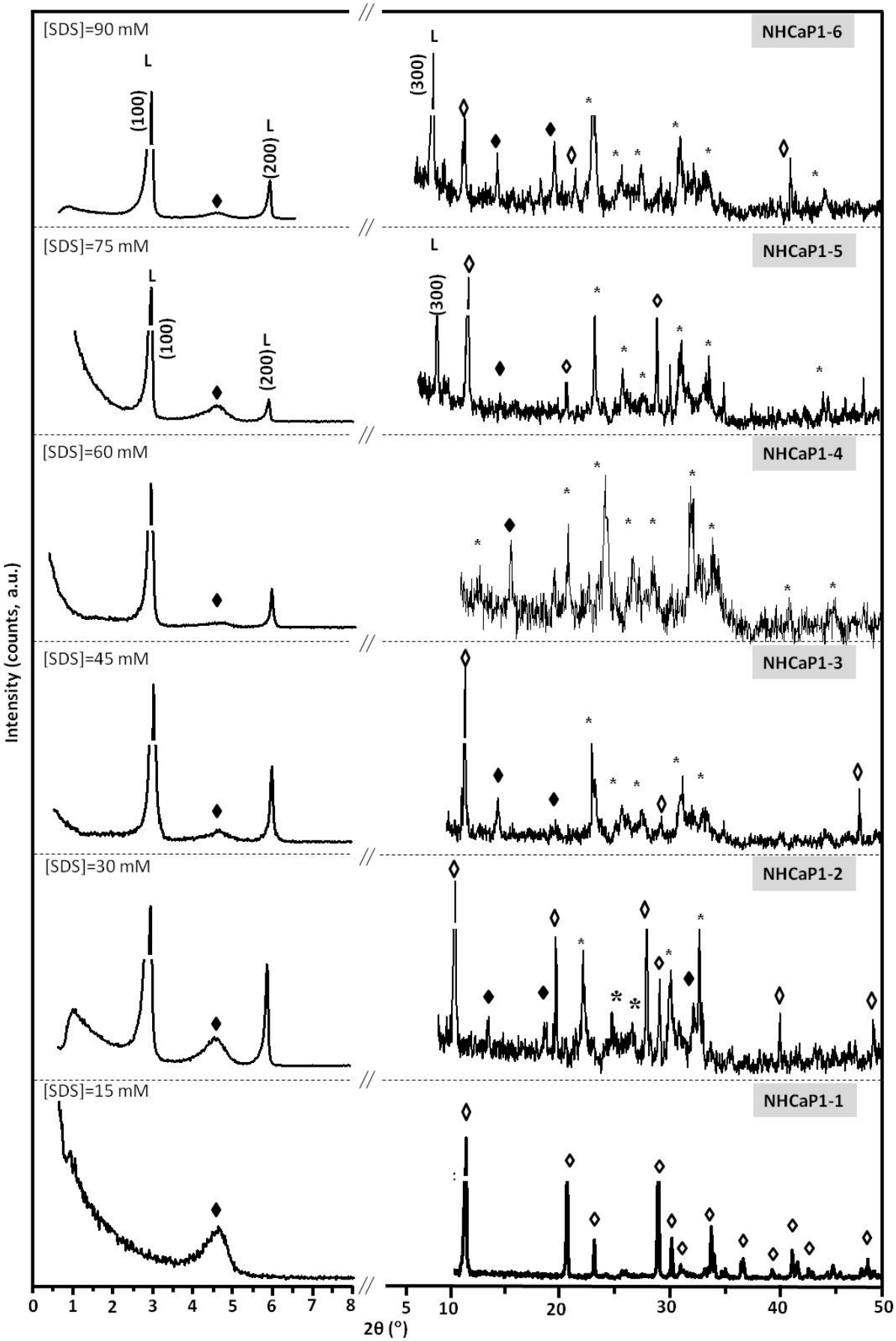

Figure II.6 Powder XRD patterns of hybrid materials (Ca/P = 1) by small angle (left) and wide angle (right), where *, ◊ and ♦ indicate HA, brushite and OCP, respectively.

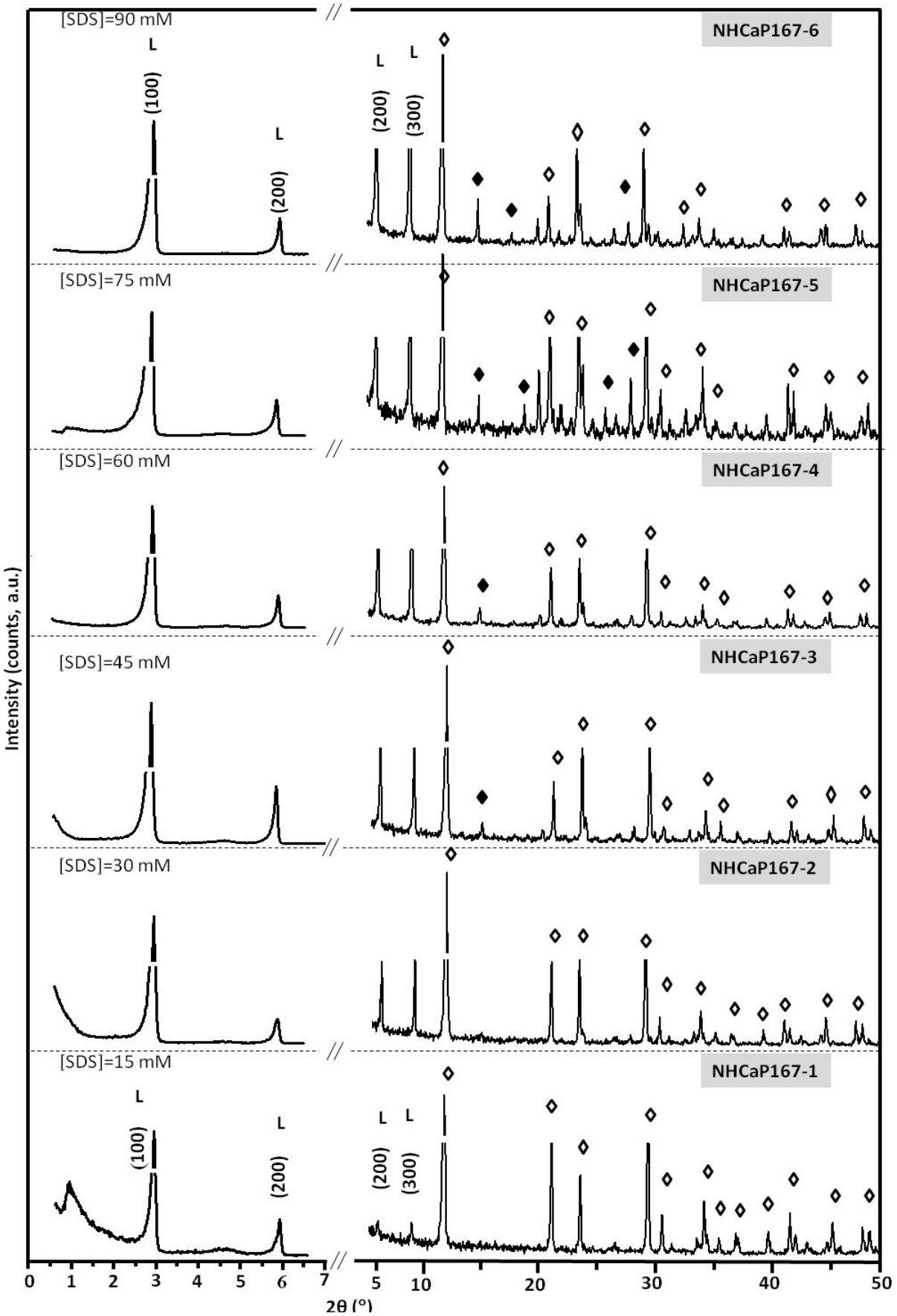

Figure II.7 Powder XRD patterns of hybrid materials (Ca/P = 1.67) by small angle (left) and wide angle (right), where ◊ and ♦ indicate brushite and OCP, respectively.

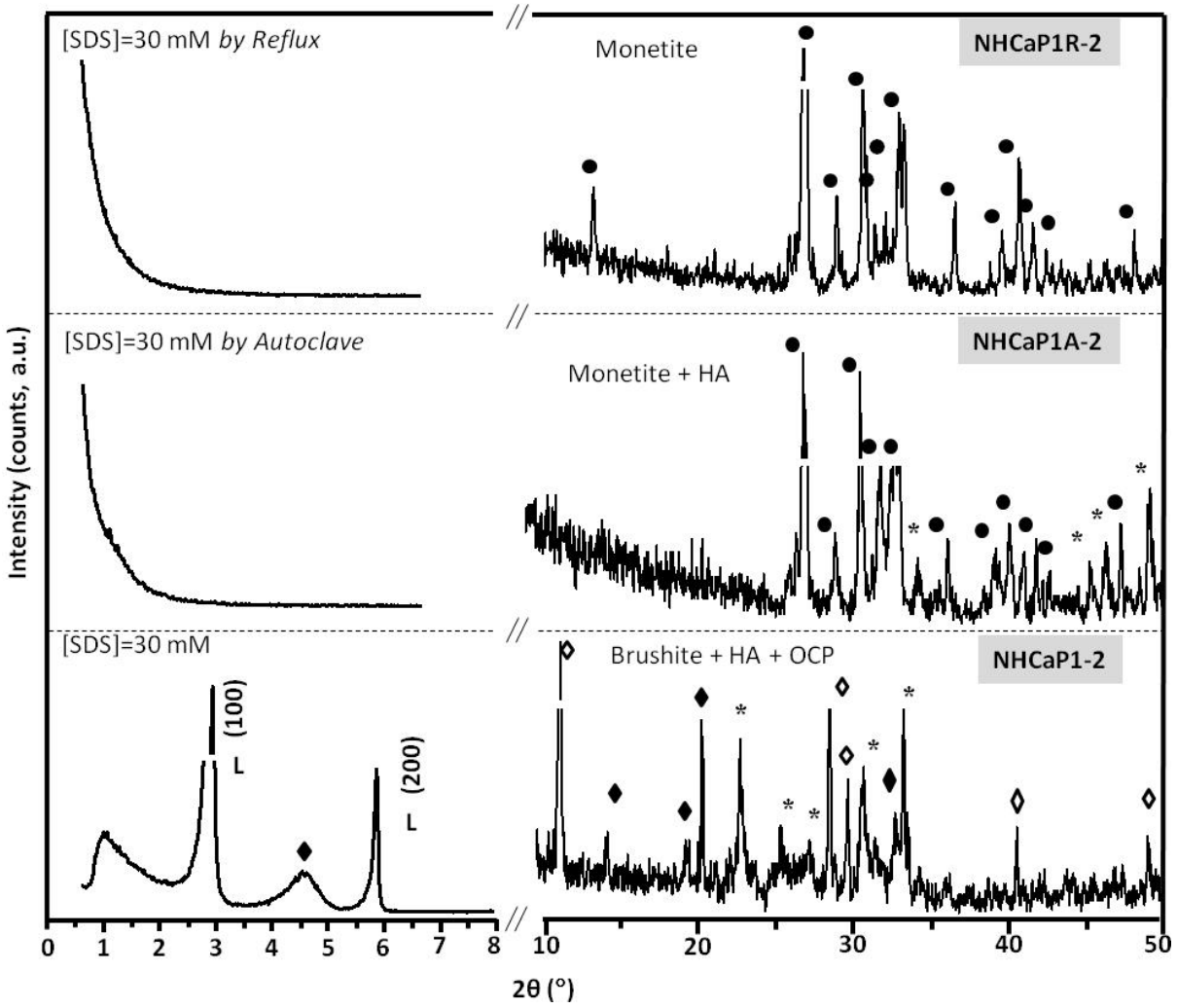

Figure II.8 SA–XRD and WA–XRD diffractograms of hybrid materials (Ca/P = 1) synthesized by using autoclave or reflux; •, *, ◊ and ♦ indicate monetite, HA, brushite and OCP, respectively. XRD patterns of NHCaP1–2 are included for reference purposes.

The interplanar spacing (d) values obtained from peaks in the SA–XRD measurement are summarized in Table II.2. According to Bragg's law ($\lambda = 2d\sin\theta$, where λ is the wavelength 1.5418 Å for Cu Kα X-ray radiation, *d* is the spacing of atomic planes and θ is the angle of incidence), the *d* spacing is figured out as d_{100} = 3.046, d_{200} = 1.52 nm, d_{300} = 1.015 nm. The d spacing ratio for these three peaks is close to 1:1/2:1/3:1. Compared with the references [5, 26], the small–angle pattern of the sample indicates the existence of long–range ordered layers of a mesostructured phase with a periodical spacing of about 3.046 nm, as evidence by peaks corresponding to the (100), (200) and (300) reflections.

Regarding the hybrid materials synthesized with **Ca/P molar ratio 1** and **[SDS] = from 15 to 90 mM**, see Figure II.6 for SA- and WA-XRD measurements. SA–XRD revealed the first two peaks of the lamellar layer, corresponding to (100) and (200) reflections, at 2θ = 2.8 and 5.8° in all samples with the exception of NHCaP1–1. Also, in all the samples of this series, a broad peak was observed at 2θ = 4.6° indexed as the (100) reflection of OCP. Therefore, materials from NHCaP1–2 to NHCaP1–6 consist of lamellar mesostructured hybrids.

For synthesized hybrid material NHCaP1–1, besides the OCP peak at 2θ = 4.6°, diffraction peaks attributable to a crystalline brushite phase are observed in the WA range. This brushite peaks were observed at 2θ = 11.6°, 20.9°, 23.4°, 29.1°, 30.5°, 31.2°, 34.1°, 37.0°, 39.6°, 41.5°, 42.0° and 48.4° for (020), (021), (040), (041), $(\bar{2}21)$, $(\bar{1}12)$, (220), (022), (061), (151), $(\bar{2}42)$ and (260) reflections, respectively.

As already mentioned, the first two peaks of the lamellar layer were observed at 2θ = 2.9° and 5.8° for (100) and (200) diffractions in all remaining hybrid materials (from NHCaP1–2 to NHCaP1–6, Figure II.6). Also, the third peak (300) of the lamellar layer was observed at 2θ = 8.8° in the wide angle X–ray diffraction pattern between 5 and 50° 2θ. Therefore, a lamellar mesostructure was detected in these samples and confirmed according to Table II.2. Regarding WA–XRD of these five materials, mixtures of brushite, HA and OCP could be indexed with diffraction peaks at 2θ = 11.7°, 14.7°, 20.0°, 23.3°, 26.2°, 28.0°, 29.8°, 31.6°, 33.8° and 47.8°; these peaks correspond to (020) of brushite; $(3\bar{1}0)$, (310) of OCP; (111), (002), (102) of HA; $(11\bar{2})$ of brushite; (211), (202) of HA and (062) of brushite, respectively, as indicated with different symbols in Figure II.6 (right).

Regarding the hybrid materials synthesized with **Ca/P molar ratio 1.67** and **[SDS] = from 15 to 90 mM**, see Figure II.7. In all synthesized materials, 100 and 200 reflections were observed in the SA region, indexed for a lamellar mesostructure and summarized as shown in Table II.2. In this series, no OCP diffraction peak was observed at 2θ = 4.6°. In the WA range crystalline brushite with one additional peak, tentatively attributable to OCP, was identified for the four hybrid materials from NHCaP167–1 to NHCaP167–4. The remaining two materials, NHCaP167–5 and NHCaP167–6, showed a diffraction pattern for a mixture of brushite and OCP phases.

Regarding the two hybrid materials synthesized with **Ca/P = 1** molar ratio and **[SDS] = 30 mM** by **reflux** and **autoclave** processes, see Figure II.8. According to SA–XRD measurements, reflux and autoclave processes did not succeed in obtaining lamellar mesostructures. In the sample prepared by autoclave process, WA–XRD measurements exhibit a mixture of calcium phosphate phases. Peaks at 2θ = 26.4°, 28.5°, 30.2°, 31.5°, 32.5°, 33.9°, 36.0°, 39.0°, 40.0°, 41.0°, 41.8°, 45.4°, 46.4° and 47.3° were identified as (002), $(11\bar{2})$, (120), $(12\bar{1})$, (201) of monetite, (202) of HA, $(\bar{1}\bar{1}2)$, (120), (003), $(1\bar{2}\bar{2})$, $(0\bar{1}3)$ of monetite, (203), (222) of HA and $(32\bar{1})$ of Monetite, respectively. In the sample prepared by reflux process, the diffraction peaks at 2θ = 13.1°, 26.4°, 28.5°, 30.2°, 31.5°, 32.5°, 33.9°, 36.0°, 39.0°, 40.0°, 41.0°, 41.8° and 47.3° were all identified as monetite [27]. In summary, reflux and autoclave processes were applied on hybrid materials obtained with Ca/P molar ratio 1 and [SDS] = 30 mM to reveal potential phase changes of calcium phosphate and mesostructure. However, these two processes were unproductive in terms of mesostructure (see Figure II.8, left). On the other hand, these processes lead to obtain monetite phase (see Figure II.8, right).

Transmission Electron Microscopy

Transmission Electron Microscopy (TEM) analysis was performed on NHCaP167–6 sample ([SDS] = 90 mM with Ca/P molar ratio 1.67), see Figure II.9.

Lamellar mesostructures forming well-arranged nano–rods were observed for this sample. As shown in this TEM image, alternating inorganic layers and template layers were arranged in one dimension to form an ordered nano-array. This ordered nano-array could be made of SDS and brushite layers. The lamellar structure exhibits a layer thickness of 1.3 nm. Therefore, this image confirms the lamellar mesostructure detected by SA–XRD. The intermediate light areas correspond to layers occupied by the hydrocarbon tails of the SDS surfactant.

The dark areas correspond to higher electron density regions of calcium phosphate, electrostatically interacting with the phosphate head groups of the surfactant.

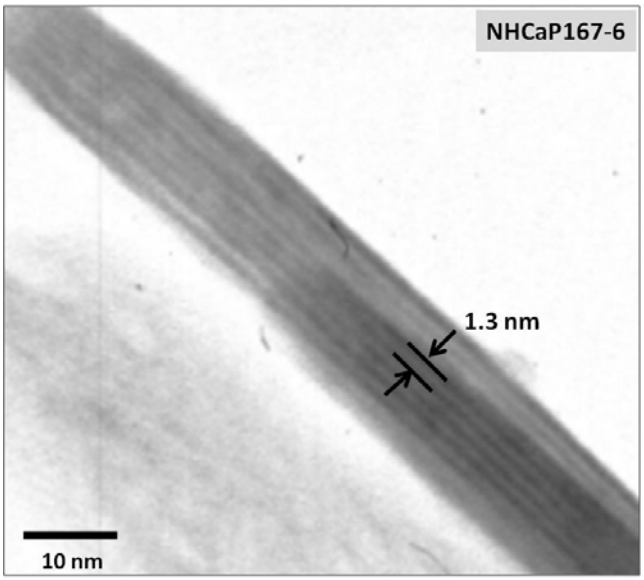

Figure II.9 TEM images of lamellar nanosostructured hybrid material (Ca/P = 1.67 and [SDS] = 90 mM).

Conclusion of Section II.2.a

By using SDS surfactant as structure directing agent, lamellar CaP has been obtained by precipitation as a fast synthesis method. Highly mesostructured lamellar calcium phosphates were synthesized with Ca/P molar ratio 1 or 1.67 and [SDS] = 15 to 90 mM, and CaP obtained phases were brushite, HA and low crystalline OCP. The optimal concentration of surfactant plays an important role both in the mesostructure formation and in the crystalline phases obtained. In this sense, when [SDS] < 30 mM and Ca/P molar ratio 1, brushite phase was always observed with and without lamellar mesostructure. When the conditions were [SDS] < 60 mM and Ca/P molar ratio 1.67, brushite phase was always observed with lamellar mesostructures. A mixture of brushite and HA, with lamellar order was synthesized at [SDS] ≥ 30 mM and Ca/P molar ratio 1. A mixture of brushite and OCP, with lamellar order was synthesized at [SDS] ≥ 60 mM and Ca/P molar ratio 1.67. According to these results, we observed two features in these materials: *(i)* lamellar structure and *(ii)* mixture of calcium phosphate phases such as hydroxyapatite and brushite in the aqueous media. Thus, we can see how the synthesis conditions play an important role for obtaining different CaP phases with mesostructure, disordered mesostructure or monetite phase without mesostructure. This last case, monetite phase without mesostructure, was observed when reflux and autoclave processes were used.

II.2.b Calcium phosphate in the presence of sodium dodecyl benzene sulphonate

The main purpose of this section was to synthesize mesostructured calcium phosphate phases using sodium dodecyl benzene sulphonate (SDBS) as structure directing agent. SDBS contains a benzene group in the surfactant polar head that would modify the curvature of the association of surfactant molecules compared with SDS. Mesostructured lamellar structures are expected to be synthesized by precipitation method in aqueous media. The hybrids were synthesized with Ca/P molar ratio 1 and [SDBS] = 15 to 90 mM. The pH was not buffered during the synthesis and therefore it was measured and the obtained values for each case are indicated in the figures.

The synthesized hybrid materials were shortly named as NHHA1–X, nanostructured hybrid hydroxyapatite with Ca/P molar ratio 1, where X indicates the number of sample (X = 1 to 4). Four hybrid materials were synthesized with [SDBS] = 15, 30, 60 and 90 mM, NHHA1–1, NHHA1–2, NHHA1–3 and NHHA1–4 samples, respectively.

Thermogravimetric and Differential Thermal Analysis

TGA and DTA curves obtained for NHHA1–1 to NHHA1–4 are shown in Figure II.10. Curves for the hybrid material prepared with [SDBS] = 15 mM differs from the rest which present a very similar TG and DTA curves, therefore, only DTA curve for [SDBS] = 90 mM is shown as representative for [SDBS] = 30, 60 and 90 mM. TGA curves exhibited a slight weight loss between room temperature and 125 °C that was attributed to the loss of physisorbed water in the samples.

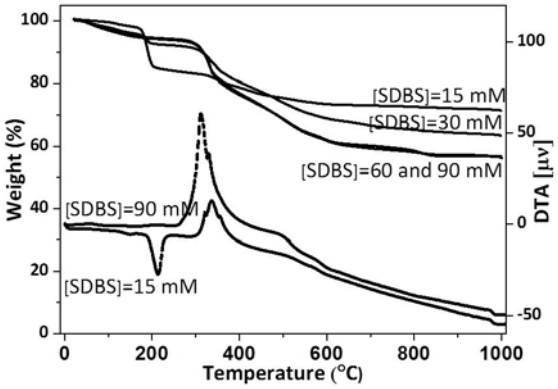

Figure II.10 Thermogravimetric and differential thermal analysis curves for hybrid materials obtained with Ca/P=1 and [SDBS]=15 to 90 mM.

For sample NHHA1–1 prepared with [SDBS] = 15 mM, a sharp weight loss with 27% is registered around 200 °C and assigned to a phase transition of brushite to monetite due to the loss of two water molecules in the crystal lattice of brushite, which gives an endothermic peak in the DTA. Also in this sample, surfactant combustion is observed around 350 °C and confirmed by exothermic peak in DTA curve. The other three samples only showed the weight loss due to surfactant combustion around 350 °C associated with exothermic processes in the DTA. The weight loss due to organic matter follows an increasing trend for all samples, in accordance with the increasing surfactant concentration in the reaction. However, the coincidence of TG curves for samples prepared with [SDBS] = 60 and 90 mM indicates that a maximum amount of incorporated organic matter is reached with [SDBS] = 60 mM.

Fourier Transform Infrared Spectroscopy

The FTIR spectra of the hybrid materials obtained with different SDBS concentrations are shown in Figure II.11.

FTIR spectrum of NHHA1–1 shows typical brushite bands while FTIR spectra of NHHA1–2, NHHA1–3 and NHHA1–4 are compatible with a characteristic HA-like spectrum. These results are consistent with the previous described TG analysis, in which only NHHA1–1 sample presents a weight loss associated to crystalline water.

Bands corresponding to other species present in the materials are listed as follows:

- *SDBS:* at 2954, 2915 and 2849 cm^{-1} for ν_{as}(CH) of the methyl group, ν_{as}(CH) and ν_{s}(CH) of the methylene groups. These bands were observed with increasing intensity as the [SDBS] increased in the synthesis.
- *PO_4^{3-} for HA and HPO_4^{2-} for brushite:* at 3540 and 3460 cm^{-1} bands for ν_{as}(OH) and ν_{s}(OH) for HPO_4^{2-} in brushite; at 1200 cm^{-1}, 1120 cm^{-1} and 1090 cm^{-1} bands for ν_{as}(PO) and ν_{s}(PO); at 790 cm^{-1} the band for δ(O-P-OH) in brushite and at 520 and 570 cm^{-1} bands for δ(OPO) in HA.
- *crystalline H_2O in brushite:* at 3260 and 3150 cm^{-1} bands for ν_{as}(OH) and ν_{s}(OH); at 1650 cm^{-1} band for δ(HOH).

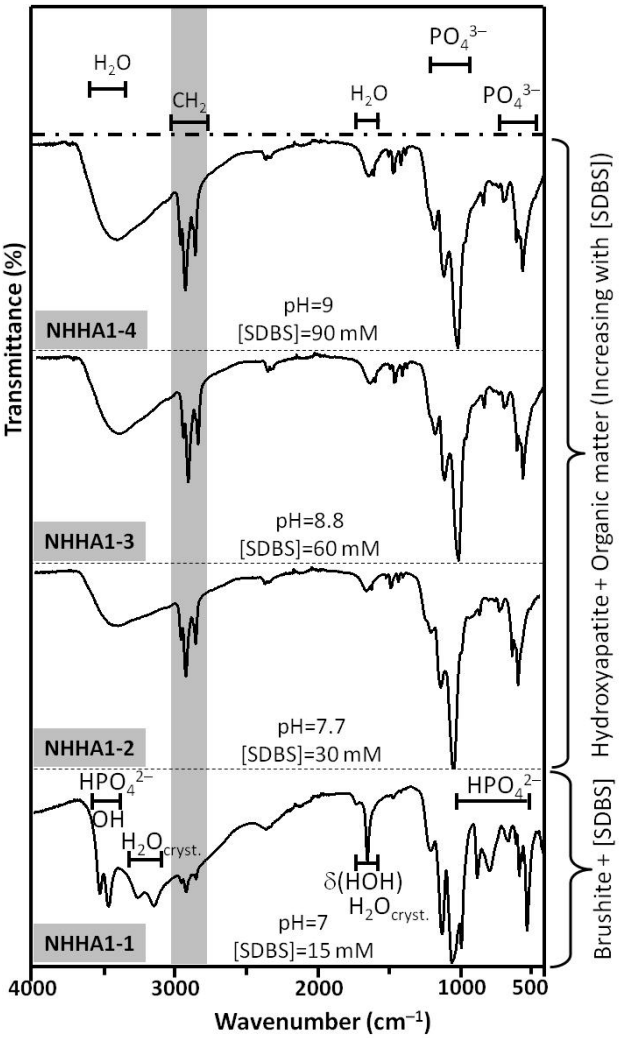

Figure II.11 FTIR spectra of hybrid materials obtained with Ca/P=1 and [SDBS]=15, 30, 60 and 90 mM. pH values measured during the synthesis are especified in the figure.

Small and wide angle X–ray Diffraction

Figure II.12 collects the small and wide angle XRD patterns of the hybrid materials synthetized in the presence of SDBS.

SA–XRD patterns showed in all samples a single shoulder–like broad diffraction peak at around 2θ = 2°. With this single X–ray peak as the only evidence, it is difficult to ascertain the existence of mesostructure arrangement, but it could be associated to disordered or discontinued lamellar structure [28]. In this hypothesis, this weak reflection is consistent with discontinuous lamellar mesostructure and would correspond to its (100) reflection at 4.6 nm of *d*–spacing.

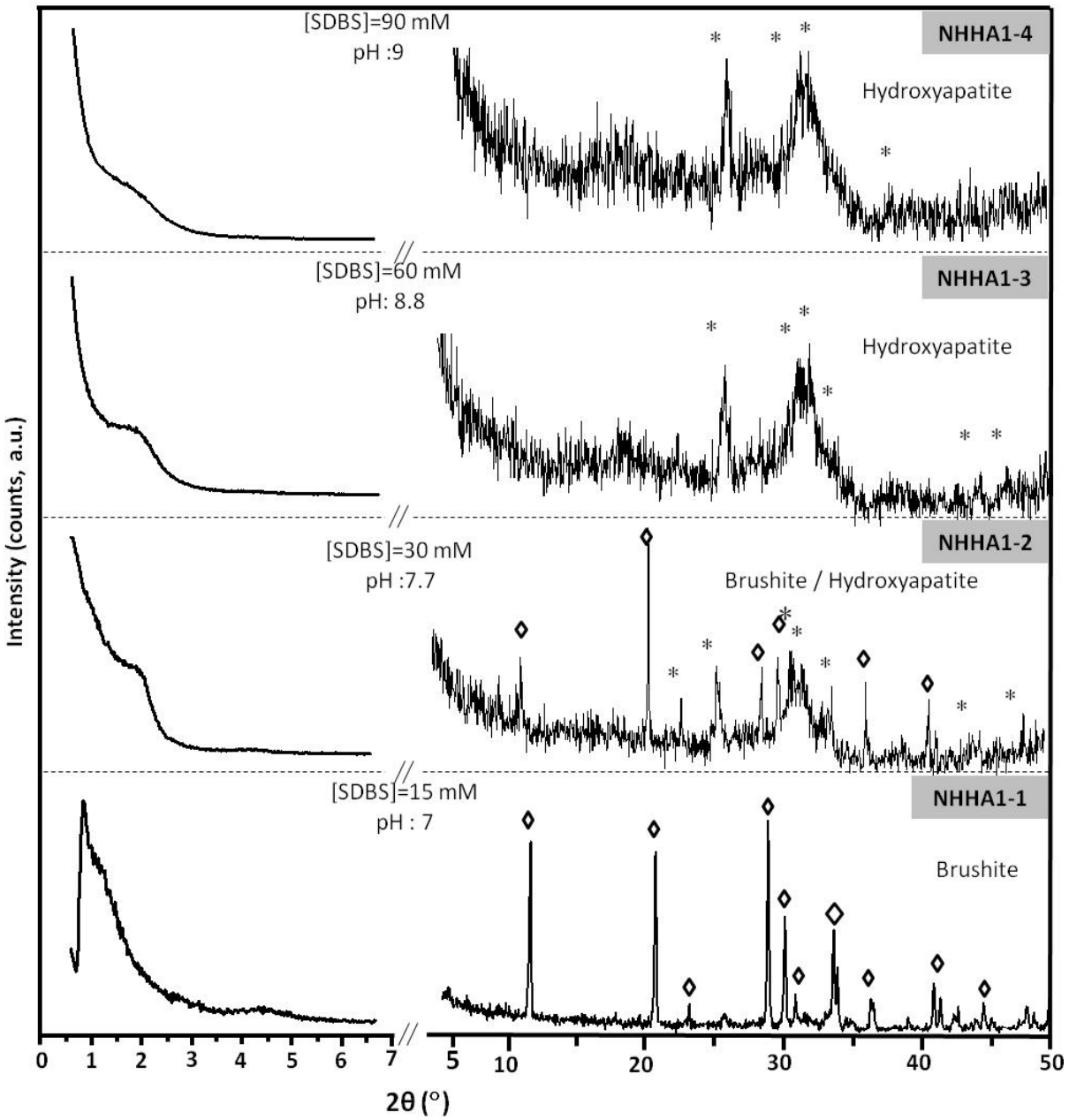

Figure II.12 Powder XRD patterns of calcium phosphate in the presence of SDBS in the small (left) and wide (right) angle ranges, where * and ◊ indicate HA and brushite, respectively.

CaP phases were identified by WA–XRD. Characteristic peaks of brushite were observed in NHHA1–1 pattern at 2θ = 11.6°, 20.9°, 23.4°, 29.1°, 30.5°, 31.2°, 34.1°, 37.0°, 41.5°, 42.0° and 48.4° for (020), (021), (040), (041), ($\bar{2}$21), ($\bar{1}$12), (220), (022), (151), ($\bar{2}$42) and (260) reflections, respectively. In NHHA1–2 sample, on the other hand, a mixture of hydroxyapatite–brushite phases is observed as follows: *(i)* brushite at 2θ = 11.68°, 20.93°, 30.50°, 34.1°, 41.5° and 42.0° for (020), (021), ($\bar{2}$21), (220), (151) and ($\bar{2}$42) reflections, and *(ii)* HA at 2θ = 21.8°, 25.9°, 31.7°, 32.2°, 46.7° and 48.7° for (200), (002), (211), (112), (222) and (312) reflections, respectively. For NHHA1–3 and NHHA1–4 samples all diffraction peaks have been indexed for HA. These results confirm the previous findings obtained by TGA and FTIR analysis.

Scanning Electron Microscopy

Surface morphology of NHHA1–3 sample with SDBS surfactant was observed by SEM (see Figure II.13). Sample morphology is formed by cloud–like or lump–like HA particles.

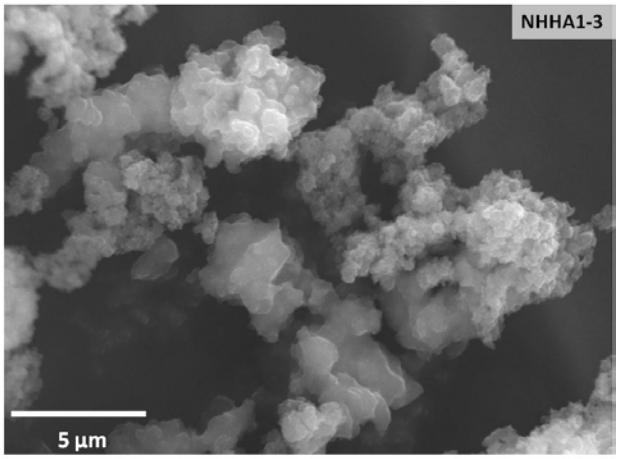

Figure II.13 Particle morphology of hybrid material.

Transmission Electron Microscopy and Electron Diffraction

Samples were also characterized by transmission electron microscopy and electron diffraction (TEM–ED). Figure II.14.a displays a TEM micrograph of NHHA1–3 sample, showing structures close to needle-like particles of HA, which is the usual HA formed by precipitation [29].

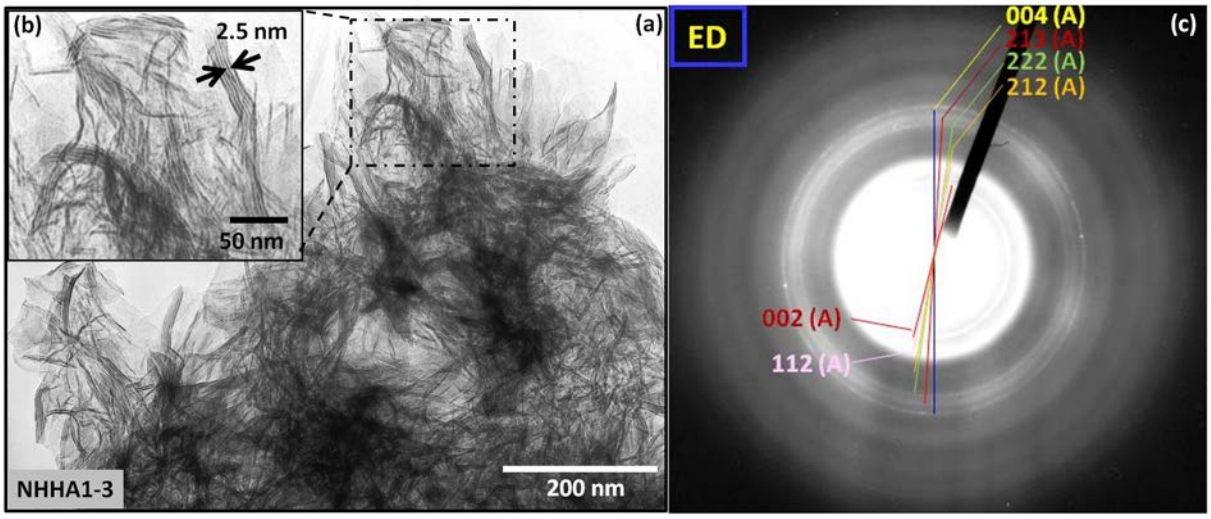

Figure II.14 (a and b) TEM images showing a discontinuous lamellar mesostructure and (c) ED pattern of an apatite phase (A) for NHA1-3 hybrid material.

Furthermore, the synthesized hybrid material exhibits HA with a lamellar mesostructure, with 2.5 nm of layer distance. Figure II.14.b is a magnification over the marked area and shows a lamellar mesostructure obtained by the presence of SDBS. Layer repetition does not go above 5 times and the formation presents a curved structure. We have described this formation as a *discontinuous lamellar mesophase*. Dark contrast areas represent higher electron density regions which correspond to HA, electrostatically interacting with the head groups of the surfactants. On the other hand, clear regions are the surfactants in mesostructured lamellar formation**.** Figure II.14.c shows the corresponding ED pattern of this sample. This pattern exhibits the presence of rings that can be assigned to a poorly crystallized apatite-like phase.

Conclusion of Section II.2.b

Brushite and a mixture of brushite and HA were observed when [SDBS] ≤ 30 mM while HA with lamellar mesostructure was observed in samples prepared at [SDBS] ≥ 60 mM. The layer spacing of lamellar mesostructures measured by TEM was around 2.5 nm. However, layer repetition does not go above 5 times and the formation presents a curved structure. We have described this formation as a *discontinuous lamellar mesophase*. The formation of this lamellar mesostructures of calcium phosphate hybrids is schematically depicted in Figure II.15.

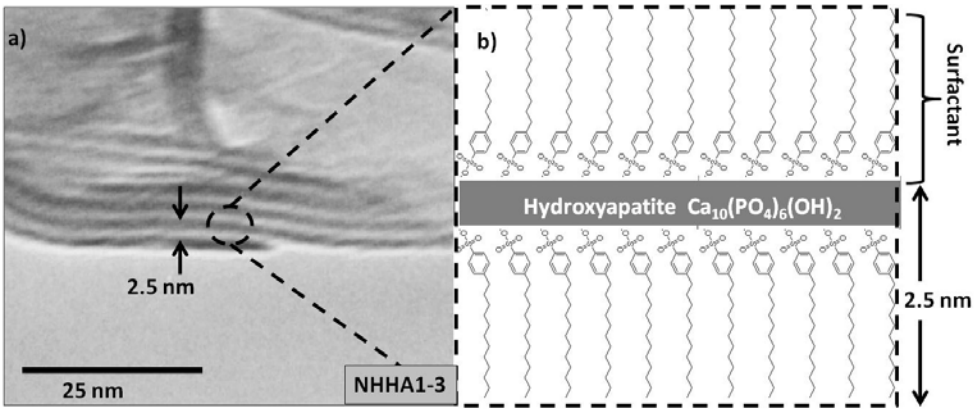

Figure II.15 a) TEM image of lamellar structure in NHHA1-3 sample and b) schematic representation of the lamellar formation by SDBS presence during CaP precipitation.

The Ca/P molar ratio of 1 used during synthesis is not appropriate for obtaining HA phase, therefore this result maybe attributable to another factor. Measurements of pH reached during the syntheses show that pH increases with the increase of surfactant concentration from 7 up to 9. Hence, the protonation of sulphate polar heads of SDBS in phosphate aqueous solution increases the pH value of the medium during the synthesis. Consequently, this phenomenon allowed us to obtain as follows: *(i)* brushite phase at [SDBS] < 30 mM (pH = 7); *(ii)* a mixture phase of calcium phosphates (brushite and HA) at 30 mM ≥ [SDBS] ≤ 60 mM and *(iii)* HA at [SDBS] ≥ 60 mM (pH = 9).

II.3 Calcium phosphate in the presence of surfactant mixture: anionic and cationic

According to our previous studies, sections II.2a and II.2b, and the study reported by *Wang* [5], it is possible to synthesize lamellar mesostructured HA using SDS, SDBS and MAP anionic surfactants as template by the molecular self-assembly method. As already reported, anionic surfactants have good interaction with calcium ions. On the other hand, the cationic surfactant CTAB ($R–N^+Me_3Br^–$) is well known to synthesize the hexagonally mesostructured silica and it hardly interacts with Ca^{2+} cations. For the first time, to synthesize hexagonal mesostructured calcium phosphate phase through the interaction between CTAB and calcium ions, SDS and SDBS anionic surfactants and MAP were used to facility their reciprocal interactions. The addition of two different surfactants into the same solution could be useful to obtain a different mesostructure than lamellar, maintaining a good interaction of the CaP ionic phase with the anionic surfactant. To obtain this kind of hybrid materials, a homogenous mixture of the surfactants would be needed in the surfactant assemblies.

II.3.a Calcium phosphate in mixed surfactants of sodium dodecyl sulphate and cetyltrimethyl ammonium bromide

This part describes the precipitation of CaPs in the presence of mixtures of surfactant such as SDS and CTAB (1:1/mol:mol). These two surfactants were added as structure directing agents due to their mesostructure formation ability, namely lamellar layers and micelles, respectively. Seven samples were synthesized and the calcium phosphate phase formed and its mesostructure were studied. Synthesized multistructured hybrid CaP materials were shortly named as MHCaP-X with Ca/P molar ratio 1, where X indicates the number of synthesized sample (X = 1 to 7).

Thermogravimetric and Differential Thermal Analysis

TGA and DTA curves for hybrid materials of this series are shown in Figure II.16. Except for hybrid material prepared with the lower surfactant concentration, *i.e.*, [SDS+CTAB]= 5 mM, all of them present similar behaviour.

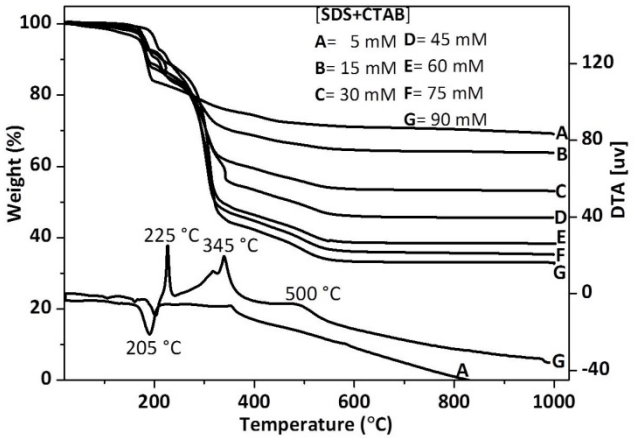

Figure II.16 Thermogravimetric and differential thermal analysis curves for MHCaP-X hybrid materials obtained with Ca/P molar ratio 1 and [SDS+CTAB] = 5 to 90 mM. DTA curve for hybrid material prepared with [SDS+CTAB]= 90 mM is shown as representative example for hybrid material prepared with [SDS+CTAB]= 15 to 90 mM.

TGA curves exhibited a slight weight loss between room temperature and 125 °C that was attributed to the loss of water adsorbed in the samples.

All samples present a weight loss around 200 °C, clearly associated with an endothermic process in the DTA curve. This behaviour is typical for the phase transition of brushite to monetite, where the two water molecules of the crystal lattice are lost (see reaction 4). Therefore, these hybrid samples may content brushite as CaP principal phase.

$$CaHPO_4{\cdot}2H_2O\ (\text{brushite}) \xrightarrow{\Delta\ ^\circ C} CaHPO_4 + 2H_2O\uparrow \qquad (4)$$

At higher temperatures, in the range 250-600 °C, the surfactant combustion is registered with a weight loss in the TGA curves associated with exothermic peaks in the DTA curves. Weight losses for this process are 12, 20, 28, 33, 44, 48 and 49%, respectively. As expected, an increase in total amount of organic matter incorporated in the hybrid materials was observed according to the increase in surfactant mixture concentration during the synthesis of materials. However, it seems to be an upper limit around 50% since there is no further incorporation of organic matter in the sample prepared with [SDS+CTAB] = 90 mM with respect to the previous with [SDS+CTAB] = 75 mM, TGA curves for these two samples are almost coincident.

Fourier Transform Infrared Spectroscopy

The FTIR spectra of hybrid materials from 5 to 90 mM of [SDS+CTAB] (Figure II.17) showed that all samples are compatible with brushite-like phases with increasing contents of organic matter. Bands present in the spectra are listed as follows:

- *SDS and CTAB*: at 2954, 2916 and 2849 cm^{-1} bands for ν_{as}(CH), ν_{as}(CH) and ν_s(CH) of CH_3 and CH_2 groups.
- R-OSO_3^{2-} group: at *ca.* 1450, 1250 and 1215 cm^{-1} bands for ν(S=O), ν_{as}(SO) and ν_s(SO).
- *HPO_4^{2-}:* at 3531 and 3466 cm^{-1} bands for ν_{as}(OH) and ν_s(OH) for HPO_4^{2-}; at 1198 cm^{-1}, 1116 cm^{-1} and 1040 cm^{-1} bands for ν_{as}(PO) and ν_s(PO); at 790 cm^{-1} the band for δ(O-P-OH) and at 518 and 575 cm^{-1} bands for δ(OPO).
- *crystalline H_2O in brushite:* at 3256 and 3149 cm^{-1} bands for ν_{as}(OH) and ν_s(OH); at 1645 cm^{-1} band for δ(HOH).

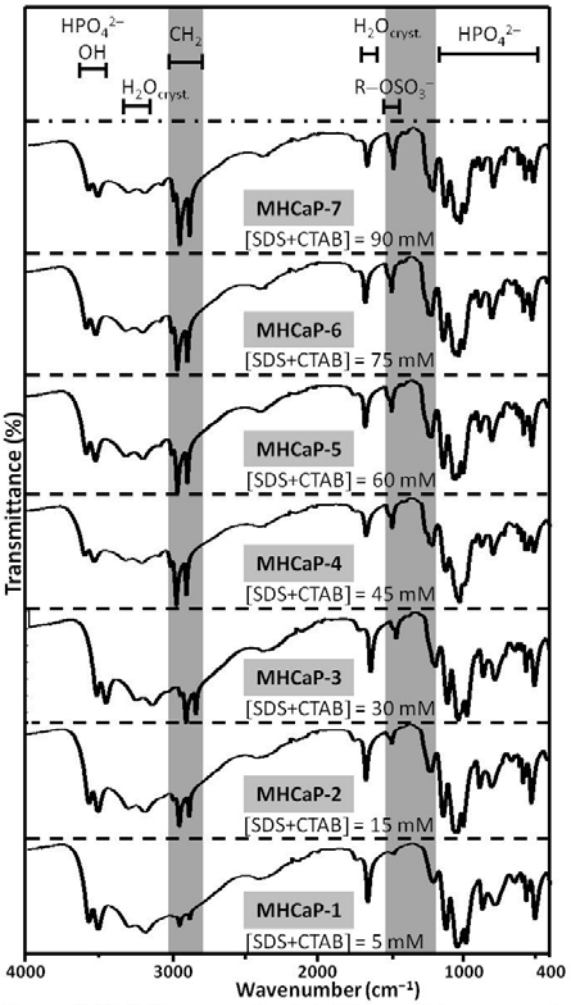

Figure II.17 FTIR spectra for hybrid materials prepared with Ca/P=1 and [SDS+CTAB]=5 to 90 mM and 1:1 molar ratio

Small and wide angle X–ray Diffraction

Figures II.18 and II.19 show the SA–XRD and WA–XRD patterns of hybrid materials to analyse the possible mesostructural order and the phase of calcium phosphate formed, respectively.

In Figure II.18 first and second peaks of a lamellar mesostructure were observed at 2θ = 2.3° and 4.6°, which can be respectively indexed to (100) and (200). The low intensity second peak could also be indexed to (100) of OCP phase. However, no OCP diffraction peaks have been identified in the WA region and furthermore, for samples prepared with [**SDS+CTAB**] > 60mM, the third peak of the lamellar structure (300) was observed at 2θ = 6.9° by WA–XRD (see Figure II.19).

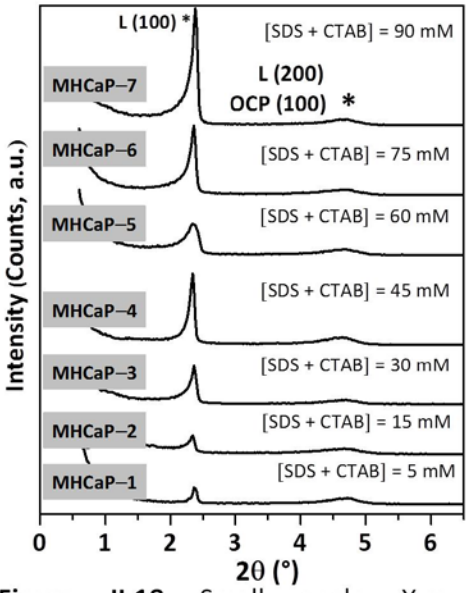

Figure II.18 Small angle X-ray diffraction patterns of hybrid materials prepared with increasing concentration of surfactant mixture.

The 100 reflexion of the lamellar mesostructure was observed as a low intensity peak for samples MHCaP-1, MHCaP-2 and MHCaP-3 prepared with [**SDS+CTAB] = 5, 15** and **30 mM**, respectively. A more intense peak was observed in MHCaP-4, MHCaP-5, MHCaP-6 and MHCaP-7 samples prepared from [**SDS+CTAB] = 45, 60, 75 and 90 mM**, respectively. Therefore, an increase in intensity of lamellar peak was observed as surfactant concentration increased during synthesis of materials.

Regarding the CaP phase obtained in the hybrid materials, the WA-XRD patterns show in all cases the characteristic diffraction peaks of brushite [23] (Figure II.19).

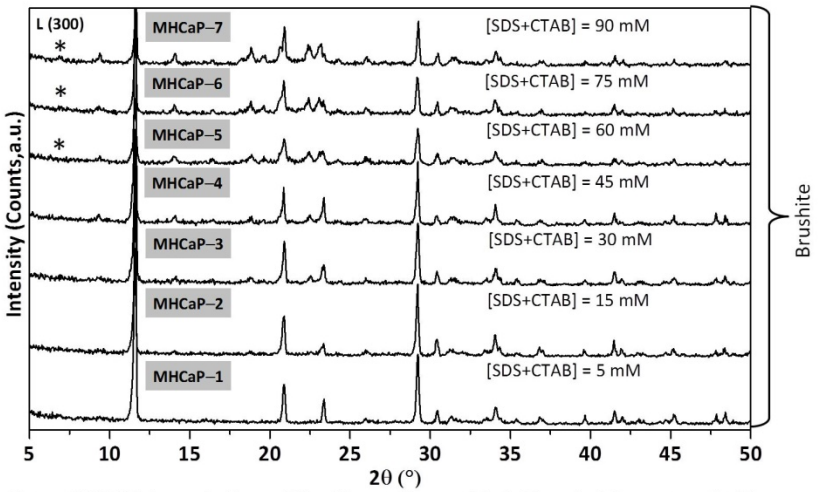

Figure II.19 Wide angle X-ray diffraction patterns of hybrid materials prepared with increasing concentration of surfactant mixture.

Transmission Electron Microscopy – Electron Diffraction

TEM micrographs show two different morphological features in MHCaP-7 sample because rods and sheets or patches of around 300 nm in size are identified (see Figure II.20.a). Inset in Figure II.20.a shows the corresponding ED pattern exhibiting rings that can be assigned to a rather poorly crystallized brushite-like phase.

The rods possess a lamellar mesostructure with 1.7 nm layer spacing and its formation may be explained due to the presence of SDS surfactant (see Figure II.20.c). Unfortunately, a deep analysis of the sheets was not possible with the transmission electron microscope since these particles rapidly decompose under the electron beam.

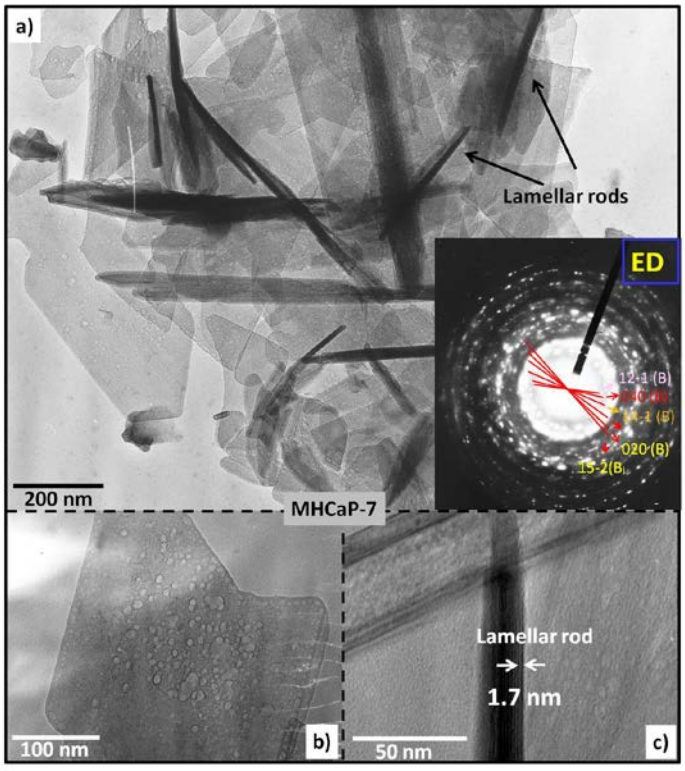

Figure II.20 TEM images of MHCaP-7 sample prepared with [SDS+CTAB] = 90 mM.

In Figure II.20.b it can be observed a bubbles formation which was appreciable in a very short time, probably due to the combustion and evaporation of organic matter form the hybrid sample, as well as evaporation of crystalline water from the brushite phase.

Conclusion of Section II.3.a

An equimolar mixture of SDS and CTAB in increasing concentrations (from 5 to 90 mM) has been used as structure directing agent to obtain a lamellar mesostructured brushite calcium phosphate. Lamellar mesostructured brushite rods were identified by TEM-ED, although the presence of sheets with no clear mesostructure was also observed.

II.3.b Calcium phosphate in mixed surfactants of sodium dodecyl benzene sulphonate and cetyltrimethyl ammonium bromide

This section describes the synthesis of mesostructured hybrid calcium phosphates by precipitation in the presence of the mixture of SDBS and CTAB. Two samples were prepared with Ca/P molar ratio 1 and surfactant mixture concentration of 30 mM with 3:1 and 1:3 SDBS/CATB molar ratios, respectively. According to Section II.2.b, we expect to obtain HA in samples from highly concentrated SDBS surfactant in aqueous media. In highly concentrated CTAB surfactant solution, with the Ca/P molar ratio 1, we expect to obtain brushite. Synthesized organic-inorganic hybrid mesostructured materials were shortly named as HMM31 for SDBS+CTAB (3:1) and HMM13 for SDBS+CTAB (1:3).

Thermogravimetric and Differential Thermal Analysis

TG and DTA curves for both hybrid materials are consistent with the presence of brushite because the sharp weight loss around 200 °C is associated with the endothermic process for crystalline water loosing, as previously commented. Surfactant combustion is confirmed by DTA exothermic processes in the 300-600 °C temperature range. The exothermic peak around 500 °C is usually present in CTAB containing samples, therefore it is intense in the hybrid material prepared with the higher ratio in CTAB, HMM13 sample.

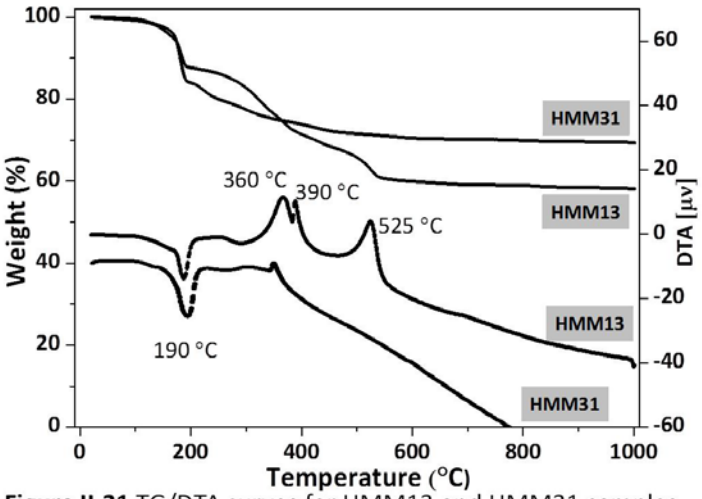

Figure II.21 TG/DTA curves for HMM13 and HMM31 samples.

Fourier Transform Infrared Spectroscopy

FTIR spectra of HMM13 and HMM31 samples prepared with SDBS+CTAB in molar ratios 1:3 and 3:1 respectively (Figure II.22) are compatible with brushite and apatite–like profiles, respectively. However, pure HA cannot be assigned for HMM31 sample only with FTIR data since the presence of brushite is pointed out from the TG/DTA data.

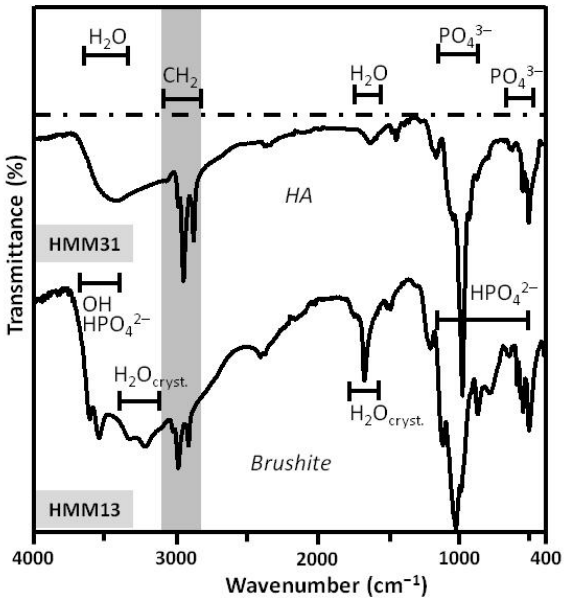

Figure II.22 FTIR spectra of hybrid materials prepared with [SDBS+CTAB] in molar ratios 1:3 and 3:1.

Small and Wide angle X–ray Diffraction

The X–ray diffraction patterns of the hybrid samples are shown in Figure II.23. By SA–XRD no clear mesostructure is detected in any of the two samples, although two broad reflections centred at 2.9° and 4.5° seem to emerge in the SA diffractogram for the sample with higher SDBS content.

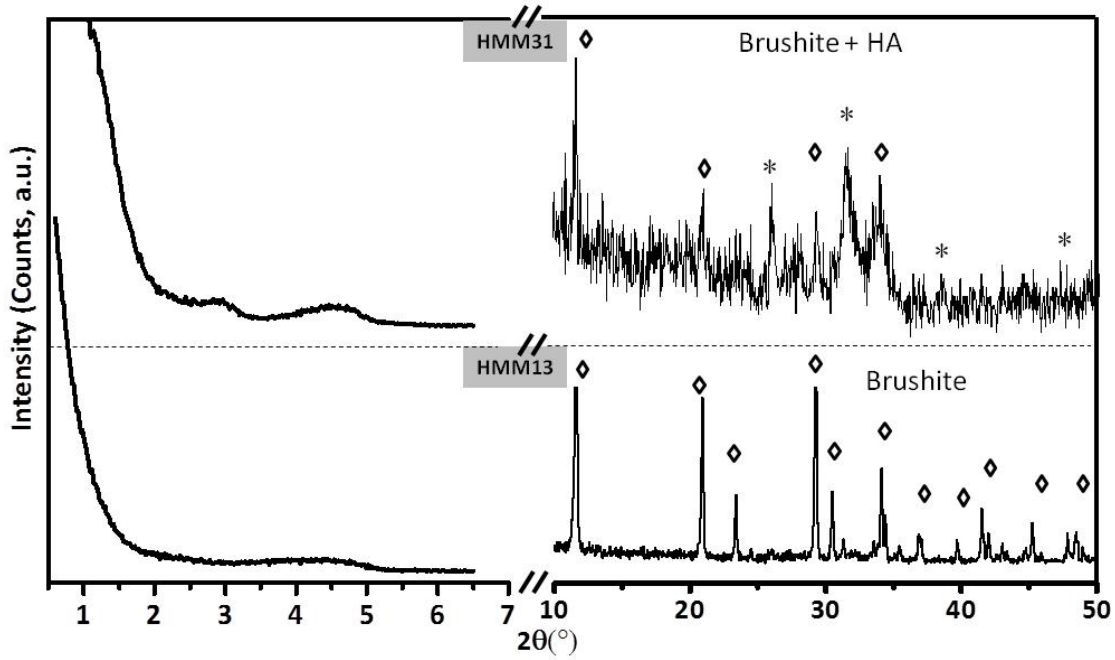

Figure II.23 Small angle (left) and wide angle (right) XRD patterns of hybrid materials HMM13 and HMM31, where * and ◊ indicate HA and brushite, respectively.

By WA–XRD, a brushite phase was clearly confirmed for HMM13 (1:3 mol ratio of SDBS+CTAB). On the other hand, a mixture of low crystalline HA and low crystalline brushite is identified for sample HMM31 (3:1 mol ratio of SDBS+CTAB). The formation of HA in this sample prepared with a Ca/P

molar ratio 1 can be explained due to a higher amount of SDBS surfactant than CTAB surfactant. The presence of higher amount of SDBS allows the pH of the medium increase during the synthesis due to the protonation of sulphonate polar head in phosphate aqueous solution (see section II.2.b). Therefore, two different CaPs have been obtained in the presence of SDBS and CTAB mixture by only changing the surfactant proportions.

Transmission Electron Microscopy

TEM images of HMM31 sample (Figure II.24) reflect the mixture of apatite and brushite phases found in the WA-XRD analysis. Two different particle morphologies are observed in the sample, nanorods identified as a low crystalline apatite in their ED pattern rings (Figures II.24 a and b, respectively) and sheets with a prismatic shape typical for brushite (Figure II.24.e). TEM images at higher magnification of the nanorods reveal a hybrid material with lamellar mesostructure having a 1.6 nm of layer spacing. The difference with the hybrid material obtained in the presence of pure SDBD (sample NHA1-3, layer spacing 2.5 nm, Figure II.14) can be attributed to the simultaneous presence of CTAB in this sample. Unfortunately, the analysis at higher magnification of the prismatic particles results in their quick decomposition, probably due to the combustion and evaporation of the organic matter and evaporation of the crystalline water of brushite under the electron beam.

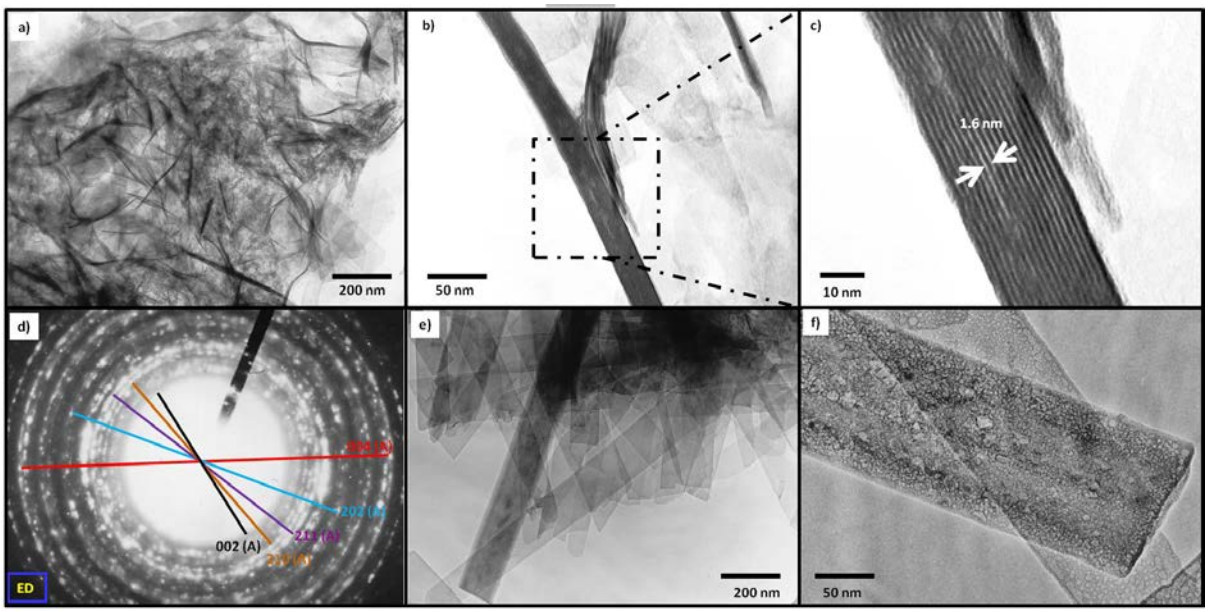

Figure II.24 TEM images of different regions in hybrid material HMM31 (SDBS+CTAB = 3:1, mol/mol). (a) Region of nanorods identified as HA by ED, (b) and (c) HRTEM images of the nanorods, (d) ED pattern of the nanorods region, (e) region of sheets with a prismatic shape typical for brushite and (f) HRTEM images of the sheets where bubbles due to decomposition are observed.

Conclusion of Section II.3.b

Two phases of calcium phosphate were obtained from Ca/P molar ratio 1 and [SDBS+CTAB] = 30 mM (1:3 and 3:1, mol:mol) by precipitation in aqueous media. The different CaP phases were obtained by

changing the molar ratio of surfactants. According to WA-XRD, crystalline brushite was obtained when SDBS+CTAB (1:3) and a mixture of low crystalline hydroxyapatite and brushite when SDBS+CTAB (3:1). Hence, surfactants ratio plays an important role on the obtained CaP phase. A higher presence of SDBS in the surfactant mixture favours the obtaining of HA, since protonation features of SDBS in aqueous media is responsible of a pH increase and HA growth, as it was justified in the case of CaP precipitation in the presence of SDBS alone. Also a lamellar mesostructure is favoured in the presence of a higher ratio of SDBS.

II.3.c Calcium phosphate in mixed surfactants of mono-n-dodecyl phosphate and cetyltrimethyl ammonium bromide

The synthesis of calcium phosphates by precipitation in the presence of the surfactants mixture MAP and CTAB is here presented. The synthesized hybrid material was prepared with [MAP+CTAB] = 240 mM, surfactant mixture in 1:1 molar ratio and Ca/P molar ratio 1. After the precipitation of the CaP the material was subjected to an autoclave process. The sample is termed LCaP.

Thermogravimetric and Differential Thermal Analysis

A total weight loss of 27% took place between RT and 500 °C. This weight loss is attributed mainly to organic matter due to the temperature range in which is produced (200-500 °C), as well as the absence in this case of a clear endothermic peak around 200 °C. This fact would exclude the presence of brushite in this sample.

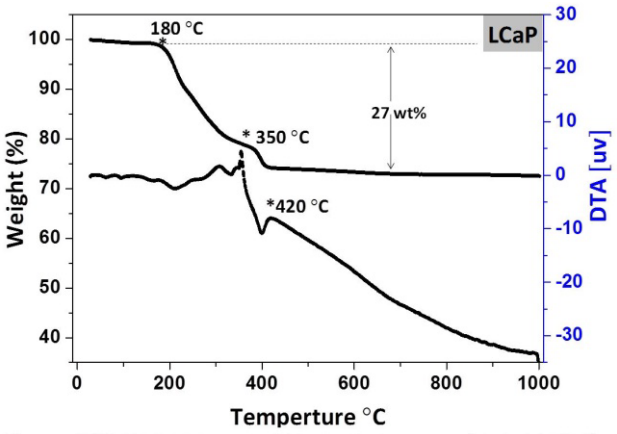

Figure II.25 Weight loss and thermal changes of hybrid LCaP sample.

Fourier Transform Infrared Spectroscopy

The FTIR spectrum of this material is shown in Figure II.26 and is similar to that of monetite together with an appreciable amount of organic matter.

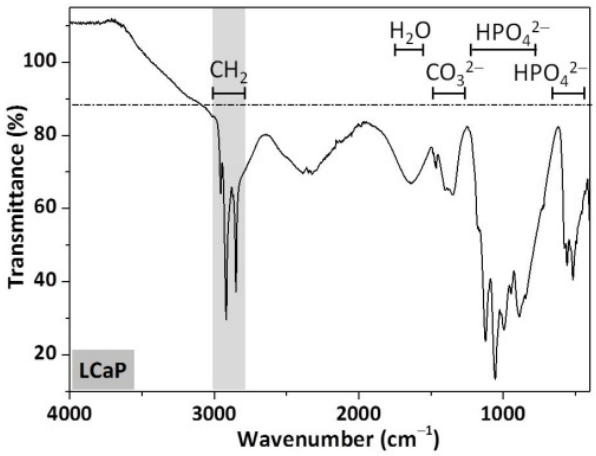

Figure II.26 FTIR spectrum of LCaP hybrid material.

Small and wide angle X–ray Diffraction

SA–XRD and WA–XRD patterns of this material are shown in Figure II.27. SA–XRD pattern showed the first and second maxima of lamellar structure (L–marked in the figure) observed at 2θ = 2.4 and 4.9°. The third maximum of the lamellar structure was observed at 2θ = 7.3° in the WA diffractogram. The calculated distances are 3.60, 1.82 and 1.21 nm for these three reflexions, which are very similar to the reported ones for lamellar HA prepared in the presence of pure MAP [5].

Intense diffraction maxima, attributable to monetite, are observed in the WA–XRD pattern at 2θ = 13.1°, 20.6°, 26.5°, 28.5°, 30.1°, 32.6°, 35.9°, 38.8°, 40.1°, 41°, 44.5°, 45.7°, 47.5°, 49.2°, 50.6° and 53.0° that can be assigned to (010), (1$\bar{2}$0), (2$\bar{2}$0), ($\bar{1}$ $\bar{1}$1), ($\bar{1}$12), (102), (0$\bar{2}$2), (120), (030), (003), ($\bar{1}$32), (3$\bar{4}$0), ($\bar{3}$22), (3$\bar{2}$2), (122) and (3$\bar{1}$2) reflections, respectively.

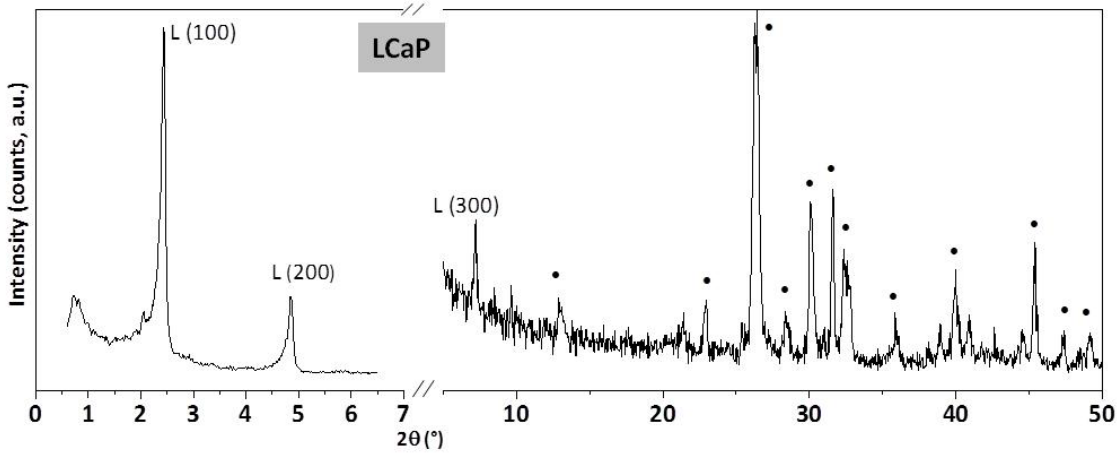

Figure II.27 Lamellar mesostructure (left) and crystalline monetite (right) as detected by SA–XRD and WA–XRD measurements respectively. • indicate monetite diffraction maxima.

Scanning Electron Microscopy

The surface morphology of the hybrid material was examined by SEM, see Figure II.28. Two different morphologies, needle and cloud–like, were observed in Figure II.28.a. Moreover a cloud-like structure formed by shell layers can be seen in Figure II.28.b.

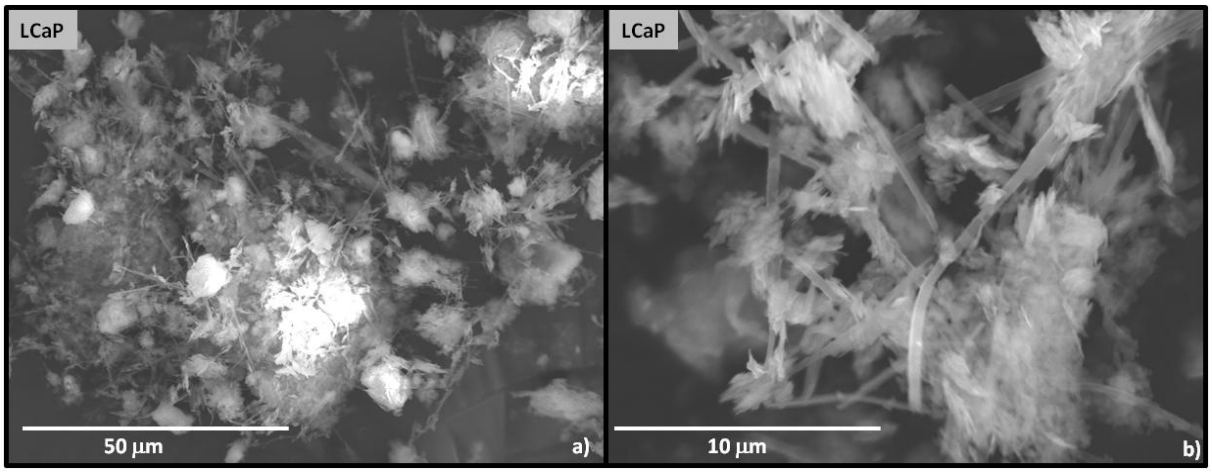

Figure II.28 SEM images of hybrid calcium phosphate obtained with MAP+CTAB (1:1) and Ca/P = 1.

Transmission Electron Microscopy

The observation of this sample by TEM was not fully useful since the sample mostly decomposes under the electron beam and a rapid bubble formation is produced (Figure II.29, right). Nonetheless, a lamellar structure with 3.5 nm of layer distance was observed in some stable prismatic rod particles. This mesostructure is probably due to the presence of MAP because of its lamellar formation features in calcium phosphates already reported [5].

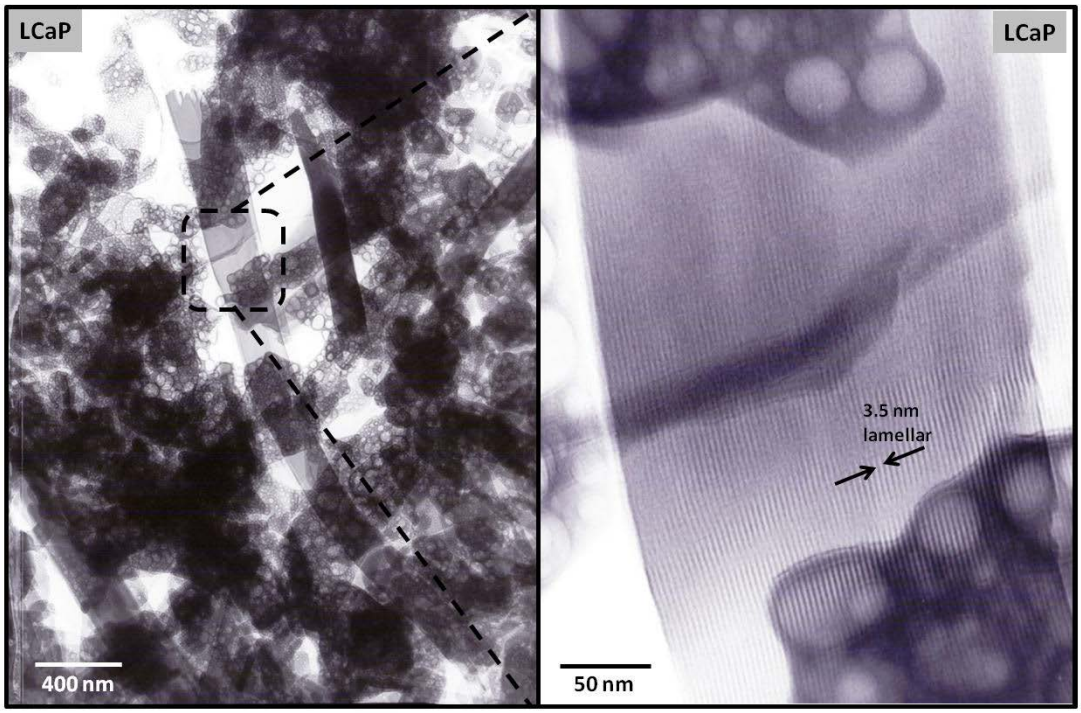

Figure II.29 TEM images at different magnifications of hybrid LCaP sample.

Conclusion of Section II.3.c

On one hand, as already found in section II.2.a, the use after the CaP precipitation of an energetic process, such as synthesis in an autoclave, leads to the achieving of monetite, a calcium phosphate phase derived from brushite but without the two water molecules. On the other hand, the hybrid sample is not stable under the TEM examination. Only particles with a clear lamellar mesostructure seem to be stable, which could point to the accomplishing of stable phases only in the case of mesostructure formation. Lamellar mesostructure would be due to the presence of MAP. The presence of CTAB does not modified the spacing distances with respect to samples prepared in the presence of pure MAP.

II.4 Calcium phosphate in the presence of a zwitterionic surfactant

A zwitterion (formerly called a dipolar ion) is a neutral molecule with a simultaneous positive and a negative electrical charge at different locations within the molecule. A zwitterionic surfactant such as EPG®BB exhibits neutral charge arising from the presence of a quaternary ammonium group and a deprotonated carboxylic acid group in its “polar” head. The aim in this section was to synthesize CaP

materials in the presence of zwitterionic surfactant by precipitation to check whether mesostructural order could be obtained.

Four materials were synthesized in 30 and 45 mM concentrations of EPG®BB surfactant by adding the solutions containing Ca^{2+} and HPO_4^{2-} ions in different order. Therefore, two synthesis methods have been assayed as follows: in the first one, the calcium salt was dissolved in EPG®BB solution and then hydrogen phosphate salt was added to it and, in the second case, hydrogen phosphate salt was dissolved in EPG®BB solution and then the calcium salt was added to the solution. Two materials synthesized with [EPG] = 30 and 45 mM with Ca^{2+} in the solution were denominated CaP1 and CaP2, respectively. The other two materials synthesized with [EPG] = 30 and 45 mM with hydrogen phosphate ions in the solution were called PCa1 and PCa2, respectively. In all cases the Ca/P molar ratio was 1.

Thermogravimetric and Differential Thermal Analysis

PCa1 and PCa2 samples showed similar results to CaP1 and CaP2 samples. Thus, TGA curves for just two samples, PCa1 and PCa2, are shown in Figure II.30. DTA curves for all the samples were also very similar and only that of PCa1 is represented in the figure. TGA curves of samples PCa1 and PCa2 show a sharp weight losses of 23 and 33% around 200 °C respectively, which occurs simultaneously with an endothermic peak in DTA. This process is attributed to the removal of crystalline water from brushite. Phase change from brushite to monetite occurred at about 200 °C when removing crystallization water molecules. Remarkably there is not apparent loss of organic matter in these samples.

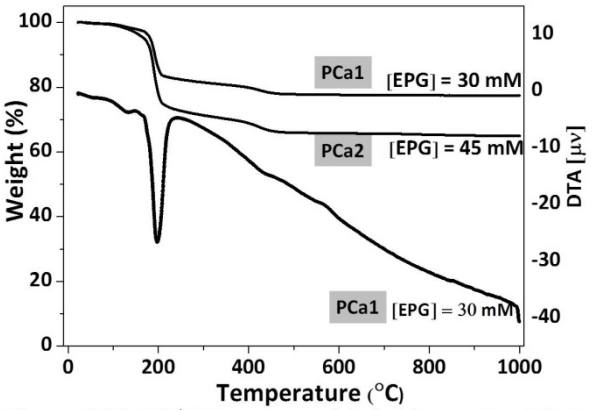

Figure II.30 TG/DTA curves of hybrid samples PCa1 and PCa2.

Fourier Transform Infrared Spectroscopy

FTIR analysis of the four samples shows brushite characteristic spectrum for each of them (see Figure II.31). As already suspected from the TG/DTA data, no bands due to ν(CH) modes from EPG®BB in the samples were observed around 2900 cm^{-1}, therefore, the absence of organic matter points to a lack of interaction between CaP and EPG®BB surfactant.

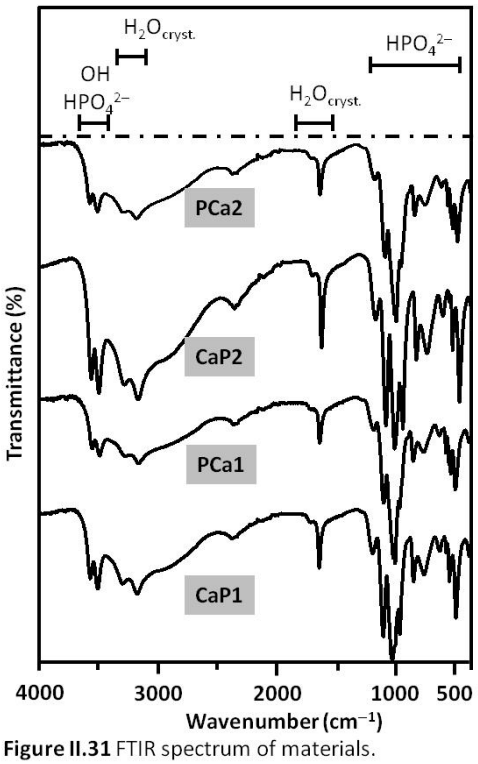

Figure II.31 FTIR spectrum of materials.

Small and wide angle X–ray Diffraction

Small and wide angle X–ray diffraction patterns of these materials are shown in Figure II.32. By WA-XRD analysis crystalline brushite was observed in all samples. Brushite peaks were detected at 2θ = 11.6°, 20.9°, 23.3°, 29.2°, 30.4°, 34.0°, 41.5°, 42.0°, 45.2°, 48.4 and 50.1° for (020), (021), (040), (041), $(\bar{2}21)$, (220), (151), $(\bar{2}42)$, $(\bar{1}71)$, (260) and(241), respectively.

By SA-XRD one broad peak is observed at 2θ = 4.6° in all samples, which could be attributable to the first diffraction maxima of the octacalcium phosphate phase (OCP) [30]. However, the width of the peak is not characteristic for a crystalline OCP phase. Furthermore, no peaks attributable to OCP were found in the WA-XRD analysis. In fact, in the diffractograms of CaP1 and CaP2 samples there appear two broad maxima, at 2θ = 1° and 4.6°, that are not clearly indexable to a mesostructure, taking into account as well that there is not a surfactant template present in these samples, in agreement with TG/DTA and FTIR analysis.

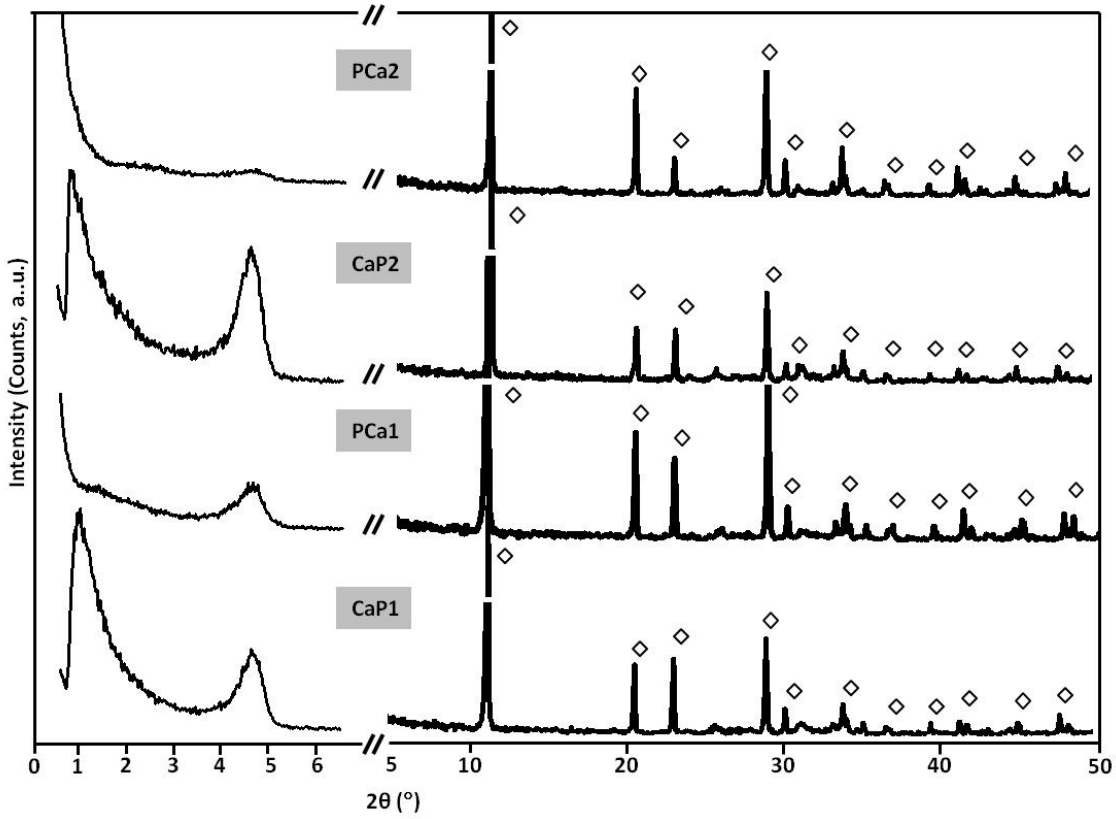

Figure II.32 Small angle (left) and wide angle (right) X–ray diffraction patterns of materials prepared in the presence of EPG®BB surfactant, where ◊ indicates brushite.

In order to better clarify the possible assignment of these two maxima an additional sample was prepared. The synthesis of the calcium phosphate phase was performed in the same experimental conditions that for samples CaP1 and CaP2, but in the absence of surfactant. The results analyzed by XRD (Figure II.33) show the same diffraction pattern in both angle regions, *i.e.*, two broad maxima at 2θ = 1° and 4.7°, and the calcium phosphate phase of brushite.

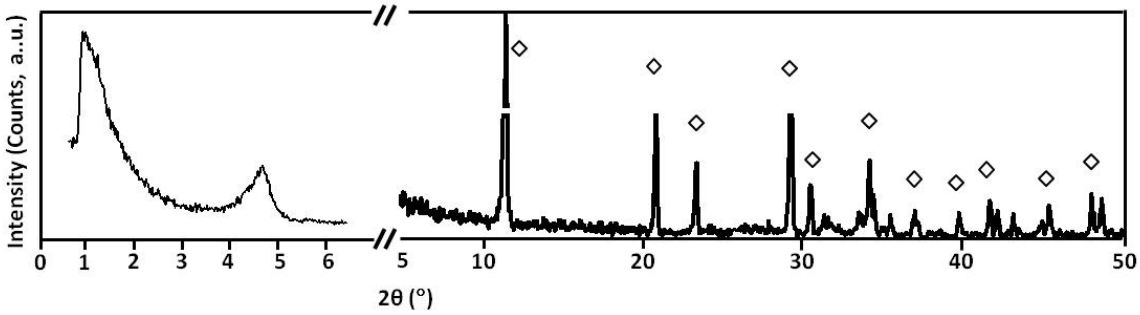

Figure II.33. Small angle (left) and wide angle (right) X–ray diffraction patterns of calcium phosphate prepared in the absence of surfactant, where ◊ indicates brushite.

In fact, these two broad maxima were already observed for samples prepared in very low surfactant concentration, such as [SDS] = 15 and 30 mM (Figure II.6, II.7 and II.8) and [SDBS] = 15 mM (Figure II.12). By now we do not have a satisfactory explanation for these two broad maxima at such a low diffraction angle, since a deeper analysis of these samples by TEM was not possible, as explained below.

Transmission Electron Microscopy

In an attempt to clarify structural aspects the CaP2 sample was subjected to TEM observation (Figure II.34). Unfortunately, this sample was not stable under the electron beam. A very quick bubble formation was observed and taking into account that this sample does not contain organic matter this fact is probably caused from the evaporation of water from the crystalline brushite.

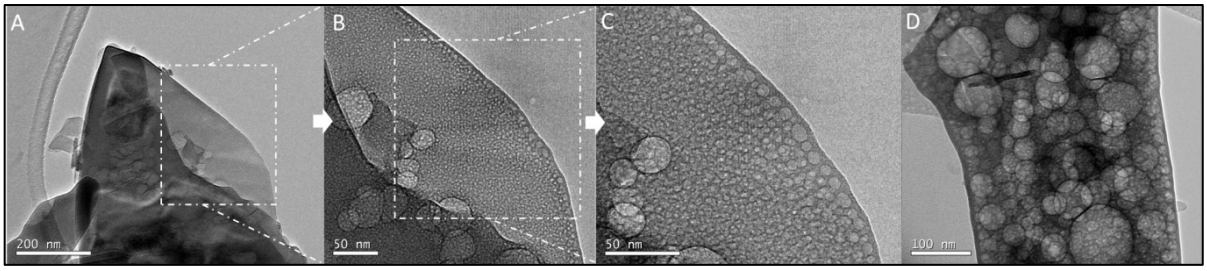

Figure II.34 TEM images of the CaP2 sample. A, B and C are different magnifications of the same particle showing rapid evolution with time. D is an image of another particle in the sample.

Conclusion of Section II.4

EPG®BB surfactant was assayed as a structure template to synthesize mesostructured calcium phosphate for the first time. However, FTIR results did not show any stretching bands from CH_2 groups of EPG®BB and no weight loss due to organic matter was detected by TGA. Therefore, we can conclude that there is no interaction between CaP and this zwitterionic surfactant. As a consequence, no defined mesostructure was observed by small angle X–ray diffraction. Crystalline brushite was identified by wide angle X–ray diffraction and this phase was not stable under the TEM analysis conditions.

II.5 Conclusions of Chapter II

The interaction of several amphiphilic molecules with silica in aqueous media has led, through the confluence between the sol-gel and supramolecular chemistries, to a variety of mesoporous silica materials which are thoroughly investigated for many industrial applications and biomedicine. In this field, the synthesis of mesostructured calcium phosphates could bring new applications due to its likely bioactivity and biocompatibility. For this reason, several authors have treated to obtain them by using similar strategies of synthesis to those used for mesostructured silica. However, the chemical behaviour in aqueous solution of both families of compounds is completely different. Therefore, at the start of this thesis, the reported data on mesostructured calcium phosphates were limited to the obtaining of apatites with lamellar structure through its precipitation in the presence of two anionic surfactants: SDS and MAP.

In this chapter precipitation of calcium phosphates was investigated in the presence of:

1) ***Anionic surfactants:*** SDS (deepening on already published) and SDBS.
2) ***Mixture of an anionic surfactant***: SDS, SDBS, or MAP, and ***one cationic***: CTAB.
3) ***Zwiterionic surfactant:*** EPG

Table II.3 summarizes the families of compounds here investigated, including the results previously reported, the most significant results of this investigation and some suggestions for the future work.

Table II.3. Main results derived from the precipitation of calcium phosphates in the presence of ionic surfactants studied in Chapter II.

Surfactant	**Previous work of others**	**Main results of this thesis**	**Suggested work for the future**
SDS	Lamelar apatite [reference 6]	• Lamelar CaPs mixture • Lamelar brushite, rods	
SDBS	----	• Discontinuous lamelar apatite (or curved lamellar), meshes	Studies of bioactivity and biocompatibility of this new phase
MAP	Lamelar apatite [refs. 5,21,22]	----	----
SDS + CTAB	----	• Lamelar brushite, rods + non-mesostructured sheets (or plates)	CTAB does not improve the structural characteristics of the hybrids obtained with pure SDS, SDBS or MAP. CTAB does not seem to interact during the formation of the CaP lamellar phase.
SDBS + CTAB	----	• Low [SDBS]: non lamelar brushite • High [SDBS]: Lamelar HA + brushite (rods – prismatic lamelas)	
MAP + CTAB	----	• Lamelar monetite prismatic rods	
EPG (carboxybetaine)	----	• Brushite (no organic matter)	The use other zwitterionic surfactant containing sulfobetaines could be a promising approach

In our study, as well as the type of surfactant(s), it was investigated the effect of: the surfactant concentration, the pH of precipitation, the Ca/P molar ratio (set in most cases to 1.0 or 1.67), and other parameters of synthesis.

The main conclusions derived from the present study are summarized as follows:

- ✓ When high concentration of SDBS was used, a poorly crystallized HA was obtained even when the Ca/P molar ratio used during synthesis was 1. This result was attributed to the increase of the pH during the synthesis from 7 up to 9, due to the protonation of sulphate polar heads of SDBS in phosphate aqueous solution.
- ✓ SDBS plays a double role, it acts as mesostructure template as well as a base.
- ✓ The use of energetic processes, such as ageing in autoclave or refluxing the material after the CaP precipitation, leads to monetite, anhydrous dicalcium phosphate.
- ✓ The hybrid materials obtained by precipitation in the presence of surfactant mixtures showed two types of particles: (i) rod particles with lamellar mesostructure and (ii) sheet-like particles with no clear mesostructure. These sheet-like particles were not stable under the TEM analysis conditions. A rapid bubble formation process is explained by the combustion of the organic matter and the evaporation of the crystallization water from brushite. However, this fact points to a stabilization of the CaP phases in the case of clear mesostructure formation, because only the lamellar rods are stable under the TEM examination.
- ✓ The lamellar mesostructure formation mechanism is showed in Figure II.35. Firstly, surfactants were added into the hydrogen phosphate solution to obtain a structure template before adding Ca^{2+} solution. By this method, brushite and poorly crystallized HA with lamellar structure were obtained with **SDS, SDBS** and with the mixtures of **SDS+CTAB, SDBS+CTAB and MAP+CTAB.** However, in the case of mixtures of surfactants, the lamellar phase seems to be due just to SDS, SDBS or MAP, and CTAB does not seem to interact during the formation of the CaP lamellar phase.

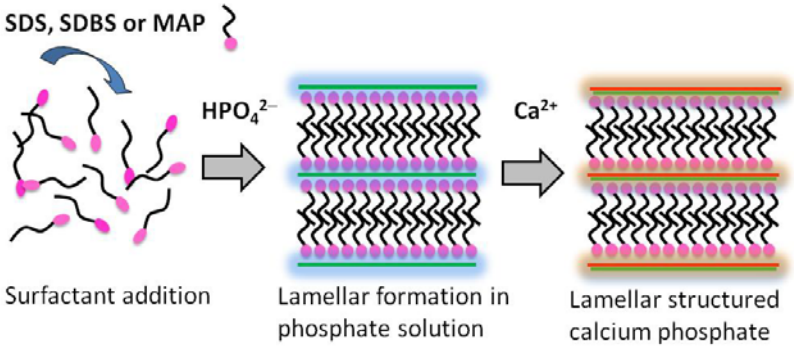

Figure II.35 Proposed mechanism for the synthesis of lamellar structured CaP in presence of SDS, SDBS or MAP surfactants.

In summary, ionic surfactants, especially anionic containing S or P in their polar heads, are useful to obtain mesostructured CaPs in lamellar mesostructure. In the future, the development of the synthesis techniques and methods for such a particular structures may be useful in the biomedical field for bone regeneration applications.

II.6 References:

1. J. B. Thompson, H. J. Kindt, B. Drake, H. G. Hansma, D.E. Morse, P. K. Hansma. *Nature* **2001**, *414*, 773-776. Bone indentation recovery time correlates with bond reforming time.

2. C. T. Kresge, M. E. Leonowicz, W. J. Roth, J. C. Vartuli, J. S. Beck. *Nature* **1992**, *359*, 710-712. Ordered mesoporous molecular sieves synthesized by a liquid-crystal template mechanism.

3. N. Kawa, Y. Oumi, T. Kimura, T. Ikeda, T. Sano. *J. Mater. Sci.* **2008**, *43*, 4198-4207. Synthesis of lamellar mesostructured calcium phosphates using n-alkylamines as structure-directing agents in alcohol/water mixed solvent systems.

4. H. Guo, F. Ye, H. Zhang. *Mater. Lett.* **2008**, *62*, 2129-2132. Tween-60 mediated synthesis of lamellar hydroxyapatite with worm-like mesopores.

5. S. Zhang, Y. Wang, K. Wei, X. Liu, J. Chen, X. Wang. *Mater. Lett.* **2007**, *61*, 1341-1345. Template-assisted synthesis of lamellar mesostructured hydroxyapatites.

6. C. Liu, X. Ji, G. Cheng. *Appl. Surf. Sci.* **2007**, *253*, 6840-6843. Template synthesis and characterization of highly ordered lamellar hydroxyapatite.

7. Y. Tokuoka, Y. Ito, K. Kitahara, Y. Niikura, A. Ochiai, N. Kawashima. *Chem. Lett.* **2006**, *35*, 1220-1221. Preparation of monetite ($CaHPO_4$) with hexagonally packed mesoporous structure by a sol-gel method using cationic surfactant aggregates as a template.

8. M. S. Schmidt, J. McDonald, E. T. Pineda, A. M. Verwilst, Y. Chen, R. Josephs, A. E. Ostafin. *Micropor. Mesopor. Mater.* **2006**, *94*, 330-338. Surfactant based assembly of mesoporous patterned calcium phosphate micron-sized rods.

9. H. Wang, L. Zhai, Y. Li, T. Shi. *Mater. Res. Bull.* **2008**, *43*, 1607-1614. Preparation of irregular mesoporous hydroxyapatite.

10. Y-H. Yang, C-H. Liu, Y-H. Liang, F-H: Lin, K. C. W. Wu. *J. Mater. Chem. B.* **2013**, *1*, 2447-2450. Hollow mesoporous hydroxyapatite nanoparticles (hmHANPs) with enhanced drug loading and pH-responsive release properties for intracellular drug delivery.

11. M. Vallet-Regí, F. Balas, D. Arcos. *Angew. Chem. Int. Ed.* **2007**, *46*, 7548-7558. Mesoporous materials for drug delivery.

12. F. Shao, L. Liu, K. Fan, Y. Cai, J. Yao. *J. Mater. Sci.* **2012**, *47*, 1054-1058. Ibuprofen loaded porous calcium phosphate nanospheres for skeletal drug delivery system.

13. C-. X. Zhao, L. Yu, A. P. J. Middelberg. *J. Mater. Chem. B.* **2013**, *1*, 4828-4833. Magnetic mesoporous silica nanoparticles end-capped with hydroxyapatite for pH-responsive drug release.

14. Y. Hong, H. Fan, B. Li, B. Guo, M. Liu, X. Zhang. *Mater. Sci. Eng. R.* **2010**, *R70*, 225-242. Fabrication, biological effects and medical applications of calcium phosphate nanoceramics.

15. S. Recillas, V. Rodriguez-Lugo, M.L. Montero, S. Viquez-Cano, L. Hernandez, V. M. Castano. *J. Ceram. Process Res.* **2012**, *13*, 5-10. Studies on the precipitation behaviour of calcium phosphate solutions.

16. Sergey V. Dorozhkin. *Front. Nanobiomed. Res.* **2014**, *2*, 219-341. Nanodimensional and nanocrystalline calcium orthophosphates.

17. N. Kawa, H. Hori, K. Tatsuo, Y. Oumi, T. Sano. *Micropor. Mesopor. Mat.* **2011**, *141*, 56-60. Unique surface property of surfactant-assisted mesoporous calcium phosphate.

18. J . Jinhua, F. Yong, Z. Lirong, Y. Hong, C. Yanli, Z. Dazhou, Z. Ping. *J. Mater. Sci.* **2011**, *46*, 3828-3834. Synthesis and characterization of multi-lamellar mesostructured hydroxyapatites using a series of fatty acids.

19. Q. Shen, H. Wei, Y. Zhao, D.-J. Wang, L.-Q. Zheng, D.-F. Xu. *Colloids Surface A.* **2004**, *251*, 87-91. Morphological control of calcium carbonate crystals by polyvinylpyrrolidone and sodium dodecyl benzene sulfonate.

20. V. Boonamnuayvitaya, C. Tayamanon, S. Sae-Ung, W. Tanthapanichakoon. *Chem. Eng. Sci.* **2006**, *61*, 1686-1691. Synthesis and characterization of porous media produced by a sol-gel method.

21. I. Soten, G. A. Ozin. *J. Mater. Chem.* **1999**, *9*, 703-710. Porous hydroxyapatite-dodecyl phosphate composite film on titania-titanium substrate.

22. A. G. Ozin, N. Varaksa, N. Coombs, J. E. Davies, D. D. Perovic, M. Ziliox. *J. Mater. Chem.* **1997**, *7*, 1601-1607. Bone mimetics: a composite of hydroxyapatite and calcium dodecylphosphate lamellar phase.

23. J. Zhang, M. Fujiwara, Q. Xu, Y. Zhu, M. Iwasa, D. Jiang. *Micropor. Mesopor. Mater.* **2008**, *111*, 411-416. Synthesis of mesoporous calcium phosphate using hybrid templates.

24. S. Han, W. Hou, W. Dang, J. Xu, J. Hu, D. Li. *Mater. Lett.* **2003**, *57*, 4520-4524. Synthesis of rod-like mesoporous silica using mixed surfactants of cetyltrimethylammonium bromide and cetyltrimethylammonium chloride as templates.

25. R. Z. LeGeros. *KARGER* **1991**, *Vol.15*. Calcium phosphates in oral biology and medicine.

26. G. Cheng, C. Liu. *Mater. Chem. Phys.* **2003**, *77*, 359-364. Preparation of lamellar mesoporous silica microspheres via SDS templates.

27. J. C. Elliott. *Elsevier Science B. V.* **1994**, 387. Structure and chemistry of the apatites and other calcium orthophosphates.

28. H. Zhao, W. He, Y. Wang, Y. Yue, X. Gao, Z. Li, S. Yan, W. Zhou, X. Zhang. *Mater. Chem. Phys.* **2008**, *111*, 265-270. Biomineralizing synthesis of mesoporous hydroxyapatite-calcium pyrophosphate polycrystal using ovalbumin as biosurfactant.

29. M. P. Ferraz, F. J. Monteiro, C. M. Manuel. *J. Appl. Biomater. Biomech.* **2004**, *2*, 74-80. Hydroxyapatite nanoparticles: a review of preparation methodologies.

30. Y. Honda, T. Anada, S. Morimoto, Y. Shiwaku, O. Suzuki. *Cryst. Growth Des.* **2011**, *11*, 1462-1468. Effect of Zn^{2+} on the physicochemical characteristics of octacalcium phosphate and Its hydrolysis into apatitic phases.

III. PRECIPITATION OF MESOSTRUCTURED CALCIUM PHOSPHATES IN THE PRESENCE OF PHOSPHOLIPIDS

III.1 Introduction

As it was previously indicated, in recent years particular attention has been paid to the preparation of mesostructured CaPs by using a templating route [1-9]. In this chapter, phospholipids (PLs) are used as structure directing agents, specifically phosphatidylcholine (PC) because is a biocompatible substance that exhibits self-assembly characteristics in water [5, 10-12]. PLs are widely distributed throughout the human body such as structural components in the cell and nucleus membranes. Due to their high biocompatibility they are receiving increasing attention in the synthesis of new biomimetic biomaterials [13-15]. PC plays an important role in many biological processes [15-18]. However until now, few studies were published about the synthesis of CaPs in the presence of PLs or PC [7, 19-22].

PC can be obtained from different sources such as egg yolk or soy bean [10]. Figure III.1 shows the schematic depiction of a PC molecule showing its main structural features: hydrophobic tails, glycerol and polar head groups. PC is an amphiphilic molecule that exhibits a tendency to self-assemble in water solutions. Polar head groups are forming outside and hydrophilic tails collected inside to form sandwich sheets called bilayers. These bilayers can form micelles and hollow spheres denoted vesicles. Critical micelle concentration and the molecular polarity and size of PC molecule determine the mesophase formed.

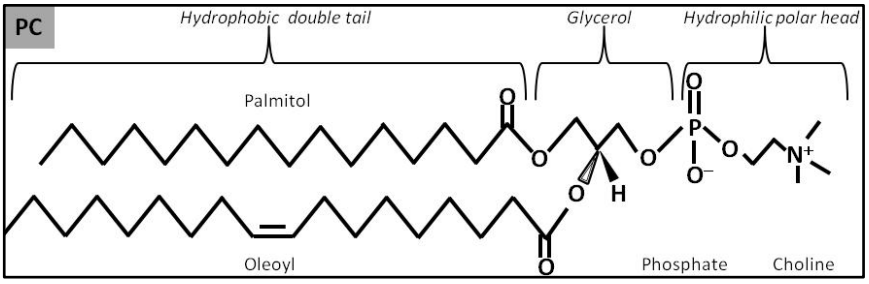

Figure III.1 Double tail, hydrophobic tails, glycerol and polar head group of phosphatidylcholine.

The idea for the experimental conditions and precipitation of CaPs in the presence of PLs was inspired by those used to obtain sponge mesoporous silica materials through a self-assembly process of PLs reported by *A. Galarneau et al* [23, 24]. In this study, phosphatidylcholine (PC) was used as template of mesoporous silica materials. Lecithin (containing 60% of PC) leaded to lamellar materials evoking multilamellar systems and vesicles formation. Then, these authors used dodecylamine as co-surfactant since the alkyl-amine was anticipated to play a role in the formation of the mesostructure given by the PLs. It promoted the decrease of the spontaneous curvature of the phospholipid bilayers. The phase transition from multilamellar mesostructures to sponge–like mesostructure was driven by the presence of dodecylamine which packs the head groups of the lecithin. Figure III.2 shows this phase transition and the sponge-like structure of the silica material obtained.

In this chapter, we aimed at synthesizing HA based hybrids with a sponge-like mesostructure, looking for a stable mesostructure that could lead to a mesoporous CaP material after removing the organic part. The precipitation of CaPs in aqueous suspensions of PLs was used to obtain new mesostructured hybrid materials CaP-PLs. The influence of several parameters of synthesis: *(i)* pH of

solutions (basic or neutral), *(ii)* Ca/P molar ratio (1.0 or 1.67) and *(iii)* the PLs source (asolectin, lecithin or lipoid) was investigated. The mesostructure of the new hybrids is characterized and mechanisms of formation of the nanostructured materials are proposed [25].

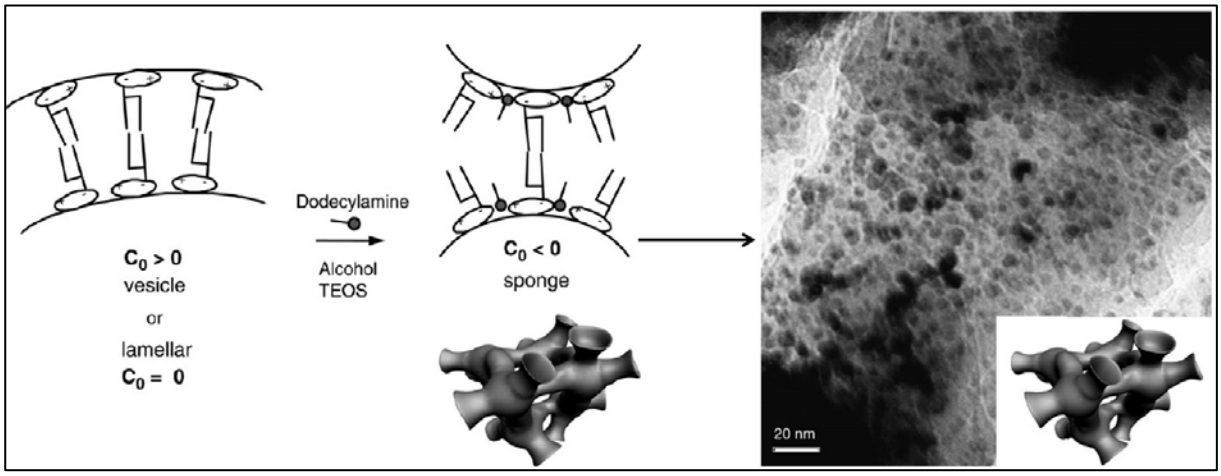

Figure III.2 *Left:* Vesicle to sponge-like phase transition by addition of dodecylamines/alcohol and silica source to lecithin vesicles. C_o denotes the spontaneous curvature of each phase. *Right*: TEM image of sponge-like silica materials showing the sponge structure. *Inset:* Schematic representation of the pore structure of sponge-like silica materials. Figure taken from ref 23: *Micropor. Mesopor. Mater.* **2007**, *104*, 103-114.

Three PLs sources with increasing contents of PC were used: *Asolectin* from soybean, which is a mixture of mainly three PLs containing about 33 % of PC (**PC33**); *L-α-Lecithin* from egg yolk, which contains about 60 % of PC (**PC60**) and *Lipoid-S100* from soybean, containing 94 % of PC (**PC94**). Table III.1 includes the experimental synthesis conditions, reactant and solvent amounts, Ca/P molar ratio and pH of the four samples discussed in this section. Hybrid materials were named as PC33, PC60, PC94–1 and PC94–2 with the numbers indicating the percentage of PC in the commercial source, respectively. Actually, many samples using different experimental conditions were synthesized but only the four most significant ones are presented in this chapter.

Table III.1 Amount of phospholipids (PLs), moles of reactants, solvents and NaOH used in the synthesis of hybrids CaP–PLs.

Samples (PLs source, % of PC)	HPO_4^{2-} (mol)	Ca^{2+} (mol)	PLs (g)	H_2O (mol)	EtOH (mol)	NaOH (mol)
PC33 (Asolectin, 33)	1	1.67	0.5	126	38	2
PC60 (Lecithin, 60)	1	1	0.5	69	38	–
PC94–1 (Lipoid, 94)	1	1	0.5	194	–	–
PC94–2 (Lipoid, 94)	1	1.67	0.5	223	–	1

To analyze the textural properties of the inorganic materials and to check whether this method could lead to mesoporous apatite-like CaPs, hybrids were calcined at high temperature to remove the organic PLs. As a representative example of calcined sample, PC33 calcined material is presented in

this chapter together with the other four hybrid samples. However, N_2 adsorption-desorption isotherms of hybrid samples, as well as calcined samples, indicated that no significant surface area and porosity was obtained in any case (results not shown).

III.2 Precipitation of calcium phosphates in the presence of phospholipids

The detailed experimental procedure of synthesis of the hybrid materials is given in section VII.4.b. The general synthetic procedure was the following: CaPs were precipitated from calcium and phosphate ions in the presence of PLs, using a modification of a method described by *Galarneau et al* for the synthesis of sponge mesoporous silica [23, 26, 27]. Next, the most relevant results obtained for physical-chemical characterization of samples are presented.

Thermogravimetric and Differential Thermal Analysis

TG and DTA results for all the hybrid materials, are shown in Figure III.3. TGA curves of samples showed continuous weight losses mostly in the interval from 225 to 500 °C. In addition, TGA curves exhibited a slight weight loss between room temperature and 125 °C that was attributed to the loss of physisorbed water. TGA of PC94–2 and PC33 samples have dissimilar curves that PC60 and PC94–1 samples.

PC33 and PC94–2, samples obtained in basic medium, present a continuous weight loss in all the interval with weigh losses of 18 % (PC33) and 14 % (PC94–2) in the 170 to 420 °C interval. These weight losses were observed together with exothermic peaks at 320 °C in the DTA curves that were assigned to the PLs combustion.

For PC60 and PC94–1 samples, obtained at neutral pH, TGA curves exhibited sharp weight losses of 7 and 14 % (PC60 and P94–1, respectively) in the 170 to 225 °C range, associated with an endothermic peak in the DTA curve. This behaviour is characteristic for crystalline water loss in CaP materials consisting in brushite phase. In the 225 to 470 °C interval weight losses of 21 and 16 % (PC60 and P94–1, respectively) were observed together with exothermic peaks at 380 °C in the DTA curves, which were assigned to the PLs combustion. Therefore, the observed differences may be attributed to different CaP phases in the hybrid materials.

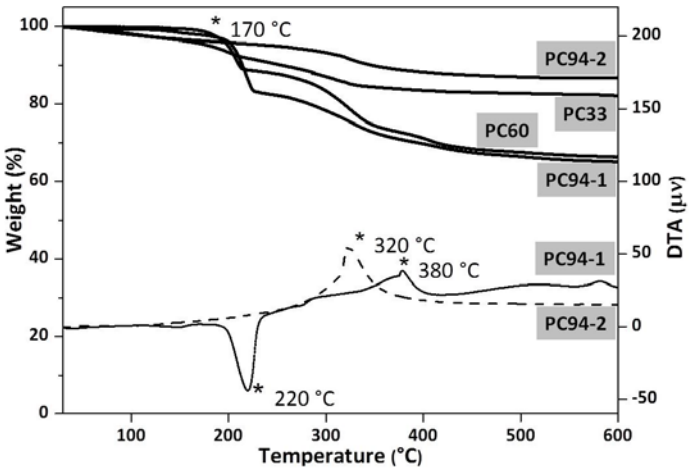

Figure III.3 Weight losses of all hybrid materials CaP-PLs by TGA and analysis of exothermic/endothermic processes by DTA. For DTA only two representative curves are shown.

Fourier Transform Infrared Spectroscopy

The FTIR spectra of the four samples studied are shown in Figure III.4, where in addition FTIR spectra of the calcined PC33 sample and for the pure PC are also included. Concordant with the information obtained by TG/DTA, two types of FTIR spectra were obtained. Thus, for PC33 and PC94–2 the spectra were analogous to those of apatite–like phases. However, the PC60 and PC94–1 FTIR spectra were similar to that of brushite [28].

In addition, FTIR spectroscopy is sensitive to the presence of specific functional groups. First, the presence of organic matter was confirmed in the four samples of hybrid materials by the bands at 2920 cm^{-1} and 2851 cm^{-1} assigned to asymmetric and symmetric stretching modes mainly from $-CH_2-$ groups. The bands of carbonyl group (C=O) present in the PLs structure appears at 1728-35 cm^{-1} in samples PC60 and PC94–1. However, the carbonyl bands are not visible in PC33 and PC94–2 spectra, *i. e.*, in the apatite containing hybrids obtained in basic media. This fact could be related to an hydrolisis of the ester group, which is catalyzed at basic pH.

Moreover, the FTIR spectra allow visualizing the relative amount of water in the hybrids. Again substantial differences were observed as a function of whether the hybrids might contain either apatite or brushite. PC60 and PC94–1 spectra exhibited the well-known bands at 3531 cm^{-1} and 3470 cm^{-1} of ν(OH) from HPO_4^{2-}, at 3260 cm^{-1} and 3154 cm^{-1} of ν(OH) and at 1647 cm^{-1} of δ(HOH) from the H_2O crystallization molecules in the brushite structure. However, in the apatite containing hybrids, PC33 and PC94–2, just a minimum amount of water, as humidity, detected by the presence of a very broad and low intensity band at about 3300 cm^{-1} was observed. FTIR spectrum of the calcined PC33 sample exhibits the bands corresponding to vibration modes for the following structural units: crystalline PO_4^{3-} group observed at 1015, 600 and 550 cm^{-1}; and CO_3^{2-} groups observed at 1423 and 860 cm^{-1}.

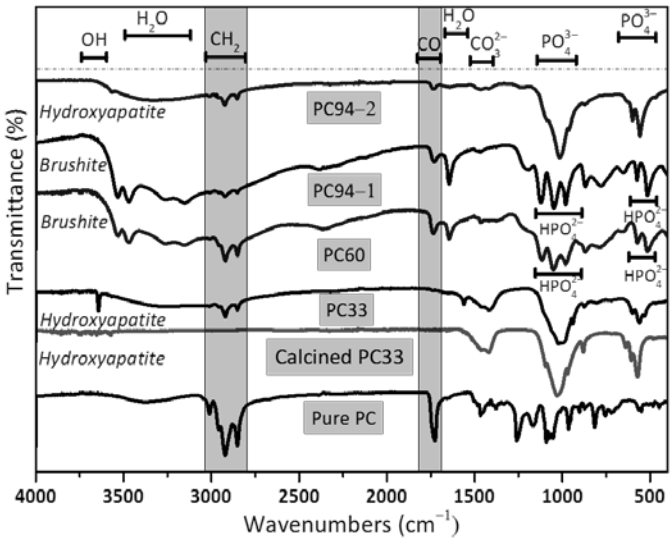

Figure III.4 FTIR analysis of hybrid materials synthesized in the presence of PLs.

The FTIR spectra of the samples also contain the bands corresponding to the vibration modes of –OH, PO_4^{3-}, CO_3^{2-} and HPO_4^{2-} groups. In general terms the following facts can be indicated:

- CO_3^{2-} bands are only present at 1470 cm^{-1} in the apatite–containing hybrids spectra, *i.e.*, the calcined PC33, PC33 and PC94–2, with more intensity in the PC33 sample.
- –OH bands from hydroxyl group of HA appear at wave numbers 3642 cm^{-1} in PC33 and 3567 cm^{-1} in PC 94–2.

- P–OH, P–O and O–P–OH bands are quite similar in the spectra of the brushite-containing hybrids, *i.e.*, PC60 and PC94–1. FTIR spectra of both hybrids are practically identical.

- However, PC33 and PC94–2 spectra present some differences: the mentioned variations in the OH bands position and two bands at 531 cm^{-1} and 1560 cm^{-1} only visible in the calcined PC33 and PC33 spectrum. Besides, the PO_4^{3-} band at 1020 cm^{-1} is broader for the calcined PC33 and PC33. These findings could be attributed to a lower homogeneity of PC33 obtained with a PLs mixture being the PC content of 33 % whereas PC94–2 was synthesised with PC of 94 % of purity.

Small and wide angle X–ray Diffraction

Figure III.5 shows the small angle (0.6 ° to 5 ° in 2θ) and wide angle (5 ° to 50 ° in 2θ) X–ray diffractograms of the four hybrid samples investigated and the calcined PC33. The small angle region was studied to detect the possible mesostructure of the hybrid materials. This fact would be confirmed by the presence of diffraction maxima in this region indicative of repetitive distances of a few nanometres in the sample structure. The wide angle XRD region was investigated to identify the CaP crystalline phases formed.

The WA-XRD patterns of samples can be explained as follows: on the one hand the two hybrids synthesised at basic pH, *i.e.*, PC33 and PC94–2 correspond to poorly crystallized apatite-like phases. No extra diffraction maxima of additional phases were obtained. The calcined PC33 sample exhibits a diffractogram concordant with an apatite-like phase with narrow maxima typical for samples subjected to a thermal treatment. The presence of a small amount of CaO was also detected in this sample. On the other hand, those diffractograms of hybrids synthesised at neutral pH were assigned to a brushite phase, although in both cases the most intense XRD reflection of monetite (002) was observed, indicative of the presence of a small amount of this phase in the hybrid materials.

In PC33 and PC60 samples less information was found in the low angle region. However, a poorly defined shoulder centred at 1.4°, equivalent to a distance of around 6 nm, was observed for PC33 pattern and a broad diffraction at 2° for PC60 that corresponds to around 4.7 nm. This weak reflections are typical of nano-ordered mesostructures with lamellar bilayer and vesicles formation [5, 29], and this will be confirmed by TEM. As observed in Figure.III5, clear diffraction maxima are present in the small angle region of PC94–1 and PC94–2 patterns at 2.0° and 1.0°, respectively that correspond to distances of 4.3 nm and 8.6 nm respectively. Observed results can be summarized as follows:

- At neutral pH: $d \leq 4.7$ nm, *d* value is smaller and the observed CaP phase is brushite,
- At basic pH: $d \geq 6$ nm, *d* value is bigger and the observed CaP phase is HA.

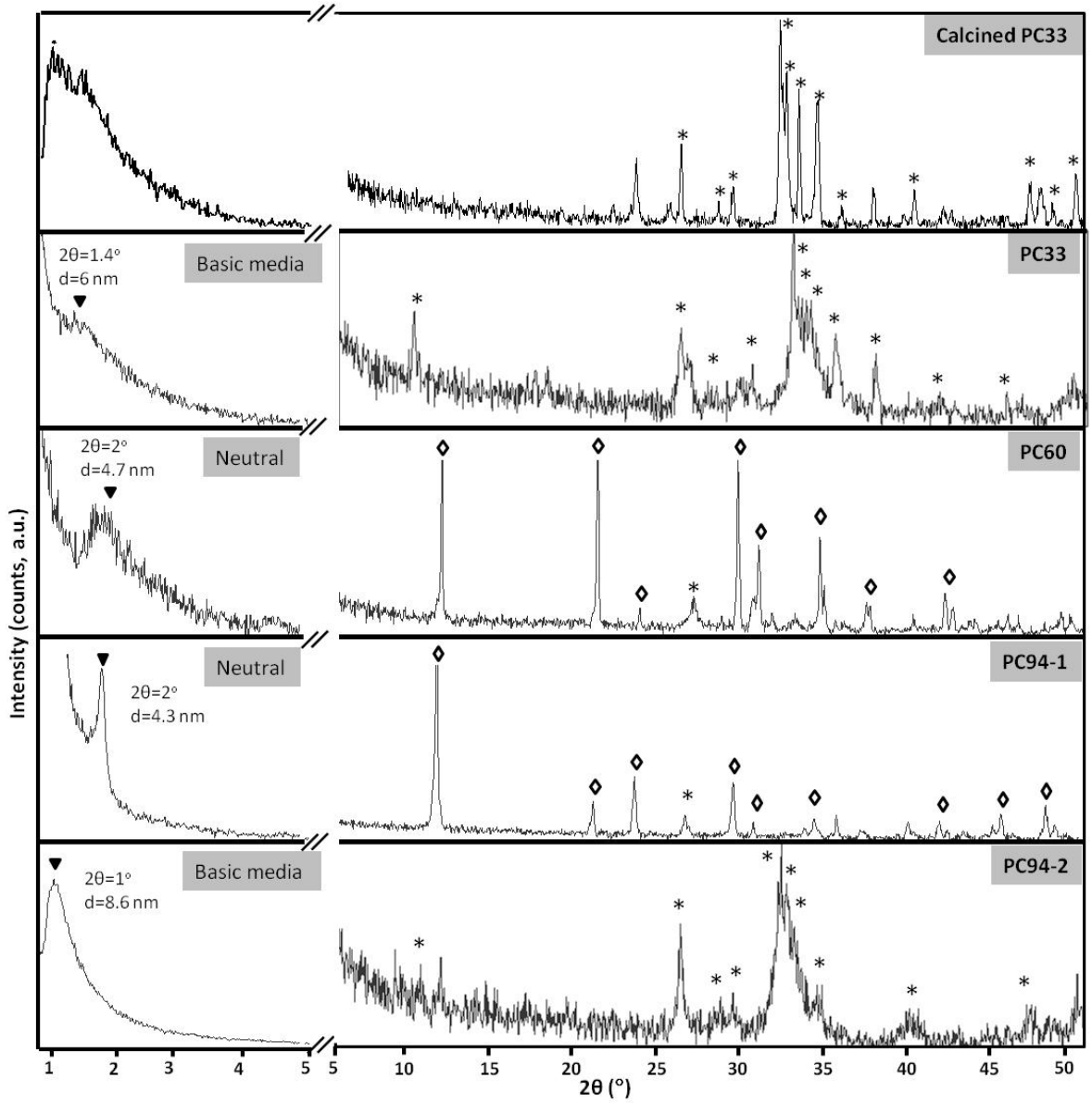

Figure III.5 Small and wide angle X–ray diffraction patterns of four hybrid materials and the calcined PC33, where * and ◊ indicate hydroxyapatite and brushite, respectively.

High Resolution Transmission Electron Microscopy

High Resolution Transmission Electron Microscopy (HRTEM) images showed that PLs and CaP are arranged with different mesostructure in four samples depending on pH and type of solutions, as well as on Ca/P molar ratio and PLs source (see Figure III.6). The calcined PC33 sample, identified by WA-XRD mainly as a HA phase, was observed according to TEM as non porous particles with an eroded surface morphology.

Obtained images of four samples PC33, PC60, PC94–1 and PC94–2 by HRTEM are shown in Figure III.7 together with a proposed scheme to explain how PLs form a mesostructure, and what kind of mesostructures were obtained. HRTEM images are interpreted as follows: *(i)* discontinuous lamellar bilayer structured hydroxyapatite with 4.2 nm size for sample PC33 [30]; *(ii)* bilayer vesicles of brushite with ~35 nm of diameter (media average) and 4.7 nm of bilayer thickness for sample PC60;

(iii) micelles structured brushite with 4.3 nm for sample PC94–1, where said micelles structure is confirmed according to *Nabakumar P. et al*.[5]; *(iv)* bilayer sponge–like [30] or worm–like structured hydroxyapatite observed with 4.3 nm for sample PC94–2.

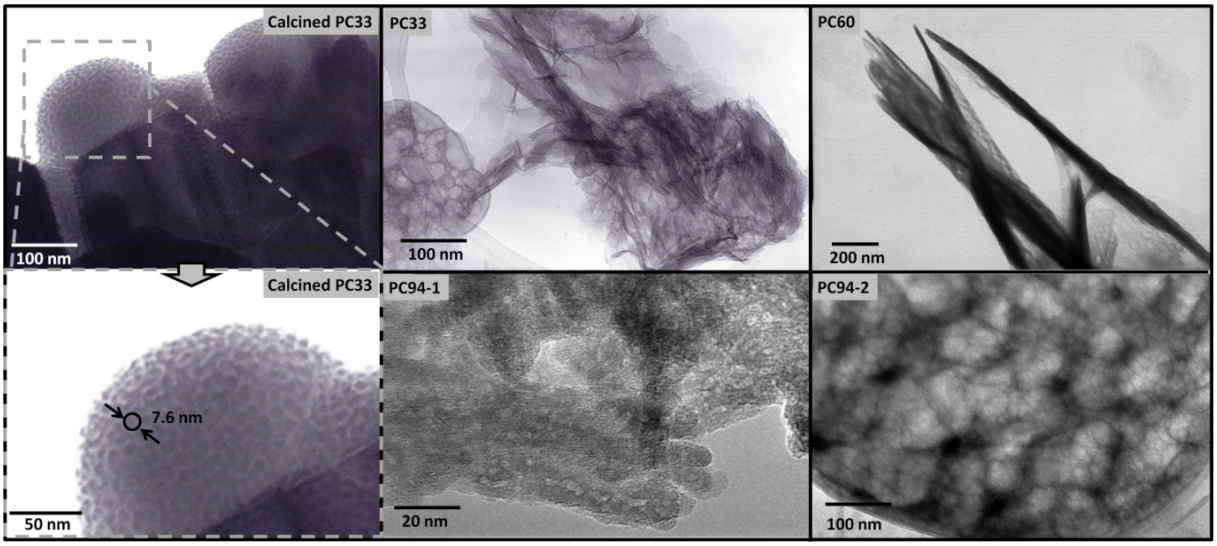

Figure III.6 HRTEM images of all materials. The CaP phases previously identified by XRD are described in the TEM images as non-porous HA (calcined PC33), HA with lamellar structures (PC33), brushite with vesicle structure (PC60), brushite with micelle structure (PC94–1) and HA phase with sponge–like structure (PC94–2).

In case of PC33, several bilayers can pile up with a spacing nano-layer of water solution separating one another; such a structure is referred to as a discontinued lamellar phase [29, 30]. For sample PC60 prepared in water/ethanol solution, the polar characteristic of water provokes the formation of bilayer vesicles of PLs with around 35 nm in diameter. The thickness of the bilayer is 4.7 nm and inside the bilayer vesicles CaP with brushite structure is present. A mechanism for the mesostructure formation in sample PC94–1 is based on micelles behavior in water solution. In a first step, PC molecules form a micelle layer in the solution. After the addition of an aqueous PO_4^{3-} solution to the aqueous PC solution, the PC–PO_4^{3-} complex, formed by many PO_4^{3-} species interacting with the surface of the micelle, is obtained. After an aqueous Ca^{2+} solution is added, a PC–calcium phosphate phase is formed because of the conformational compatibility between the micelle and the calcium phosphate. The micelle acts as a nucleating point for the growth of brushite crystals at an adequate aging temperature and time.

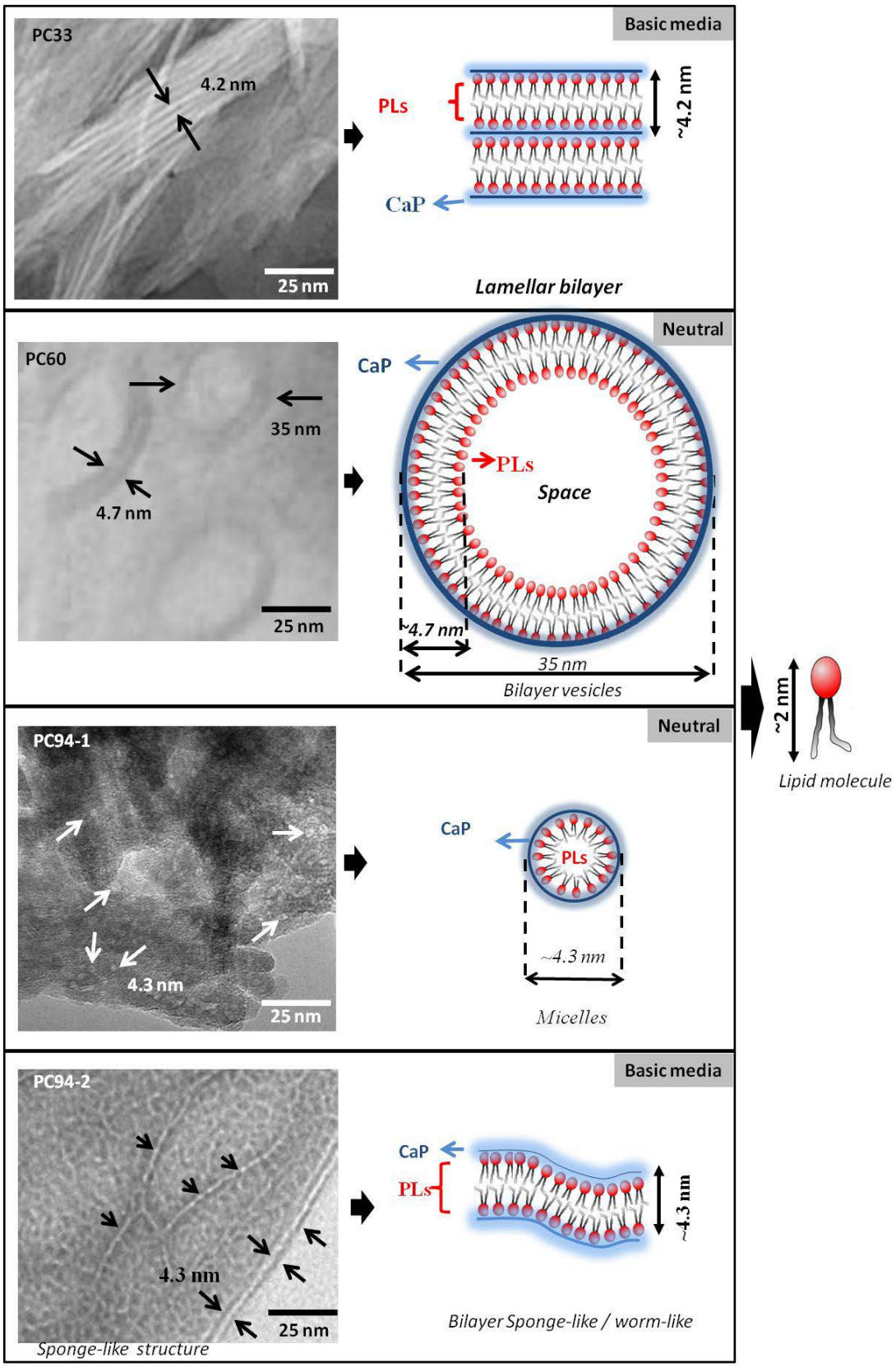

Figure III.7 HRTEM micrographs of calcium phosphate hybrids in the presence of PLs (left). Schematic representation of the PL and CaP arrangements (right).

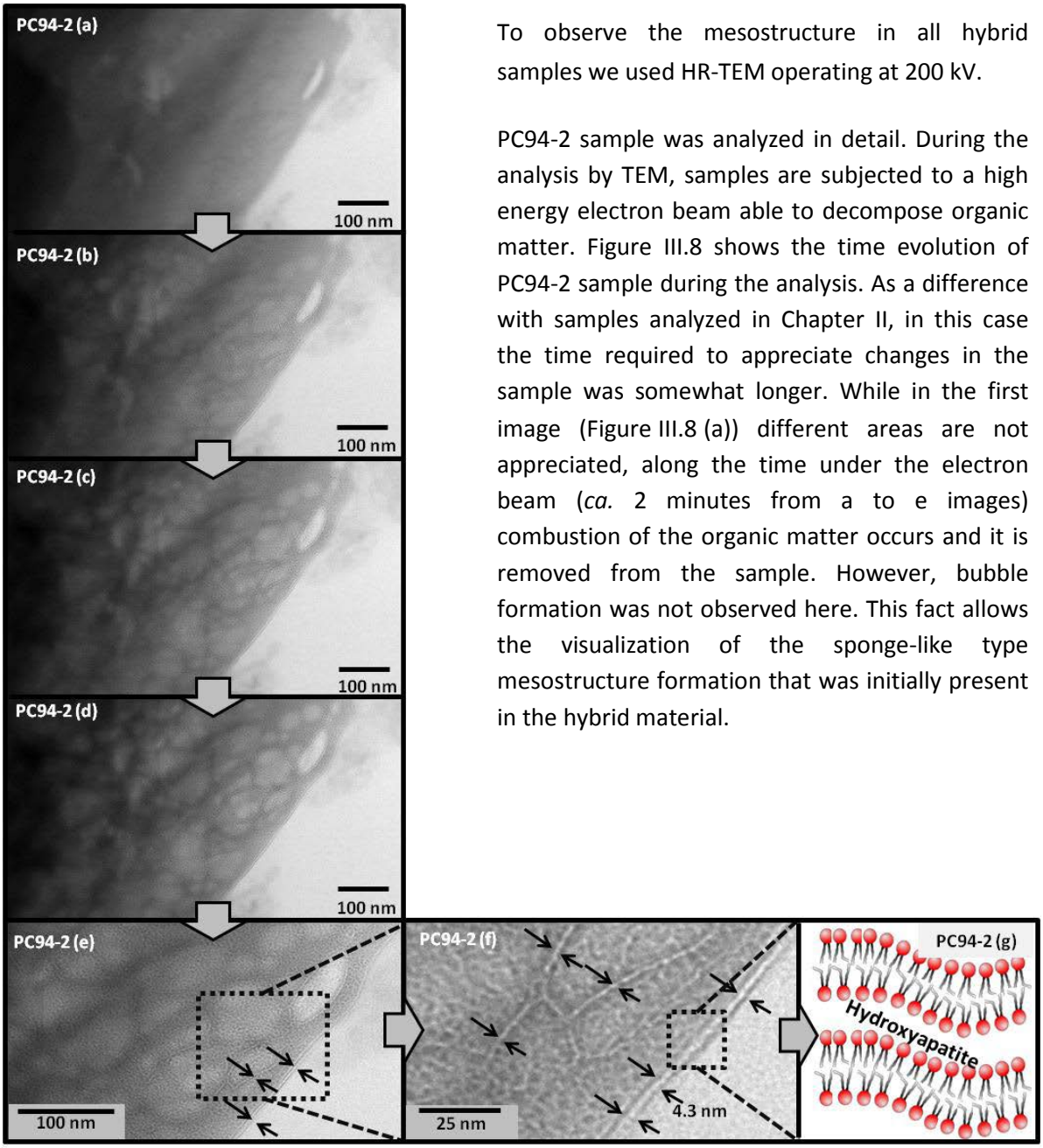

To observe the mesostructure in all hybrid samples we used HR-TEM operating at 200 kV.

PC94-2 sample was analyzed in detail. During the analysis by TEM, samples are subjected to a high energy electron beam able to decompose organic matter. Figure III.8 shows the time evolution of PC94-2 sample during the analysis. As a difference with samples analyzed in Chapter II, in this case the time required to appreciate changes in the sample was somewhat longer. While in the first image (Figure III.8 (a)) different areas are not appreciated, along the time under the electron beam (*ca.* 2 minutes from a to e images) combustion of the organic matter occurs and it is removed from the sample. However, bubble formation was not observed here. This fact allows the visualization of the sponge-like type mesostructure formation that was initially present in the hybrid material.

Figure III.8 Temporal evolution of PC94-2 sample analyzed by TEM operating at 200 kV. (g) Schematic representation of the CaP-PLs arrangement as sponge-like hybrid material, PC94-2.

III.3 Conclusions of Chapter III

Organic–inorganic hybrid materials were synthesised by precipitation of calcium phosphates in phospholipids (PLs) suspensions. As PLs source, different commercial preparations were used, all of them containing phosphatidylcholine (PC) as main PL in proportions of 33% (asolectin), 60% (lecithin) and 94% (lipoid). Ca^{2+} and HPO_4^{2-} ions were managed by different purity of PLs in ethanol and water dispersions: the PLs mixtures (*i.e.* asolectin and lecithin) were prepared in a mixture of water and ethanol. Lipoid was suspended in pure distilled water. The inorganic components of the hybrids were

poorly crystallized HA, when pH of medium was basic and the Ca/P molar ratio was 1.67 for samples PC33 and PC94-2. The observed CaP phase was brushite ($CaHPO_4 \cdot 2H_2O$) for neutral pH and Ca/P = 1.0. No mesoporous materials were obtained by removing the organic matter via calcination. Instead, dense HA phase was obtained. FTIR analysis reveals a possible hydrolysis of the ester group of PC in samples prepared under basic pH. However, all samples present in FTIR the bands corresponding to CH_2 groups, and moreover, thermogravimetric analysis data confirmed the presence of organic matter in the materials showing weight losses in the range of 220 °C and 470 °C around 20% in brushite containing hybrids, and around 17% in apatite ones. Furthermore, TEM analysis reveals that four different nanostructures were obtained: *(i) lamellar bilayer* with a spacing of 4.2 nm (apatite, asolectin), *(ii) bilayer vesicles* around of 35 nm in diameter (brushite, lecithin) and 4.7 nm in thickness of vesicles, *(iii) micelles* with sizes of approximately 4.3 nm (brushite, lipoid), and *(iv) bilayer sponge–like* or *worm–like tubular* mesostructures with 4.3 nm thickness of disordered bilayer sponge–like structure (apatite, lipoid).

Since the organic part of these hybrid materials is a biocompatible PL, they could be considered as drug delivery platforms via the encapsulation of a drug within the organic matter in these PL-CaP hybrid materials.

III.4 References:

1. M. Vallet-Regí, D. Arcos. *Curr. Nanosci.* **2006**, *2*, 179-189. Nanostructured hybrid materials for bone tissue regeneration.

2. C. Liu, X. Ji, G. Cheng. *Appl. Surf. Sci.* **2007**, *253*, 6840-6843. Template synthesis and characterization of highly ordered lamellar hydroxyapatite.

3. P. Benedicte, Z. Thomas. *Mater. Sci. Eng. C.* **2005**, *25*, 553-559. Calcium phosphate precipitation in catanionic templates.

4. N. Kawa, H. Hori, K. Tatsuo, Y. Oumi, T. Sano. *Micropor. Mesopor. Mat.* **2011**, *141*, 56-60. Unique surface property of surfactant-assisted mesoporous calcium phosphate.

5. N. Pramanik, T. Imae. *Langmuir* **2012**, *28*, 14018-14027. Fabrication and characterization of dendrimer-functionalized mesoporous hydroxyapatite.

6. Y-.T. Huang, M. Imura, Y. Nemoto, C-.H. Cheng, Y. Yamauchi. *Sci. Technol. Adv. Mat.* **2011**, *12*, 045005. Block-copolymer-assisted synthesis of hydroxyapatite nanoparticles with high surface area and uniform size.

7. M. S. Schmidt, J. McDonald, E. T. Pineda, A. M. Verwilst, Y. Chen, R. Josephs, A. E. Ostafin. *Micropor. Mesopor. Mater.* **2006**, *94*, 330-338. Surfactant based assembly of mesoporous patterned calcium phosphate micron-sized rods.

8. N. Kawa, Y. Oumi, T. Kimura, T. Ikeda, T. Sano. *J. Mater. Sci.* **2008**, *43*, 4198-4207. Synthesis of lamellar mesostructured calcium phosphates using n-alkylamines as structure-directing agents in alcohol/water mixed solvent systems.

9. M. Bauer, U. Schubert, M. Gottschaldt, A. Schallon, C. Pietsch, F. Gonnert, P. Recknagel, A. Press, *Cell-specific targeting using nanostructured polymer and/or lipid and polymethine dye delivery systems*. **2015**, Universitaetsklinikum Jena, Germany; Friedrich-Schiller-Universitaet Jena . p. 37pp.

10. J. Garcia-Martinez, P. Brugarolas, S. Dominguez-Dominguez. *Micropor. Mesopor. Mater.* **2007**, *100*, 63-69. Ordered circular mesoporosity induced by phospholipids.

11. H. Zhai, X. Chu, L. Li, X. Xurong, R. Tang. *Nanoscale* **2010**, *2*, 2456-2462. Controlled formation of calcium-phosphate-based hybrid mesocrystals by organic-inorganic co-assembly.

12. L. Zerkoune, A. Angelova, S. Lesieur. *Nanomaterials* **2014**, *4*, 741-765, 25 pp. Nano-assemblies of modified cyclodextrins and their complexes with guest molecules: incorporation in nanostructured membranes and amphiphile nanoarchitectonics design.

13. X. Liu, H. Bai, L. Zhang, E. Wang. *Adv. Planar Lipid Bilayers Liposomes* **2008**, *7*, 203-220. Lipid-based strategies in inorganic nano-materials and biomineralization.

14. N. V. Beloglazova, I. Yu Goryacheva, P. S. Shmelin, V. Kurbangaleev, S. De Saeger. *J. Mater. Chem. B* **2015**, *3*, 180-183. Preparation and characterization of stable phospholipid-silica nanostructures loaded with quantum dots.

15. C. C. Tester, D. Joester. *Methods Enzymol* **2013**, *532*, 257-76. Precipitation in liposomes as a model for intracellular biomineralization.

16. T. Li, Y. Deng, X. Song, Z. Jin, Y. Zhang. *B. Korean Chem. Soc.* **2003**, *24*, 957-960. The formation of magnetite nanoparticle in ordered system of the soybean lecithin.

17. S. Bhandary, S. Das, R. Basu, P. Nandy. *J. Nanoeng. Nanomanuf.* **2014**, *4*, 209-214. Influence of calcium phosphate nanoparticle in promotion of liposomal fusion.

18. Z. Yang, C. Zhang, L. Huang. *Colloids Surf. B. Biointerfaces* **2014**, *116*, 265-9. Quartz crystal microbalance for comparison of calcium phosphate precipitation on planar and rough phospholipid bilayers.

19. E. D. Eanes, A. W. Hailer, J. L. Costa. *Calcif. Tissue Int.* **1984**, *36*, 421-430. Calcium phosphate formation in aqueous suspensions of multilamellar liposomes.

20. E. D. Eanes, A. W. Hailer. *Calcif. Tissue Int.* **1985**, *37*, 390-394. Liposome-mediated calcium phosphate formation in metastable solutions.

21. T. Anada, Y. Takeda, Y. Honda, K. Sakurai, O. Suzuki. *Bioorg. Med. Chem. Lett.* **2009**, *19*, 4148-4150. Synthesis of calcium phosphate-binding liposome for drug delivery.

22. S. Zhang, K. Kawakami, L. K. Shrestha, G. C. Jayakumar, J. P. Hill, K. Ariga. *J. Phys. Chem. C* **2015**, *119*, 7255-7263. Totally Phospholipidic Mesoporous Particles.

23. A. Galarneau, G. Renard, M. Mureseanu, A. Tourrette, C. Biolley, M. Choi, R. Ryoo, F. R. Di, F. Fajula. *Micropor. Mesopor. Mater.* **2007**, *104*, 103-114. Synthesis of sponge mesoporous silicas from lecithin/dodecylamine mixed-micelles in ethanol/water media: A route towards efficient biocatalysts.

24. A. Galarneau, M. Mureseanu, S. Atger, G. Renard, F. Fajula. *New J. Chem.* **2006**, *30*, 562-571. Immobilization of lipase on silicas. Relevance of textural and interfacial properties on activity and selectivity.

25. J. Yu, X. Zhao, B. Cheng, Q. Zhang. *J. Solid State Chem.* **2005**, *178*, 861-867. Controlled synthesis of calcium carbonate in a mixed aqueous solution of PSMA and CTAB.

26. P. Laveille, L. T. Phuoc, J. Drone, F. Fajula, G. Renard, A. Galarneau. *Catal. Today* **2010**, *157*, 94-100. Oxidation reactions using air as oxidant thanks to silica nanoreactors containing GOx/peroxidases bienzymatic systems.

27. M. Mureseanu, A. Galarneau, G. Renard, F. Fajula. *Langmuir* **2005**, *21*, 4648-55. A new mesoporous micelle-templated silica route for enzyme encapsulation.

28. S. V. Dorozhkin. *J. Mater. Sci.* **2007**, *42*, 1061-1095. Calcium orthophosphates.

29. M. Tiemann, M. Froeba. *Chem. Commun.* **2002**, 406-407. Mesoporous aluminophosphates from a single-source precursor.

30. G. Tresset. *PMC Biophys.* **2009**, *2*, 3. The multiple faces of self-assembled lipidic systems.

IV. HYDROXYAPATITE COATINGS ON MESOPOROUS SILICA NANOSPHERES

IV.1 Introduction

Mesoporous silica nanospheres (MSNSs) are widely investigated in recent years for biomedical applications including the loading of anticancer drugs or the incorporation of magnetic thermoseeds to be used in hyperthermia treatments [1]. Nowadays, the drug delivery from MSNSs injected in the bloodstream is considered as an important approach for targeted tumor therapy [2-6]. The most relevant information on MSNSs has been presented in Chapter I.

On the other hand, SiO_2–CaO–P_2O_5 mesoporous bioactive glasses (MBGs) have been proposed for bone regeneration applications. These glasses exhibit the excellent textural properties (high surface area and pore volume) and mesopore order similar to pure silica mesoporous materials, together with a remarkable quick of the *in vitro* bioactive response [7]. MBGs have been also investigated for other clinical applications including gene transfection [8], encapsulation of proteins [9], tumor treatment [10], scaffold processing [11, 12] or drug delivery [13]. In some of these applications their use as nanoparticles (NPs) could bring considerable advantages. For instance, their use as drug nanocarriers for intracellular delivery due to cellular uptake of NPs, and the possibility of systemic administration through the blood stream. However, to our best knowledge no ternary SiO_2–CaO–P_2O_5 MBG–NPs have been synthetized. In recent years, several close approaches in which we found inspiration were reported, including:

(i) The synthesis of bioactive binary SiO_2–CaO template glasses by M. Vallet-Regí [14],
(ii) The synthesis of binary mesoporous SiO_2–CaO NPs, by Wu *et al* [15],
(ii) The coating of hydroxyapatite (HA) NPs by mesoporous silica, by Anderson *et al* [16],
(iii) The functionalization of MSNSs with phosphonic acid, by Jin *et al* [17],
(iv) The synthesis of ternary SiO_2–CaO–P_2O_5 MBGs adding biologically relevant elements, by Shruti *et al* [18].

The present study tries to coat MCM–41 type MSNSs with HA NPs which would greatly improve their bioactivity and biocompatibility when used for bone therapy [19-22]. In addition, the HA coating could act as a nanogate allowing the controlled release under specific conditions – a pH decrease, for instance – of the biomolecules contained in the mesopores [23]. However, the synthesis of bioactive silica-based materials with such multifunctional properties still remains a significant challenge**.** The nanospheres coated by CaP NPs would exhibit well interconnected pore structures and excellent *in vitro* bioactivity useful for biomedical applications [24-28].

As it was indicated, the main objective of this memory was the synthesis of mesostructured calcium phosphates. The synthesis and characterization of CaPs obtained in the presence of ionic surfactants and phospholipids were described in Chapters II and III. In this Chapter, we changed the strategy by using MSNSs with hexagonal MCM–41 structure as nano-ordered structure core to lead Ca^{2+} and HPO_4^{2-} ions to obtain HA NPs coatings as the nanospheres shell.

The procedure attempted to obtain MSNSs coated by HA NPs involved two steps: *(1)* the synthesis of MSNSs ranging 150 – 250 nm of diameter and around 2 nm of pore diameter; *(2)* the coating of MSNSs by HA by using several approaches including: *(i)* the simultaneous precipitation of CaP on

MSNSs surface during the MSNSs sol-gel synthesis [29], *(ii)* to mantain the MSNSs soaked in a sol precursor of CaP and *(iii)* to wet the MSNSs several times with a sol precursor of CaP [30], and *(iv)* to functionalize the MSNSs with organic chains containing phosphate-like groups and then to wet them with a sol precursor of CaP [31]. For only one case (section IV.3), the co-synthesis of CaP and MSNSs, the strategy used does not implie the use of presynthesized MSNSs. Table IV.1 shows the approaches of synthesis and the sample codes.

Table IV.1 Coating strategies, sample code and section of this Chapter where they will be described.

Section	Strategy of Synthesis		Sample Code
IV.2	Synthesis of mesoporous silica nanospheres		***MSNSs***
IV.3	Co-synthesis of CaP and MSNSs		***MSNS–HA–1***
IV.4	Soaking MSNSs into a sol precursor of CaP		***MSNS–HA–2***
IV.5	Wetting several times the MSNSs by a sol precursor of CaP		***MSNS–HA–3***
IV.6	Functionalization of MSNSs with phosphate-like groups and subsequent wetting with a sol precursor of CaP		
	IV.6.1	Co-condensation and post-synthesis with diethylphosphatoethyl-triethoxysilane, DEPETES	***NSFD1***, ***NSFD2, NSFD***
	IV.6.2	Wetting of DEPETES functionalized MSNSs	***NSFD–HA***
	IV.6.3	Co-condensation with 3-trihydroxysilylpropyl methylphosphonate, THSMP	***NSFT***
	IV.6.4	Wetting of THSMP functionalized MSNSs	***NSFT–HA***

IV.2 Synthesis of mesoporous silica nanospheres, MSNSs sample

Regarding all the experimental strategies investigated in this Chapter to obtain core@shell MSNS@CaP composites, Sections IV.4, IV.5, IV.6.1 and IV.6.2 use MSNSs as starting material to be coated with CaP by different methods: soaking, wetting and functionalization and wetting, respectively. On the other hand, in Section IV.3, the sol-gel synthesis of MSNSs was performed simultaneously to the precipitation of the CaP. Therefore, we will start describing the synthesis and characterization of MSNSs that were used as reactants in Sections IV.4, IV.5 and IV.6.

There are many methods to synthesize the MSNSs [2, 17]. In the present study our method was based on hydrolysis and condensation of silicon alkoxydes in the presence of structure directing agents and following a modified Stöber method. The synthesis procedure is detailed in Chapter VII.4.c. Briefly, CTAB was mixed with basic aqueous solution at 80 °C and stirred until a homogeneous solution was obtained. After that, TEOS as silica source was slowly added with stirring for two hours. Finally, the mixture was filtered, washed thoroughly with water/ethanol (1:1) and dried. The surfactant was removed by calcination. Next step was the physical and chemical characterization of the obtained MSNSs material.

Fourier Transform Infrared Spectroscopy

FTIR spectrum of MSNSs is shown in Figure IV.1. A typical spectrum of silica was observed exhibiting the following bands: at 1044 cm^{-1} a strong band of the asymmetric stretching mode ν_s(SiO) of SiO_2; a shoulder at around 970 cm^{-1} attributed to the stretching mode of the Si-O bonds of the silanol groups of the silica surface; a medium band at 800 cm^{-1} for the symmetric stretching mode ν_s(SiO) of SiO_2; and a strong band at 432 cm^{-1} for the bending mode δ(SiOSi) of SiO_2.

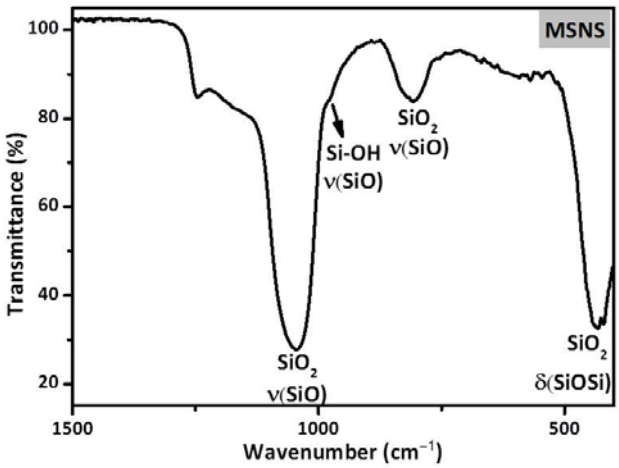

Figure IV.1 FTIR spectrum of mesoporous silica nanospheres (MSNSs).

Small and wide angle X–ray Diffraction

Figure IV.2 shows the SA-XRD and WA-XRD patterns of MSNSs. SA-XRD pattern shows three diffraction maxima at 2.6°, 4.4° and 5.1° in 2θ, which can be respectively indexed to (10), (11) and (20) reflections of a 2D hexagonal arrangement, being the unit cell parameter a_o= 39.7 Å (a_o= $2d_{100}/\sqrt{3}$, for d_{100} = 34.3 Å). These positions are easily indexable, q_1, q_2 and q_3 are positions of the peaks 1, 2 and 3. We observed following relations $q_2=q_1x\sqrt{3}$, $q_3=q_1x\sqrt{4}$...

For WA-XRD the MSNSs diffractogram shows only a diffuse maximum centred at 23° characteristic of amorphous silica.

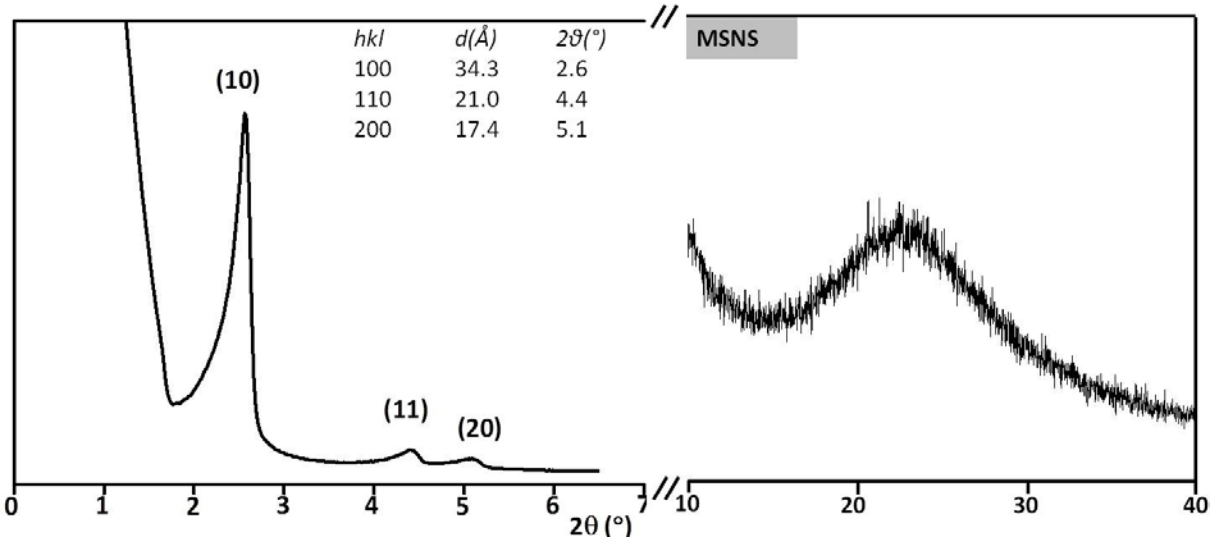

Figure IV.2 SA–XRD (left) and WA–XRD (right) patterns of MSNS. The diffraction patterns were assigned to a 2D-hexagonally arranged mesoporous lattice and to amorphous silica, respectively.

N_2 Adsorption–Desorption Isotherms

Figure IV.3 shows the N_2 adsorption-desorption isotherm, and as an inset, the pore diameter distribution of MSNSs [5].

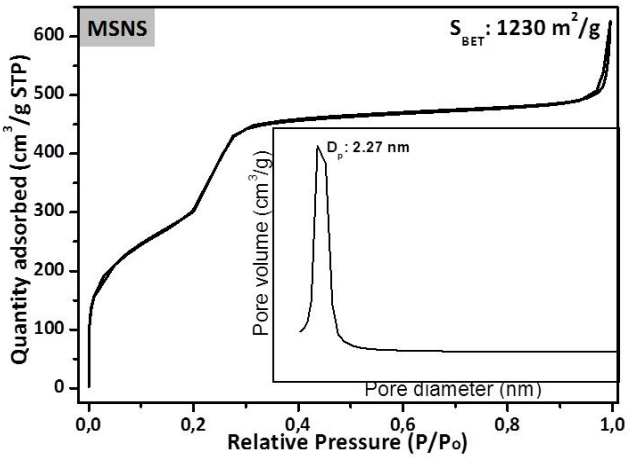

Figure IV.3 Adsorption-desorption isotherms and pore diameter of MSNS.

Through these measurements it was obtained a maximum in the pore size distribution at 2.27 nm and a BET surface area of 1230 m^2/g. MSNSs sample exhibits type IV BET isotherms with no observed hysteresis loop, confirming the presence of a cylindrical, one-dimensional channel-like mesoporous structure in the nanospheres. The N_2 isotherms present a sharp inflection at a relative pressure of 0.2–0.3, which corresponds to the capillary condensation and evaporation within channel-type uniform mesopores. In addition, a secondary step at a P/P_o above 0.95 is observed, attributed to condensation in textural porosity, *i.e.*, in the macropores formed between the nanoparticles after the drying process.

Scanning Electron Microscopy

The spherical morphology of particles in MSNS sample is revealed by the SEM micrograph in Figure IV.4.

SEM image shows homogenously dispersed nanospheres with sizes ranging between 150 and 320 nm in diameter. The mean value of 100 nanospheres measured is 228 ± 30 nm.

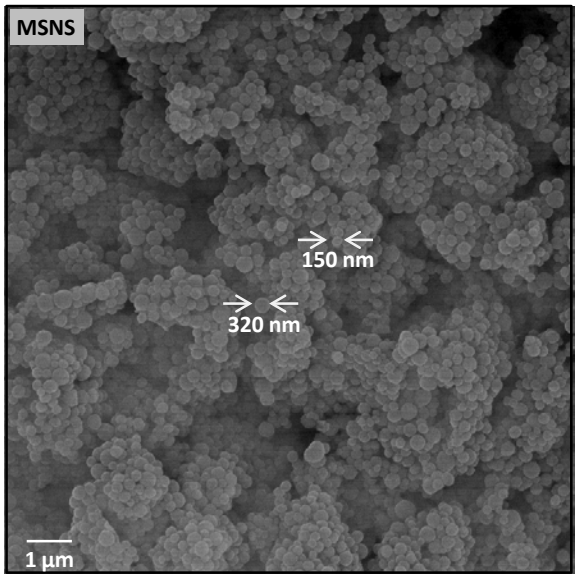

Figure IV.4 Surface morphology of MSNSs observed by SEM.

Transmission Electron Microscopy

Figure IV.5 shows two TEM micrographs of MSNSs. As shown in the left side micrograph, the silica nanoparticles exhibit spherical shape, while the micrograph in the right side details their ordered mesopores hexagonal arrangement. Spacing between mesoporous silica channels was measured at 2.5 nm.

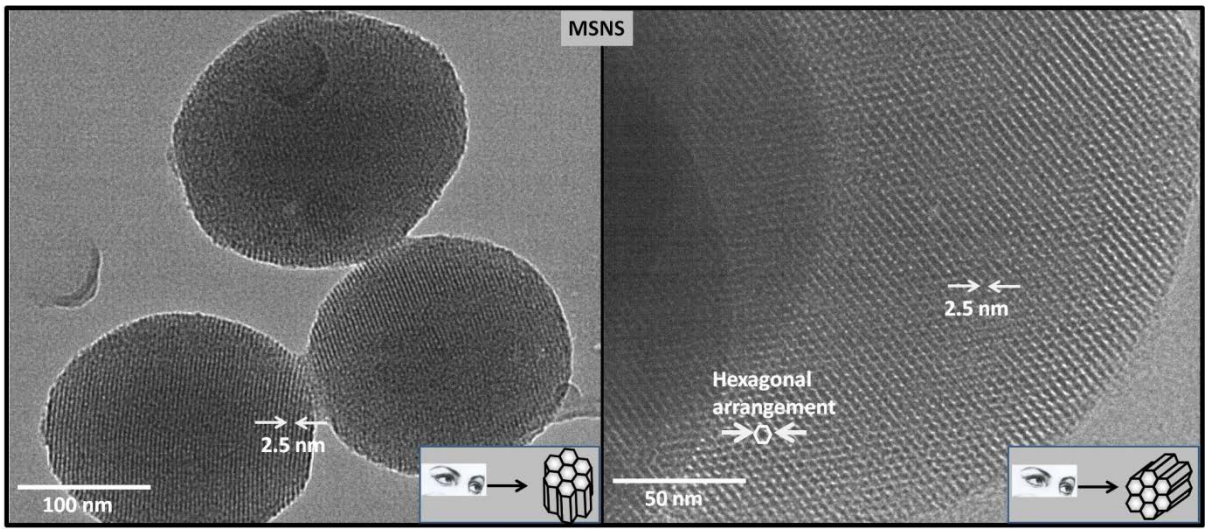

Figure IV.5 TEM micrographs of MSNS showing the nanospheres (left) and a higher magnification image to observe better their pore arrangement.

Conclusion of Section IV.2: Synthesis of mesoporous silica nanospheres, MSNSs sample

MSNSs were obtained as monodispersed particles with sizes between 150 and 320 nm of diameter and a high surface area of 1230 m^2/g. These MSNSs were used as reference to compare with modified MSNSs investigated in the next sections.

IV.3 Precipitation of calcium phosphate simultaneous to the formation of mesoporous silica nanospheres, *MSNS–HA–1 sample*

In this approach MSNSs were treated to coat by HA–NPs in one step involving two simultaneous processes as follows: *(i)* precipitation of HA and *(ii)* synthesis of MSNSs. Accordingly, Ca^{2+} and phosphate ions were added into the solution containing TEOS at the onset of silica condensation (for a more detailed description of the synthesis method, see Chapter VII). Hence, the aim was to provide interactions between silica, Ca^{2+} and phosphate ions during the silica condensation to synthesize homogeneous silica@CaP composites with the silica MSNSs coated by nanocrystalline HA. Calcium and phosphate precursor solutions were added in a Ca/P molar ratio of 1.67. Furthermore, the Stöber method uses sodium hydroxide to catalyze the silicate precursor hydrolysis and this basic medium favours the HA formation.

On the other hand, if Ca^{2+} and phosphate ions penetrated into the silica mesopores they could increase their interaction with silica matrix. This would increase the homogeneity of silica-HA composites. The main goal was to achieve ionic interactions between silicate, Ca^{2+} and phosphate ions. The following text describes the characterization of the sample obtained, MSNS-HA-1.

Fourier Transform Infrared Spectroscopy

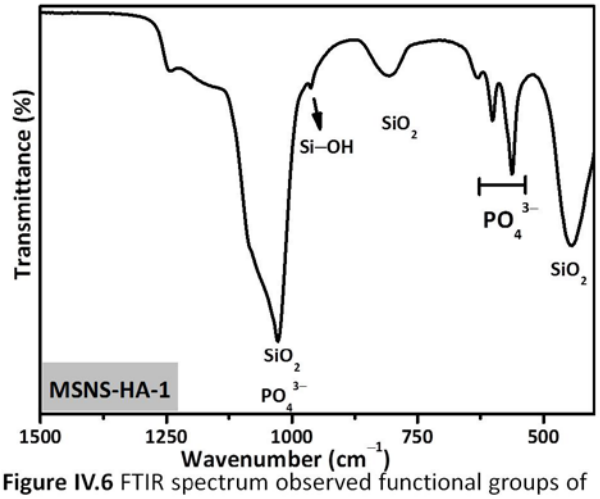

Figure IV.6 FTIR spectrum observed functional groups of MSNS-HA-1 sample.

FTIR spectrum of MSNS–HA–1 is shown in Figure IV.6. The spectrum shows overlapping bands in the 1100-1000 cm^{-1} range corresponding to the stretching mode of ν(SiO) and ν(PO) for SiO_2 and PO_4^{3-} groups, respectively. For silica also appear the bands for the stretching mode ν(SiO) at 806 cm^{-1} and at 950 cm^{-1} for the silanol surface groups, as well as the δ(SiOSi) bending mode at 443 cm^{-1}. Finally, bands at 601 and 563 cm^{-1} that were assigned to δ(OPO) bending modes of PO_4^{3-} in crystalline environment were visible. These two peaks of phosphate are characteristic of crystalline phosphate [32]. Hence, the FTIR spectrum of MSNS–HA–1 contains both bands of silica and bands of phosphate in a crystalline environment which hints at the simultaneous formation of SiO_2 and HA.

Small and wide angle X–ray Diffraction

Figure IV.7 shows the SA–XRD and WA–XRD patterns of MSNS–HA–1. SA–XRD pattern shows four diffraction maxima at 2θ = 2.2 °, 3.9 °, 4.5 ° and 6.0 ° , which can be respectively indexed to (100), (110), (200) and (210) reflections of a 2D hexagonal arrangement in the MSNSs [33], being the unit cell parameter a_o= 45.8 Å ($a_o = 2d_{100}/\sqrt{3}$, for d_{100} = 39.7 Å). The first four peaks of MSNS–HA–1 sample by SA–XRD confirm that the 2D mesoporous hexagonal arrangement is present, but do not confirm if some interaction was established between SiO_2, Ca^{2+} and phosphate ions.

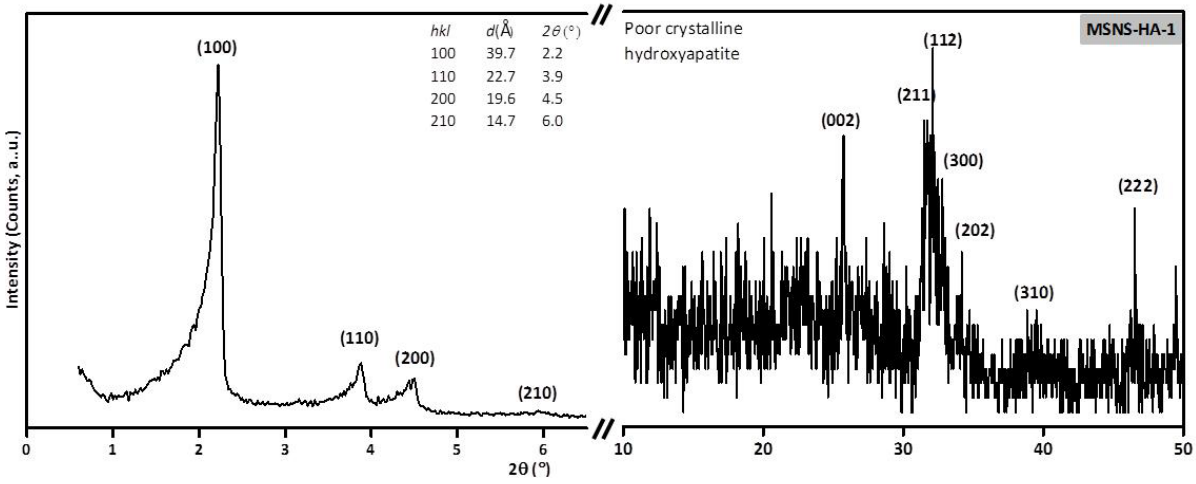

Figure IV.7 SA–XRD (left) and WA–XRD (right) patterns of MSNS–HA–1. The diffraction maxima in the SA-XRD pattern were indexed to a 2D hexagonally arranged mesoporous material. The poorly defined diffraction maxima in the WA-XRD pattern were assigned to a very poorly crystallized HA phase.

WA–XRD pattern can be indexed as a poorly crystalline HA. As it can be observed in Figure IV.8 (right) the diffuse diffraction maxima in the pattern were assigned to the (002), (211), (112), (300), (202), (310) and (222) reflections of HA (International Centre for Diffraction Data (ICDD) Powder Diffraction File No. 9-432). The calcination temperature selected for the synthesis or this material was 550 °C, enough to remove the surfactant whereas the hexagonal order in the MSNSs is maintained, avoiding at the same time further modifications in the HA phase formed if higher temperatures were used. Differently from WA-XRD data of MSNSs where a diffuse maximum centred at 23° characteristic of amorphous silica is registered, here we observed poorly crystalline HA in MSNS-HA-1 sample.

N_2 Adsorption–Desorption Isotherms

Figure IV.8 shows nitrogen adsorption and desorption isotherm of MSNS–HA–1. The Figure also includes the S_{BET} surface area and the pore size diameter distribution. This isotherm is analogous to previously reported for MCM–41 materials [34]. The S_{BET} was 594 m^2/g and the pore size distribution exhibited two maxima at 0.6 nm and 2.6 nm, respectively. In general, isotherm displays a decrease of N_2 adsorption capacity in the presence of the HA phase compared with pure silica MSNSs with surface area 1235 m^2/g (see section IV.2).

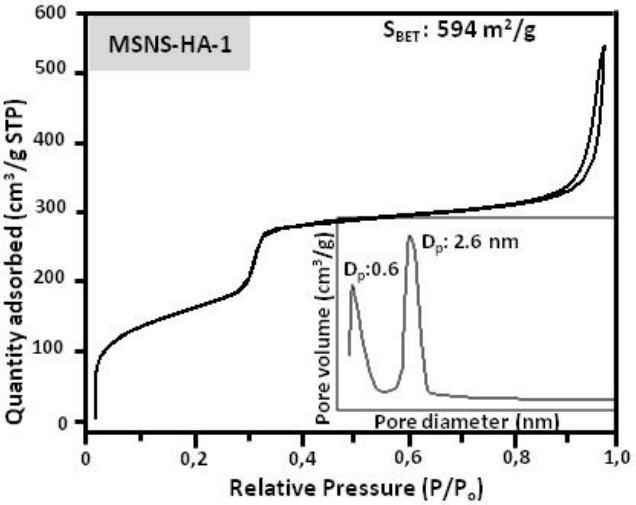

Figure IV.8 N_2 adsorption-desorption isotherms and pore diameters of MSNS-HA-1 sample.

However, the surface area of the silica nanospheres is not totally coated because the composite material still shows mesoporous features with a remarkable surface area of 594 m^2/g. This result indicated that HA is not completely absorbed within the accessible mesopores of material. Hence, after simultaneous synthesis of MSNSs and HA, the S_{BET} of the sample decreased around 52 %.

Transmission Electron Microscopy

In Figure IV.9 TEM micrographs of MSNS–HA–1 are shown. Particles with three different features can be distinguished as follows: *(i)* uncoated MSNSs, *(ii)* nanorods and *(iii)* nanoparticles which are identified as HA. The silica particles exhibited spherical shape with ordered mesopore channels arrangement. However, great differences in particle size were found, MSNSs around 60 nm and around 320 nm of diameter.

Spacing between mesoporous silica channels were 2.5 nm as can be observed in Figure IV.9.d. Moreover, Figures IV.9.b and IV.9.d shows some HA nanoparticles and HA nanorods. These needle-like HA nanorods formed are similar to those reported by *Zhao, Grigoriadou* and *Verma* [35-37]. To sum up, TEM results show that the precipitation method of CaP simultaneously with the synthesis of

ordered mesoporous silica nanospheres yield MSNSs with high dispersity in particle diameters and a CaP phase with a fairly heterogeneous distribution of the HA phase.

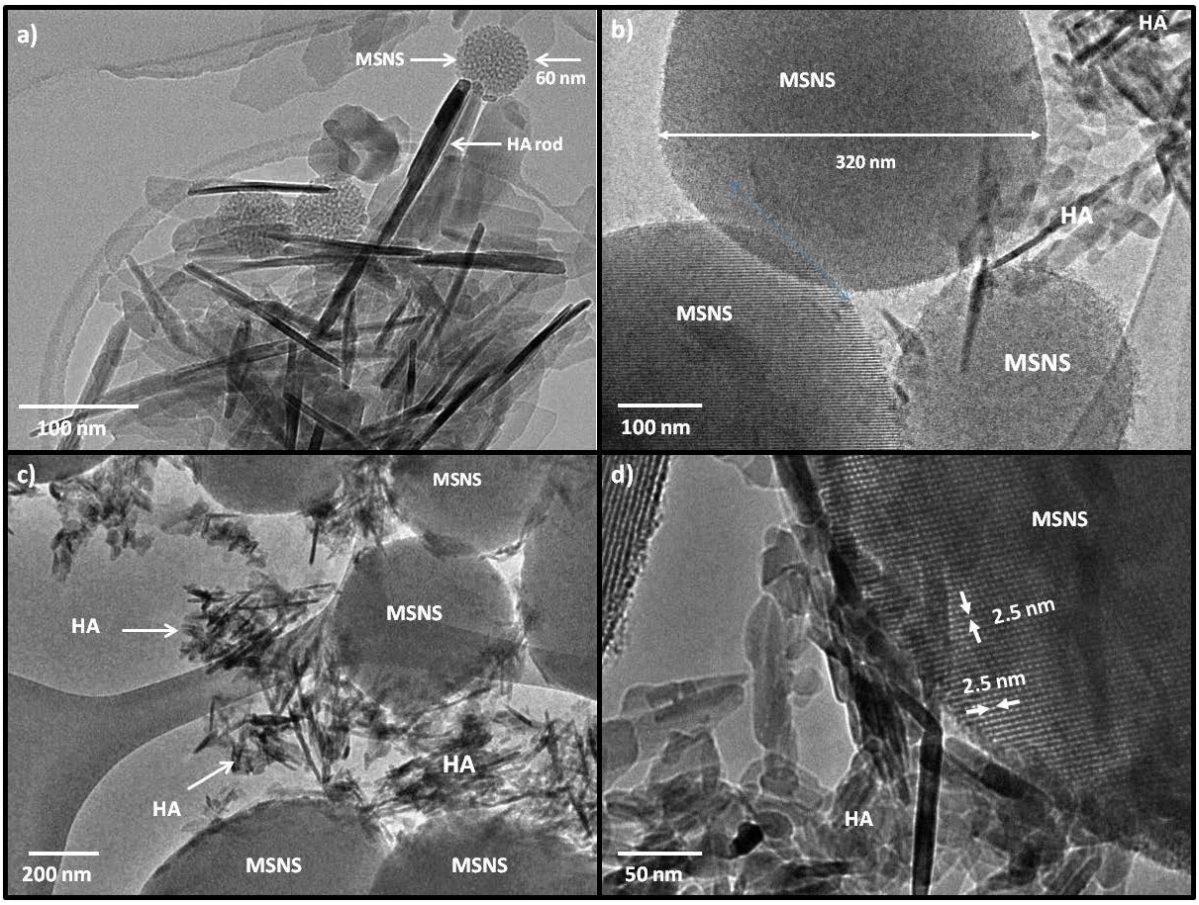

Figure IV.9 TEM micrographs of MSNS–HA–1 showing MSNSs and HA nanorods.

Conclusion of Section IV.3: Precipitation of calcium phosphate simultaneous to the formation of mesoporous silica nanospheres, MSNS–HA–1 sample

Poorly crystallized HA nanorods and mesoporous silica spheres with a high polydispersity in particle diameter were separately observed by this method. The objective of using the hexagonal structure of MSNSs as core was not reached because the interactions between CaP (HA) and silicate ions were poor. However, the presence of HA could confer bioactive features to the material obtained with this approach. According to the analyses, the presence of HA NPs in the sample decreased the textural properties of MSNSs (surface area and porosity). Figure IV.10, schematically depicts the synthesis of MSNS–HA–1 sample, showing how HA nanorods and MSNSs were separately obtained.

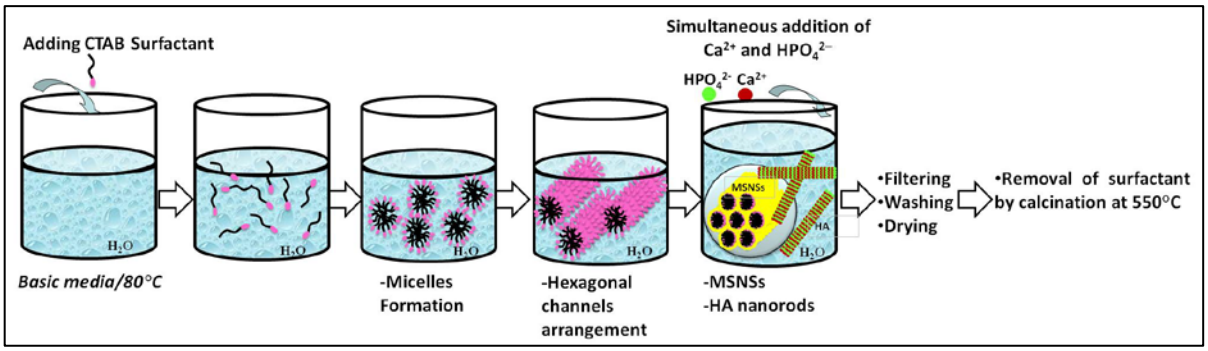

Figure IV.10 Schematic depiction of MSNS–HA–1 synthesis by simultaneous addition of Ca^{2+} and phosphate ions together with the silica precursor TEOS.

IV.4 Soaking mesoporous silica nanospheres into a sol precursor of calcium phosphate, *MSNS–HA–2 sample*

In this approach the synthesis of silica@CaP nanocomposites was attempted by soaking pure silica MSNSs in a sol precursor of CaP. After that, the material was filtered and characterized to check if silica@CaP composites were formed. This strategy of synthesis is here described for the first time. In detail, the synthesis procedure can be divided in the next steps, as it is schematically explained in Figure IV.11:

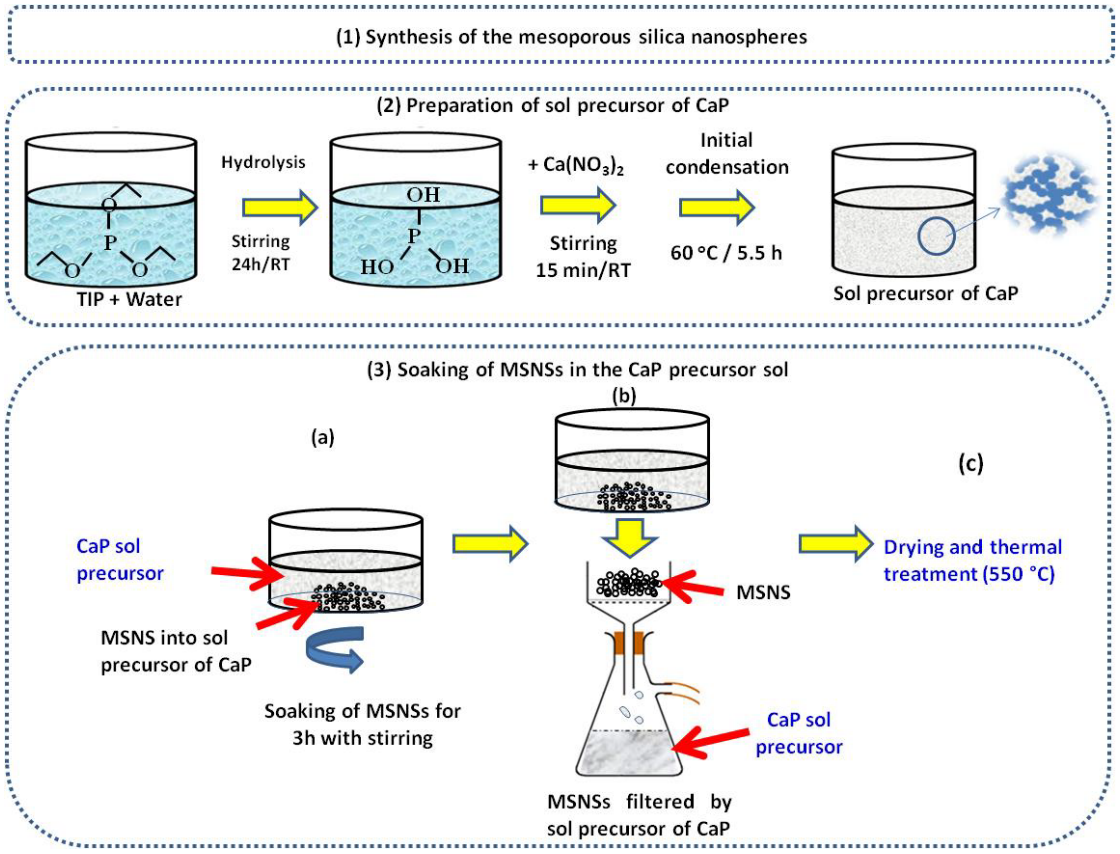

Figure IV.11 Schematic representation of method used showing how the CaP sol precursor is prepared and then used to soak the MSNSs.

(1) Synthesis of the silica nanospheres MSNSs to be used as core,

(2) Soaking of MSNSs for 3 h with stirring in the sol precursor of CaP followed by a filtration. We had speculated that this process could be enough to obtain an appropriate interaction between Ca^{2+} and HPO_4^{2-} ions and the silica matrix.

(3) The MSNSs soaked in the sol precursor of CaP were heated in air at 550 °C trying to obtain HA. The sample obtained after this process was termed as MSNS–HA–2.

Fourier Transform Infrared Spectroscopy

FTIR spectrum of MSNS–HA–2 in the range between 2000 and 400 cm^{-1} is shown in Figure IV.12. The assignation of the bands present in the spectrum is as follows:

- *SiO_2*: at 1050 cm^{-1} for ν_{as}(SiO) and at 800 cm^{-1} for ν_s(SiO) stretching modes; at 435 cm^{-1} for δ(SiOSi) bending mode.
- *PO_4^{3-}:* at 548 cm^{-1} for δ(OPO) of PO_4^{3-} in an amorphous environment.
- *H_2O*: at 1630 cm^{-1} for δ(HOH) of physisorbed water.

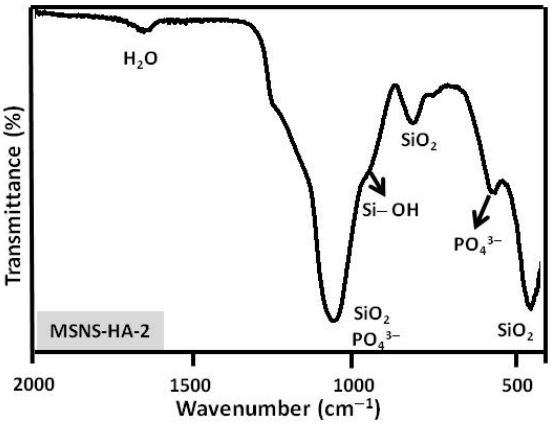

Figure IV.12 FTIR spectrum of sample MSNS–HA–2.

Therefore, the presence of CaP in the sample can be deduced by the band at 548 cm^{-1}, which was not visible in the MSNSs spectrum (Figure IV.1).

Small and wide angle X–ray Diffraction

Figure IV.13 shows the SA–XRD and WA–XRD patterns of MSNS–HA–2 sample. SA–XRD pattern shows two diffuse diffraction maxima at 2θ = 2.44 ° and 4.2 °, which can be respectively indexed to (100) and (110) reflections of a 2D hexagonal arrangement in the MSNSs, being the unit cell parameter a_o= 42.8 Å (a_o= $2d_{100}/\sqrt{3}$, for d_{100} = 37 Å).

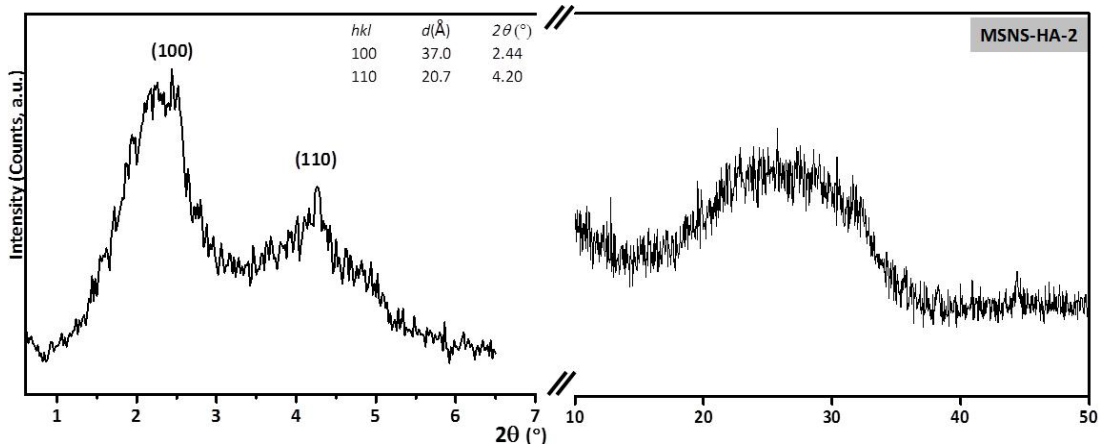

Figure IV.13 SA–XRD and WA–XRD patterns of MSNS–HA–2 sample.

Thus, after soaking the silica nanospheres in sol precursor of CaP, only two XRD maxima with very low intensity were visible in the XRD pattern. This fact reveals a decrease in the hexagonal order of MSNS–HA–2 compared with the initial MSNSs, see Figure IV.2.

Regarding the WA–XRD pattern in Figure IV.13 (right), no clear diffraction maxima were observed, indicating the absence of crystalline phases in MSNS–HA–2. Although some maxima for poorly crystallized HA seem to emerge from the background of the wide diffuse band between 20 and 37 ^{o} in 2θ, the WA–XRD diagram is not conclusive at all in this regard.

N_2 Adsorption–Desorption Isotherms

Figure IV.14 shows nitrogen adsorption and desorption isotherm of MSNSs and MSNS–HA–2. The Figure also includes the S_{BET} surface area value and the pore size diameter distribution (inset). The analysed sample is compared with the initial untreated MSNSs used as reference.

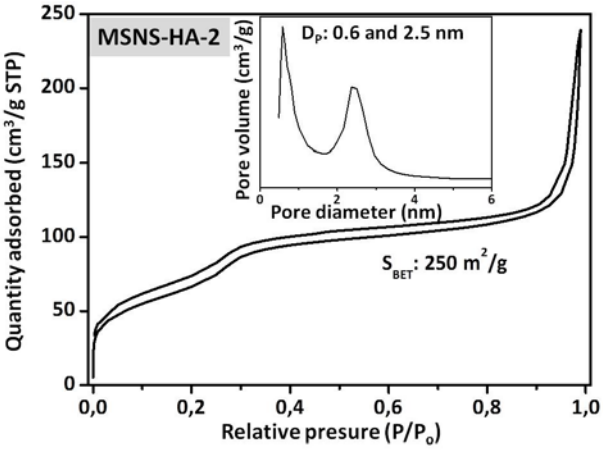

Figure IV.14 N_2 adsorption-desorption isotherms and pore size distributions (insets) of MSNS–HA–2. Surface area values and maxima in the pore diameter distribution are also included.

For MSNS–HA–2 S_{BET} was 250 m^2/g and the pore size distribution exhibited two maxima for D_p of 0.6 nm and 2.5 nm, respectively. As observed in the Figure, MSNS–HA–2 sample displays a decrease of N_2 adsorption capacity after the soaking and filtration treatment compared with pure silica MSNSs, which exhibit a S_{BET} of 1230 m^2/g and a maximum in the pore size distribution at D_p of 2.27 nm. However, the surface area of the silica nanospheres of MSNS–HA–2 sample should not be totally coated by HA, because it still shows mesoporous features and a quite remarkable S_{BET} of 250 m^2/g.

This result could indicate that CaP particles are not completely located within the accessible mesopores of material. Hence, after the treatment with the sol precursor for calcium phosphate, the S_{BET} decreased around 80 % with respect to pure MSNSs.

Transmission Electron Microscopy – Energy Dispersive X–ray Spectroscopy

Figure IV.15 shows several TEM micrographs of the MSNS–HA–2 sample. TEM images show that the initial nanospheres have changed their morphology, from spherical NPs to ellipsoid shaped NPs. Also, the 2D hexagonal array of mesopores has disappeared, although a radial porosity is observed. These ellipsoid shaped NPs seem to be formed by a unique phase with mean elemental composition in Si:P:Ca of 50:25:25, analyzed by EDS in several NPs. These results indicate that the composition of the initial SiO_2 nanospheres has also changed.

A few particles with different morphology were identified by TEM in some regions of the sample and their analysis by EDS gave values mainly for Ca and P, being Si in a minimum proportion. Therefore, some particles of a CaP phase were also formed.

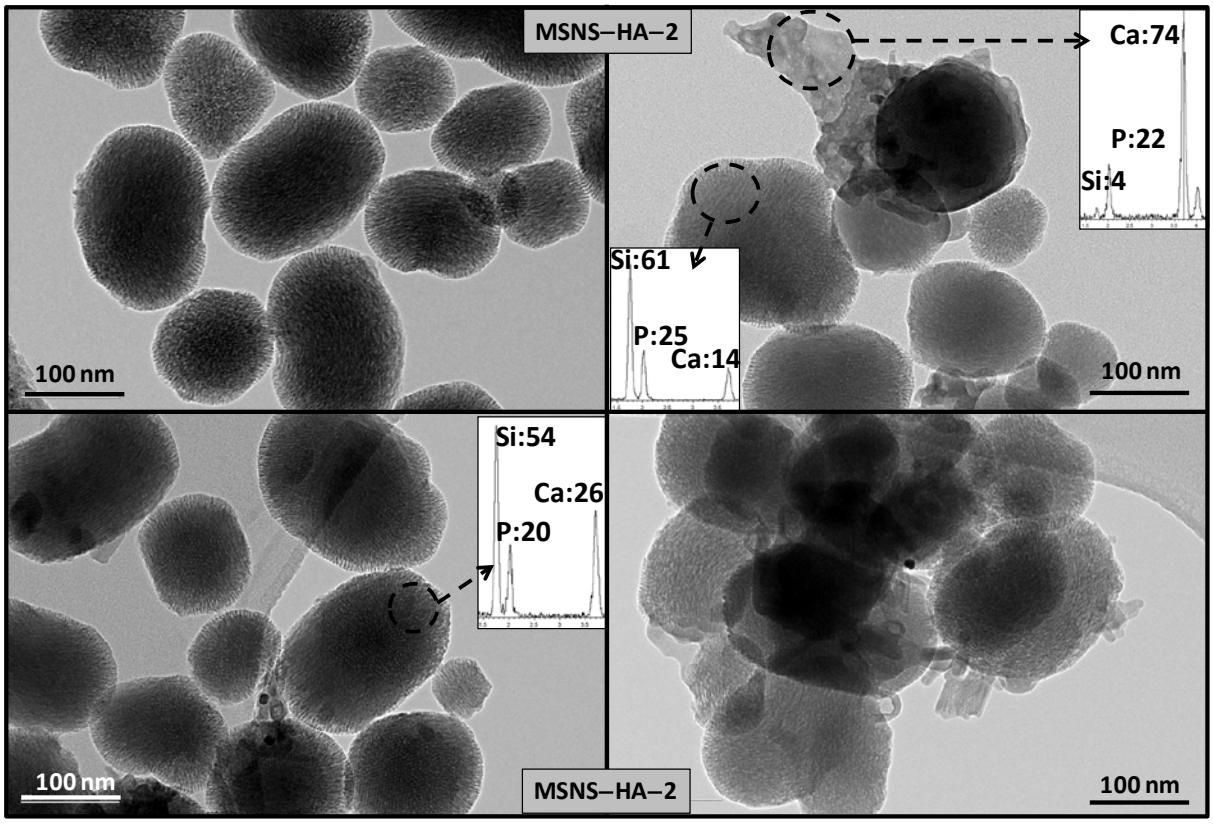

Figure IV.15 TEM micrographs of MSNS–HA–2 showing ellipse–like MSNSs and few particles identified as a CaP phase (up, right). The values of Si, Ca and P elemental composition (atomic %) analyzed by EDS are indicated as insets.

In vitro bioactivity test

Simulated body fluid (SBF) solution, proposed by *Kokubo et al* [38, 39], is used to perform *in vitro* simulations of *in vivo* conditions. Several revisions of the SBF solution have been proposed, including one in 2003 which took into account the fact that a large proportion of calcium and magnesium species present in serum is bound to proteins and hence unavailable for apatite precipitation [40]. According to Kokubo and Takadama's paper [38], a bioactive material is a material on which bone–like hydroxyapatite will form selectively after it is immersed in a serum–like

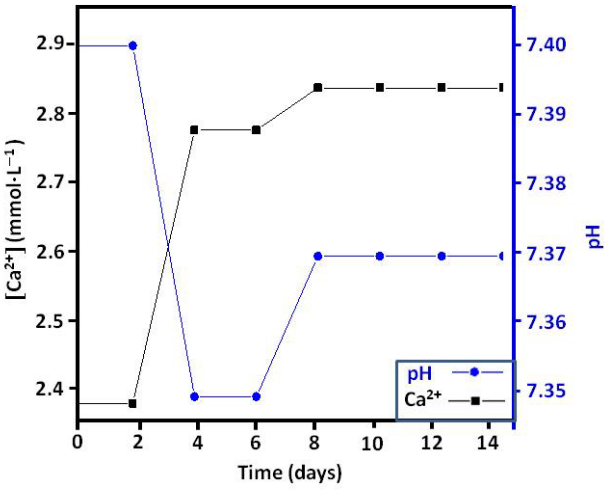

Figure IV.16 Variations of calcium content and pH values of the SBF after soaking the MSNSs-HA-2 sample.

solution. Since 1990, the use of SBF for *in vitro* bioactivity testing has been reported [41]. In the present study, the bioactivity tests in SBF were performed to confirm the apatite formation ability on the MSNS–HA–2 surface.

The *in vitro* bioactivity of MSNS–HA–2, *i.e.*, its ability to be coated by an apatite–like layer after soaking in a simulated body fluid (SBF), was tested as follows: 42 mg of MSNS–HA–2 compacted into a pellet were soaked in 8.4 mL of SBF for three different time intervals up to 15 days. After the soaking period, the pellet was gently washed with water and ethanol and dried at 80 °C for 24 h.

Figure IV.16 shows the variation of Ca^{2+} concentration and pH in the SBF with the soaking time of MSNS–HA–2 measured in an ILyte Electrolyte Analyzer. As observed in the Figure, calcium levels increased quickly during the first 4 days, after that it increased slowly until 8 days. Thereafter, the calcium concentration remained stable until the end of the assay.

The pH evolution follows a profile different to that of $[Ca^{2+}]$ showing in the first 6 days a slight decrease from the initial 7.40 to 7.35 and it is unchanged in a value of 7.37 until the end of the assay. These results could indicate that a Ca^{2+}–H^{+} exchange occurs between the sample and the SBF solution, mainly in the first 6 days of assay.

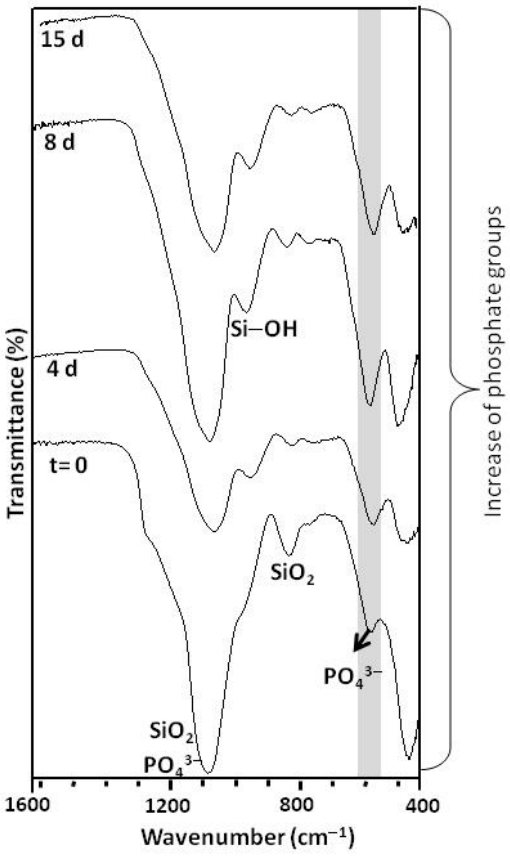

Figure IV.17 FTIR spectra of bioactive MSNSs–HA-2 sample, from 0 to 15d.

FTIR spectroscopy was carried out to evaluate the changes in the sample surface as a function of soaking time. Figure IV.17 collects the FTIR spectra of MSNS–HA–2 before and after different times in SBF. Before soaking (t=0) the spectrum shows characteristic absorption bands of amorphous phosphate groups at 600 cm^{-1} with low intensity, and silica bands at 1040, 800 and 470 cm^{-1} already observed in Fig IV.12. An increase in the intensity of the amorphous phosphate absorption band is observed after 4 days in SBF combined with a decrease in the definition of the silicate bands. Both effects are more visible when the soaking time increased to 8 and 15 days.

Figure IV.18 shows the SEM micrographs of the sample before and after soaking in SBF for 8 days. MSNSs are clearly seen as spheres before soaking in SBF (Figure IV.18, left), t = 0. SEM micrograph after 8 days in SBF reveals that the sample surface undergoes some changes because new particles are formed (Figure IV.18, right).

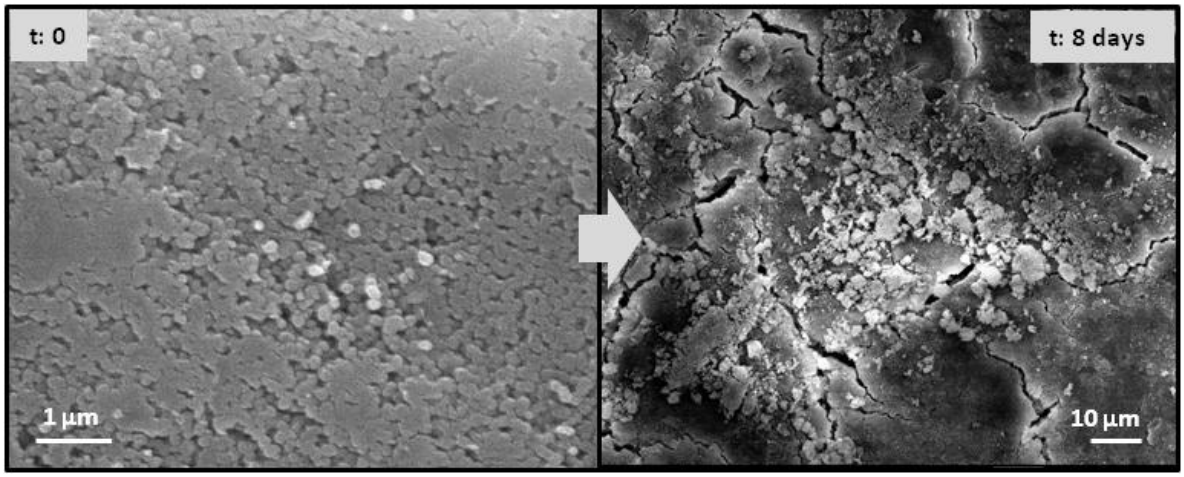

Figure IV.18 SEM micrographs of MSNS–HA–2 surface before and after 8d in SBF.

Conclusion of Section IV.4: Soaking mesoporous silica nanospheres into a sol precursor of calcium phosphate

The MSNSs were soaked for 3 h in a sol precursor of CaP and then filtered. 2D hexagonal ordered mesoporous silica NPs were intended to be used as structure core to be covered by HA. The synthesis procedure was schematically explained in Figure IV.11. By this procedure the sample obtained exhibited the following features: ellipse-like NPs and an elemental composition different from the initial SiO_2, containing Si, Ca and P. Moreover, a significant decrease in porosity and decrease in surface area of *ca.* 80% was found by N_2 adsorption, although the surface area is 250 m^2/g, which is still valid for bioapplications. Therefore, this procedure affects mesoporosity, composition and shape of mesoporous silica nanospheres. Also, this material shows a moderate in vitro bioactivity in SBF.

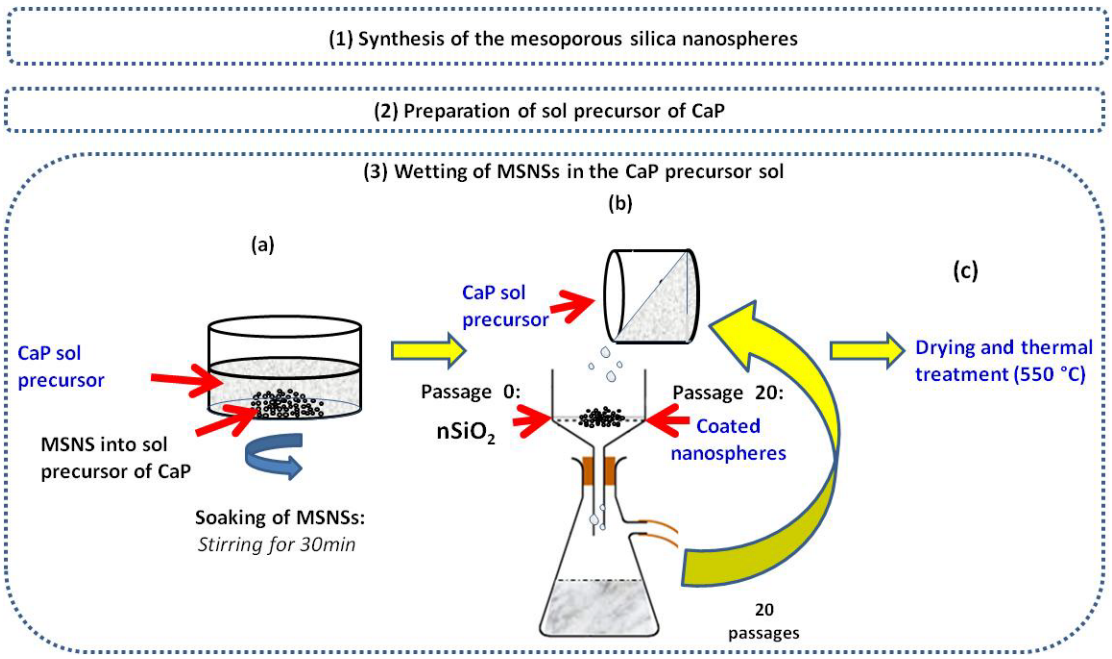

Figure IV.19 Schematic representation of method used showing the wetting process of the MSNSs into the precursor sol of CaP.

IV.5 Wetting mesoporous silica nanospheres into a sol precursor of calcium phosphate, *MSNS–HA–3* sample

In this case, the core@shell material (MSNSs@CaP) was treated to be obtained by soaking the MSNSs in the sol precursor of CaP for a short period of time and subsequently performing a filtration and repeated washings with the sol for 20 times. That is, the filtered solution was poured again over the filter containing the nanospheres, repeating the process for 20 times. With this procedure, schematically depicted in Figure IV.19 (previous pag), we were trying to mimic a dip-coating method. The obtained sample was called MSNS–HA–3. The main difference with the previous study was the soaking time in sol precursor of CaP (30 min), avoiding a long soaking time which seems to affect in a high extend the MSNSs, as described in the previous section.

Fourier Transform Infrared Spectroscopy

The FTIR spectrum of MSNS–HA–3 is shown in Figure IV.20 and compared with FTIR spectrum of uncoated MSNS. The bands were assigned as follows:

- *SiO_2*: at ca. 1050 and at 802 cm^{-1} the bands for stretching modes ν(SiO). At 432 cm^{-1} bending mode δ(SiOSi).
- *PO_4^{3-}:* at ca. 1050 cm^{-1} the band for stretching mode ν(PO) and at 600 and 565 cm^{-1} for δ(OPO).

The HA presence in the sample can be confirmed by phosphate bands observed at 600 and 565 cm^{-1} revealing the presence of PO_4^{3-} in a crystalline environment [42].

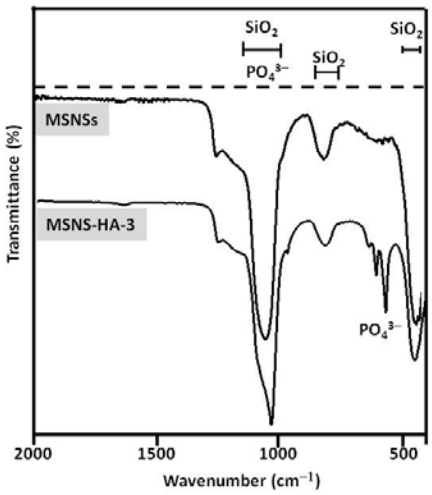

Figure IV.20 FTIR spectra and functional groups of MSNS and MSNS-HA-3 samples.

Small and wide angle X–ray Diffraction

Figure IV.21 (left) shows the SA–XRD pattern of MSNS-HA-3 to analyze the possible hexagonal order in the nanospheres, compared with MSNSs.

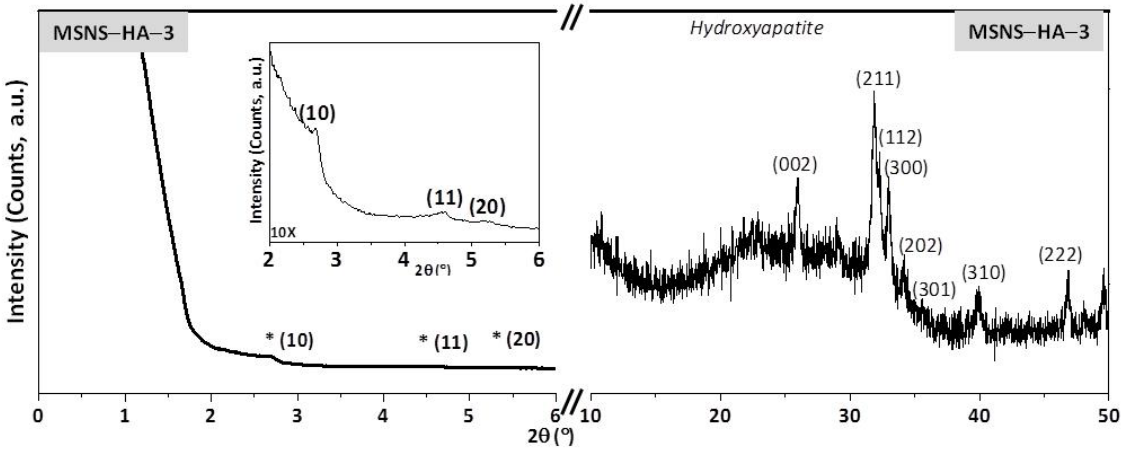

Figure IV.21 The possible nanostructural order shown by SA–XRD (left) and diffuse maxima indexed for poorly crystallized HA shown by WA–XRD (right) for MSNS-HA-3.

SA–XRD pattern of sample shows three diffraction maxima with low intensity at 2θ = 2.6°, 4.4° and 5.1°, which can be respectively indexed to (100), (110) and (200) reflections of a 2D hexagonal arrangement.

For WA–XRD, the sample shows the poorly defined diffraction maxima assigned to a very low crystalline HA phase. As it can be observed in the Figure, the diffuse diffraction maxima in the diffractogram were assigned to the (002), (211), (112), (300), (202), (301), (310) and (222) reflections of a HA phase (ICDD Powder Diffraction File No. 9-432). Thus, while the WA–XRD pattern for MSNSs shows only a diffuse maximum centred at 25 ° characteristic of amorphous silica, WA–XRD pattern of sample MSNS–HA–3 can be assigned to a poorly crystallized HA.

N_2 Adsorption–Desorption Isotherms

Figure IV.22 shows N_2 adsorption and desorption isotherms of MSNS–HA–3. The Figure also includes the S_{BET} surface area and the pore size diameter distribution.

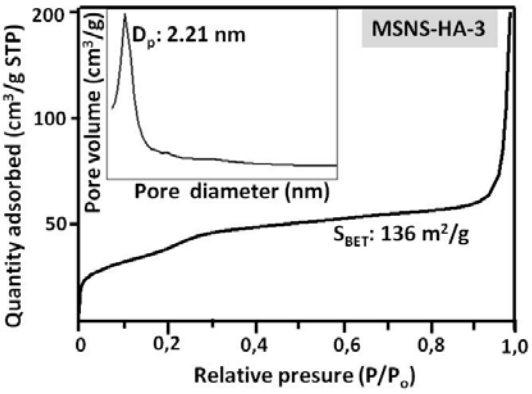

Figure IV.22 N_2 adsorption-desorption isotherms and pore diameter of MSNS–HA–3.

As observed in the Figure, the S_{BET} was 136 m^2/g and the pore size distribution exhibited maxima at 2.21 nm. In general, isotherms display a decrease of N_2 adsorption capacity after coating compared with pure silica MSNSs with a S_{BET} of 1235 m^2/g. However, the pore diameter is maintained, from 2.27 nm to 2.21 nm, indicating that the accessible pores preserve the initial diameter. This fact would be indicative of a partial coverage of the silica nanospheres, leaving pores without an entrance blockage. This fact also discard occupation of the cylindrical channels or internal surface by the HA. The composite material still shows mesoporous features with quite enough surface area. Hence, after the treatment with the sol, the S_{BET} decreased around 90 %.

Transmission Electron Microscopy

Figure IV.23 shows TEM images of MSNSs and MSNS–HA–3 samples. For MSNSs, SiO_2 nanospheres in the range 150-250 nm of diameter, exhibiting highly ordered 2D hexagonal mesoporous structure are observed. After sol filtration repeated times and thermal treatment (MSNS–HA–3 sample), the nanospheres appeared fully coated by HA nanoparticles as identified by the XRD analysis. Nanospheres of silica coated by hydroxyapatite phase are clearly observed in MSNS–HA–3 sample with homogeneous size of around 250 nm of diameter. The sol filtration method allows a fairly homogeneous distribution of HA nanoparticles layer throughout the mesoporous silica nanospheres surface. Elemental composition analyzed by EDS gives values for Si:P:Ca of 59:17:24 (atomic %) when registered in the centre of the covered nanospheres. However, for the particles near the borders of the nanospheres values for Si:P:Ca of 2:38:60 (atomic %) were obtained. The silicon content

decreased as expected for a calcium phosphate composition, which in addition possesses a Ca/P molar ratio of 1.58, very close to the corresponding ratio in HA, 1.67.

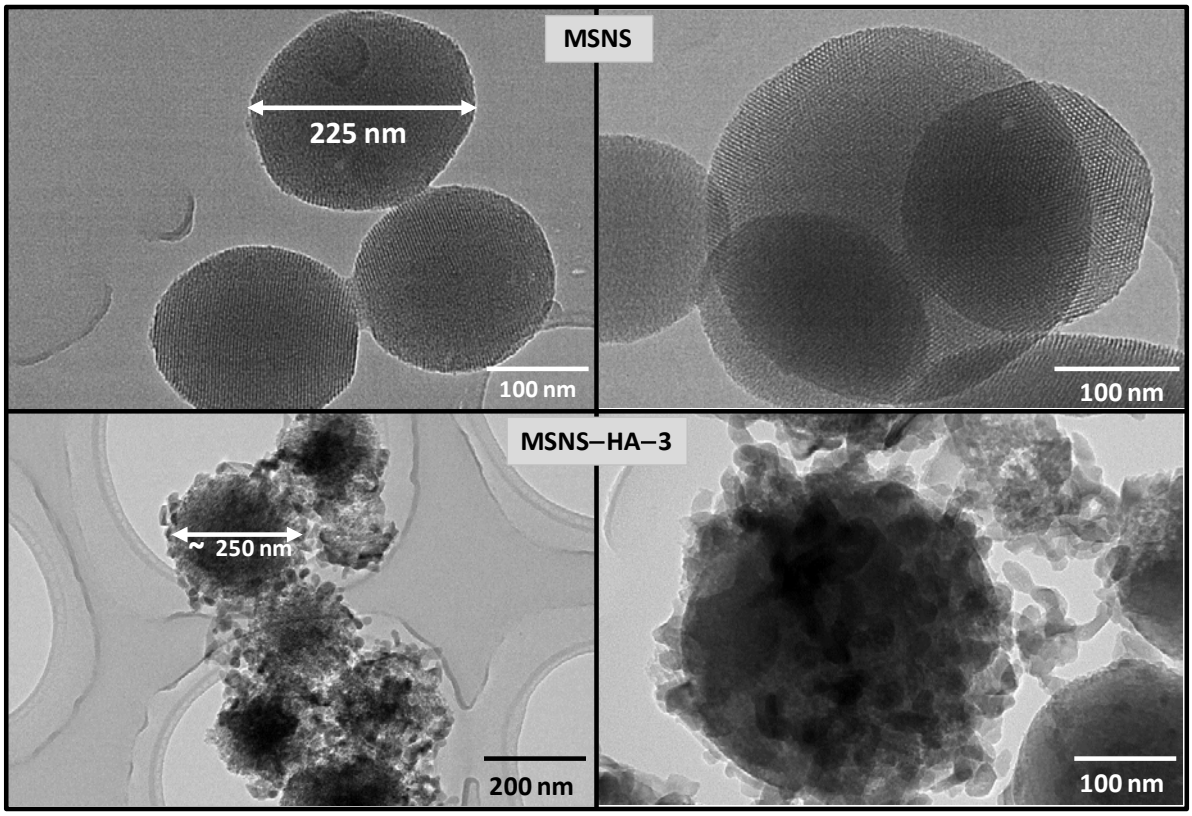

Figure IV.23 TEM images of MSNSs (before wetting by sol precursor of CaP) and MSNS–HA–3 (after wetting by sol precursor of CaP).

Conclusion of Section IV.5: Wetting mesoporous silica nanospheres into a sol precursor of calcium phosphate

MSNS coated with HA were synthesized by wetting MSNSs in a sol precursor of CaP for a short time and subsequently filtering and washing the nanospheres with the sol for 20 times, resembling a dip–coating method. The differences with our previous study in section IV.4 were *(i)* the soaking time of the MSNSs in sol precursor of CaP that was now only 30 min instead of 3 h and *(ii)* the wetting procedure with the sol up to 20 times. Final sample was calcined in air at 550 °C to obtain HA phase. Our goal here was to check if the soaking time plays an important role on the shape, composition and mesoporosity of MSNSs.

For MSNS–HA–3, the presence of HA and its interaction with the silica mesoporous structure were confirmed by TEM, FTIR and WA–XRD. By SA–XRD, the very low intense diffraction maxima indicated the presence of a 2D hexagonal mesoporous order still present after HA coating. The S_{BET} surface area was 136 m^2/g, indicating a decrease of N_2 adsorption capacity of around 90% with respect to uncoated MSNS with a S_{BET} surface area of 1235 m^2/g. The pore diameter is maintained in the sample treated with the sol, therefore, the formed HA is not inside the pores but capping the entrance in

most of them. TEM images confirm the formation of HA NPs covering the surface of MSNSs. Moreover, homogenously formed nanospheres were observed by TEM. As opposed to MSNS–HA–2, in this case no ellipse–like nanospheres were observed. These results confirm the effect of soaking time over nanospheres composition, shape and mesoporosity.

This new route could be used to improve the bioactivity and biocompatibility of nanospheres designed for clinical applications in bone regeneration. Specific applications will require wetting levels that allow us to reach different textural properties. The composite is thought to be suitable as bone filler material where a biodegradable and osteoconductive implant with a localized release of biologically active substances is required.

IV.6 Functionalization of nanospheres with phosphate–like groups and subsequent wetting into a sol precursor of CaP

The application of nanotechnology in the field of drug delivery has brought many innovations on the surface functionalization of inorganic nanomaterial-based delivery vehicles, such as MSNSs. The ability to functionalize the surface of silica groups of mesoporous nanospheres with organic entities make them suitable as a new platform for various biotechnological and biomedical applications [13, 43-57]. Here, the abundant silanol groups (Si–OH) on the silica surface of MSNSs were functionalized with molecules containing phosphate-like groups such as diethylphosphatoethyltriethoxysilane (DEPETES) [17, 58-60] and 3-trihydroxysilylpropyl methylphosphonate (THSMP), see Figure IV.24.

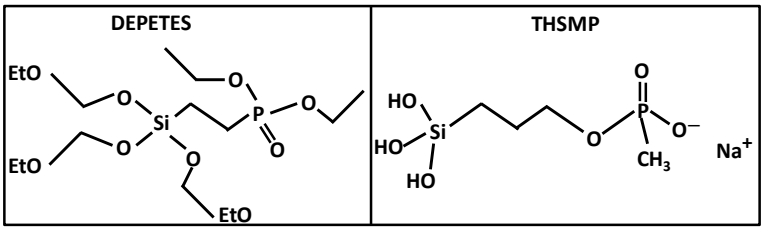

Figure IV.24 Chemical structure of DEPETES and THSMP.

The following two subsequent steps were used to achieve the main goal of this study: *(i)* functionalization of MSNSs with phosphate–like groups and *(ii)* using these groups as binding moieties between silica surface and Ca^{2+} and HPO_4^{2-} ions to coat the MSNSs with HA NPs. This novel approach gives us an opportunity to synthesize the nanostructured HA onto the surface of prefunctionalized silica. Co-condensation and post-synthesis methods were used to obtain the MSNSs functionalized with phosphate–like groups.

Co-condensation method (direct synthesis) allows synthesizing the silica phases functionalized with phosphate–like groups in the presence of surfactant. By this method, it is possible to prepare mesostructured silica phases with DEPETES and THSMP in the presence of surfactants leading to materials with organic residues covalently anchored to the pore walls. *Post–synthesis* method allows preparing the pre-synthesized MSNS with phosphate-like groups. This method carries out in two steps: *(i)* first MSNSs are synthesized by addition of the silica source (TEOS) into a surfactant

template in water solution and, once the surfactant is removed, *(ii)* MSNSs are then functionalized with the alkoxysilanes.

Regarding the silanes used for phosphate-like functionalization, DEPETES can be used in co-condensation as well as in post-synthesis methods. However, THSMP is only appropriate for co-condensation because it already possesses the silanol groups or hydrolized alkoxysilane moiety. Therefore, the following samples were prepared:

Two samples with DEPETES obtained by co-condensation containing 10 and 20% mol of DEPETES with respect to TEOS, **NSFD1** and **NSFD2** samples, and one sample with DEPETES obtained by post-synthesis, **NSFD** sample. The amount of DEPETES used for each sample is explained in section VII.5.c. The obtained samples are named NSFD1, NSFD2 and NSFD (**N**ano**s**pheres pre**f**unctionalized by **D**EPETES).

The sample functionalized with THSMP was prepared by co-condensation and it is named **NSFT** (**N**ano**s**pheres pre**f**unctionalized by **T**HSMP).

The functionalized samples were extracted with acidified ethanol solution to remove surfactant as described in section VII.5.c. Then, all functionalized samples were subjected to a wetting process in a sol precursor of CaP and they are named **NSFD–HA** and **NSFT–HA** for DEPETES and THSMP, respectively.

IV.6.1 Functionalization of nanospheres with diethylphosphatoethyltriethoxysilane: *by post-synthesis for NSFD sample*, and by co-condensation for *NSFD1* and *NSFD2* samples

Thermogravimetric and Differential Thermal Analysis

The TG/DTA curves, as well as weight loses, for the samples obtained with DEPETES are shown in Figure IV.25. TGA curves show continuous weight loses from 180 to ~450 °C, due to organic matter combustion. Moreover, TGA curves exhibit a small weight loss between room temperature and 150 °C that was attributed to the physisorbed water loss.

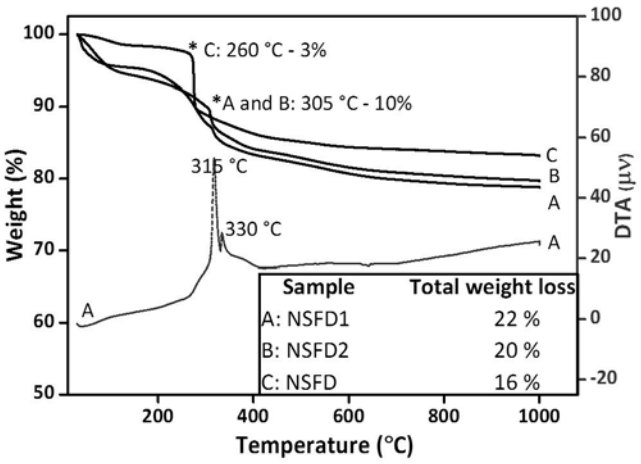

Figure IV.25 TG/DTA curves of samples functionalized with DEPETES.

Samples functionalized by co-condensation are subjected to a solvent extraction to remove the surfactant. With this method it is not usual the complete removal of the surfactant, being common a remained amount of around 5% wt. Samples NSFD1 and NSFD2 present different TGA curves, as well as a bigger amount of organic matter, that the sample prepared by post-synthesis NSFD, in which the surfactant is completely removed by calcination before organic functionalization.

Fourier Transform Infrared Spectroscopy

The FTIR spectra for all samples functionalized with DEPETES are shown in Figure IV.26. Typical spectrum of silica was obtained. The presence of a small amount of DEPETES in all samples was confirmed by the low intensity bands of ν(CH) from CH_2 groups and δ(OPO) from phosphonate groups.

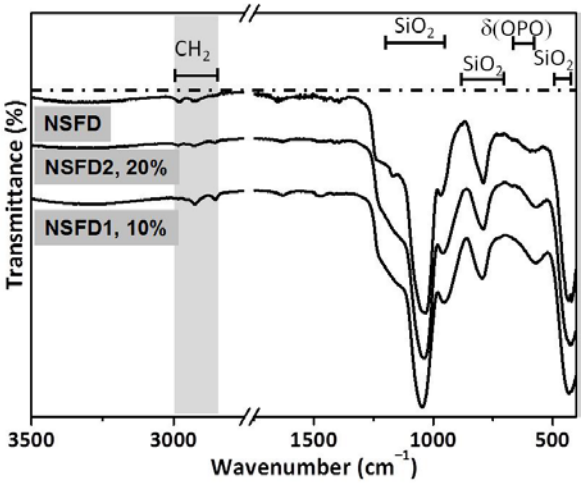

Figure IV.26 FTIR spectra of MSNPs functionalized with DEPETES after extraction of surfactant.

Small angle X–ray Diffraction

Figure IV.27 shows the SA–XRD patterns of these three samples. In total four XRD maxima were observed that can be indexed on a hexagonal lattice typical of MSNSs [33]. An interplanar spacing was around $d_{100} \approx 40$ for (d_{hkl} = 100). As shown in the figure, other three peaks were observed around d(Å) = 22 and 19 and 15 nm for 2θ = 2.2°, 3.8°, 4.4 and 5.8°, respectively.

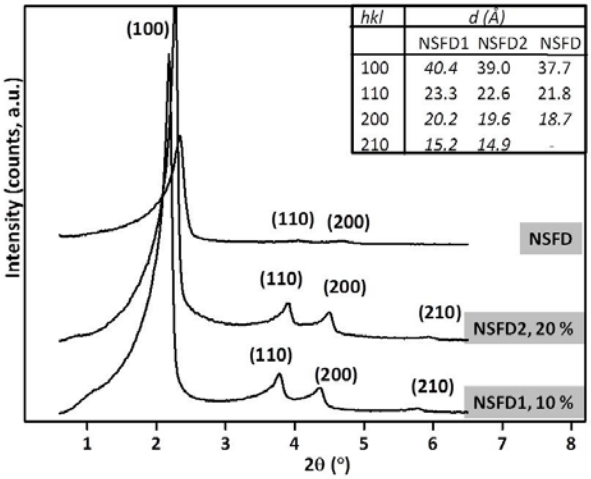

Figure IV.27 Small angle XRD of MSNSs functionalized with DEPETES via co–condensation and post synthesis.

N_2 Adsorption–Desorption Isotherms

Pore surface area and pore diameter data of the samples were obtained by nitrogen adsorption and desorption isotherms (Figure IV.28).

All samples are based on a model mesoporous adsorbent exhibiting a pore structure in the form of hexagonal arrays of uniform tubular channels of controlled width [61]. The well-defined reversible type IV isotherms obtained in all samples correspond to MCM–41 type. This is a type IV BET isotherm of mesoporous materials with an adsorption curve step between relative pressures P/P_o of 0.2 and 0.4 [62]. The following values of BJH pore diameter (D_p) and BET surface area (S_{BET}) were obtained:

- NSFD D_p = 0.8 and 1.9 nm ; S_{BET} = 878 m^2/g
- NSFD1, 10 % D_p = 2.5 nm ; S_{BET} = 1190 m^2/g
- NSFD2, 20 % D_p = 0.6 and 2.3 nm ; S_{BET} = 920 m^2/g

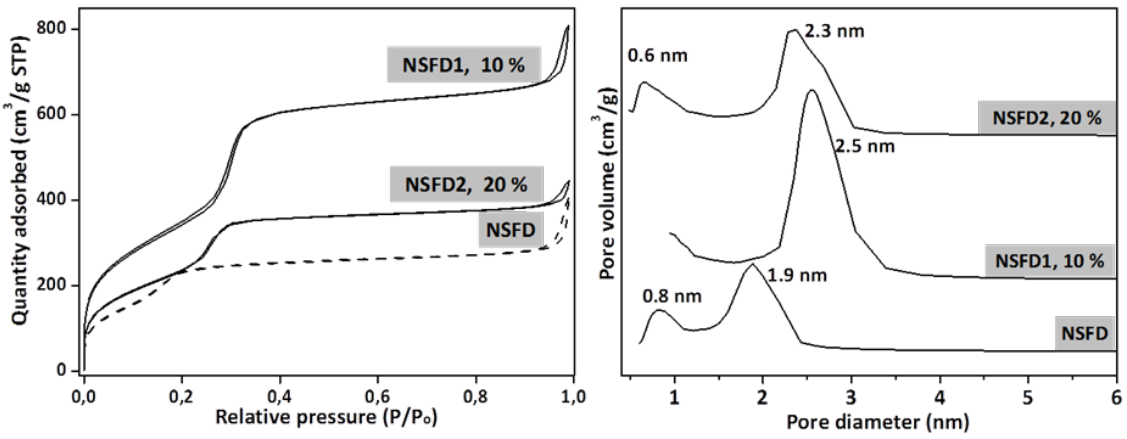

Figure IV.28 N_2 adsorption-desorption isotherms (left) and pore diameter data (right) of the samples obtained by nitrogen adsorption and desorption isotherms.

Scanning Electron Microscopy and Energy Dispersive X–ray Spectroscopy

The morphology of the samples is observed by SEM images in Figure IV.29. These micrographs show that all samples consist on monodisperse spherical nanoparticles. The particle size seems bigger in the case of co-condensation using 20% of DEPETES, being between 170 and 250 nm for all the samples. DEPETES presence was confirmed by phosphorous detection in the EDS analysis, being the P content very similar for the three samples although slightly bigger for the sample obtained by post-synthesis.

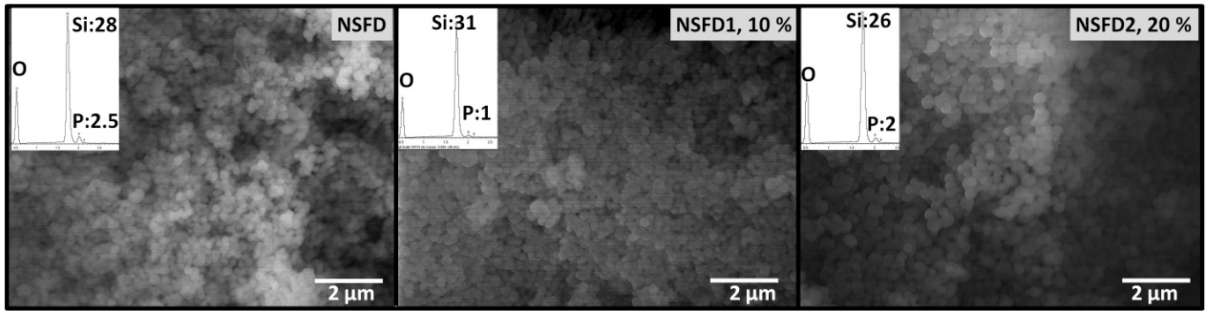

Figure IV.29 SEM micrographs of the DEPETES functionalized MSNSs.

Conclusion of Section IV.6.1: Functionalization of mesoporous silica nanospheres with diethylphosphatoethyltriethoxysilane

MSNSs functionalized with phosphate groups of DEPETES were prepared via two functionalization methods, co-condensation and post-synthesis. The presence of DEPETES was confirmed by the content in organic matter, EDS and FTIR analysis, observing phosphonate groups and hydrocarbon chains. All samples show a high specific surface area according to BET model. These results confirm that the DEPETES functionalization has not decreased the surface area to a high extent. In addition, the hexagonal arrangement was observed by WA–XRD. Therefore, the typical mesoporous silica nanospheres were no structurally affected. The sample selected for the next step is NSFD, the obtained via post-synthesis, due to its slightly higher content in phosphorous.

IV.6.2 Wetting of DEPETES functionalized MSNSs via post-synthesis into a sol precursor for CaP, NSFD–HA sample

Fourier Transform Infrared Spectroscopy

The FTIR spectra of the NSFD–HA sample is shown in Figure IV.30 together with NSFD sample, before sol treatment. The band attributed to the bending mode δ(OPO) from phosphate groups is more intense after sol treatment. *C–H stretching bands* in NSFD-HA sample could not be observed due to calcinations in the HA preparation process.

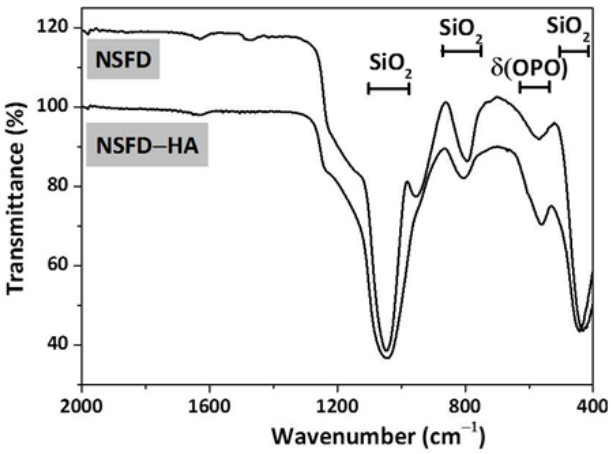

Figure IV.30 FTIR spectra of MSNSs functionalized with DEPETES via post–synthesis, before and after being wetted in the precursor sol for CaP.

Small and Wide X–ray Diffraction

SA–XRD and WA–XRD analysis were used to determine the mesostructure and crystalline phase in NSFD-HA sample, see Figure IV.31. Due to the wetting of the MSNSs functionalized with DEPETES with the sol precursor of CaP, the three peaks of hexagonal structure were observed with very low intensity by SA–XRD (Figure IV.30, left). These three peaks can be indexed on the hexagonal arrangement of MCM–41 material, corresponding to a interplanar spacing d_{100} ≈ 37.5 Å (d_{hkl} = 100). Besides the broad maximum of amorphous SiO_2, a potential nanocrystallized hydroxyapatite phase was detected in the WA-XRD pattern after wetting in the sol precursor of CaP. Poorly defined diffraction maxima can be assigned to the (002), (112) and (222) reflections of an HA–like phase.

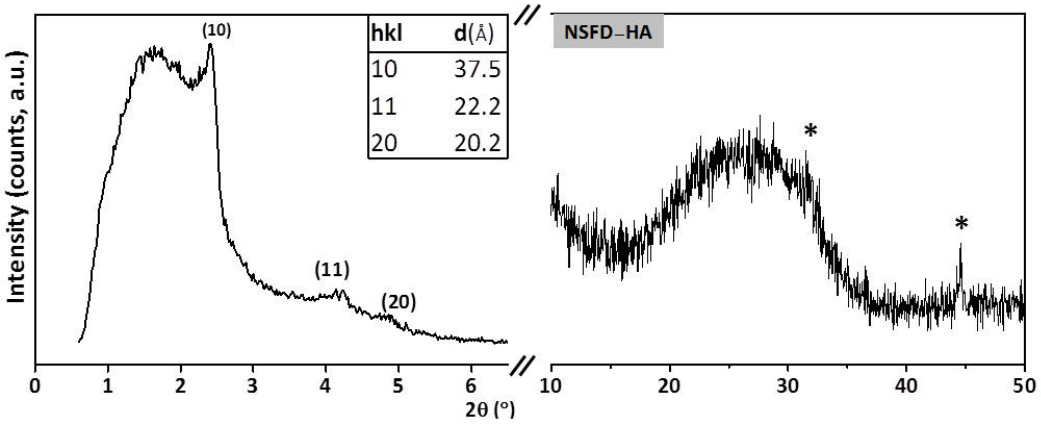

Figure IV.31 SA–XRD (left) and WA–XRD (right) of NSFD–HA sample, where * indicates HA.

N_2 Adsorption–Desorption Isotherms

Nitrogen adsorption–desorption isotherms of NSFD after being soaked in the CaP precursor sol are shown in Figure IV.32. The sample exhibit similar type IV isotherm that before being soaked, demonstrating the features of typical mesoporous materials. The surface area was S_{BET} was 335 m^2/g, which is lower than the typical for MSNSs materials. It has decreased around 62% compared with NSFD. Pore size distribution exhibited a maximum at 1.8 nm.

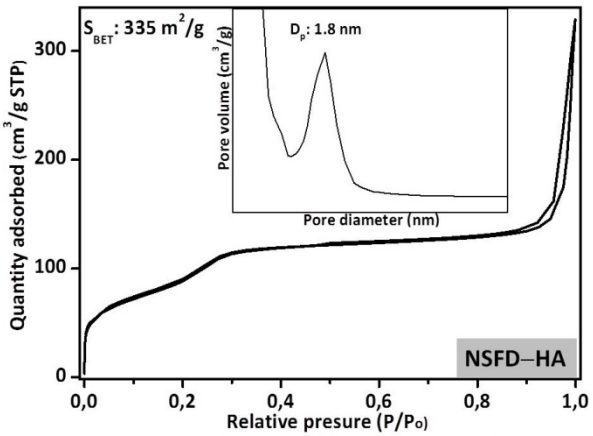

Figure IV.32 N_2 adsorption/desorption isotherms of NSFD–HA sample.

Transmission Electron Microscopy

TEM micrographs of different regions of the NSFD–HA sample presented in Figure IV.33 show nanospheres possessing mesopore ordered structure. The shape of nanospheres is not modified after wetting them with the sol precursor of CaP. The nanospheres seem to be covered by a phase rich in Ca and P, as the EDS analysis in several nanospheres indicates.

There is also presence of other nanoparticles in which the 0.7 nm spacing could be attributed to the interplanar distance (001) of hydroxyapatite. Therefore, the sol coating method allows a fairly homogeneous distribution of an HA layer throughout the ordered MSNSs.

Conclusion of Section IV.6.2: HA coating of mesoporous silica nanospheres functionalized with diethylphosphatoethyltriethoxysilane by post–synthesis

In this study, an easy synthesis route for making multifunctional silica@HA composite material is presented. Our goal was to coat MSNSs with HA and make it a bioactive material for biomedical applications. The MSNSs with HA particles were prepared by wetting MSNSs functionalized with DEPETES into a precursor sol for CaP. Then, they were subjected to a thermal treatment at high temperature to obtain the HA phase of interest for its bioactive properties. The obtained product could be useful in biomedical applications. This system exhibits a potential application in the fields of drug delivery based on its possible bioactive and mesoporous properties.

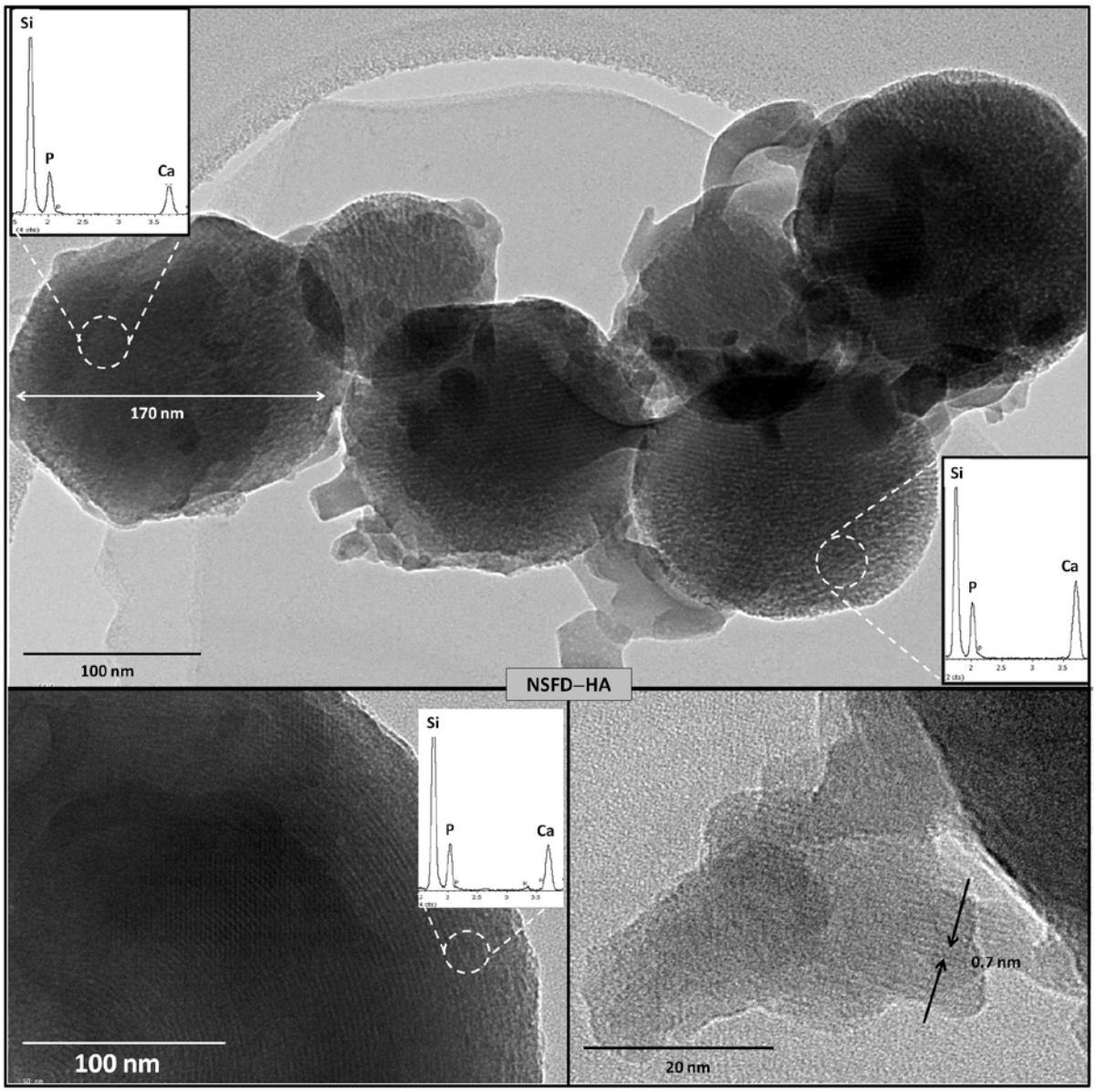

Figure IV.33 TEM images of NSFD–HA sample.

IV.6.3 Functionalization of nanospheres with 3–trihydroxysilylpropyl methylphosphonate *by co-condensation, NSFT sample*

During synthesis the molar ratios of used reactants were as follows: 1 TEOS / 0.3 THSMP.

Thermogravimetric and Differential Thermal Analysis

TG/DTA were used to detect the presence of surfactant and THSMP and the results are shown in Figure IV.34. TG curve exhibited a weight loss between room temperature and ~100 °C that was

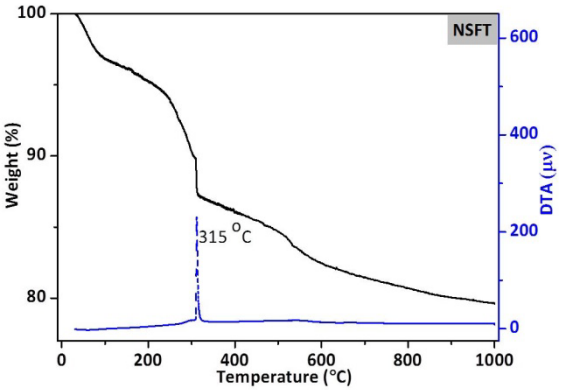

Figure IV.34 TG/DTA curves for MSNSs functionalized with THSMP.

attributed to physisorbed water. The organic matter loss of THSMP and residual surfactant from the extraction method was estimated around 13 %.

Fourier Transform Infrared Spectroscopy

The FTIR spectrum is shown in Figure IV.35. A typical spectrum of silica was obtained for this sample. In addition, the following bands confirming the presence of THSMP are observed:

- *Phosphonate bending region*: at 577 cm^{-1} for δ(OPO).
- *CH stretching region for THSMP*: at 2981 and 2926 cm^{-1} for ν_{as}(CH) and ν_{s}(CH), respectively.

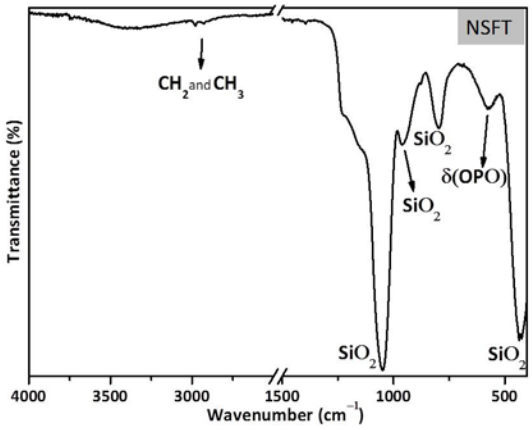

Figure IV.35 FTIR spectrum of MSNSs functionalized with THSMP.

Small angle X–ray Diffraction

SA–XRD analysis was used to determine the mesostructure of the nanospheres functionalized with THSMP (Figure IV.36). An interplanar spacing $d_{100} \approx 39.8$ Å was observed (d_{hkl} = 100). Four peaks observed in SA–XRD 2θ region can be indexed on a hexagonal lattice typical of MCM–41 type, confirming that the 2D hexagonal order is achieved during the co-condensation with the used TEOS/THSMP proportion.

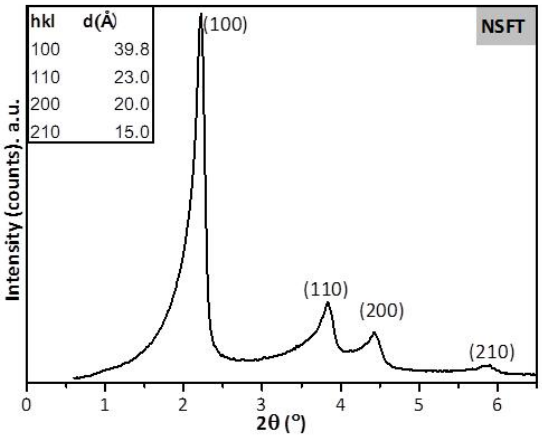

Figure IV.36 Small angle XRD of MSNPS functionalized with THSMP.

N_2 Adsorption–Desorption Isotherms

BET surface area and pore diameter data of the sample were calculated from the nitrogen adsorption and desorption isotherms in Figure IV.37. The sample exhibits a hexagonal array of uniform tubular mesoporous channels that is confirmed the Type IV isotherms with no observed hysteresis loop. It shows a well–defined step in the adsorption curve between partial pressures P/P_o of 0.2 and 0.4. Pore diameter distribution calculated by BJH showed two maxima at 0.8 and 2.7 nm. A BET surface area of 1316 m^2/g was calculated.

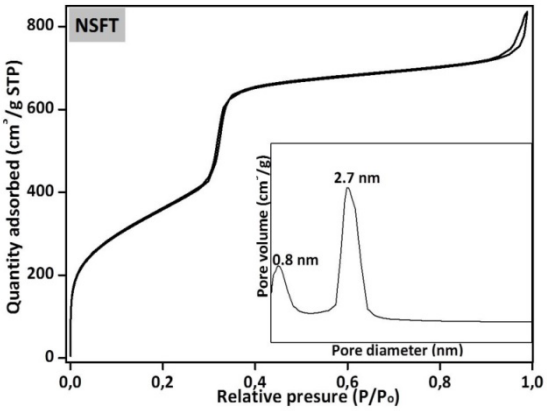

Figure IV.37 N_2 adsorption/desorption isotherms of NSFT sample. Inset: pore size distribution.

Scanning Electron Microscopy and Energy Dispersive X–ray Spectroscopy

Morphology of particles in sample is revealed by SEM micrographs in Figure IV.38. SEM image indicates that NSFT sample is formed by monodisperse spherical nanoparticles with 235 nm in average diameter. THSMP presence was confirmed by EDS analysis where a peak for phosphorous is observed.

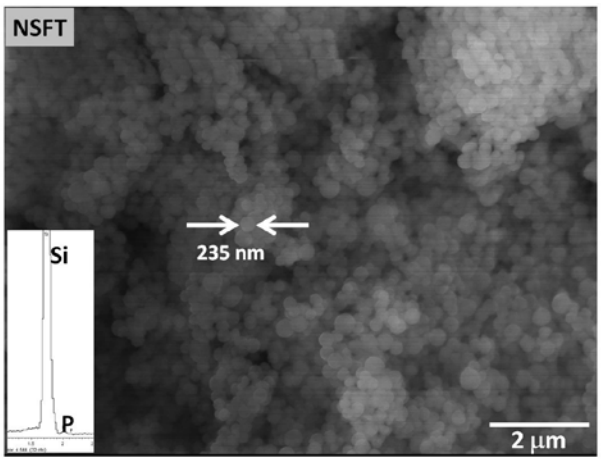

Figure IV.38 Nanospheres were observed by SEM image in NSFT sample.

Transmission Electron Microscopy

Figure IV.39 shows the TEM micrographs of NSFT. The nanospheres, homogeneous in size, with an average diameter of 200 nm, exhibit a highly ordered hexagonal mesoporous structure. Therefore, functionalization with THSMP by co-condensation in the TEOS/THSMP molar ratio used of 1:0.3 did not affect the mesoporous structure of MSNSs. The presence of THSMP phosphate–like groups was again confirmed by EDS with phosphorous and silicon values of 2 and 97 atomic %, respectively, dismissing the content in carbon and oxygen (see inset, Figure IV.39).

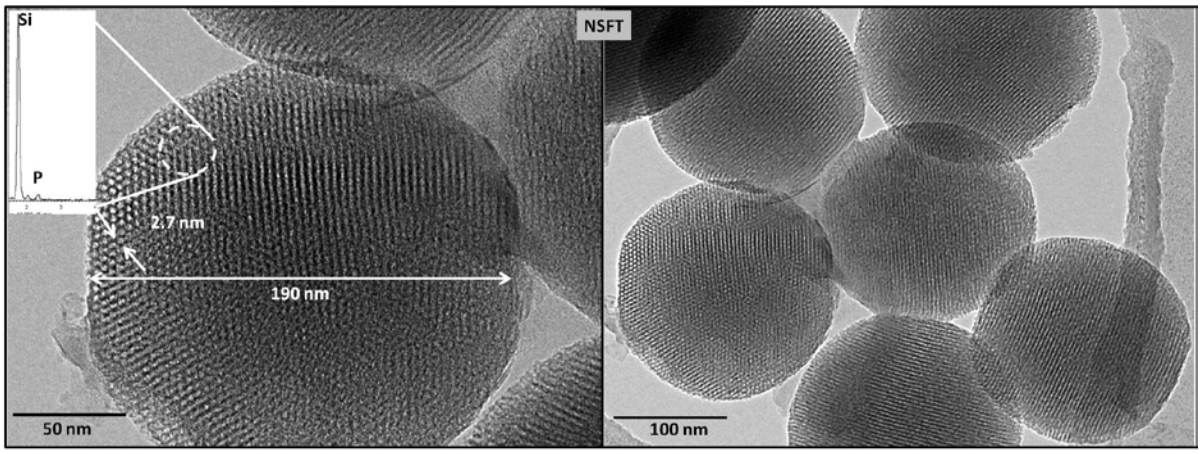

Figure IV.39 TEM images of MSNSs functionalized with THSMP via co-condensation method.

Conclusion of Section IV.6.3: Functionalization of mesoporous silica nanospheres with 3–trihydroxysilylpropyl methylphosphonate by co–condensation

Hexagonally ordered MSNSs were functionalized using phosphate-like groups of THSMP by co-condensation (molar ratios of reactants: TEOS/THSMP = 1/0.3). According to N_2 adsorption analysis, the synthesized sample shows a typical mesoporous isotherm with 1316 m^2/g of BET surface area and pore diameter of 2.7 nm. The diameters of nanospheres are quite homogeneous around 200 nm as observed by TEM. TEM micrographs also show the 2D hexagonal order. The presence of THSMP in the nanospheres was confirmed by EDS and FTIR studies. The MSNSs have been functionalized with phosphate–like groups to facilitate the interaction with Ca^{2+} ions to obtain HA NPs on the MSNSs external surface, which was attempted in the next section.

IV.6.4 Wetting of THSMP functionalized mesoporous silica nanospheres with a sol precursor of CaP, NSFT–HA sample

Fourier Transform Infrared Spectroscopy

The FTIR spectrum of sample NSFT–HA is shown in Figure IV.40. In this case the FTIR spectrum is compatible with silica as well as a calcium phosphate phase possessing PO_4^{3-} in crystalline environment. Presence of carbonate groups is also identified in the spectrum.

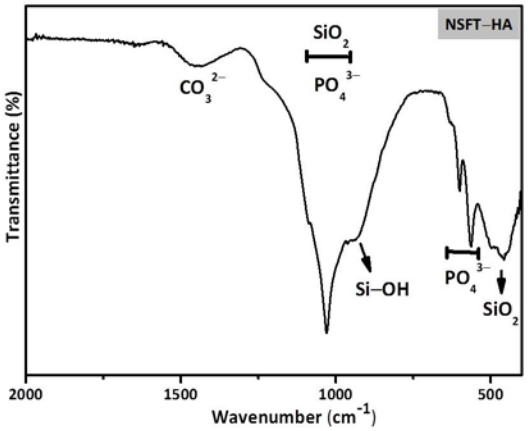

Figure IV.40 FTIR spectra of NSFT–HA sample.

X–ray Diffraction

SA–XRD and WA–XRD patterns of NSFT–HA sample are shown in Figure IV.41. Mesostructure was not observed in SA–XRD analysis.

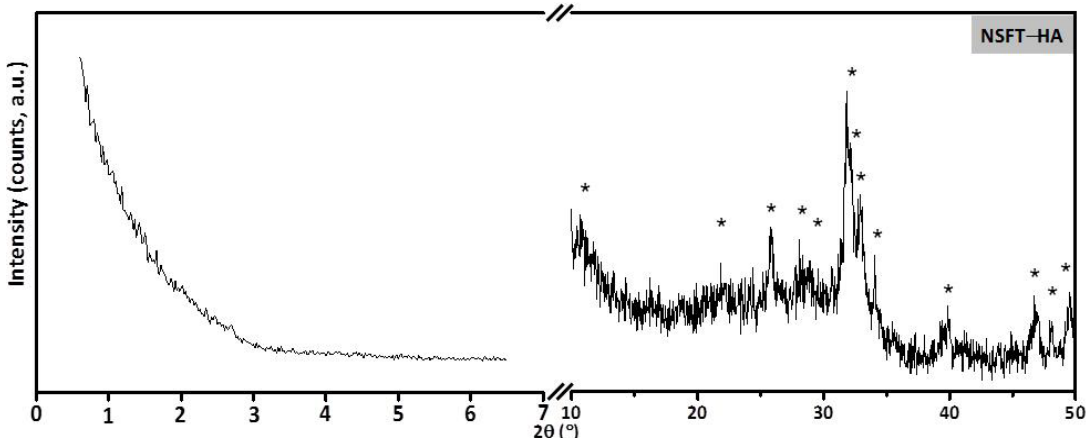

Figure IV.41 SA/WA–XRD analysis of HA coating of MSNSs functionalized with THSMP, where * indicates hydroxyapatite.

According to WA–XRD, a nanocrystallized HA phase was observed in NSFT–HA sample. The diffraction maxima can be assigned to the (100), (101), (002), (102), (210), (211), (112), (300), (202), (310), (322), (312) and (213) reflections of an HA–like phase.

N_2 Adsorption–Desorption Isotherms

Figure IV.42 shows N_2 adsorption-desorption isotherms of NSFT–HA. NSFT–HA sample exhibits a non-porous behaviour, with a surface area of 30 m^2/g, as a great decrease of N_2 adsorption capacity. The

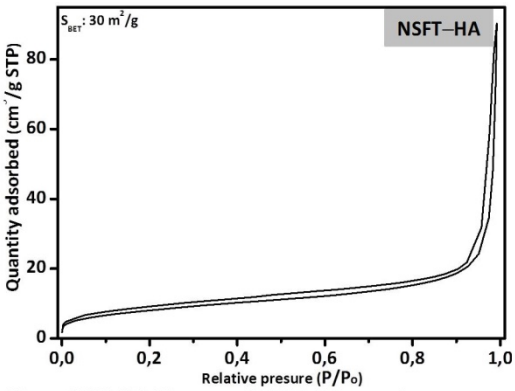

Figure IV.42 TEM images of NSFT–HA sample.

decrease in surface area compared to the uncoated sample was around 97 %. This fact could be indicating a pore blocking due to the HA coating of the MSNSs in the external surface.

Transmission Electron Microscopy – Energy Dispersive X–ray Spectroscopy

TEM micrographs of the functionalized MSNSs (NSFT) and the functionalized MSNS subjected to soaking and wetting treatment by the precursor sol of CaP (NSFT-HA) are shown in Figure IV.43.

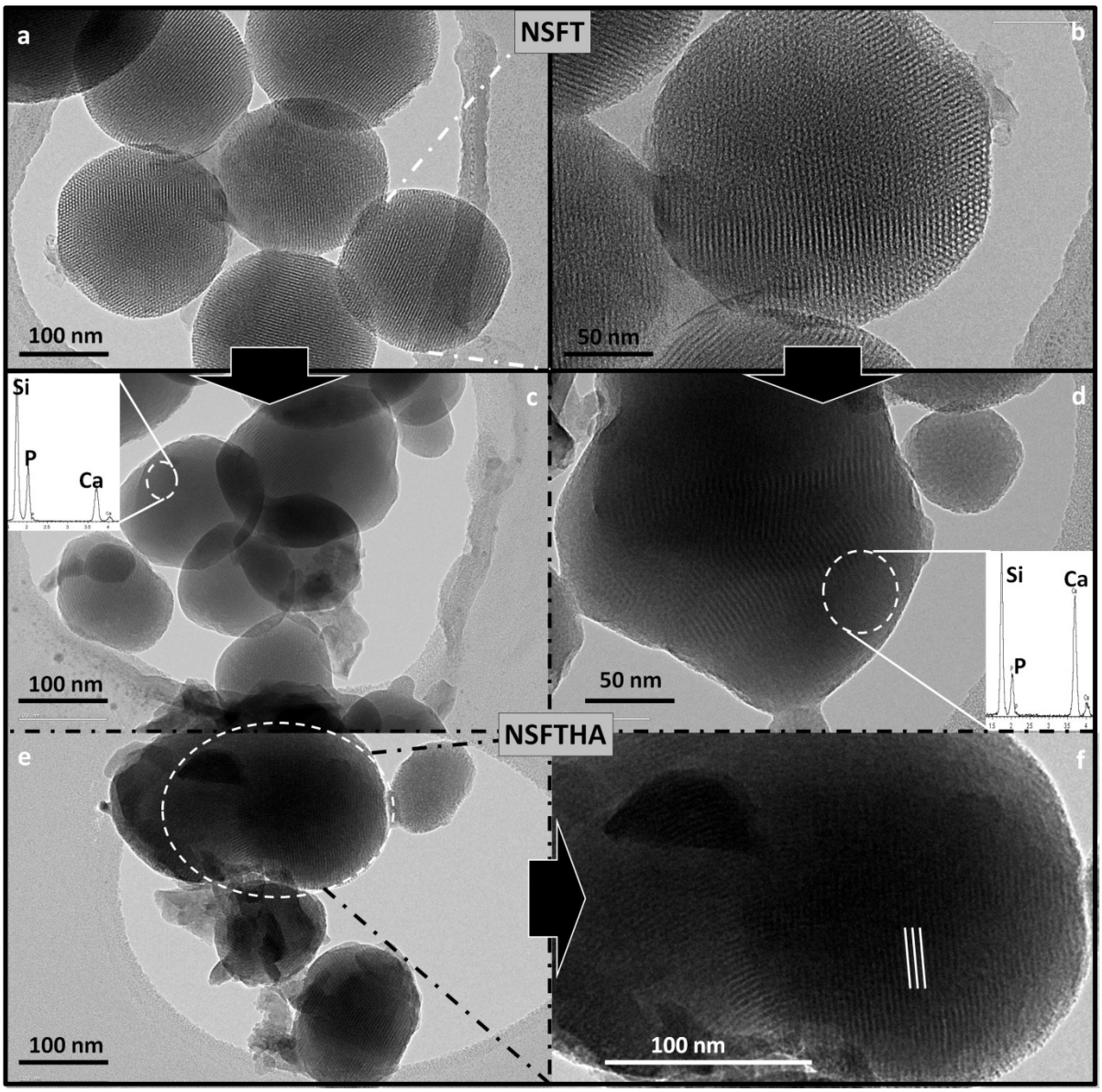

Figure IV.43 TEM–EDS of the functionalized NSFT sample (a, b) and the NSFT–HA sample (c, d, e, f).

TEM images of NSFT, just described in the previous section, show nanospheres monodisperse in size were the 2D hexagonal arrangement of mesopores is clearly observed (Figures IV.43.a and b). Nanoparticles more irregular in size were observed for NSFT–HA sample, which could be explained considering that the soaking process may deform the nanospheres, as it was discussed for sample MSNS-HA-2 (Figure IV.43.c and d). The nanoparticles seem to be covered by a new layer, although the presence of the channels is still perceptible underneath this layer (Figure IV.43.d. and f).

The presence of a CaP phase in NSFT–HA sample was confirmed by EDS analysis. The measured contents (atomic %) of Ca, P and Si were 14, 29 and 57 for Figure IV.43.c, and 35, 15 and 50 for Figure IV.43.d, respectively.

Conclusion of Section IV.6.4: Hydroxyapatite coating of mesoporous silica nanospheres functionalized with 3–trihydroxysilylpropyl methylphosphonate by co–condensation

MSNSs have been functionalized with phosphate–like groups of THSMP by a co-condensation method, and then coated with an HA layer by soaking and wetting them in a precursor sol for CaP, as explained in the scheme of Figure IV.44. As observed by TEM images with this approach core@shell structure of MSNS@HA has been successfully obtained. The nanoparticles were observed with a non-porous surface area, as confirmed by N_2 adsorption measurements. The presence of HA would improve the bioactivity and biocompatibility properties of the mesoporous silica nanospheres.

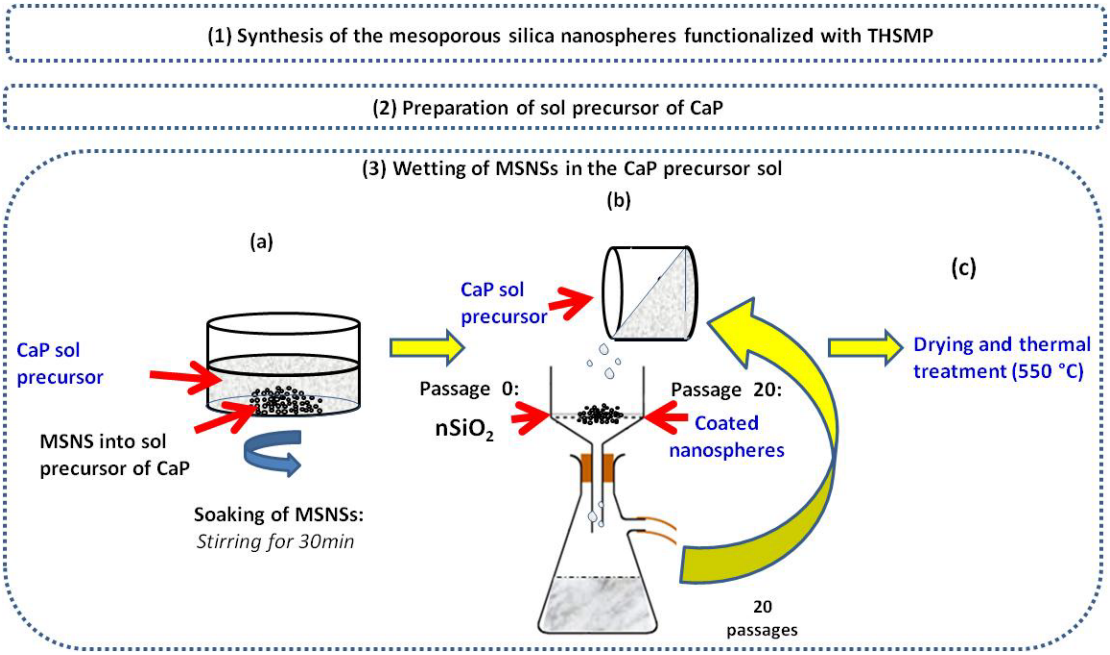

Figure IV.44 Schematic depiction of the overall process and detailed steps of wetting of the MSNS in the sol to obtain NSFT–HA.

IV.7 Summary and conclusions of Chapter IV

The present study tried to coat MCM–41 type MSNS with HA NPs or HA layer which would greatly improve their bioactivity and biocompatibility. Mesoporous silica nanospheres with 2D hexagonal MCM–41 structure of were attempted to be used as nano-ordered structure core to obtain HA coatings as shell onto the external surface of the MSNSs. According to this goal, the conclusions derived from each synthetic route are as follows:

- *MSNSs* were synthesized as silica nanospheres exhibiting 2D hexagonal MCM-41 type mesoporous order and high surface area (S_{BET} = 1230 m^2/g).

- **Co-synthesis of CaP and MSNSs, *MSNS–HA–1* sample.** The precipitation of CaP method was used simultaneously to the synthesis of MSNSs by sol-gel chemistry. Poorly crystallized HA rods and silica nanospheres polydisperse in size were separately observed as a mixture of independent particles (S_{BET} 594 m^2/g). Thus, with this approach our objective was not reached because no interactions between CaP and silicate ions took place.

- **Soaking of MSNSs into a sol precursor of CaP, *MSNS–HA–2* sample.** In this case the soaking time into the sol affected the shape, composition and mesoporosity of the original MSNSs. Pure SiO_2 mesoporous nanospheres become ellipsoids with a Si, Ca and P composition and a radial mesoporosity around 80% lower. The obtained material revealed a slow bioactive response in SBF.

- **Wetting of MSNSs by a sol precursor of CaP, *MSNS–HA–3* sample.** MSNS coated with HA NPs were successfully obtained when the soaking time into the sol is minimized to 30 min and subsequently the nanoparticles are subjected to a wetting process trying to mimic a dip-coating process. With this wetting process the MSNSs are not altered in shape neither in composition. TEM images confirm the formation of HA NPs covering the surface of MSNSs. The surface area reduction of sample is around 90 % (S_{BET} 136 m^2/g).

- **Functionalization of MSNSs with phosphate-like groups and subsequent wetting into a sol precursor of CaP.** Last section was designed to ascertain the functionalization of MSNS with phosphate-like groups such as DEPETES or THSMP. The functionalized MSNSs exhibited 2D hexagonal arrangement and highly porous materials were obtained with specific surface areas between 878 and 1316 m^2/g. The goal was to facilitate the interaction of phosphate-like groups of MSNSs with Ca^{2+} ions to obtain HA NPs. This would give a possible interaction between silica, Ca^{2+} and phosphate ions in order to obtain HA NPs or a HA layer coating the surface of the MSNSs. The following results were obtained:

    - MSNSs were successfully functionalized with DEPETES by co-condensation for NSFD1 and NSFD2 and by post-synthesis for NSFD samples.

    - The functionalized NSFD exhibiting a slightly higher P content was wetted by sol filtration. This method allows a fairly homogeneous distribution of an HA layer throughout the MSNSs, as well as some HA nanoparticles. Specific surface area is still 335 m^2/g, indicating that the surface is not totally covered.

    - MSNSs were functionalized with THSMP by co-condensation with a BET surface area of 1316 m^2/g, NSFT sample.

    - NSFT sample was wetted by sol filtration. The nanospheres were coated with a HA layer. As observed by TEM with this approach core@shell structure of MSNS@HA has been successfully obtained. The nanoparticles were observed with a non-porous surface area, as confirmed by N_2 adsorption measurements. Surface area decreased around 97 %, S_{BET} = 30 m^2/g.

Figure IV.45 depicts the method used in sections IV.6.1 and IV.6.3; the nanospheres are functionalized with phosphate–like groups and then subjected to a soaking and wetting procedures trying to be coated by HA NPs or HA layer.

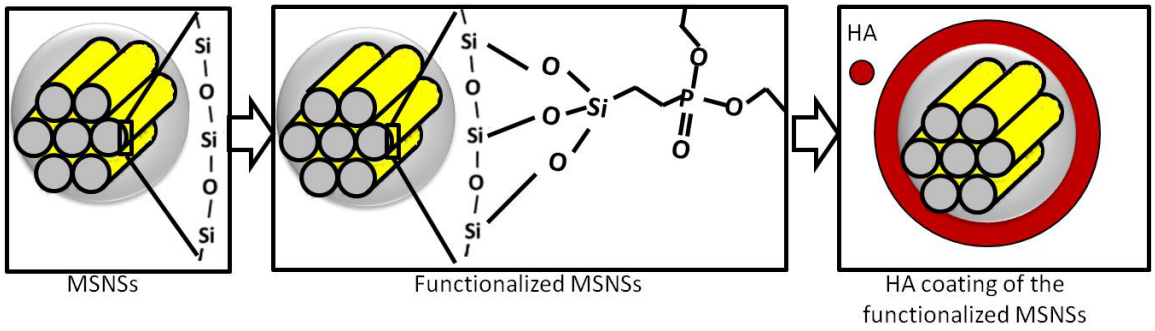

Figure IV.45 Schematic representation of the nanospheres prefunctionalized with phosphate–like groups and then coated with HA.

IV.8 References:

1. M. Vallet-Regí, E. Ruiz-Hernandez, B. González, A. Baeza. *J. Biomater. Tissue. Eng.* **2011**, *1*, 6-29. Design of smart nanomaterials for drug and gene delivery.

2. D. Arcos, A. López-Noriega, E. Ruiz-Hernandez, O. Terasaki, M. Vallet-Regí. *Chem. Mater.* **2009**, *21*, 1000. Ordered Mesoporous Microspheres for Bone Grafting and Drug Delivery.

3. M. Yu, S. Jambhrunkar, P. Thorn, J. Chen, W. Gu, C. Yu. *Nanoscale* **2013**, *5*, 178-183. Hyaluronic acid modified mesoporous silica nanoparticles for targeted drug delivery to CD44-overexpressing cancer cells.

4. C. He, S. W. Kim, D. S. Lee. *J. Controlled Release* **2008**, *127*, 189-207. In situ gelling stimuli-sensitive block copolymer hydrogels for drug delivery.

5. M. Vallet-Regí, F. Balas, D. Arcos. *Angew. Chem. Int. Ed.* **2007**, *46*, 7548-7558. Mesoporous materials for drug delivery.

6. E. J. Anglin, L. Cheng, W. R. Freeman, M. J. Sailor. *Adv. Drug Delivery Rev.* **2008**, *60*, 1266-1277. Porous silicon in drug delivery devices and materials.

7. M. Vallet-Regí. *J. Intern. Med.* **2010**, *267*, 22-43. Nanostructured mesoporous silica matrices in nanomedicine.

8. C. Wu, W. Fan, J. Chang. *J. Mater. Chem. B.* **2013**, *1*, 2710-2718. Functional mesoporous bioactive glass nanospheres: synthesis, high loading efficiency, controllable delivery of doxorubicin and inhibitory effect on bone cancer cells.

9. L. E. Vera-Avila, E. Garcia-Salgado, M. P. Garcia de Llasera, A. Pena-Alvarezi. *Anal. Biochem.* **2008**, *373*, 272-280. Binding characteristics of bovine serum albumin encapsulated in sol-gel glasses: An alternative for protein interaction studies.

10. D. Arcos, R. P. del Real, M. Vallet-Regí. *J. Biomed. Mater. Res.* **2003**, *65A*, 71-78. Biphasic materials for bone grafting and hyperthermia treatment of cancer.

11. S. Yue, P. D. Lee, G. Poologasundarampillai, J. R. Jones. *Acta Biomater.* **2011**, *7*, 2637-2643. Evaluation of 3-D bioactive glass scaffolds dissolution in a perfusion flow system with X-ray microtomography.

12. M. N. Rahaman, D. E. Day, B. S. Bal, Q. Fu, S. B. Jung, L. F. Bonewald, A. P. Tomsia. *Acta Biomater.* **2011**, *7*, 2355-2373. Bioactive glass in tissue engineering.

13. D. Arcos, M. Vallet-Regí. *Acta Mater.* **2013**, *61*, 890. Bioceramics for drug delivery.

14. A. Martinez, I. Izquierdo-Barba, M. Vallet-Regí. *Chem. Mater.* **2000**, *12*, 3080-3088. Bioactivity of a CaO-SiO_2 Binary Glasses System.

15. C. Wu, J. Chang, W. Fan. *J. Mater. Chem.* **2012**, *22*, 16801. Bioactive mesoporous calcium-silicate nanoparticles with excellent mineralization ability, osteostimulation, drug-delivery and anti bacterial properties for filling apex roots of theet.

16. J. Andersson, S. Areva, B. Spliethoff, M. Linden. *Biomaterials* **2005**, *26*, 6827-6835. Sol-gel synthesis of a multifunctional, hierarchically porous silica/apatite composite.

17. Y. G. Jin, S. Z. Qiao, Z. P. Xu, J. C. Diniz da Costa, G. Q. Lu. *J. Phys. Chem. C.* **2009**, *113*, 3157-3163. Porous Silica Nanospheres Functionalized with Phosphonic Acid as Intermediate-Temperature Proton Conductors.

18. S. Shruti, A. J. Salinas, G. Lusvardi, G. Malavasi, L. Menabue, M. Vallet-Regí. *Acta. Biomater.* **2013**, *9*, 4836-4844. Mesoporous bioactive scaffolds prepared with cerium-, gallium- and zinc-containing glasses.

19. M. Vallet-Regí, E. Ruiz-Hernandez. *Adv. Mater.* **2011**, *23*, 5177-5218. Bioceramics: From Bone Regeneration to Cancer Nanomedicine.

20. V. Mourino, A. R. Boccaccini. *J. R. Soc. Interface.* **2010**, *7*, 209-227. Bone tissue engineering therapeutics: controlled drug delivery in three-dimensional scaffolds.

21. M. Vallet-Regí. *Chem. - Eur. J.* **2006**, *12*, 5934-5943. Ordered mesoporous materials in the context of drug delivery systems and bone tissue engineering.

22. L. Cui, H. Lin, W. Guo, D. Xiang, D. Zhou, T. Zhang, F. Qu. *J. Sol-Gel Sci. Technol.* **2014**, *72*, 106-113. A novel pH-responsive controlled release system based on mesoporous silica coated with hydroxyapatite.

23. C-. X. Zhao, L. Yu, A. P. J. Middelberg. *J. Mater. Chem. B.* **2013**, *1*, 4828-4833. Magnetic mesoporous silica nanoparticles end-capped with hydroxyapatite for pH-responsive drug release.

24. H.- S. Yun, S.- E. Kim, Y.- T. Hyun. *Mater. Chem. Phys.* **2009**, *115*, 670-676. Preparation of bioactive glass ceramic beads with hierarchical pore structure using polymer self-assembly technique.

25. Y.- H. Liang, C.-H. Liu, S.-H. Liao, Y.-Y. Lin, H.-W. Tang, S.-Y. Liu, I. R. Lai, K. C. W. Wu. *ACS Appl. Mater. Interfaces* **2012**, *4*, 6720-6727. Cosynthesis of Cargo-Loaded Hydroxyapatite/Alginate Core-Shell Nanoparticles (HAP@Alg) as pH-Responsive Nanovehicles by a Pre-gel Method.

26. H.-C. Wu, T.- W. Wang, M. C. Bohn, F.-H. Lin, M. Spector. *Adv. Funct. Mater.* **2010**, *20*, 67-77. Novel Magnetic Hydroxyapatite Nanoparticles as Non-Viral Vectors for the Glial Cell Line-Derived Neurotrophic Factor Gene.

27. M. Kester, Y. Heakal, T. Fox, A. Sharma, G. P. Robertson, T. T. Morgan, E. I. Altinoglu, A. Tabakovic, M. R. Parette, S. Rouse, V. Ruiz-Velasco, J. H. Adair. *Nano. Lett.* **2008**, *8*, 4116-4121. Calcium Phosphate Nanocomposite Particles for In Vitro Imaging and Encapsulated Chemotherapeutic Drug Delivery to Cancer Cells.

28. M. Zhu, Y. Zhu, B. Ni, N. Xie, X. Lu, J. Shi, Y. Zeng, X. Guo. *ACS Appl. Mater. Interfaces* **2014**, *6*, 5456-5466. Mesoporous silica nanoparticles/hydroxyapatite composite coated implants to locally inhibit osteoclastic activity.

29. S. Zhang, Y. Wang, K. Wei, X. Liu, J. Chen, X. Wang. *Mater. Lett.* **2007**, *61*, 1341-1345. Template-assisted synthesis of lamellar mesostructured hydroxyapatites.

30. S. Sanchez-Salcedo, M. Vila, I. Izquierdo-Barba, M. Cicuendez, M. Vallet-Regí. *J. Mater. Chem.* **2010**, *20*, 6956-6961. Biopolymer-coated hydroxyapatite foams: a new antidote for heavy metal intoxication.

31. Y. G. Jin, S. Z. Qiao, Z. P. Xu, C. J. C. Diniz, G. Q. Lu. *J. Phys. Chem. C.* **2009**, *113*, 3157-3163. Porous silica nanospheres functionalized with phosphonic acid as Intermediate-temperature proton conductors.

32. G. Malavasi, L. Menabue, M. C. Menziani, A. Pedone, A. J. Salinas, M. Vallet-Regí. *J. Sol-Gel Sci. Technol.* **2013**, *67*, 208-219. New insights into the bioactivity of SiO_2-CaO and SiO_2-CaO-P_2O_5 sol-gel glasses by molecular dynamics simulations.

33. J. S. Beck, J. C. Vartuli, W. J. Roth, M. E. Leonowicz, C. T. Kresge, K. D. Schmitt, C. T. W. Chu, D. H. Olson, E. W. Sheppard. *J. Am. Chem. Soc.* **1992**, *114*, 10834-10843. A new family of mesoporous molecular sieves prepared with liquid crystal templates.

34. D. Zhao, Y. Wan, W. Zhou. *Wiley-Vch.* **2013**, *517*. Ordered mesoporous materials.

35. X.-Y-. Zhao, Y.-J. Zhu, B.-Q. Lu, F. Chen, C. Qi, J. Zhao, J. Wu. *Mater. Res. Bull.* **2014**, *55*, 67-70. Hydrothermal synthesis of hydroxyapatite nanorods using pyridoxal-5'-phosphate as a phosphorus source.

36. I. Grigoriadou, N. Nianias, A. Hoppe, Z. Terzopoulou, D. Bikiaris, J. Will, J. Hum, J. A. Roether, R. Detsch, A. R. Boccaccini. *Compos. Part B.* **2014**, *60*, 49-59. Evaluation of silica-nanotubes and strontium hydroxyapatite nanorods as appropriate nanoadditives for poly(butylene succinate) biodegradable polyester for biomedical applications.

37. G. Verma, K. C. Barick, N. Manoj, A. K. Sahu, P. A. Hassan. *Ceram. Int.* **2013**, *39*, 8995-9002. Rod-like micelle templated synthesis of porous hydroxyapatite.

38. T. Kokubo, H. Takadama. *Biomaterials* **2006**, *27*, 2907-2915. How useful is SBF in predicting in vivo bone bioactivity?

39. T. Kokubo. *J. Non-Cryst. Solids* **1990**, *120*, 138-151. Surface chemistry of bioactive glass ceramics.

40. A. Oyane, H.-M. Kim, T. Furuya, T. Kokubo, T. Miyazaki, T. Nakamura. *J. Biomed. Mater. Res.* **2003**, *65A*, 188-195. Preparation and assessment of revised simulated body fluids.

41. C. Wu, Y. Xiao. *Bone Tissue Regener. Insights* **2009**, *2*, 25-29. Evaluation of the in vitro bioactivity of bioceramics.

42. S. Padilla, J. Román, S. Sánchez-Salcedo, M. Vallet-Regí. *Acta. Biomater.* **2006**, *2*, 331-342. Hydroxyapatite/SiO_2-CaO-P_2O_5 glass materials: in vitro bioactivity and biocompatibility.

43. Y. Zhao, B. G. Trewyn, I. I. Slowing, V. S. Y. Lin. *J. Am. Chem. Soc.* **2009**, *131*, 8398-8400. Mesoporous silica nanoparticle-based double drug delivery system for glucose-responsive controlled release of insulin and cyclic AMP.

44. R. Singh, J. W. Lillard. *Exp. Mol. Pathol.* **2009**, *86*, 215-223. Nanoparticle-based targeted drug delivery.

45. Y. B. Patil, S. K. Swaminathan, T. Sadhukha, L. Ma, J. Panyam. *Biomaterials* **2009**, *31*, 358-365. The use of nanoparticle-mediated targeted gene silencing and drug delivery to overcome tumor drug resistance.

46. T. Xia, M. Kovochich, M. Liong, H. Meng, S. Kabehie, S. George, J. I. Zink, A. E. Nel. *ACS Nano.* **2009**, *3*, 3273-3286. Polyethyleneimine coating enhances the cellular uptake of mesoporous silica nanoparticles and allows safe delivery of siRNA and DNA constructs.

47. V. Cauda, A. Schlossbauer, J. Kecht, A. Zurner, T. Bein. *J. Am. Chem. Soc.* **2009**, *131*, 11361-11370. Multiple core-shell functionalized colloidal mesoporous silica nanoparticles.

48. S. Shylesh, A. Wagner, A. Seifert, S. Ernst, W. R. Thiel. *Chem. - Eur. J.* **2009**, *15*, 7052-7062. Cooperative acid-base effects with functionalized mesoporous silica nanoparticles: Applications in carbon-carbon bond-formation reactions.

49. Y.-F. Han, F. Chen, Z. Zhong, K. Ramesh, L. Chen, E. Widjaja. *J. Phys. Chem. B.* **2006**, *110*, 24450-24456. Controlled synthesis, characterization, and catalytic properties of Mn_2O_3 and Mn_3O_4 nanoparticles supported on mesoporous silica SBA-15.

50. J. Lu, M. Liong, Z. Li, J. I. Zink, F. Tamanoi. *Small* **2010**, *6*, 1794-1805. Biocompatibility, biodistribution, and drug-delivery efficiency of mesoporous silica nanoparticles for cancer therapy in animals.

51. J. Kobler, K. Moeller, T. Bein. *ACS Nano.* **2008**, *2*, 791-799. Colloidal suspensions of functionalized mesoporous silica nanoparticles.

52. M. Vallet-Regí, M. Vila. *Key Eng. Mat.* **2010**, 392. Advanced bioceramics in nanomedicine and tissue engineering.

53. J. Lu, E. Choi, F. Tamanoi, J. I. Zink. *Small* **2008**, *4*, 421-426. Light-activated nanoimpeller-controlled drug release in cancer cells.

54. R. Mortera, J. Vivero-Escoto, I. I. Slowing, E. Garrone, B. Onida, V. S. Y.-Lin. *Chem. Commun.* **2009**, 3219-3221. Cell-induced intracellular controlled release of membrane impermeable cysteine from a mesoporous silica nanoparticle-based drug delivery system.

55. J. Wang, H. Liu, F. Leng, L. Zheng, J. Yang, W. Wang, C. Z. Huang. *Micropor. Mesopor. Mater.* **2014**, *186*, 187-193. Autofluorescent and pH-responsive mesoporous silica for cancer-targeted and controlled drug release.

56. A. L. Doadrio, J. M. Sanchez-Montero, J. C. Doadrio, A. J. Salinas, M. Vallet-Regi. *Micropor. Mesopor. Mater.* **2014**, *195*, 43-49. A molecular model to explain the controlled release from SBA-15 functionalized with APTES.

57. S. Mohapatra, S. R. Rout, R. Narayan, T. K. Maiti. *Dalton Trans.* **2014**, *43*, 15841-15850. Multifunctional mesoporous hollow silica nanocapsules for targeted co-delivery of cisplatin-pemetrexed and MR imaging.

58. I. V. Melnyk, V. P. Goncharyk, L. I. Kozhara, G. R. Yurchenko, A. K. Matkovsky, Y. L. Zub, B. Alonso. *Micropor. Mesopor. Mater.* **2012**, *153*, 171-177. Sorption properties of porous spray-dried microspheres functionalized by phosphonic acid groups.

59. O. A. Dudarko, Y. L. Zub, M. Barczak, A. Dabrowski. *Glass Phys. Chem.* **2011**, *37*, 596-602. Template synthesis of mesoporous silicas containing phosphonic groups.

60. Y-. C. Pan, H.- H. G. Tsai, J.- C. Jiang, C.- C. Kao, T.- L. Sung, P.- J. Chiu, D. Saikia, J.- H. Chang, H.- M. Kao. *J. Phys. Chem. C.* **2012**, *116*, 1658-1669. Probing the nature and local structure of phosphonic acid groups functionalized in mesoporous silica SBA-15.

61. K. S. W. Sing. *Adv. Colloid Interface Sci.* **1998**, *76-77*, 3-11. Adsorption methods for the characterization of porous materials.

62. S. Brunauer, L. S. Deming, W. E. Deming, E. Teller. *J. Am. Chem. Soc.* **1940**, *62*, 1723-1732. A theory of the van der Waals adsorption of gases.

V. COATING OF MESOPOROUS SILICA NANOSPHERES WITH FLUORESCENT HYDROXYAPATITE NANOPARTICLES

V.1 Introduction

Materials based on hydroxyapatite (HA) exhibit good biocompatibility and osteoconductivity [1, 2]. Thus, they are widely used in Orthopaedics and Dentistry [3]. HA structure can accept numerous ionic substitutions including lanthanide ions. Therefore, in recent years several strategies have been developed to produce luminescent HA nanoparticles (NPs) doped with Eu^{3+}, Eu^{2+}, Ce^{3+}, Eu^{3+}/Y^{3+} or Pb^{2+} ions [4-7], that could be used as luminescent labels or luminescent drug carriers [8]. Moreover, small amounts of a doping ion (0.5–2 mol %) induce luminescence in HA–based materials [4]. The emitted wavelength (colour) can be modified by selecting a specific dopant or a combination of dopants. In general, the luminescence intensity of a material is dependent on the concentration of the doping ions, the crystal structure and the degree of crystallinity of the host material. In this study nanocrystalline HA is the host material and Eu^{3+} and Y^{3+} the doping ions.

On the other hand, as it was explained in Chapters I.3 and IV, silica mesoporous matrices are potential drug carriers because of their textural features including: *(i)* ordered pore network, homogeneous in size (pore diameter, Dp ≈ 2-10 nm); *(ii)* high pore volume; *(iii)* high surface area; and *(iv)* silanol (Si–OH) rich surface. The functionalization of Si–OH groups allows tailoring at demand the drug loading and release. These unique features make mesoporous materials excellent candidates for controlled drug-delivery systems (DDSs), and intensive research was carried out in this topic in the last decade [9-14].

As a continuation of the research developed in Chapter IV, the aim in this chapter is the coating of MCM–41 mesoporous silica nanospheres (MSNSs) by europium–doped HA NPs, to develop new biocompatible luminescent HA/MSNSs based materials. If successful results are achieved, MSNSs coated by europium-doped HA NPs would be promising biomaterials with fluorescent properties that after optimization could be highly appropriate for biomedical applications [7, 15, 16]. Such applications include: luminescent labels, luminescent drug carriers, biological probes, biological labelling and red fluorescent probes that follow an excitation in the visible domain [17-19].

V.2 Materials synthesis

Experimental conditions to obtain the MSNSs coated with europium–doped HA NPs were inspired in those used to obtain lanthanide–doped HA and silica materials reported by *S. Dembski* [7, 20]. First, HA was precipitated in the presence of Eu^{3+} ions in a suspension of previously prepared MSNSs. The final step was completed by addition of Poly(ethyleneimine), PEI, (M_w=750.000 g/mol), that is used to stabilize the particles [7]. Citric acid was used in the preparation of one of the samples as chelating ligand of metal ions [20]. This chapter was developed during a short research stay and therefore, the syntheses were carried out at the Institute of Inorganic Chemistry of the University of Duisburg Essen. Synthesized lanthanide (Eu^{+3})–doped HA/MSNSs composites were shortly named as LDHASix where x indicates the number of synthesized sample. Four samples were synthesised by using the synthesis conditions detailed in Table VII.3 of the Chapter VII and briefly described in Table V.1.

Table V.1 Calcium, monohydrogen phosphate and europium ion concentrations used to coat 0.25 g of MSNPs.

Samples	MSNPs (g)	Ca^{2+} (mM)	HPO_4^{2-} (mM)	Eu^{3+} (mM)
LDHASi1	0.25	19.7	11.94	0.2
LDHASi2	0.25	2462.5	1492.5	25
LDHASi3	0.25	0.1905	0.116	0.00075
LDHASi4	0.25	2437.5	1458.8	50

As far as possible, all synthesized samples of FHA (Fluorescent HA)/MSNSs composites were characterized during the period of stay at the mentioned German institution. Therefore, the most representative samples were analysed with the results presented below. These analysed FHA/MSNSs samples are compared with MSNSs used as reference.

Fourier Transform Infrared Spectroscopy

The FTIR spectra of the four samples investigated and that of reference MSNSs are shown in Figure V.1. A typical spectrum of mesoporous silica was obtained for MSNSs. For FHA/MSNSs samples, the spectra were analogous to those of apatite–like phases. Thus, the FTIR spectra of FHA/MSNSs samples exhibit the following bands of the characteristic functional groups:

- SiO_2:

  At 1054 cm^{-1} for νas(SiO) symmetric stretching mode, at 968 cm^{-1} for υ(SiO) stretching mode of Si-OH groups, at 805 cm^{-1} for νs(SiO) and at 440 cm^{-1} for δ(SiOSi) bending mode.

- PO_4^{3-}:

  At 1024 for ν_{as}(PO) stretching mode; 605 and 553 cm^{-1} for δ(OPO) bending mode.

- CO_3^{2-}:

  In the 1450-1400 cm^{-1} interval for ν(CO).

The HA presence in synthesized samples of FHA/MSNSs can be confirmed by the observed FTIR bands of phosphate in LDHASi2 and LDHASi4. In addition, these samples present in their FTIR spectra normal vibration bands of carbonate groups, suggesting that the apatite phase is hydroxycarbonate apatite (HCA).

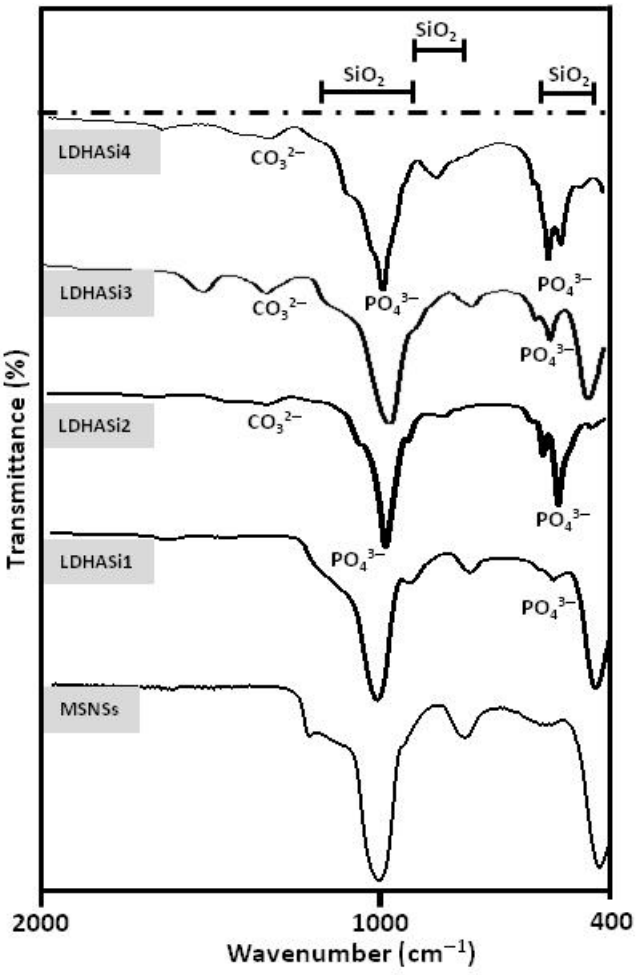

Figure V.1 FTIR spectra of FHA/MSNSs samples

The coexistence of the adsorption bands coming from phosphate and silica can be observed in the spectra of LDHASi1 and LDHASi3. That way, LDHASi1 spectrum is very similar to that of the reference, although bands that can be assigned to PO_4^{3-} bending modes are also present. In LDHASi3 the situation is analogous but with an increase in the intensity of the phosphate bands. Finally, in the FTIR spectrum of LDHASi4 certain anomalies in the shape of the bands suggest that another calcium phosphate phase such as brushite could co−precipitate with the HA phase that, in any case, would be the majority calcium phosphate phase.

Small and wide angle X − ray Diffraction

Figure V.2 shows the small and wide angle XRD patterns of pure MCM−41 silica nanospheres, used as reference, and also the patterns of the FHA/MSNSs composites synthesised in this chapter.

The MSNSs XRD pattern, registered in the small angle region, shows three diffraction maxima at 2θ = 2.3 °, 4.07 ° and 4.7 °, which can be respectively indexed to the (10), (11) and (20) reflections of a 2D hexagonal arrangement with MCM−41 structure [21]. However, the diffractogram of LDHASi2 shows only a low intensity maximum at 2θ = 2.3 ° that can be assigned to the (10) reflection of the hexagonal phase. This could indicate that after the process to coat the silica nanospheres with Eu^{3+}−doped HA NPs, only the highest intensity maximum remained visible. For LDHASi3 and LDHASi4, no diffraction maxima were observed, indicative of the absence of hexagonal order.

The MSNSs XRD pattern, registered in the wide angle region, shows only a diffuse maximum centred at 25 ^{o} characteristic of amorphous silica. A low crystalline HA phase was observed in the diffractogram of LDHASi1. The diffraction maxima can be assigned to the (100), (101), (111), (002), (210), (211), (202), (310), (222) and (213) reflections of HA (ICDD Powder Diffraction File No. 9-432). However in LDHASi2, two weak reflections were observed at 2θ = 26.0 ^{o} and 31.7 ^{o} which could be indexed to the (002) and (211) reflections of an apatite−like phase [22]. For LDHASi3 and LDHASi4, very low crystalline HA was observed because the diffraction maxima of HA are wider and a lower number of reflections, assigned to (002), (211), (310) and (222), were now observed. Therefore, in terms of increasing HA crystallinity, the four samples would be classified as follows: LDHASi2, LDHASi3, LDHASi4, and LDHASi1.

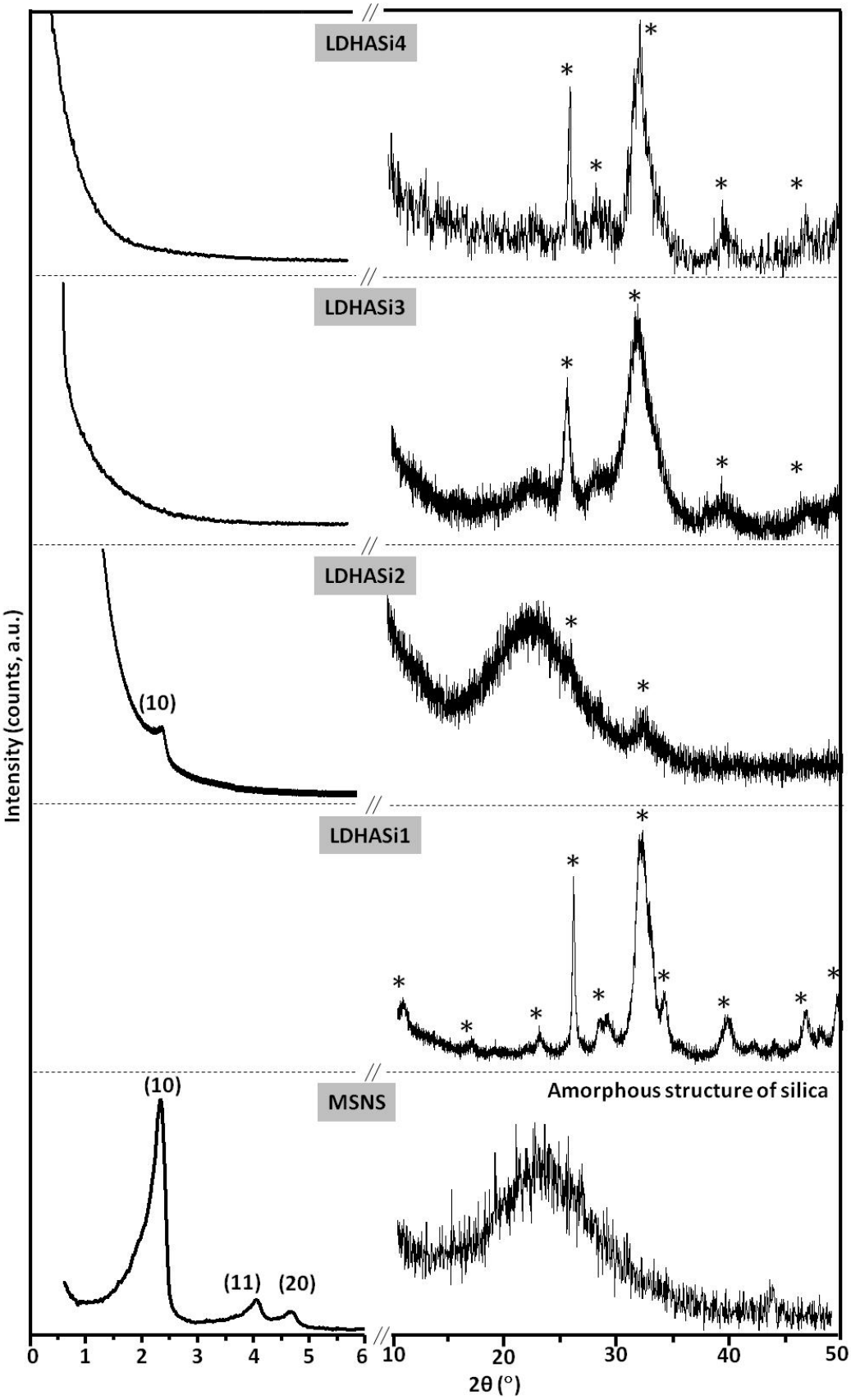

Figure V.2 Small and wide angle XRD patterns of reference (MSNSs with MCM-41 structure) and the synthesized materials, where * indicates HA.

Scanning Electron Microscopy, Energy Dispersive X–ray Spectroscopy and Elemental Analysis

The surface morphology of MSNSs before and after coating with europium–doped HA was studied by SEM (Figure V.3). Micrograph of the uncoated material shows the typical pseudo–spherical shape of mesoporous MCM–41 NPs obtained via sol-gel in the presence of structure directing agents and using the Stöber modified method. However, the morphology of samples containing FHA NPs is completely different. For LDHASi1, two morphologies of HA NPs and nanospherical MSNSs with average diameter of 170 nm were observed, and the presence of calcium, phosphorous and silicon in LDHASi1 (left) was confirmed by EDS with 46.3, 37.2 and 16.5 %, respectively. According to EDS analysis, we found major proportion of silicon in LDHASi1. The Ca/P ratio was calculated as 1.24 which could corresponds to a calcium-deficient HA (CDHA) phase together with amorphous CaP.

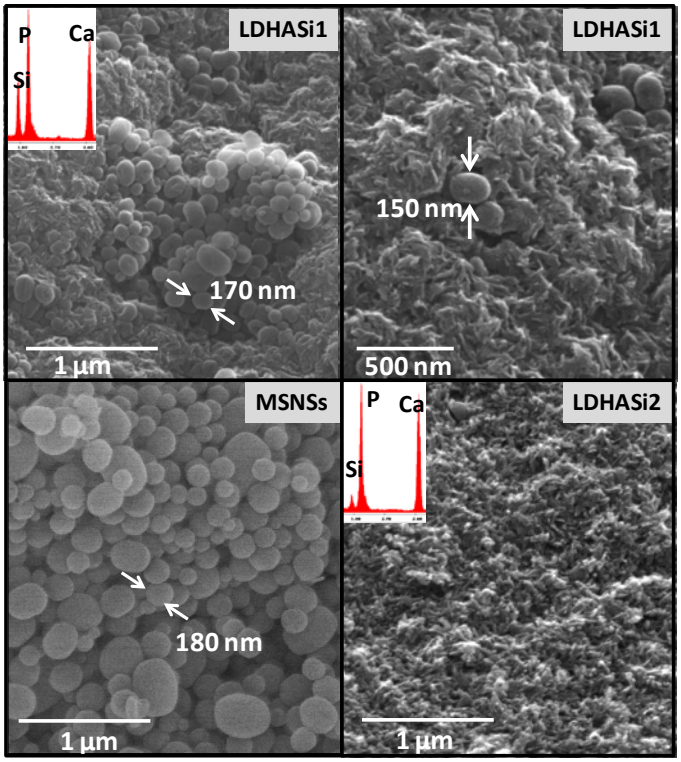

Figure V.3 Surface morphology of samples MSNSs, LDHASi1 and LDHASi2 observed by SEM.

As a difference from the other samples, the surface morphology of LDHASi2 shows homogeneous rod–like HA nanoparticles with around 60 nm in length and 15 nm in width. No visible nanospheres of silica in LDHASi2 were observed by SEM. Moreover the presence of calcium, phosphorous and silicon was confirmed by EDS analysis with 55.9, 40.7 and 3.5 %, respectively. Accordingly to this, LDHASi2 includes a low content of silicon. The Ca/P ratio was 1.36 which corresponds to a CDHA phase.

The content in PEI, ($H(NHCH_2CH_2)_nNH_2$), in the samples was measured from the nitrogen present in its amino groups, by using CHN elemental analysis as shown Table V.2. This Table also contains the calcium, phosphorous and silicon percentages in the samples measured by EDS analysis in the SEM microscope.

Table V.2 Ca, P and Si contents obtained by SEM–EDS (at-%) and N content (wt-%) by CHN analysis.

Element	LDHASi1	LDHASi2	Method
Ca	46.3	55.9	SEM-EDS (At-%)
P	37.2	40.7	
Si	16.5	3.5	
N	1.1	2.4	CHN Elemental Analysis (wt %)

In the synthesis of LDHASi1 sample the relative proportion of silica NPs respect to Ca^{2+} and HPO_4^{2-} ions was very high, and consequently the silicon content is high. And, as it was expected, LDHASi2 contains higher amounts of Ca and P because in this case the proportion of these elements was very high compared with the amount of silica NPs added during the synthesis.

Transmission Electron Microscopy

In Figure V.4 TEM micrographs of MSNSs, LDHASi1 and LDHASi2 are shown. Hexagonally meso–structured MSNSs were shown as reference for comparison. In the micrograph of sample LDHASi1 it can be visualized that MSNSs were completely coated by fluorescent HA. Therefore, a stronger interaction between europium-doped HA NPs and MCM-41 nanospheres can be inferred. TEM image of LDHASi2 sample shows that the nanospheres have not been coated by nanocrystalline HA, in other words, ellipse-shaped MSNSs and europium–doped HA phase are not interacting with each other. In any case HA nanocrystals are homogeneous in size and forming groups into similar shapes.

In this Chapter and Chapter IV.4, similar materials were obtained by different synthetic methods, and similar results were observed. However, in this study, the difference is the synthesis of CaP in the presence of europium ions. In both chapters, MSNSs coated HA NPs were observed, and the morphology of the obtained HA phase was compared with that reported by Linden *et al* [23]. Separated nanospheres and HA phase were observed in some of the samples according to TEM images. In any case (before or after the coating process), some nanospheres were ellipsoid shaped due to the synthesis conditions.

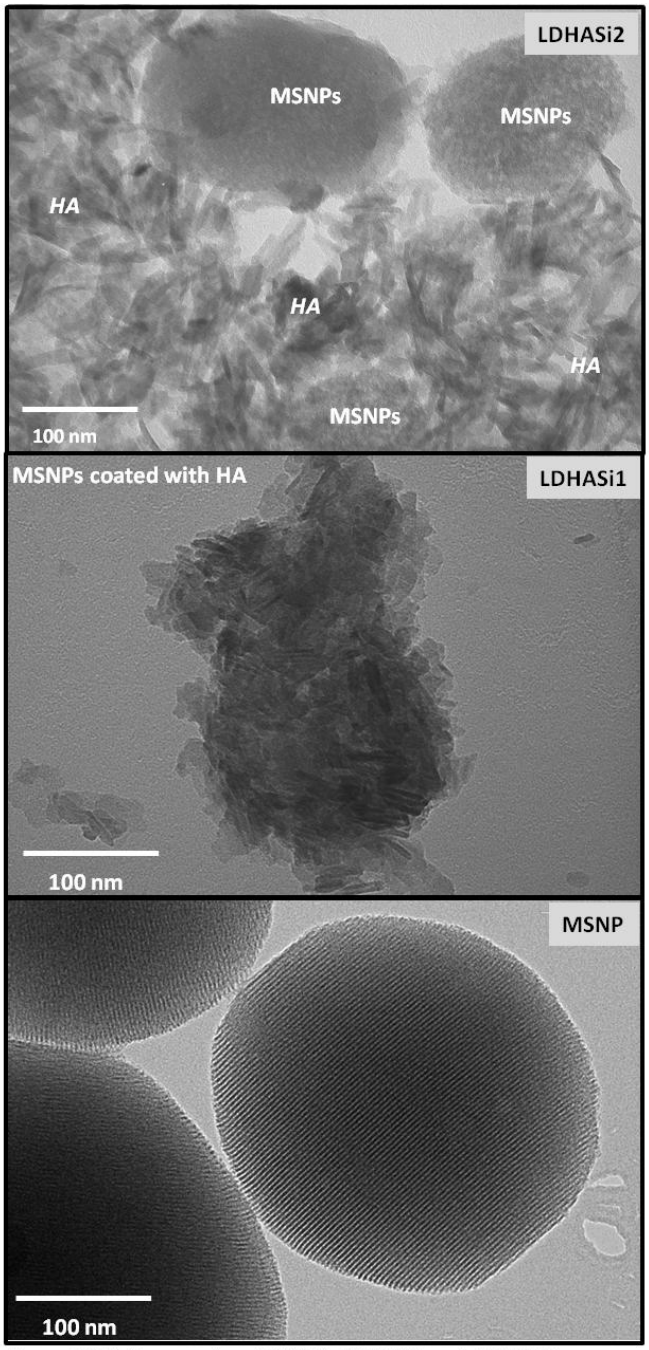

Figure V.4 Micrographs of MSNP, LDHASi1 and LDHASi2 observed by TEM.

Ultraviolet Spectroscopy

The luminescent properties of samples were analysed by UV–light absorption at λ = 254 nm [20]. According to the low Eu^{3+} contents showed in Table V.1, LDHASi1 and LDHASi3 did not show fluorescent emission when exposed to the ultraviolet light source, and this fact could be explained in one case due to the low concentration of europium ions when a solution of europium−doped CaP (≤ 0.2 mM) was prepared. In LDHASi2 and LDHASi4, the luminescent characteristic (red−light emission) was observed because the concentration of prepared solution of europium−doped CaP was 25 and 50 mM, respectively.

V.3 Conclusions of Chapter V

A new method for coating silica materials with europium-doped HA was proposed. The luminescent FHA/MSNSs composites were synthesized including different amounts of Eu^{3+} ions via a modified precipitation method for HA. Some FHA/MSNSs composites exhibited red luminescence of lanthanides under UV light; luminous intensity was dependent on the amount of Europium ion. Furthermore, biocompatible and bioactive properties should be expected for these nanocomposites due to their HA coating. The fluorescent characteristics and XRD results of the synthesized samples are summarized in Table V.3.

Table V.3 Fluorescent characteristics and XRD results of samples.

Samples	Fluorescence	Crystalline phase (XRD)
LDHASi1	Colourless	Crystalline HA
LDHASi2	Red-light	Apatite–like phase
LDHASi3	Colourless	Low crystalline HA
LDHASi4	Red-light	Low crystalline HA

The synthesis procedure of MSNSs coated with fluorescent doped HA is schematically depicted in Figure V.5. Four samples of MSNSs and europium-doped HA composites were synthesised by modified precipitation, and the observed results were compared with pure MSNSs (MCM–41 type) used as reference. According to Figure V.5, the MSNSs were coated by precipitation with fluorescent HA (red−light emission). Then the MSNSs were stabilized with PEI (shown by drawing). LDHASi2 and LDHASi3 were synthesized as FHA/MSNSs composites. Moreover, the presence of moderately crystalline HA was confirmed by WA-XRD.

In summary, MSNSs of MCM-41 type has been used as intended core during the precipitation of Europium−doped HA as shell component. HA crystallinity in the samples increased in the following sequence: LDHASi2, LDHASi3, LDHASi4 and LDHASi1. FHA/MSNSs (red-light emission) composites have been confirmed by UV light in LDHASi2 and LDHASi4. According to these results, Europium−doped HA/MSNSs composites were successfully synthesized reaching the main objective of this Chapter. The structure as core@shell (MSNS@HA) was observed in sample LDHASi1 by TEM. However, it did not show fluorescent emission due to lower proportion of Eu^{3+} in its synthesis.

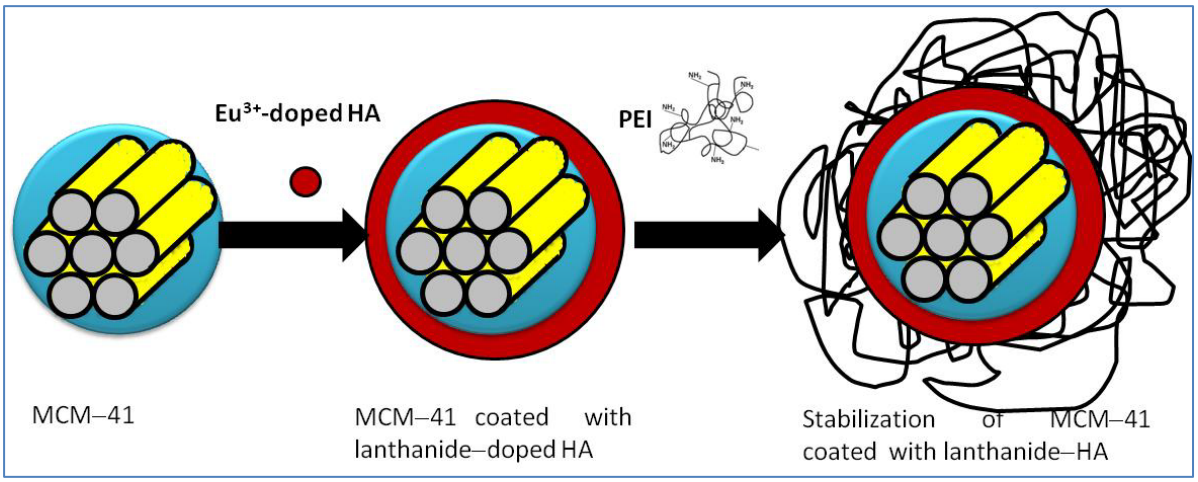

Figure V.5 Proposed mechanisms for the coating of MSNSs with FHA and subsequent stabilization with a polycationic polymer such as PEI.

V.4 References:

1. H. A. Lowenstam, S. Weiner. *Oxford University Press: New York* **1989**. On Biomineralization.
2. S. Mann. *Chem. Unserer Zeit* **1986**, *20*, 69-76. Biomineralization: A new branch of bioinorganic chemistry.
3. S. V. Dorozhkin, M. Epple. *Angew. Chem. Int. Edit.* **2002**, *41*, 3130-3146. Biological and medical significance of calcium phosphates.
4. A. Doat, F. Pelle, A. Lebugle. *J. Solid State Chem.* **2005**, *178*, 2354-2362. Europium-doped calcium pyrophosphates: Allotropic forms and photoluminescent properties.
5. R. Ternane, M. T. Cohen-Adad, G. Panczer, C. Goutaudier, C. Dujardin, G. Boulon, N. Kbir-Ariguib, M. Trabelsi-Ayedi. *Solid State Sci.* **2002**, *4*, 53-59. Structural and luminescent properties of new Ce^{3+} doped calcium borophosphate with apatite structure.
6. M. Mehnaoui, R. Ternane, G. Panczer, M. Trabelsi-Ayadi, G. Boulon. *J. Phys. Condens. Matter.* **2008**, *20*, 275227/1-275227/6. Structural and luminescent properties of new Pb^{2+}-doped calcium chlorapatites $Ca_{(10-x)}Pb_x(PO_4)_6.Cl_2$ ($0 \leq x \leq 10$).
7. M. Neumeier, A. L. Hails, A. S. Davis, S. Mann, M. Epple. *J. Mater. Chem.* **2011**, *21*, 1250-1254. Synthesis of fluorescent core-shell hydroxyapatite nanoparticles.
8. S. P. Mondejar, A. Kovtun, M. Epple. *J. Mater. Chem.* **2007**, *17*, 4153-4159. Lanthanide-doped calcium phosphate nanoparticles with high internal crystallinity and with a shell of DNA as fluorescent probes in cell experiments.
9. S. Wang. *Micropor. Mesopor. Mater.* **2008**, *117*, 1-9. Ordered mesoporous materials for drug delivery.

10. M. Vallet-Regí, F. Balas, D. Arcos. *Angew. Chem. Int. Ed.* **2007**, *46*, 7548-7558. Mesoporous materials for drug delivery.

11. M. Vallet-Regí, A. Ramila, R. P. del Real, J. Perez-Pariente. *Chem. Mater.* **2001**, *13*, 308-311. A new property of MCM-41: drug delivery system.

12. F. Tang, L. Li, D. Chen. *Advanced Materials* **2012**, *24*, 1504-1534. Mesoporous Silica Nanoparticles: Synthesis, Biocompatibility and Drug Delivery.

13. D. Zhao, Y. Wan, W. Zhou. *Wiley-Vch.* **2013**, *517*. Ordered mesoporous materials.

14. C. Argyo, V. Weiss, C. Bräuchle, T. Bein. *Chem. Mater.* **2013**, *26*, 435-451. Multifunctional Mesoporous Silica Nanoparticles as a Universal Platform for Drug Delivery.

15. W. Wang, D. Shi, J. Lian, Y. Guo, G. Liu, L. Wang, R. C. Ewing. *Appl. Phys. Lett.* **2006**, *89*, 183106/1-183106/3. Luminescent hydroxylapatite nanoparticles by surface functionalization.

16. A. Doat, M. Fanjul, F. Pelle, E. Hollande, A. Lebugle. *Biomaterials* **2003**, *24*, 3365-3371. Europium-doped bioapatite: a new photostable biological probe, internalizable by human cells.

17. F. Chen, Y.- J. Zhu, K.- H. Zhang, J. Wu, K.-W. Wang, Q.-L. Tang, X.- M. Mo. *Nanoscale Res. Lett.* **2011**, *6*, 67-69. Europium-doped amorphous calcium phosphate porous nanospheres: preparation and application as luminescent drug carriers.

18. A. Lebugle, F. Pelle, C. Charvillat, I. Rousselot, J. Y. Chane-Ching. *Chem. Commun.* **2006**, 606-608. Colloidal and monocrystalline Ln^{3+} doped apatite calcium phosphate as biocompatible fluorescent probes.

19. A. Doat, F. Pelle, N. Gardant, A. Lebugle. *J. Solid State Chem.* **2004**, *177*, 1179-1187. Synthesis of luminescent bioapatite nanoparticles for utilization as a biological probe.

20. S. Dembski, M. Milde, M. Dyrba, S. Schweizer, C. Gellermann, T. Klockenbring. *Langmuir* **2011**, *27*, 14025-14032. Effect of pH on the synthesis and properties of luminescent SiO_2/calcium phosphate: Eu^{3+} core-shell nanoparticles.

21. J. S. Beck, J. C. Vartuli, W. J. Roth, M. E. Leonowicz, C. T. Kresge, K. D. Schmitt, C. T. W. Chu, D. H. Olson, E. W. Sheppard. *J. Am. Chem. Soc.* **1992**, *114*, 10834-10843. A new family of mesoporous molecular sieves prepared with liquid crystal templates.

22. S. V. Dorozhkin. *J. Mater. Sci.* **2007**, *42*, 1061-1095. Calcium orthophosphates.

23. J. Andersson, S. Areva, B. Spliethoff, M. Linden. *Biomaterials* **2005**, *26*, 6827-6835. Sol-gel synthesis of a multifunctional, hierarchically porous silica/apatite composite.

VI. CONCLUSIONS

VI. Conclusions

Chapter II. Precipitation of Mesostructured Calcium Phosphates in the Presence of Ionic Surfactants

- Ionic surfactants, namely anionic, containing S or P atoms in their polar head, such as SDS, SDBS and MAP, can be used to obtain mesostructured organic-inorganic hybrids based in CaPs.

- The interaction of amphiphilic molecules of surfactant with calcium and phosphate ions, during the CaP precipitation from aqueous solutions, yield hybrid materials exhibiting lamellar or discontinuous lamellar mesostructures, but no mesoporous order.

- In the synthesis conditions, *i.e.*, Ca/P molar ratio 1 and 1.67, surfactant concentration from 15 to 90 mM and 240 mM and pH not buffered, the CaP most common phases present in the lamellar hybrids were brushite, hydroxyapatite or monetite.

- SDS is a suitable surfactant to obtain highly mesostructured lamellar CaP hybrids.

- Relatively high SDBS concentrations and Ca/P molar ratio of 1 yield discontinuous lamellar or curved lamellar mesostructures, forming meshes, of poorly crystallized HA. The formation of HA at this low Ca/P molar ratio is attributed to the pH increase (7 to 9) of medium due to the protonation of the sulphate polar heads of SDBS.

- The mixture of an anionic surfactant, such as SDS, SDBS or MAP, with the cationic cetyltrimethyl ammonium bromide (CTAB) produces hybrids with mesostructure analogous to that obtained with the pure anionic surfactants, suggesting a non-effective interaction of CTAB with calcium and phosphate ions.

- TEM analysis of materials obtained using a surfactant mixture shows two types of particles: *(i)* rod-like particles exhibiting lamellar mesostructure and (ii) sheet-like particles unstable under the electron beam. The bubbles formed when these sheet-like particles were investigated, attributed to the organic matter combustion and to the removal of crystallization water molecules in brushite, avoid the identification of the possible mesostructure in the sheet-like particles.

- The use of energetic synthesis procedures, such as ageing in an autoclave or refluxing after the CaP precipitation, leads to monetite, a CaP phase derived from brushite after remove the two water molecules of crystallization.

- The use of EPG, a zwitterionic surfactant containing one carboxybetaine group, as mesostructure template for CaP fails and no interactions with calcium and phosphate ions are detected. For the future, the investigation of another zwitterionic surfactant containing a sulfobetaine groups is suggested.

Chapter III. Precipitation of Mesostructured Calcium Phosphates in the Presence of Phospholipids

- The precipitation of CaPs in phospholipids (PLs) suspensions containing different concentrations of phosphatidylcholine (PC) yields to the synthesis of CaP-PLs hybrid materials.

- The inorganic components of the hybrids are poorly crystallized HA, when pH is basic and Ca/P molar ratio 1.67, and brushite at pH neutral and Ca/P = 1.

- The organic matter content is similar in both hybrid types, around 20% in brushite-containing hybrids and around 17% in HA-containing ones. CaP-PLs hybrid materials subjected to a thermal process to remove the organic matter evolve to non-porous HA. Since no mesoporous materials were obtained after calcination, this Chapter has been focused in the characterization of the CaP-PLs hybrid materials.

- TEM analysis of hybrids revealed four types of nanostructures: *(i) lamellar bilayer* with 4.2 nm in thickness of layer (apatite, asolectin), *(ii) bilayer vesicles* around 35 nm in diameter of vesicles and 4.7 nm in thickness of bilayer (brushite, lecithin), *(iii) micelles* of about 4.3 nm in diameter (brushite, lipoid) and *(iv) bilayer sponge–like* or *worm–like tubular* mesostructures with 4.3 nm in thickness of disordered bilayer sponge–like structure (apatite, lipoid).

- Since both components of CaP-PLs hybrid materials are biocompatible they can be investigated as drug delivery platforms via the encapsulation of a drug within the phospholipid structure of the hybrid.

Chapter IV. Hydroxyapatite Coatings on Mesoporous Silica Nanospheres

In this chapter, MCM–41 mesoporous silica nanospheres (MSNSs) were tried to be coated with HA nanoparticles or with a HA layer, to expand the clinical applications of both materials. According to this goal, the conclusions derived from each synthetic route attempted are:

- Co-synthesis of CaP and MSNSs. The CaP precipitation simultaneous to the sol-gel synthesis of MSNSs yield a mixture of independent particles of poorly crystallized HA rods and polydisperse MSNSs (S_{BET} 594 m^2/g).

- Soaking of MSNSs into a sol precursor of CaP. First, pure SiO_2 MSNSs (S_{BET} = 1230 m^2/g) were synthesized. After soaking them in the sol precursor of CaP for 3 hours, the nanospheres (S_{BET} = 250 m^2/g) convert in ellipsoids with the elements Si, Ca, P and O in their composition. The ellipsoids exhibit a radial mesopore channels arrangement close to the particles surface. Moreover, the obtained material exhibits a moderate *in vitro* bioactive response in simulated body fluid.

- Wetting of MSNSs by a sol precursor of CaP. In this approach, pure SiO_2 MSNSs (S_{BET} = 1230 m^2/g) were synthesized first, then soaked for 30 minutes in the sol precursor of CaP and subsequently subjected to a washing process mimicking a dip-coating procedure with the sol. TEM images after wetting confirm the successful formation of HA NPs covering the MSNSs

surface. In this case, the S_{BET} of the coated material suffer a drastic decrease of ≈90 % compared to the initial MSNSs. Unlike the previous method, in this approach MSNSs are not altered in shape neither in composition.

- Functionalization of MSNSs with phosphate-like groups and subsequent wetting into a sol precursor of CaP. MSNSs were functionalized with diethylphosphatoethyl triethoxysilane (DEPETES) or 3-trihydroxysilylpropylmethylphosphonate (THSMP) to facilitate the subsequent interaction of their phosphate-like groups with calcium ions and then phosphate ions in the sol.

    - DEPETES-functionalized MSNSs exhibiting MCM-41 hexagonal arrangement and high S_{BET} (878 to 1190 m^2/g) were synthesized by co-condensation or post-synthesis. After functionalization, P-containing MSNSs were wetted with a sol precursor of CaP. A homogeneous distribution of a HA layer around the MSNSs and some HA NPs are observed by TEM. S_{BET} of 335 m^2/g indicates a partial coating of the MSNSs surface.

    - MSNSs were functionalized with THSMP by a co-condensation method. The obtained material exhibits a high S_{BET} of 1316 m^2/g. THSMP-functionalized MSNSs were wetted with a sol precursor of CaP. TEM analysis showed that a *core@shell* structure MSNS@HA was obtained. Coated MSNSs are non-porous showing a decrease in S_{BET} of around 97% regarding the initial MSNSs.

Chapter V. Coating of Mesoporous Silica Nanospheres with Fluorescent Hydroxyapatite Nanoparticles

- The precipitation of Eu^{3+} doped HA (fluorescent HA, FHA) in the presence of MCM-41 type MSNSs yields to the synthesis of FHA/MSNSs composites.

- Some FHA/MSNSs composites exhibit the red luminescence of lanthanides under UV light. The luminous intensity is dependent on the amount of Eu^{3+} ion in the composite.

- A *core@shell* structure (MSNS@HA) is observed by TEM for one of the samples investigated. However, this sample does not show a fluorescent emission due to its low Eu^{3+} content.

VII. APPENDIX: EXPERIMENTAL PART

VII.1 Tables for the interpretation of FTIR spectra of synthetized materials

The next tables resume the assignments used to analyze the FTIR results of the materials prepared in this thesis. The following abbreviations are used: w: weak, m: medium; s: strong; vs: very strong; sh: shoulder; shp: sharp; br: broad.

Organic matter from surfactants

Wavenumber (cm^{-1})	Vibration mode	Functional group Structural unit	Assignment
2950 (w)	ν_{as} (CH)	CH_3 group	Asymmetric stretching mode of the C-H bonds of the methyl group
2916 (s)	ν_{as} (CH)	CH_2 group	Asymmetric stretching mode of the C-H bonds of the methylene group
2850 (m)	ν_{s} (CH)	CH_2 group	Symmetric stretching mode of the C-H bonds of the methylene group

Silica

Wavenumber (cm^{-1})	Vibration mode	Functional group Structural unit	Assignment
3500-3300 (br)	ν (OH)	H_2O	Stretching mode of the O-H bonds of the physisorbed water
1630	δ (HOH)	H_2O	Bending mode of the H-O-H bonds of the physisorbed water
1050 (vs)	ν_{as} (SiO)	SiO_2	Asymmetric stretching mode of the Si-O bonds of the silica network
950-910 (sh)	ν (SiO)	Si-OH	Stretching mode of the Si-O bonds of the silanol groups of the silica surface
800 (m)	ν_{s} (SiO)	SiO_2	Symmetric stretching mode of the Si-O bonds of the silica network
440 (s)	δ (SiOSi)	SiO_2	Bending mode of the Si-O-Si bonds of the silica network (siloxane bonds)

Calcium phosphates: HAp $Ca_{10}(PO_4)_6(OH)_2$

Wavenumber (cm^{-1})	Vibration mode	Functional group Structural unit	Assignment
3800-3000 (br) 3400 (br)	ν (OH)	H_2O	Stretching mode of the O-H bonds of the adsorbed water
3500 (w) or 3572 (w)	ν (OH)	OH	Stretching mode of the O-H bond of the hydroxyl group
1630	δ (HOH)	H_2O	Bending mode of the H-O-H bonds of the adsorbed water
1087 (s) 1046 (s) 1032 (s)	ν_{as} (PO)	PO_4^{3-}	Asymmetric stretching mode of the P-O bonds of the phosphate groups
960 (w)	ν_{s} (PO)	PO_4^{3-}	Symmetric stretching mode of the P-O bonds of the phosphate groups
600 (s) 574 (m) 560 (m) Two or three bands	δ (OPO)	PO_4^{3-} in crystalline environment	Bending mode of the O-P-O bonds of the phosphate groups in crystalline environment
470 (w) or 460	δ (OPO)	PO_4^{3-}	Bending mode of the O-P-O bonds of the phosphate groups

Calcium phosphates: Carbonated HAp $Ca_{10}(PO_4,CO_3)_6(OH)_2$

Wavenumber (cm^{-1})	Vibration mode	Functional group Structural unit	Assignment
1550 **1500** 1465 1430 **1410**	ν (CO)	CO_3^{2-}	Stretching mode of the C-O bonds of the carbonate group
1087 (s) 1046 (s) 1032 (s)	ν_{as} (PO)	PO_4^{3-}	Asymmetric stretching mode of the P-O bonds of the phosphate groups
970 (w)	ν_s (PO)	PO_4^{3-}	Symmetric stretching mode of the P-O bonds of the phosphate groups
883 875 870 (m)	δ (OCO)	CO_3^{2-}	Bending mode of the C-O bonds of the carbonate group
600 (s) 574 (m) 560 (m) Two or three bands	δ (OPO)	PO_4^{3-} in crystalline environment	Bending mode of the O-P-O bonds of the phosphate groups in crystalline environment
470 (w) or 460	δ (OPO)	PO_4^{3-}	Bending mode of the O-P-O bonds of the phosphate groups

Calcium phosphates: Brushite $CaHPO_4 \cdot 2H_2O$

Wavenumber (cm^{-1})	Vibration mode	Functional group Structural unit	Assignment
3540 (s)	ν_{as} (OH)	OH	Asymmetric stretching mode of the O-H bonds of the monohydrogenphosphate group
3460 (s)	ν_s (OH)	OH	Symmetric stretching mode of the O-H bonds of the monohydrogenphosphate group
3260 (m)	ν_{as} (OH)	H_2O	Asymmetric stretching mode of the H-O-H bonds of the crystalline water
3150 (m)	ν_s (OH)	H_2O	Symmetric stretching mode of the H-O-H bonds of the crystalline water
1650-1640 (shp, s)	δ (HOH)	H_2O	Bending mode of the H-O-H bonds of the crystalline water
1092 (s) 1060 (sh) 1020 (s)	ν_{as} (PO)	HPO_4^{2-}	Asymmetric stretching mode of the P-O bonds of the phosphate groups
970 (m) 870 (m)	ν_s (PO)	HPO_4^{2-}	Symmetric stretching mode of the P-O bonds of the phosphate groups
790 (m) 660 (m)	δ (OPO)	HPO_4^{2-}	Bending mode of the O-P-O bonds of the phosphate groups
580 (w) 520 (w)	δ (OPO)	HPO_4^{2-}	Bending mode of the O-P-O bonds of the phosphate groups

VII.2 Characterization Techniques

Thermogravimetric and Differential Thermal Analysis (TG/DTA)

Thermogravimetric analyses were used to investigate the weight losses of synthesized materials during the temperature treatment. Calcium phosphate phase changes as well as exothermic/endothermic processes of synthesized materials were observed by DTA. In the cases in which TGA curve exhibited a small weight loss between room temperature and 125 °C this fact was attributed to the loss of water physisorbed in samples. TG/DTA was performed in air at a flow rate of 100 ml min^{-1} and a heating rate of 10 °C min^{-1} between 30 and 1000 °C on a Perkin–Elmer Pyris Diamond thermobalance. Platinum crucible was used as sample holder and alumina as reference.

Elemental Analysis of Carbon, Hydrogen and Nitrogen

Elemental analysis was performed on a Perkin–Elmer 2400 CHN thermo analyzer at the Elemental Microanalysis CAI of Universidad Complutense de Madrid.

During the short research stay at the Inorganic Chemistry Center of the University of Duisburg–Essen, the contents of carbon, hydrogen and nitrogen were determined by standard combustion analysis with EA 1110 instrument (CE Instruments).

Fourier Transform Infrared Spectroscopy (FTIR)

FTIR was used to identify the functional groups of synthesized materials. FTIR spectra were collected by using a Nicolet iS10 spectrometer equipped with a Goldengate® attenuated total reflectance (ATR) device. FTIR is typically operated in the range between 400 and 4000 cm^{-1}. OMNIC spectroscopy software package from Nicolet was used for the treatment of the FTIR spectra.

During the short research stay, FTIR spectra were collected by using Bruker–Vertex 70 FTIR spectrometer in the range between 400 and 4000 cm^{-1}. In this case, OPUS spectroscopy software package for FTIR was used.

Powder X–ray Diffraction (XRD)

The XRD analyses were carried out using a Philips X´Pert MPD diffractometer (Philips Electronics NV, Eindhoven, Netherlands) with Cu K_α radiation (λ=1.5418 Å) at the X–ray diffraction CAI of Universidad Complutense de Madrid operated by Dr. Fernando Conde.

Small–angle XRD was used to examine the mesostructures in synthesized materials and wide–angle XRD was used to examine the crystalline phases of CaP in synthesized samples. Wide–angle X–ray was collected over the range 2θ = 5–50°, with a step size of 2θ = 0.04° and a counting time per step of 1 s. Small–angle X–ray diffractions were collected over the range 2θ = 0.6–6.5°, with a step size of 2θ = 0.02° and a counting time per step of 5 s.

During the short research stay, synthesized materials were characterised by using X–ray diffraction (Bruker D8 Advance: Cu K_α radiation, λ=1.5418 Å). The diffractograms were collected over the range 2θ = 10–50°, with a step size of 2θ = 0.01 ° and a counting time of 102 s per step for wide–angle XRD. The range of small–angle XRD was between 0.95 and 6 °.

Nitrogen Adsorption Isotherms

The surface area and pore size measurements of hybrid materials were performed by nitrogen adsorption/desorption analysis at –196 °C on ASAP 2010 and 2020 porosimeter (Micromeritics Co, Norcross GA, USA). Prior to the analysis, powder samples were degassed at 125 °C for 24 h under a vacuum lower than 5 μmHg. The surface area was determined by Brunauer–Emmett–Teller (BET) method [1,2]. The pore diameter distribution was obtained by the Barrett–Joyner–Halenda (BJH) method [1,2].

Transmission Electron Microscopy – Electron Diffraction (TEM–ED)

TEM was performed to analyze the mesostructures and crystalline phases in synthesized materials on a JEOL JEM–2100 microscope operating at 200 kV in the National Centre of Electron Microscopy at Universidad Complutense de Madrid. I want to thank Dr. Mª Luisa Ruiz González for measuring samples prepared by precipitation of CaP during the synthesis of mesoporous silica nanospheres (MSNSs). All synthesized samples were prepared by dispersing a small amount of powder materials in butanol or water with an ultrasonicator bath. After sonication, suspensions were deposited by 2–3 drops of suspension on a perforated carbon–coated copper grid.

During my short research stay in Germany, synthesized materials were examined by JEOL 1200 microscope operating at 120 kV.

Scanning Electron Microscopy and Energy Dispersive X–ray Spectroscopy (SEM–EDS)

The surface morphology of synthesized materials was studied by Scanning Electron Microscopy coupled with Energy Dispersive X–ray Spectroscopy. SEM–EDS analysis was carried out using a JEOL JSM 6335F Microscope at the National Center of Electron Microscopy of Universidad Complutense de Madrid**.** For this purpose, synthesized samples were mounted onto a copper stud, dried at 70 °C for 24 h under vacuum, and coated with a carbon film.

During my short research stay in Germany, the surface morphology of mesoporous silica coated with fluorescent HA was studied by SEM–EDS. This analysis was carried out using a FEI ESEM Quanta 400 FEG coupled with EDX detector S–UTW–Si(Li). For this purpose, the surface morphology of mesoporous silica coated with fluorescent HA samples were mounted onto a copper stud and coated with a film of gold–palladium (80:20).

Determination of Ca^{2+} concentration and pH value after SBF test

Variation in the Ca^{2+} concentration and pH value in solution were determined on an ILyte Na^+, K^+, Ca^{2+} pH analyzer.

Ultraviolet spectroscopy

During the short research stay, the intense luminescence of europium–doped hybrid materials was observed by using a UV lamp (λ = 254 nm) [3].

VII.3 Commercial Products

For the synthesis of the materials here described, the following products have been commercially acquired from different companies.

Sigma–Aldrich: Calcium chloride dihydrate, $CaCl_2{\cdot}2H_2O$; calcium nitrate tetrahydrate, $Ca(NO_3)_2{\cdot}4H_2O$; sodium phosphate dibasic dihydrate, $Na_2HPO_4{\cdot}2H_2O$; sodium dodecyl benzene sulphonate, $C_{18}H_{29}O_3SNa$; sodium dodecyl sulphate, $C_{12}H_{25}NaO_4S$; cetyltrimethyl ammonium bromide, $C_{19}H_{42}NB$; Empigen®BB surfactant 35%, $CH_3(CH_2)_{8-14}CH_2N^+(CH_3)_2CH_2COO^-$; *asolectin* from soybean (mixture of phospholipids); *L*-*α*-Lecithin from egg yolk; tetraethyl orthosilicate, $Si(OC_2H_5)_4$; triethylphosphite, $(C_2H_5O)_3P$; 3-trihydroxysilylpropyl methylphosphonate 42%, $CH_3P(O)(ONa)O(CH_2)_3Si(OH)_3$; sodium hydroxide, NaOH; Toluene; sodium chloride, NaCl; sodium hydrogen carbonate, $NaHCO_3$; potassium chloride, KCl; di-potassium hydrogen phosphate trihydrate, $K_2HPO_4{\cdot}3H_2O$; magnesium chloride hexahydrate, $MgCl_2{\cdot}6H_2O$; calcium chloride, $CaCl_2$; sodium sulfate, Na_2SO_4; tris-hydroxymethyl aminomethane, $(HOCH_2)_3CNH_2$ (Tris); poly(ethyleneimine), $H(NHCH_2CH_2)_nNH_2$; yttrium chloride hexahydrate 99.9%, $YCl_3{\cdot}6H_2O$.

Merck: Diammonium hydrogenphosphate, $(NH_4)_2HPO_4$.

Riedel–de Haën: Calcium nitrate tetrahydrate, $Ca(NO_3)_2{\cdot}4H_2O$.

ABCR GmbH: Diethylphosphatoethyltriethoxysilane 92% (DEPETES), $C_{12}H_{29}O_6PSi$.

Lipoid GmbH: Lipoid-S100 from soybean.

Alfa–Aesar: Mono-alkyl phosphate (MAP), $C_{12}H_{27}O_4P$; Europium (III) nitrate hexahydrate 99.9%, $Eu(NO_3)_3{\cdot}6H_2O$.

Panreac: Ethanol absolute 99.5 %; ammonia 25 %; hydrochloric acid 37 %.

Deionized water was further purified by passage through a Milli-Q Advantage A-10 Purification System (Millipore Corporation) to a final resistivity of 18 MΩ cm or above.

VII.4 Preparation of Simulated Body Fluid

Simulated Body Fluid (SBF) was prepared by *Kokubo* method . The following powder reagent grade chemicals have to be stocked in a desiccator. Milli-Q water is used for the preparation of SBF [4].

(1) sodium chloride,
(2) sodium hydrogen carbonate,
(3) potassium chloride,
(4) di-potassium hydrogen phosphate trihydrate,
(5) magnesium chloride hexahydrate,
(6) calcium chloride,
(7) sodium sulfate,
(8) tris-hydroxymethyl aminomethane,
(9) 1M (mol/1) hydrochloric acid,
(10) pH standard solutions, (pH 4, 7 and 9)

Protocol for preparing SBF:

1- All bottles and wares were washed with 1N–HCl solution, neutral detergent, and ion–exchanged and distilled water, and then dried.
2- 500 ml of ion–exchanged and distilled water was put into one liter polyethylene bottle, and the bottle was then covered with a watch glass.
3- The water in the bottle was stirred with a magnetic stirrer, dissolving the reagents one by one in the order as given in Table VII.1 (each one once the previous reagent was completely dissolved).
4- The temperature of the solution in the bottle was adjusted at 36.5 °C with a water bath, and solution pH was adjusted at pH 7.40 by stirring the solution and titrating 1N–HCl solution (when the pH electrode is removed from the solution, the water used for washing the electrode was added to the solution).
5- The solution was transferred from the polyethylene bottle to a volumetric glass flask.
6- Total volume of solution was then adjusted to one liter by adding ion–exchanged and distilled water and shaking the flask at 20 °C.
7- The solution was transferred from the flask to a polyethylene or polystylene bottle, and the bottle was stored in a refrigerator at 5–10 °C (if any substance precipitated during storage, the SBF solution was rendered invalid and not used).

Table VII.1 Reagents for preparing SBF (1 liter)

Order	Reagent	Amount
1	NaCl	7.996 g
2	$NaHCO_3$	0.350 g
3	KCl	0.224 g
4	$K_2HPO_4 \cdot 3H_2O$	0.228 g
5	$MgCl_2 \cdot 6H_2O$	0.305 g
6	1N-HCl (about 90% of total amount of HCl to be added)	40 mL
7	$CaCl_2$	0.278 g
8	Na_2SO_4	0.071 g
9	$(HOCH_2)_3CNH_2$	6.057 g

VII.5 Description of Synthesis

VII.5.a Synthesis of Calcium Phosphate in the Presence of Surfactants (Chapter II)

First, 0.4175 M or 0.25 M $CaCl_2 \cdot 2H_2O$ and 0.25 M $Na_2HPO_4 \cdot 2H_2O$ solutions were prepared in volumetric flask as stock solutions. 25 ml of each solution were taken from stocks when necessary.

Calcium Phosphate in the Presence of Sodium Dodecyl Sulphate

Nanostructured CaPs were synthesized by precipitation as previously reported [5]. Fast crystallization and precipitation of CaP is achieved by this method due to the rapid interaction between Ca^{2+} and HPO_4^{2-} ions in water solution.

SDS was dissolved in the $Na_2HPO_4 \cdot 2H_2O$ solution and surfactant amounts used are as follows: 0.2163 g, 0.4326 g, 0.6489 g, 0.8651 g, 1.0814 g and 1.2977 g for 15 mM, 30 mM, 45 mM, 60 mM, 75 mM and 90 mM of SDS concentration in the final reaction volume, respectively.

Samples were classified in two series as a function of the Ca/P molar ratio relation of 1 and 1.67. All samples were synthesized without buffering the pH. The molar ratios of materials are respectively: 1 $Na_2HPO_4 \cdot 2H_2O$ / 1 and 1.67 $CaCl_2 \cdot 2H_2O$ / 0.12 – 0.24 – 0.36 – 0.48 – 0.6 and 0.72 of SDS / 445 H_2O. The general procedure is described as follows: over 25 ml of $Na_2HPO_4 \cdot 2H_2O$ solution (0.25 M) heated at 40 °C, the corresponding amount of SDS was slowly added under stirring. The resulting solution was stirred at 40 °C during 20 min, and then 25 ml of $CaCl_2 \cdot 2H_2O$ solution (0.25 or 0.4175 M) was added drop by drop. The mixture was stirred at 40 °C for 1 h and then was left to stay at 37 °C for 24 h. The processes of reflux and autoclave were performed respectively at 80 and 125 °C for 24 h for 30 mM concentration of SDS surfactant. Finally, the mixture was filtered, washed with Milli-Q water, and dried in the oven.

Calcium Phosphate in the Presence of Sodium Dodecyl Benzene Sulphonate

The starting materials are calcium chloride dehydrate, sodium phosphate dibasic dihydrate and sodium dodecyl benzene sulphonate as surfactant. SDBS was dissolved in the $Na_2HPO_4 \cdot 2H_2O$ solution and surfactant amounts used are as follows: 0.2613 g, 0.5227 g, 1.0454 g and 1.5681 g for 15 mM, 30 mM, 60 mM and 90 mM of SDBS concentration in the final reaction volume, respectively.

All samples were prepared with molar ratio relation of Ca/P = 1 and synthesized without buffering the pH. The molar ratios of materials are: 1 $Na_2HPO_4 \cdot 2H_2O$ / 1 $CaCl_2 \cdot 2H_2O$ / 0.12 – 0.24 – 0.48 – 0.72 of SDBS / 445 H_2O, respectively. The general procedure is described as follows: over 25 ml of $Na_2HPO_4 \cdot 2H_2O$ solution (0.25 M) heated at 40 °C, the corresponding amount of SDBS was slowly added under stirring. The resulting solution was stirred at 40 °C during 20 min, and then 25 ml of $CaCl_2 \cdot 2H_2O$ (0.25 M) were added drop by drop. The mixture was stirred at 40 °C for 1 h and then was left to stay at 37 °C for 24 h. Finally, the mixture was filtered, washed with Milli-Q water, and dried in the oven.

Calcium Phosphate in the Presence of the Surfactants Mixture: Sodium Dodecyl Sulphate/CetylTrimethyl Ammonium Bromide

SDS and CTAB surfactants were separately dissolved in half the volume of $Na_2HPO_4 \cdot 2H_2O$ solution (12.5 mL, 0.25 M) and surfactant amounts used are as follows: 0.007 g, 0.216, 0.432, 0.65 g, 0.865, 1.08 g and 1.3 g of SDS and 0.1 g, 0.27 g, 0.546, 0.82 g, 1.1 g, 1.37 g and 1.64 g of CTAB surfactant for 0.5 mM, 0.15 mM, 30 mM, 45 mM, 60 mM, 75 mM and 90 mM of [SDS + CTAB, 1:1] in the final reaction volume, respectively.

All samples were prepared with molar ratio relation of Ca/P = 1 and synthesized without buffering the pH. The molar ratios of materials are: 1 $Na_2HPO_4 \cdot 2H_2O$ / 1 $CaCl_2 \cdot 2H_2O$ / 0.004 – 0.012 – 0.024 – 0.036 – 0.048 – 0.06 and 0.072 of SDS + CTAB (1:1) / 445 H_2O, respectively.

The general procedure is described as follows: over 12.5 ml of $Na_2HPO_4 \cdot 2H_2O$ solution (0.25 M) heated at 40 °C, the corresponding amount of SDS or CTAB was slowly added under stirring. These solutions were mixed and the resulting solution was stirred at 40 °C during 20 min, and then 25 ml of $CaCl_2 \cdot 2H_2O$ (0.25 M) was added drop by drop. The mixture was stirred at 40 °C for 1 h and then was left to stay at 37 °C for 24 h. Finally the mixture was filtered, washed with Milli-Q water, and dried in the oven.

Calcium Phosphate in the Presence of the Surfactants Mixture: Sodium Dodecyl Benzene Sulphonate/CetylTrimethyl Ammonium Bromide

SDBS and CTAB surfactants were separately dissolved in half the volume of $Na_2HPO_4 \cdot 2H_2O$ solution (12.5 mL, 0.25 M) and the amounts of surfactants used for [SDBS+CTAB] 30 mM are as follows: 0.39204 g of SDBS and 0.1366 g of CTAB for 3:1 molar ratios; 0.13068 g of SDBS and 0.41001 g of CTAB for 1:3 molar ratios.

All samples were prepared with molar ratio relation of Ca/P = 1 and synthesized without buffering the pH. The molar ratios of materials are: 1 $Na_2HPO_4 \cdot 2H_2O$ / 1 $CaCl_2 \cdot 2H_2O$ / 0.18 and 0.06 of SDBS / 0.06 and 0.18 of CTAB / 445 H_2O, respectively.

The general procedure is described as follows: over 12.5 ml of $Na_2HPO_4.2H_2O$ solution (0.25 M) heated at 40 °C, the corresponding amount of SDBS or CTAB was slowly under stirring. These solutions were mixed and the resulting solution was stirred at 40 °C during 20 min, and then 25 ml of $CaCl_2 \cdot 2H_2O$ (0.25 M) was added drop by drop. The mixture was stirred at 40 °C for 1 h and then was left to stay at 37 °C for 24 h. Finally, the mixture was filtered, washed with Milli-Q water and dried in the oven.

Calcium Phosphate in the Presence of the Surfactants Mixture: Monoalkyl Phosphate/CetylTrimethyl Ammonium Bromide

Several samples with different CTAB/MAP molar ratio and increasing surfactants mixture concentration were prepared. The sample described in the chapter was prepared with the following molar ratios of reactants: 1 $Na_2HPO_4{\cdot}2H_2O$ / 1 $CaCl_2{\cdot}2H_2O$ / 0.12 MAP / 0.12 CTAB / 52 H_2O and synthetized without buffering the pH. Final surfactant mixture concentration in the reaction volume is 240 mM. An autoclave process was performed after the synthesis by precipitation method.

The procedure is described as follows: 0.3654 g of MAP and 0.5 g of CTAB were dissolved in $Na_2HPO_4{\cdot}2H_2O$ solution (2.0349 g in 7.5 mL of H_2O). The resulting solution was stirred at 40 °C during 30 min, and then $CaCl_2{\cdot}2H_2O$ (1.6809 g in 2.5 mL of H_2O) were added drop by drop. The mixture was slowly stirred at 40 °C for 1 h and then stirred at R.T. for 16 hours (overnight). Finally, a process of autoclave was performed at 100 °C for 24 h. The mixture was filtered, washed with Milli-Q water, and dried in the oven.

Calcium Phosphate in the Presence of the Zwitterionic Surfactant

EMPIGEN BB 35% surfactant (EPG) was dissolved in water to a concentration of 60 and 90 mM (30 and 45 mM of surfactant in the final reaction volume, respectively) and surfactant amounts used were 1.17 and 1.75 ml of EPG 30% to prepare 25 mL of solution.

Sample preparation solutions had the Ca/P molar ratio 1 and pH value was not buffered. The molar ratios of material: 1 $Na_2HPO_4{\cdot}2H_2O$ / 1 $CaCl_2{\cdot}2H_2O$ / 0.68 and 1.02 of EPG / 445 H_2O, respectively. Four samples were synthesized by adding calcium and phosphate sources as follows:

(i) For samples CaP1 and CaP2: over 25 mL of the EPG solution heated a 40 °C, 0.92 g of $CaCl_2{\cdot}2H_2O$ were slowly added under stirring. The resulting solution was stirred at 40°C during 20 min, and then 25 ml of $Na_2HPO_4{\cdot}2H_2O$ (0.25 M) were added drop by drop.

(ii) For samples PCa1 and PCa2: over 25 mL of the EPG solution heated at 40 °C, 1.11 g of $Na_2HPO_4{\cdot}2H_2O$ were slowly added under stirring. The resulting solution was stirred at 40·°C during 20 min, and then 25 ml of $CaCl_2{\cdot}2H_2O$ (0.25 M) were added drop by drop.

The mixture was stirred at 40°C for 1h and then was left to stay at 37 °C for 24 h. Finally, the mixture was filtered, washed with Milli-Q water, and dried in the oven.

VII.5.b Synthesis of Calcium Phosphate in the Presence of Phospholipids (Chapter III)

The reactants used in the syntheses were: calcium chloride dihydrate, sodium phosphate dibasic dihydrate and sodium hydroxide. Three Phospholipids (PLs) sources with increasing contents of Phosphatidylcholine (PC) were used: *Asolectin* from soybean, containing about 33% of PC (PC33), *L–α–Lecithin* from egg yolk, about 60% of PC (PC60) and *Lipoid–S100* from soybean, containing 94% of PC (PC94). In some cases ethanol absolute 99.5% was used as co-solvent.

Table VII.2 shows amounts of solvents, reactants and Ca/P molar ratio. Synthesized materials were named as PC33, PC60, PC94–1 and PC94–2 with the numbers indicating the percentage of PC in the commercial reagent, respectively.

Table VII.2 Amount of phospholipids (PLs), moles of reactants, solvents and NaOH used in the synthesis of hybrids CaP–PLs. Ca/P molar ratios are also included.

Samples (PLs source, % of PC)	HPO_4^{2-} (mol)	Ca^{2+} (mol)	PLs (g)	H_2O (mol)	EtOH (mol)	NaOH (mol)
PC33 (Asolectin, 33)	1	1.67	0.5	126	38	2
PC60 (Lecithin, 60)	1	1	0.5	69	38	–
PC94–1 (Lipoid, 94)	1	1	0.5	194	–	–
PC94–2 (Lipoid, 94)	1	1.67	0.5	223	–	1

The general synthetic procedure was the following: CaPs were precipitated from calcium and phosphate ions in the presence of PLs, using a modification of a method described by *Galarneau et* al for the synthesis of sponge mesoporous silica [6].

The experimental procedure is described as follows: Firstly, 0.5 g of PC33 or PC60 was stirred in a solvent mixture of ethanol and water at room temperature and stirring at 1200 rpm overnight, until a homogeneous suspension was formed. Similarly, 0.5 g of PC94–1 or PC94–2 was stirred in water. Amounts of solvent mixture of ethanol–water and water were given in Table VII.2. Secondly, $Na_2HPO_4{\cdot}2H_2O$ was dissolved in deionised water by stirring at R.T. $CaCl_2{\cdot}2H_2O$ was dissolved in EtOH or water by stirring until obtaining a homogeneous solution. Phosphate, calcium, and PLs solutions were separately prepared from each other. Finally, calcium and phosphate solutions were added into the PLs solution drop by drop under the stirring of 500 rpm at R.T. for 15 min, and the mixture solution was left under stirring 15 min to obtain a homogenous solution. The mixture was left 24 h at room temperature for aging and then it was filtered and washed five times with 50 ml of H_2O/EtOH (1/1;v/v) and dried at 50 °C for 24 h. PC33 sample was calcinated at 700 °C for 8h and subsequently designated calcinated PC33.

VII.5.c Synthesis of Hydroxyaptite coatings on Mesoporous Silica Nanospheres (Chapter IV)

- *Synthesis of mesoporous silica nanospheres, MSNSs sample*

Synthesis of the nanospherical particles of mesoporous silica MCM-41 type with hexagonal pore arrangement, was performed by sol-gel chemistry in the presence of structure directing agents and following a modified *Stöber* method [7], as follows: 1g of CTAB was dissolved in 480 ml of water containing 3.5 ml of NaOH [2M] under stirring. The solution was heated at 80 °C and then 5 ml of TEOS as SiO_2 source was slowly added into mixture at 0.25 ml. min^{-1} using a syringe pump. The mixture was stirred at 700 rpm at 80 °C for 2 h. The material was filtered, washed thoroughly with water/ethanol (v/v : 50 ml / 50 ml) and dried in the vacuum oven at 80°C overnight. The surfactant

template was removed by heating at 550 °C for 6 h using a heating ramp of 2.5 °C/min. The obtained hexagonal mesoporous nanospherical silica particles were named as MSNSs sample.

- *Co–precipitation of calcium phosphate on mesoporous silica nanospheres, MSNS–HA–1 sample*

In the synthesis, the following molar ratios of reactants were used: 1 TEOS / 0.1223 CTAB / 0.3125 NaOH / 1190 H_2O / 0.4175 Ca / 0.25 TIP, respectively.

1 g of CTAB was mixed with 480 ml of water and added 3.5 ml of NaOH (2M) under stirring. The mixture was heated at 80 °C and stirred until colourless homogeneous mixture for 45 min. 5 ml of TEOS was slowly added into mixture at 0.25 ml min^{-1} by a syringe pump. 5 min later after adding TEOS, 20 ml of $CaCl_2{\cdot}2H_2O$ 0.4175 M and 20 ml of $Na_2HPO_4{\cdot}2H_2O$ 0.25 M were simultaneously added drop by drop into the solution. Then the mixture was mixed at 700 rpm at 80 °C for 2 hours. The sample was obtained after filtering, washing thoroughly with water–ethanol (v/v: 50/50) and drying in the vacuum oven at 80 °C overnight. To remove surfactant and keep the hexagonal form, a calcination process was performed at 550 °C for 6 h and heating rate of 2.5 °C min^{-1}.

- *Soaking and Wetting of silica nanospheres into a sol precursor of calcium phosphate, MSNS–HA–2 and MSNS–HA–3 samples*

Molar ratios of reactants were used such as: 1 TIP / 1.67 $CaCl_2{\cdot}2H_2O$ / 4 TEOS / 0.5 CTAB / 1.25 NaOH / 4762 H_2O, respectively.

Preparation of hexagonal mesoporous silica nanospheres (MSNSs): 1 g of CTAB was mixed with 480 ml of water and added 3.5 ml of NaOH (2M) under stirring. The mixing was heated at 80 °C and stirred until colourless homogeneous mixture for 45 min. After that, 5 ml of TEOS was slowly added into mixture at 0.25 ml min^{-1} by a syringe pump. Then the mixture was mixed at 700 rpm at 80 °C for 2 hours. The ordered nanospherical silicate was obtained after filtering, washing thoroughly with water/ethanol (v/v: 50/50) and drying in the vacuum oven at 80 °C overnight. To remove surfactant, a calcination process was performed at 550 °C for 6 h and heating rate of 2.5 °C min^{-1}. The obtained hexagonal mesoporous nanospherical silica particles were named as MSNSs.

The CaP sol preparation for coating MSNSs: The sol solution was prepared following a reported method [8]. Firstly, TIP was hydrolysed in water (in a 1:4 molar ratio) for 24 hours. Secondly, 4 M calcium nitrate aqueous solution was added to hydrolyzed phosphite solution, in a Ca/P ratio equal to 1.67, which corresponds to HA phase. The mixture was stirred for 15 min and subsequently was aged at 60 °C for 5 h and 30 min. The CaP sol solution is prepared for coating the MSNSs.

Coating MSNSs with nano–crystalline Apatite by CaP Sol Filtration: For soaking the nanospheres into a CaP sol, 0.3 g of pre–synthesized MSNSs (as white powder) was stirred for 3 h and filtered by sol precursor, and for wetting the nanospheres with a CaP sol, same 0.3 g of pre–synthesized MSNSs was stirred in sol for 30 min and filtered by the same sol solution for 20 times using 0.45 µm Tecnokroma®

cellulose membrane filter. Then, MSNSs coated with HA was dried at 60 °C overnight. To obtain hydroxyapatite, final sample was calcinated in air at 550 °C for 6 h with 2.5 °C min^{-1}.

- *Prefunctionalization of nanospheres with phosphate–like groups and subsequent wetting into a sol precursor of CaP*

The synthesis was prepared by *Y. G. Jin* method [9] and the following molar ratios of reactants were used: 1 TEOS / 0.1225 CTAB/ 0.3125 NaOH / 1205 H_2O.

By co–condensation method:

The corresponding amount of THSMP or DEPETES were used: 1TEOS / 0.3 THSMP / 0.1107 DEPETES 10% / 0.25 DEPETES 20 %.

1 g of CTAB was mixed with 480 ml of water and added 3.5 ml of NaOH (2M) under stirring. The mixing was heated at 80 °C and stirred until colourless homogeneous mixture for 45 min. After that, 5 ml of TEOS was slowly added into mixture at 0.25 ml min^{-1} by a syringe pump and stirred for 15 min. Then, 0.8 and 1.78 ml of DEPETES 10 % and 20 % or 0.5 ml of THSMP was added and the mixture was stirred at 700 rpm at 80 °C for 2 h. The sample of MSNSs functionalized with DEPETES or THSMP was obtained after filtering, washing thoroughly with water/ethanol (v/v: 250/250) and drying overnight in the vacuum oven at 80 °C. To remove the CTAB surfactant by *J. I. Zink* method [10], as–synthesized particles were suspended in 60 ml of methanol and 2.3 ml of 12 M HCl. The solution was refluxed for 10 h, and the synthesized samples were filtered and washed with 100 ml of methanol: water (v:v).

By post–synthesis method:

The corresponding amount of DEPETES was used: 1 TEOS / 0.07 for DEPETES.

0.5 g of pre–synthesized MSNSs as powder was mixed in 30 ml of toluene under nitrogen gas and stirred 2 hours. Then, 0.5 ml of DEPETES was added under nitrogen gas, and the mixture was refluxed at 110 °C overnight. The sample was filtered and washed by toluene: ethanol (50:50 / v:v), and dried overnight at 50 °C.

Soaking and wetting of mesoporous silica nanospheres into a sol precursor of CaP, NSFD–HA and NSFT–HA samples

The sol precursor for coating the nanospheres functionalized with DEPETES and THSMP has been prepared as previously explained in the section "*The CaP sol preparation for coating MSNSs*". The coating of prefunctionalized nanospheres can be explained as follows:

0.35 g of MSNSs functionalized with DEPETES (as white powder) was stirred in sol for 15 min and filtered by the same sol precursor for 5 times; similarly, 0.40 g of MSNSs functionalized with THSMP

was stirred in sol for 30 min and filtered by the same sol solution for 20 times using 0.45 µm Tecnokroma® cellulose membrane filter. Then, the final samples were dried at 40 °C overnight. To obtain hydroxyapatite, final samples were calcinated in air at 550 °C for 8 h with 2.5 °C min^{-1}.

VII.5.d Synthesis of Mesoporous Silica Nanospheres with Fluorescent Hydroxyapatite Nanoparticles (Chapter V)

Europium–doped hybrid materials were synthesized by *S. Dembski* and *M. Epple* methods [3, 11]. The starting materials used in this work included $Ca(NO_3)_2{\cdot}4H_2O$ and $(NH_4)_2HPO_4$ as calcium and phosphate source, respectively. PEI, Poly(ethyleneimine) (M_w 750.000 g mol^{-1}, 2 g L^{-1}), is used to stabilize the particles [11]. Europium source is $Eu(NO_3)_3{\cdot}6H_2O$. Milli-Q water and ethanol absolute 99.5%, were used for prepare the solution in this study. As silica source, MSNSs (type MCM–41) as structure template were synthesized previously following a modified Stöber method described in Section VII.3.d, *preparation of hexagonal mesoporous silica nanospheres (MSNSs)*, and used during the synthesis [7].

On the other hand, hexagonally structured MSNS coated by fluorescent HA was synthesized by precipitation of CaP in the presence of Eu^{3+} ions in a suspension of MSNSs [11-13].

Table VII.3 Amounts of MSNSs, solvents and reactants used for the synthesis of MSNSs coated by fluorescent HA.

	MSNPs (g)	Ca^{2+} (mM)	HPO_4^{2-} (mM)	Eu^{3+} (mM)	PEI (2mg mL^{-})	Citric acid anhydrous	H_2O (mL)	EtOH (mL)
LDHASi1	0.25	19.7	11.94	0.2	10 mL		75	5
LDHASi2	0.25	2462.5	1492.5	25	10 mL		40	10
LDHASi3	0.25	0.1905	0.116	0.00075	375 mg in15 mL	11.6 mmol	40	25
LDHASi4	0.25	2437.5	1458.8	50	10 mL		40	5

MCM–41 mesoporous silica material as white powder was mixed in EtOH solution and sonicated for 15 min. Secondly, aqueous solutions of Ca^{2+}:Eu^{3+} and HPO_4^{2-} were added, separately. The mixture was stirred for 1 h at R.T. Then, to remove supernatants, the mixture was centrifuged at 3500 rpm for 15 min and re–dispersed in enough amount of water. PEI was added into mixture and sonicated for 15 min, and then the mixture was centrifuged again and dried overnight at 60 °C. In all synthesis, Ca/P molar ratio was kept as 1.67 and pH value is 10–12 by addition of 2 M of NaOH. The amounts and concentration of reactants used are presented in Table VII.3.

VII.6 References:

1. S. J. Gregg, K. S. W. Sing. Adsorption Surface Area and Porosity, 2nd ed. Academic Press, New York, 1982.

2. S. Lowell, J. E. Shields, M. A. Thomas, M. Thommes. Characterization of Porous Solids and Powders: Surface Area, Pore Size and Density. Particle Technology Series, Vol. 16, 2004, Springer Science+Business Media B.V.

3. S. Dembski, M. Milde, M. Dyrba, S. Schweizer, C. Gellermann, T. Klockenbring. *Langmuir* **2011**, *27*, 14025-14032. Effect of pH on the synthesis and properties of luminescent SiO_2/calcium phosphate: Eu^{3+} core-shell nanoparticles.

4. L. B. A. Macon, T. B. Kim, E. M. Valliant, K. Goetschius, R. K. Brow, D. E. Day, A. Hoppe, A. R. Boccaccini, I. Y. Kim, C. Ohtsuki, T. Kokubo, A. Osaka, M. Vallet-Regí, D. Arcos, L. Fraile, A. J. Salinas, A. V. Teixeira, Y. Vueva, R. M. Almeida, M. Miola, C. Vitale-Brovarone, E. Verné, W. Höland, R. J. Jones. *J. Mater. Sci.: Mater. Med.* **2015**, *26*, 1-10. A unified in vitro evaluation for apatite-forming ability of bioactive glasses and their variants.

5. C. Liu, X. Ji, G. Cheng. *Appl. Surf. Sci.* **2007**, *253*, 6840-6843. Template synthesis and characterization of highly ordered lamellar hydroxyapatite.

6. A. Galarneau, G. Renard, M. Mureseanu, A. Tourrette, C. Biolley, M. Choi, R. Ryoo, F. R. Di, F. Fajula. *Micropor. Mesopor. Mater.* **2007**, *104*, 103-114. Synthesis of sponge mesoporous silicas from lecithin/dodecylamine mixed-micelles in ethanol/water media: A route towards efficient biocatalysts.

7. W. Stöber, A. Fink, E. Bohn. *J. Colloid Interf. Sci.* **1968**, *26*, 62. Controlled growth of monodisperse silica spheres in the micron size range.

8. S. Sánchez-Salcedo, M. Vila, I. Izquierdo-Barba, M. Cicuendez, M. Vallet-Regí. *J. Mater. Chem.* **2010**, *20*, 6956-6961. Biopolymer-coated hydroxyapatite foams: a new antidote for heavy metal intoxication.

9. Y. G. Jin, S. Z. Qiao, Z. P. Xu, C. J. C. Diniz, G. Q. Lu. *J. Phys. Chem. C.* **2009**, *113*, 3157-3163. Porous silica nanospheres functionalized with phosphonic acid as Intermediate-temperature proton conductors.

10. H. Meng, M. Xue, T. Xia, Z. Ji, D. Y. Tarn, J. I. Zink, A. E. Nel. *ACS Nano* **2011**, *5*, 4131-4144. Use of size and a copolymer design feature to Improve the biodistribution and the enhanced permeability and retention effect of doxorubicin-loaded mesoporous silica nanoparticles in a murine xenograft tumor model.

11. M. Neumeier, A. L. Hails, A. S. Davis, S. Mann, M. Epple. *J. Mater. Chem.* **2011**, *21*, 1250-1254. Synthesis of fluorescent core-shell hydroxyapatite nanoparticles.

12. V. Sokolova, M. Epple. *Nanoscale* **2011**, *3*, 1957-1962. Synthetic pathways to make nanoparticles fluorescent.

13. L. Armelao, S. Quici, F. Barigelletti, G. Accorsi, G. Bottaro, M. Cavazzini, E. Tondello. *Coord. Chem. Rev.* **2010**, *254*, 487-505. Design of luminescent lanthanide complexes: From molecules to highly efficient photoemitting materials.

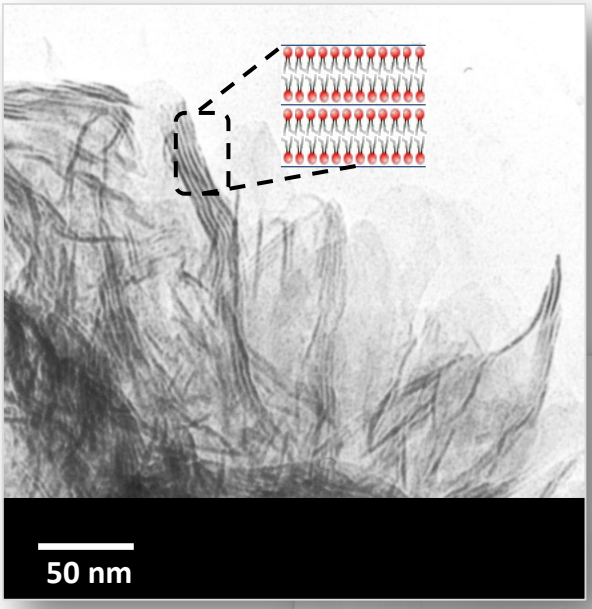
50 nm

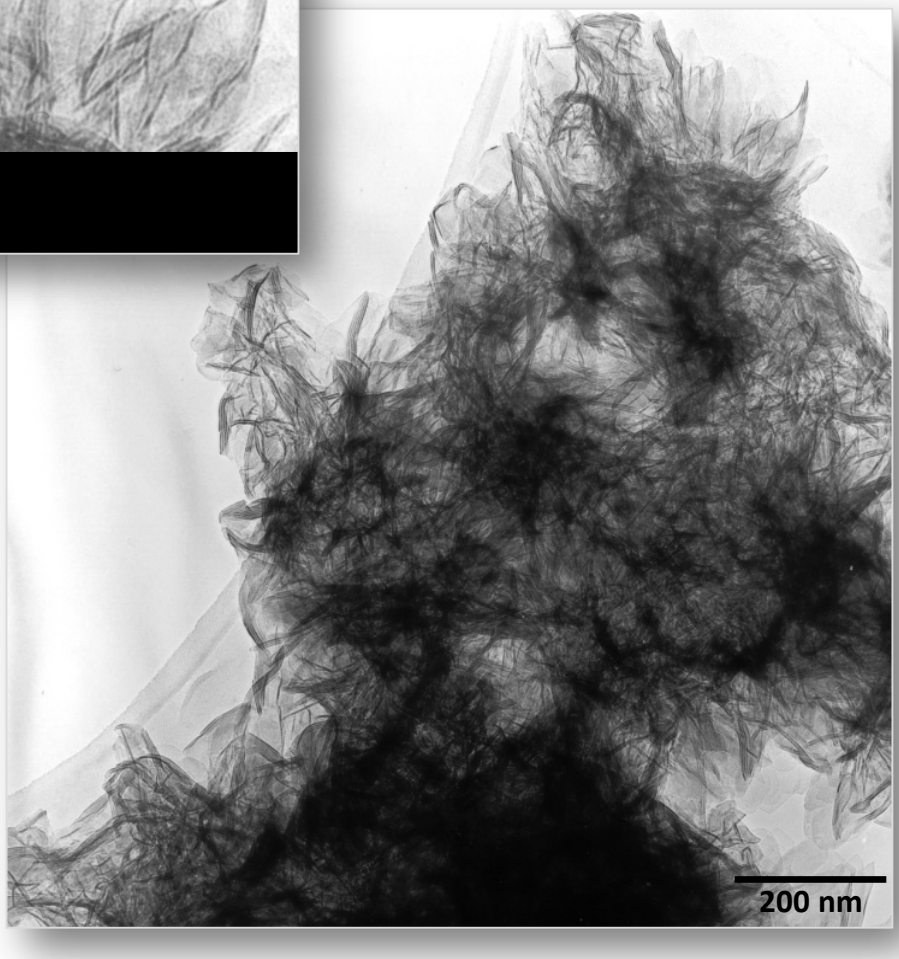
200 nm